

# **New threats to the ozone layer: Exploring ozone-depleting substances in the troposphere and stratosphere**

By

**Karina Adcock**

A thesis submitted to the School of Environmental Sciences of the  
University of East Anglia, in partial fulfilment of the  
requirements for the degree of Doctor of Philosophy

May 2020

This copy of the thesis has been supplied on condition that anyone who consults it is understood to recognise that its copyright rests with the author and that use of any information derived there from must be in accordance with current UK Copyright Law. In addition, any quotation or extract must include full attribution.



# Abstract

---

The release into the atmosphere of trace gases that contain chlorine and bromine can significantly impact stratospheric ozone depletion. The production and consumption of many ozone-depleting substances has been phased out under an international agreement called the Montreal Protocol on Substances that Deplete the Ozone Layer. Further monitoring is required to ensure the overall abundance of ozone-depleting substances continues to decrease in the atmosphere. This thesis focuses on East Asia which is a region where there can be rapid transport of ozone-depleting substances into the stratosphere and where continuing emissions of many ozone-depleting substances have been reported in recent years. In this thesis, a variety of halogenated trace gases were measured in air samples collected at ground level measurement sites and during aircraft campaigns via a gas chromatograph mass spectrometer system (GC-MS) to investigate new threats to the ozone layer.

As part of the StratoClim project, a number of halogenated trace gases were analysed in air samples collected on board the Geophysica high altitude research aircraft over the Mediterranean, Nepal and northern India during the summers of 2016 and 2017 to investigate the composition of the Asian summer monsoon in the upper troposphere and lower stratosphere. Chlorinated very short-lived ozone-depleting substances (VSLs) were found to be enhanced above mixing ratios measured in the tropical tropopause layer in 2013-2014. This indicates that large emissions of chlorinated VSLs in East and South Asia can be rapidly transported by the Asian monsoon into the lower stratosphere, before they have broken down to insignificant levels, and therefore they can contribute to ozone depletion. Chlorinated VSLs contribute only a small fraction of the total amount of chlorine in the tropopause region and the lower stratosphere. However, their contribution could delay the long-term recovery of the ozone layer.

This thesis also presents updated long-term trends and global annual emissions of CFC-113a ( $\text{CCl}_3\text{CF}_3$ ). The mixing ratios of CFC-113a are still increasing substantially and global atmospheric emissions of CFC-113a remained at about  $1.7 \text{ Gg yr}^{-1}$  between 2012 and 2016 after an increase in emissions in 2010–2012. Complementary ground-based observations in Taiwan suggest the presence of persistent emissions of CFC-113a in East Asia. The emissions are relatively small and it is possible they are due to the few remaining allowed uses of CFC-113a.

Furthermore, atmospheric observations of multiple halogenated trace gases in Taiwan used with backward trajectory modelling found that CFC-11 ( $\text{CCl}_2\text{F}_2$ ) emissions coming from eastern China had increased from  $12 (10-14) \text{ Gg yr}^{-1}$  in 2008–2011 to  $19 (14-23) \text{ Gg yr}^{-1}$  in 2014–2018. This is about one-quarter of global emissions and the increase contributed to the recently discovered global increase in CFC-11 emissions. These results independently support the findings of other recent studies. The increase in emissions is possibly due to illegal production of CFC-11.

## **Access Condition and Agreement**

Each deposit in UEA Digital Repository is protected by copyright and other intellectual property rights, and duplication or sale of all or part of any of the Data Collections is not permitted, except that material may be duplicated by you for your research use or for educational purposes in electronic or print form. You must obtain permission from the copyright holder, usually the author, for any other use. Exceptions only apply where a deposit may be explicitly provided under a stated licence, such as a Creative Commons licence or Open Government licence.

Electronic or print copies may not be offered, whether for sale or otherwise to anyone, unless explicitly stated under a Creative Commons or Open Government license. Unauthorised reproduction, editing or reformatting for resale purposes is explicitly prohibited (except where approved by the copyright holder themselves) and UEA reserves the right to take immediate 'take down' action on behalf of the copyright and/or rights holder if this Access condition of the UEA Digital Repository is breached. Any material in this database has been supplied on the understanding that it is copyright material and that no quotation from the material may be published without proper acknowledgement.

# Acknowledgments

---

I will start by thanking my supervisor Johannes Laube whose endless support with every aspect of this work made the completion of my PhD journey possible. I could not have hoped for a better supervisor. Thanks also go to my co-supervisors David Oram and Bill Sturges for all their help during supervisor meetings, for providing me with data, reading lots of my drafts and many other things.

Special thanks also go to Claire Reeves, who helped me considerably with my thesis, especially with the emission estimates of CFC-11 and CFC-113a and while not actually one of my supervisors may as well have been. I also want to thank Emma Leedham Elvidge who was incredibly supportive when I was first learning how to use the AutoSpec instrument. I am also extremely grateful to Lauren Gooch who was Johannes PhD student before me and whose measurements and analysis were the foundation I built a lot of my work on.

I extend my appreciation and gratitude to the many people at the University of East Anglia who also measured air samples and generously shared their data with me including Johannes Laube, Lauren Gooch, David Oram and Geoffrey Lee without which this thesis would not have been possible.

This thesis also draws on work from multiple different campaigns and I want to thank all the people involved especially those who collected air samples in Bachok, Malaysia; Cape Grim, Tasmania; Tacolneston, United Kingdom; and the two sites in Taiwan. Additionally, I am grateful to everyone who worked on the CARIBIC project, the StratoClim project and the staff from the NOAA Global Monitoring Division.

I am thankful to everyone who provided me with output from the NAME atmospheric dispersion model including Matthew Ashfold (University of Nottingham), Marios Panagi and Zoe Fleming (University of Leicester) and in particular Norfazrin Mohd Hanif, who was a PhD student in the same office as me at the University of East Anglia. I also want to thank Bärbel Vogel from Jülich Research Centre for providing me with the output from the CLaMS model.

Finally, I am grateful to my parents who have tolerated me being a full-time student for the past 20 years and without their enthusiastic support and encouragement none of this would have been possible.

# Table of Contents

---

<b>Chapter 1: Introduction .....</b>	<b>9</b>
1.1 The ozone layer .....	9
1.2 The circulation of the air in the stratosphere.....	10
1.3 The formation of the ozone hole .....	12
1.4 Impacts of the ozone hole .....	13
1.5 Montreal Protocol on Substances that Deplete the Ozone Layer.....	13
1.6 Halogenated substances in the atmosphere .....	15
1.6.1 Chlorofluorocarbons.....	17
1.6.2 Halons.....	18
1.6.3 Hydrochlorofluorocarbons .....	18
1.6.4 Hydrofluorocarbons.....	19
1.6.5 Perfluorocarbons and other perfluorinated compounds .....	19
1.6.6 Carbon tetrachloride .....	20
1.6.7 Methyl chloroform .....	20
1.6.8 Methyl halides .....	20
1.6.9 Very short-lived ozone-depleting substances.....	21
1.7 Aims and rationale .....	22
References .....	25
<b>Chapter 2: Methods .....</b>	<b>29</b>
2.1 Gas chromatography - mass spectrometry (GC-MS).....	29
2.2 Sample collection .....	30
2.3 Sample preparation – the inlet system .....	31
2.4 The AutoSpec system.....	33
2.5 Instrument setup .....	35
2.5.1 Typical measurement day.....	38
2.6 Data processing .....	39
2.7 Entech instrument.....	40
2.8 Stability of substances in standards.....	40
2.8.1 Purpose of a working standard .....	40
2.8.2 Purpose of intercomparison measurements .....	40
2.8.3 Description of standards .....	41
2.8.4 Intercomparison methodology.....	42

2.8.5 Intercomparison results .....	44
2.8.6 Drift correction .....	46
2.8.7 Calculating the mixing ratios in the standards .....	48
2.9 Atmospheric models .....	50
References .....	51
<b>Chapter 3: Aircraft-based observations of ozone-depleting substances in the upper troposphere and lower stratosphere in and above the Asian summer monsoon.....</b>	<b>54</b>
3.1 Introduction .....	55
3.2 Methods .....	57
3.2.1 Aircraft campaigns .....	57
3.2.2 Analytical technique .....	58
3.2.3 CLaMS backward air mass trajectories .....	62
3.2.4 Equivalent Chlorine (ECl) .....	63
3.2.5 Equivalent Effective Stratospheric Chlorine (EESC) .....	63
3.3 Results and discussion .....	66
3.3.1 Well mixed ozone-depleting substances .....	66
3.3.2 Very short-lived ozone-depleting substances .....	67
3.3.3 CLaMS backward trajectories .....	70
3.3.4 Equivalent Chlorine (ECl) .....	71
3.3.5 Mean age-of-air tracer comparison .....	74
3.3.6 Fractional Release Factors (FRFs) .....	75
3.3.7 Equivalent Effective Stratospheric Chlorine (EESC) .....	78
3.4 Conclusions .....	83
Acknowledgements .....	84
References .....	85
<b>Chapter 4: Continued increase of CFC-113a (CCl<sub>3</sub>CF<sub>3</sub>) mixing ratios in the global atmosphere: emissions, occurrence and potential sources .....</b>	<b>93</b>
4.1 Introduction .....	94
4.2 Methods .....	95
4.2.1 Analytical technique .....	95
4.2.2 Sampling .....	96
4.2.3 Emission modelling .....	98
4.2.4 Dispersion modelling .....	102
4.3 Results .....	103
4.3.1 Long-term atmospheric trends and estimated global annual emissions of CFC-113a and CFC-113 .....	103

4.3.2 Global distributions of CFC-113a .....	108
4.3.2.1 Enhancement above background mixing ratios .....	108
4.3.2.2 Interhemispheric gradient of CFC-113a .....	113
4.3.2.3 Measurements of CFC-113a in the stratosphere.....	114
4.4 Possible sources of CFC-113a .....	116
4.5 Conclusions .....	118
Acknowledgements .....	119
References .....	120
<b>Chapter 5: Investigation of East Asian emissions of CFC-11 using atmospheric observations in Taiwan.....</b>	<b>127</b>
5.1 Introduction .....	128
5.2 Methods.....	130
5.2.1 Analytical technique .....	130
5.2.2 Identification of CFC-11 source regions .....	131
5.2.3 Correlations of CFC-11 with other trace gases .....	132
5.2.4 Estimation of CFC-11 emissions from China .....	133
5.2.5 Estimation of changes in CFC-11 emissions from China .....	134
5.3 Results and discussion.....	134
5.3.1 CFC-11 mixing ratios in Taiwan.....	134
5.3.2 CFC-11 source regions .....	135
5.3.3 Correlations of CFC-11 with other trace gases .....	140
5.3.4 CFC-11 emissions from China .....	142
5.3.5 Changes in CFC-11 emissions from China .....	147
5.3.6 Comparison to global CFC-11 emissions.....	149
5.4 Conclusions .....	150
Acknowledgements .....	150
References .....	151
<b>Chapter 6: Summary, conclusions and future work .....</b>	<b>157</b>
6.1 Outline of major research findings.....	158
6.1.1 Transport of chlorine-containing very short-lived ozone-depleting substances by the Asian summer monsoon .....	158
6.1.2 CFC-113a mixing ratios and emissions in the atmosphere .....	160
6.1.3 CFC-11 mixing ratios and emissions in East Asia .....	161
6.2 Suggestions for future work and policy implications .....	162
6.2.1 Transport of chlorine-containing very short-lived ozone-depleting substances by the Asian summer monsoon .....	162

6.2.2 CFC-113a mixing ratios and emissions in the atmosphere.....	163
6.2.3 CFC-11 mixing ratios and emissions in East Asia .....	164
6.2.4 Further research directions.....	165
References.....	166
<b>Appendix .....</b>	<b>169</b>
A1. Intercomparison results.....	169
A2. AMO-16 and AMA-17 mixing ratios .....	173
A3. NAME footprints .....	176
A4. CFC-11 emission estimates .....	194

# Chapter 1: Introduction

---

This thesis aims to investigate ozone-depleting substances of interest, with a special focus on East Asia. The ozone layer is a part of the stratosphere that blocks harmful ultraviolet radiation from reaching the Earth's surface. In the stratosphere there is a large-scale overturning circulation, where air enters the stratosphere in the tropics and is transported to the poles. The release of industrially produced ozone-depleting substances leads to additional free radicals in the polar vortex, that catalyse ozone destruction reactions, and causes the formation of the 'ozone hole', in late winter and early spring. This increases the risk of people developing skin cancers. Consequently, the Montreal Protocol on Substances that Deplete the Ozone Layer was introduced to phase out the production and consumption of ozone-depleting substances. There are many different types of ozone-depleting substances that have different atmospheric lifetimes, that vary in their effectiveness at depleting ozone, and that come from a variety of natural and anthropogenic sources.

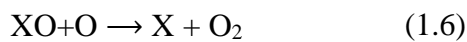
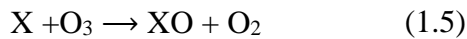
## 1.1 The ozone layer

The stratosphere is a layer of the atmosphere between roughly 12 km and 50 km above the Earth's surface. There is a broad peak in ozone mixing ratios in the stratosphere that is referred to as the ozone layer. The chemistry of the stratosphere is dominated by the reactions of ozone ( $O_3$ ). In the stratosphere, a continual reaction cycle, called the Chapman Cycle, converts between ozone and oxygen (Chapman, 1930). Molecular oxygen is two oxygen atoms bonded together,  $O_2$ . In the stratosphere, short wavelength ultraviolet radiation splits molecules of  $O_2$  into O atoms ( $<240$  nm) (Eq. 1.1). One of these atomic oxygen's can then combine with another  $O_2$  to form ozone which is three oxygen atoms bonded together (Eq. 1.2). Another molecule ( $M$ ), usually another oxygen or nitrogen, absorbs the excess energy released during the reaction. Ozone itself is also broken down by short wavelength ultraviolet radiation i.e. photolysis ( $<320$  nm) (Eq. 1.3) or by reaction with O (Eq. 1.4), to reform the oxygen molecule and the reaction cycle can then begin again.



On the one hand, solar radiation decreases with decreasing altitude as the radiation is absorbed by  $O_2$  and  $O_3$  overhead. This causes the rate of reaction of Eq. 1.1 to decrease sharply with decreasing altitude, and as this is the effective source of  $O_3$  via Eq. 1.2, there is less  $O_3$  at lower altitudes. On the other hand, oxygen is required to form ozone and as altitude increases the amount of oxygen decreases. Therefore, the observed maximum in ozone, at 20-30 km altitude, largely reflects a balance between these features (Jacob, 1999).

The Chapman mechanism alone would lead to much higher ozone mixing ratios than are observed. This is due to the presence of additional ozone loss reactions where ozone reacts with free radical catalysts (X), such as nitric oxide (NO), hydroxyl radical (OH), atomic chlorine (Cl), and atomic bromine (Br). The most basic of these reaction cycles can be generalised as in Equations 1.5-1.7. Free radicals have an unpaired electron, and this makes them highly reactive. The free radical is not destroyed in the reaction and this means it can go on to take part in thousands more reactions and destroy a huge amount of ozone before it is eventually removed. Therefore, a small amount of these compounds can have a large impact on stratospheric ozone levels.



X= NO, OH, Cl...

The natural cycles of ozone loss and formation are balanced. However, this balance has been disturbed by an increase in free radicals from anthropogenic emissions of ozone-depleting substances. Further details on different source gas types are given in Section 1.6. Ozone-depleting substances, such as chlorofluorocarbons (CFCs), first began to be used on a large scale in the 1960s and were widely used as refrigerants and aerosol propellants as they are generally non-toxic and inert. However, this inertness means that they have negligible loss mechanisms in the troposphere. Once in the stratosphere, the gases are exposed to strong ultraviolet radiation and break down mostly through photolysis and reaction with O (Ko et al., 2013). This forms chlorine and bromine free radicals that are highly reactive and act as catalysts in the destruction of ozone into oxygen in the above chemical reactions (Molina and Rowland, 1974). These additional free radicals speed up the natural process of ozone destruction.

## 1.2 The circulation of the air in the stratosphere

The transportation of air from the troposphere to the stratosphere occurs primarily at the tropics. Convective processes in the troposphere lead to vertical transport of hot moist air towards a region termed the tropical tropopause layer (TTL). At the tropical tropopause layer, further vertical transport is inhibited by the temperature inversion between the troposphere and the stratosphere. Air will usually only pass through this layer and enter the stratosphere if it has enough latent heat energy. The stratosphere has a large-scale overturning circulation called the meridional circulation or the Brewer-Dobson circulation. The air enters in the tropics and then slowly moves polewards and descends at middle and high latitudes. This circulation causes the altitude of the tropopause to be higher in the tropics and lower in the Poles. The slow-moving circulation and transportation take place on the order of years.

Global distribution of ozone varies significantly by latitude and season. As ozone-poor air in the troposphere is transported upwards into the stratosphere in the tropics, it is exposed to sunlight overhead that breaks down the oxygen and forms ozone (Eq. 1.1-1.2). Due to this process, ozone is mostly formed in the tropics. Air is then transported

to the mid-latitudes and the poles. This leads to a build-up of ozone in the North and South Pole and so under natural conditions there are higher ozone mixing ratios at the poles than in the tropics.

The strength of this transport varies seasonally and is strongest in the wintertime and springtime in each hemisphere (Holloway and Wayne, 2010). Consequently, there is a build-up of ozone and the highest ozone mixing ratios in the spring in each hemisphere. Polewards transport is much weaker in the summer and autumn. Also, during the summer in the polar regions, there is continuous daylight and therefore continuous breakdown of ozone by solar radiation. Therefore, ozone decreases gradually toward its lowest values in autumn. Then this seasonal cycle begins again. This is what the ozone layer is naturally like without human interference.

Due to the Brewer-Dobson circulation, ozone-depleting substances enter the stratosphere in the tropics where they are transported upwards and exposed to UV radiation that breaks them down and forms free radicals (Figure 1.1). Most of these free radicals are initially converted into ‘reservoir’ species, for example ClONO<sub>2</sub> (chlorine nitrate), HOCl (hypochlorous acid) and HCl (hydrochloric acid), by reactions with NO<sub>x</sub>, HO<sub>x</sub> or ClO<sub>x</sub> species (Equations 1.8-1.10) (Holloway and Wayne, 2010).



Reservoir species are relatively stable and can ‘store’ radicals in an inactive form, which prevents them from reacting with ozone (Holloway and Wayne, 2010). These reservoir species are transported polewards via the Brewer-Dobson circulation and are then either removed from the stratosphere or repartitioned into radicals (Holloway and Wayne, 2010).

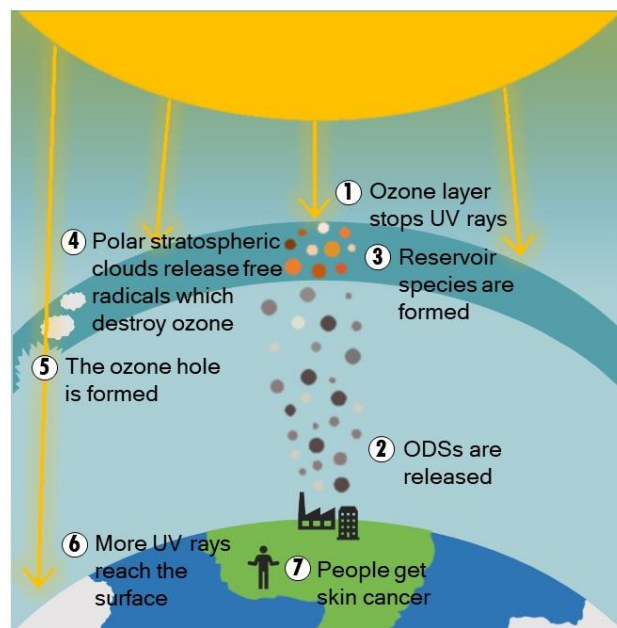
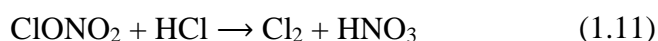


Figure 1.1: Schematic of the formation of the ozone hole.

### 1.3 The formation of the ozone hole

The ozone hole is an area with very low levels of ozone in the stratosphere over Antarctica. The ozone hole was discovered in 1984 and is mainly caused by anthropogenic compounds that contain chlorine and bromine (Molina and Rowland, 1974; Chubachi, 1984; Farman et al., 1985). In the Antarctic during the winter, it gets cold enough ( $<200\text{ °K}$ ) to form clouds in the stratosphere called polar stratospheric clouds (PSCs) (Holloway and Wayne, 2010). These clouds contain stratospheric particles such as ice, soot, sulfuric acid ( $\text{H}_2\text{SO}_4$ ) and nitric acid hydrate ( $\text{HNO}_3$ ) which provide reaction sites where the reservoir species can be converted heterogeneously to their radical forms, which destroy ozone (Holloway and Wayne, 2010). For example:



The release of anthropogenic chlorine and bromine containing substances into the atmosphere leads to more of these compounds in Antarctica. These compounds are confined to the polar vortex that forms over the Antarctic during the wintertime and springtime. The polar vortex is a very strong westerly circulation that effectively traps this air in the polar region (Holloway and Wayne, 2010). Due to a lack of sunlight in mid-winter, the ozone hole forms during late winter and early spring when sunlight returns and drives the photochemical reactions that very rapidly destroy ozone (Eq. 1.5-1.7). This typically occurs in September and October. Then at the beginning of the Antarctic summer (in about November) the atmosphere warms, the polar vortex breaks down and the ozone hole is ‘filled in’ (Holloway and Wayne, 2010).

An ozone hole also occurs during the springtime over the Arctic in about March. However, these ozone holes are more infrequent and less severe than in the Antarctic.

The Antarctic continent is surrounded by the Southern Ocean leaving it meteorologically isolated whereas the Arctic is not as isolated. Therefore, its wind flow is more often disturbed by external weather systems. This makes the Arctic polar vortex more distorted and warmer than the Antarctic polar vortex, which leads to fewer polar stratospheric clouds and therefore less ozone depletion (Holloway and Wayne, 2010). In the Antarctic, total ozone values in early springtime are nearly two-thirds below normal values. Whereas in the Arctic total ozone values are 0-30 % below normal. It has also been found that in the mid-latitudes ozone values are about 3-5 % below normal values. In the tropics, ozone-depleting substances have very little effect on ozone levels as ozone levels are naturally low in the tropics (Salawitch et al., 2019).

#### **1.4 Impacts of the ozone hole**

Ultraviolet (UV) radiation is categorised into three types based on its wavelength, UV-A, UV-B & UV-C. UV-C radiation is the most harmful radiation with the shortest wavelengths. Fortunately, it is entirely absorbed by the ozone layer. UV-A wavelengths are the longest and the least harmful. UV-A radiation is only weakly absorbed by the ozone layer and causes premature ageing of the skin and some skin cancers (Salawitch et al., 2019).

UV-B radiation has wavelengths of 280 to 315 nm. It is partially absorbed by the ozone layer and ozone depletion causes more UV-B radiation to reach the Earth's surface. In humans, increased exposure to UV-B radiation increases the risks of skin cancer, cataracts and suppresses the immune system (Salawitch et al., 2019). Excessive UV-B exposure can also damage terrestrial plant life, including agricultural crops, single-celled organisms, and aquatic ecosystems (Salawitch et al., 2019). Increased levels of UV-B radiation are known to accelerate the degradation of some materials (Andrady et al., 2011). Additionally, ozone is a greenhouse gas and so any changes to its mixing ratios has an impact on climate change.

#### **1.5 Montreal Protocol on Substances that Deplete the Ozone Layer**

It was first suggested in 1974 that chlorine-containing compounds could break down ozone in the stratosphere (Molina and Rowland, 1974). Evidence of this was found in 1984 when very low levels of ozone, 'the ozone hole', were first measured over Antarctica (Chubachi, 1984). The discovery of the ozone hole and its negative effects lead to the international agreement called the Montreal Protocol on Substances that Deplete the Ozone Layer to phase out the use of ozone-depleting substances. The Montreal Protocol requires stepwise reductions of production and consumption of a selection of ozone-depleting substances called controlled substances (UNEP, 2019). Production is the amount of controlled substances produced, minus the amount destroyed by technologies (UNEP, 2019). Consumption is the amount of production plus imports minus exports (UNEP, 2019). For a number of compounds there are exceptions for "essential uses" where no acceptable substitutes are available (UNEP, 2019). The agreement was created in 1987 and entered into force in 1989. Since then

there have been many adjustments and amendments to the Montreal Protocol, introducing faster phase out schedules and adding more compounds to the list of controlled substances (Figure 1.2).

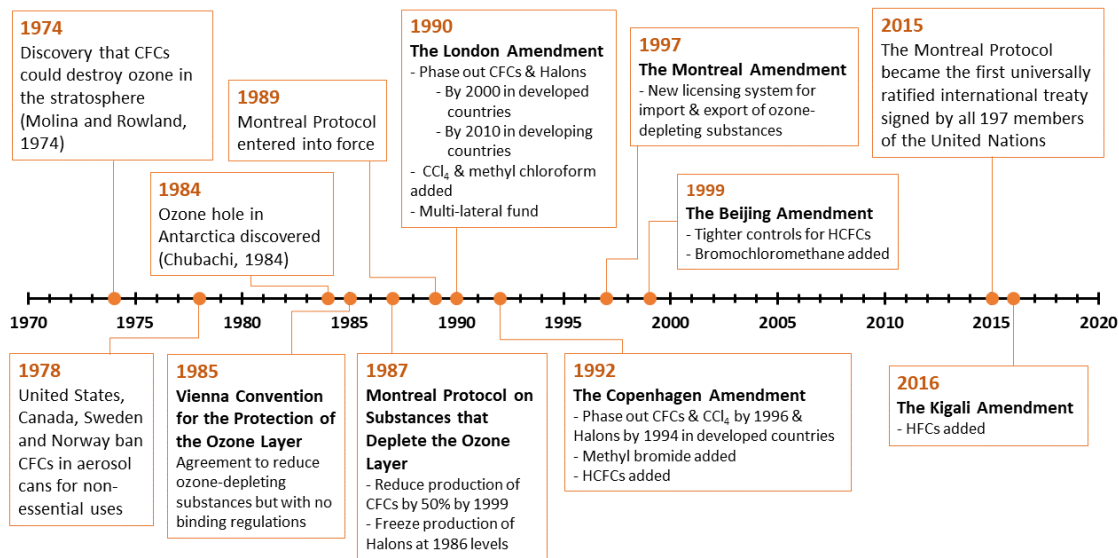


Figure 1.2: Timeline of events relevant to the ozone hole including the Montreal Protocol and its amendments (UNEP, 2019).

The Montreal Protocol originally separated country members into two groups: Non-Article 5 countries (developed countries) and Article 5 countries (developing countries). Countries with an annual per capita consumption and production of ozone-depleting substances of less than 0.3 kg are classified as Article 5 countries (UNEP, 2019). All other countries are Non-Article 5 countries. There are 147 out of 196 countries classified as Article-5 countries (MLF, 2020). Article 5 countries have longer phase-out schedules in order to allow time and funding to make necessary adjustments to industry and technology. In the Kigali Amendment in 2016, Article 5 countries were further separated into two groups with different phase out schedules for hydrofluorocarbons (HFCs). Article 5 Group 2 countries are: Bahrain, India, the Islamic Republic of Iran, Iraq, Kuwait, Oman, Pakistan, Qatar, Saudi Arabia and the United Arab Emirates (UNEP, 2019). All other Article 5 countries are in Group 1.

In 1990, the Multilateral Fund (MLF) for the implementation of the Montreal Protocol was established to provide financial assistance to Article 5 countries to help them comply with the requirements of the Montreal Protocol (MLF, 2020). The Fund is financed through contributions from non-Article 5 countries and it supports activities such as the conversion of manufacturing processes and technical assistance (MLF, 2020).

The Montreal Protocol has generally been very successful. There is mostly strong compliance with its regulations and as a result, the overall abundance of ozone-depleting substances is decreasing in the atmosphere (Engel and Rigby et al., 2018). In

response, ozone levels in most parts of the stratosphere stopped decreasing in the late 1990s and remained roughly constant since ~2000 (Braesicke and Neu et al., 2018). Some parts of the ozone layer are starting to show signs of recovery. The size of the Antarctic ozone hole has been decreasing since the year 2000 (Solomon et al., 2016). Outside the polar regions, upper stratospheric ozone has increased by 1–3 % per decade since 2000 (Braesicke and Neu et al., 2018). The ozone layer is expected to return to 1980 levels by the middle of 21<sup>st</sup> century, assuming continued compliance with the Montreal Protocol (Braesicke and Neu et al., 2018). In addition to this, as many ozone-depleting substances are also strong greenhouse gases the Montreal Protocol has had the additional benefit of reducing the human contribution to climate change (Velders et al., 2007).

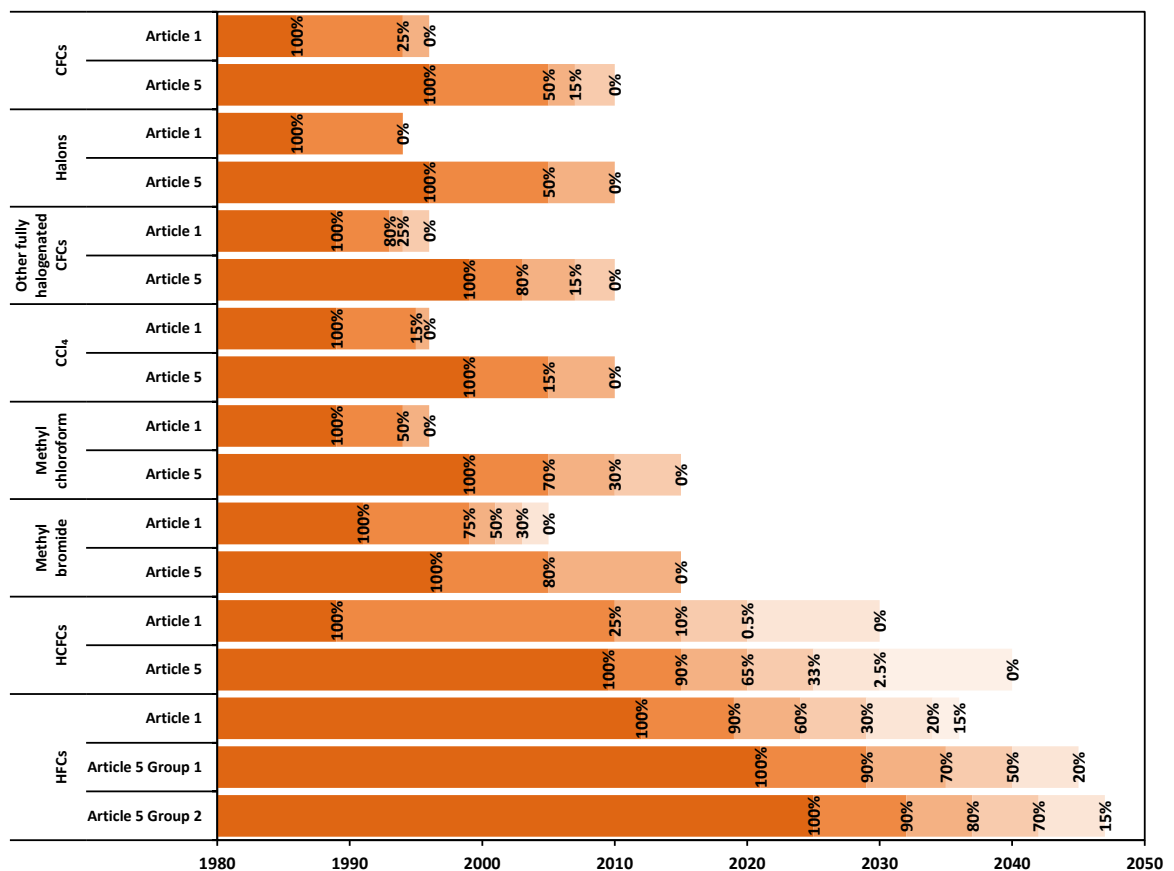


Figure 1.3: The step-down phase out schedule of compounds controlled by the Montreal Protocol (UNEP, 2019).

## 1.6 Halogenated substances in the atmosphere

This section discusses halogenated substances and their impact on stratospheric ozone depletion and climate change. The various subgroups of halogenated substances are introduced along with their atmospheric lifetimes, atmospheric trends, natural and anthropogenic sources, and the global legislation that affects their production and consumption.

- **Halogens** – are the five elements in Group 7 in the periodic table: fluorine, chlorine, bromine, iodine and astatine.
- **Halocarbons** – are compounds that contain halogens and carbon.
- **Ozone-depleting substances (ODSs)** – are compounds that break down when they reach the stratosphere to form free radicals, which catalyse the destruction of ozone (Section 1.1).
- **Trace gases** – are gases with very low atmospheric abundances. They are defined as gases that represent less than 1 % of the Earth’s atmospheric composition.

Halocarbons that contain chlorine and bromine are typically ozone-depleting substances as they break down in the stratosphere to form chlorine and bromine free radicals.

Bromine is about 60 times more efficient, on a per atom basis, at destroying ozone than chlorine (Daniel and Velders et al., 2006). There are three factors that contribute to this:

- 1) brominated compounds are photolysed at longer wavelengths than chlorinated compounds resulting in a higher percentage of free bromine atoms than chlorine.
- 2) Bromine reservoir species are formed inefficiently and are readily photolysed.
- 3) Coupling between bromine- and chlorine-catalysed processes potentiates chlorine and bromine for further ozone destruction (Eq.1.13-1.15)(Daniel et al., 1999).



Fluorine containing compounds are not generally considered to be ozone-depleting substances as the fluorine is converted into F and FO which are then very rapidly converted into hydrogen fluoride (HF), a stable reservoir species that does not react with ozone (Ravishankara et al., 1994; Wallington et al., 1995). In addition, although iodine can participate in ozone destruction reactions, due to rapid tropospheric loss of iodine-containing compounds very little iodine reaches the stratosphere (Daniel and Velders et al., 2010).

Other major ozone-depleting substances are methane (CH<sub>4</sub>) and nitrous oxide (N<sub>2</sub>O) which both have natural and anthropogenic sources. The reactions of CH<sub>4</sub> and H<sub>2</sub>O with energetically excited oxygen, O(<sup>1</sup>D), produce HO<sub>x</sub> species (H, OH and HO<sub>2</sub>) and nitrous oxide is a source of NO<sub>x</sub> species (NO and NO<sub>2</sub>), that act as catalysts in ozone destruction cycles (Eq. 1.5-1.7).

Methane, nitrous oxide and halocarbons are all also greenhouse gases. Whilst they are only trace gases, they make significant contributions to climate change because these species have strong absorption bands in the infrared spectrum in areas where CO<sub>2</sub> absorbs weakly. Due to the dual contributions to ozone depletion and climate change, the overall effects of these compounds can differ. As ozone itself is a greenhouse gas,

species that cause ozone depletion can have an indirect cooling effect (Daniel et al., 1995). The reverse is also true, if ozone levels increase, as the ozone hole reduces, this will cause more global warming. Also increased absorption of infrared radiation by greenhouse gases leads to stratospheric cooling and changes in stratospheric circulation, which can increase ozone levels (Carpenter and Daniel et al., 2018).

### 1.6.1 Chlorofluorocarbons

Chlorofluorocarbons (CFCs) are compounds that consist of chlorine, fluorine and carbon. They are ozone-depleting substances and greenhouse gases. The three most abundant CFCs in the atmosphere (the major CFCs) are CFC-12 ( $\text{CCl}_2\text{F}_2$ ), CFC-11 ( $\text{CCl}_3\text{F}$ ) and CFC-113 ( $\text{CCl}_2\text{FCClF}_2$ ). Other minor CFCs include CFC-13, CFC-112, CFC-112a, CFC-113a, CFC-114, CFC-114a and CFC-115. CFCs are relatively unreactive and have long atmosphere lifetimes of decades to centuries. For example, CFC-11 has a lifetime of about 52 years and CFC-115 has a lifetime of about 640 years (WMO, 2018).

Chlorofluorocarbons were first created by Belgian scientist, Frédéric Swarts, in the 1890s who replaced chlorine in carbon tetrachloride ( $\text{CCl}_4$ ) with fluorine to make CFC-11 ( $\text{CCl}_3\text{F}$ ) and CFC-12 ( $\text{CCl}_2\text{F}_2$ ). In the late 1920s, Thomas Midgley, Jr. improved the process of synthesis and led the effort to use CFC as a refrigerant to replace ammonia ( $\text{NH}_3$ ), chloromethane ( $\text{CH}_3\text{Cl}$ ), and sulfur dioxide ( $\text{SO}_2$ ), which were commonly used at the time but can be toxic. DuPont began producing CFCs commercially in the 1930s and they first began to be used on a large scale in the 1960s and 70s. They are used in a wide range of applications, most commonly as refrigerants, aerosol propellants, solvents and foam blowing agents (Kim et al., 2011).

It was initially thought that these compounds were safe to release into the atmosphere as they were very unreactive and so they were widely used and their mixing ratios increased rapidly in the atmosphere. It was later discovered that when these compounds reach the stratosphere they are broken down by strong ultraviolet radiation and form chlorine free radicals, which destroy ozone (Section 1.1).

CFCs are regulated under the Montreal Protocol, which came into force in 1989, and since then production and consumption of CFCs have been phased out, by 1996 in developed countries and 2010 in developing countries, with a few essential use exceptions (Figure 1.3). Production of most of these compounds has now almost completely stopped, although there continues to be emissions from equipment and products made with CFCs before the ban, referred to as a 'bank'. Mixing ratios of the major CFCs are decreasing in the atmosphere (Engel and Rigby et al., 2018).

### 1.6.2 Halons

Halons are compounds consisting of carbon, bromine, fluorine and sometimes chlorine. Halons are strong ozone-depleting substances as they contain bromine, which as previously mentioned, is 60 times more effective than chlorine at destroying ozone (Daniel and Velders et al., 2006). They have atmospheric lifetimes of the order of years to decades (WMO, 2018). Halons are strong greenhouse gases but due to their influence on ozone depletion, they have a net negative effect on radiative forcing (Daniel et al., 1995). Halons are used almost exclusively as fire extinguishers (HTOC, 2018). Halons were phased out under the Montreal Protocol by 1994 in developed countries and 2010 in developing countries, except for some essential use exemptions (Figure 1.3). Due to the Montreal Protocol mixing ratios of Halon-1211 ( $\text{CBrClF}_2$ ), Halon-2402 ( $\text{CBrF}_2\text{CBrF}_2$ ), and Halon-1202 ( $\text{CBr}_2\text{F}_2$ ) have been declining and the growth rate of Halon-1301 ( $\text{CF}_3\text{Br}$ ) is beginning to level off (Engel and Rigby et al., 2018).

### 1.6.3 Hydrochlorofluorocarbons

Hydrochlorofluorocarbons (HCFCs) are compounds consisting of hydrogen, chlorine, fluorine and carbon. HCFCs are similar to CFCs but because they contain hydrogen, HCFCs are readily broken down by hydroxyl radicals (OH) in the troposphere. This breakdown means only a small portion of HCFC molecules reach the stratosphere where they are destroyed by photolysis and they therefore contribute less to ozone depletion. Also, this means they have shorter atmospheric lifetimes than CFCs, of the order of years to decades. HCFCs are also greenhouse gases but due to tropospheric destruction, HCFCs contribute less to global warming than CFCs.

HCFCs were developed as short-term replacement compounds for the applications of stronger ozone-depleting substances as they were phased out during the first stage of the Montreal Protocol. HCFCs were mainly used to replace CFCs and therefore were used in similar applications such as refrigerants, solvents and foam-blowing agents. Since HCFCs still have some contribution to ozone depletion, they are only considered interim replacements for CFCs and are currently being phased out under the Montreal Protocol. They will be phased out by 2030 in Non-Article 5 countries and 2040 in Article 5 countries (Figure 1.3).

HCFCs were first developed in the 1980s and their mixing ratios have been increasing since then. HCFCs are now beginning to be phased out under the Montreal Protocol and the growth rates of the major HCFCs (HCFC-22, HCFC-141b and HCFC-142b) are slowing down (Engel and Rigby et al., 2018). By far the most abundant HCFC is HCFC-22, followed by HCFC-141b and HCFC-142b. Other minor HCFCs include HCFC-124, HCFC-123, HCFC-133a, HCFC-31 and HCFC-225ca.

#### **1.6.4 Hydrofluorocarbons**

Hydrofluorocarbons (HFCs) are compounds consisting of hydrogen, fluorine and carbon. They are not considered to be ozone-depleting as they do not contain chlorine or bromine. Despite this, some HFCs were added to the list of controlled substances under the Montreal Protocol by the Kigali Amendment in 2016. This is because HFCs were often used as second-generation replacement compounds after the phase out of CFCs and HCFCs and they are strong greenhouse gases so contribute to climate change. Their production and consumption will be phased down by 80-85 % between 2019 and 2047 (Figure 1.3).

HFC-134a is the most abundant HFC and is commonly used for mobile air conditioning in vehicles (Montzka and Velders et al., 2018). The second most abundant HFC is HFC-23, which is mainly produced as a by-product during production of HCFC-22 (Montzka and Velders et al., 2018). Other minor HFCs are used in a similar variety of applications to CFCs and HCFCs, such as refrigerants, foam-blowing agents, aerosol propellants, fire extinguishers and dry etching agents (Montzka and Velders et al., 2018). HFCs have variable atmospheric lifetimes of less than a year to hundreds of years (WMO, 2018). Mixing ratios of HFCs first began increasing in the 1990s and they continue to increase in the atmosphere (Montzka and Velders et al., 2018). The compounds that will replace HFCs after they are phased out are still being researched and developed but some possibilities include carbon dioxide, ammonia, hydrocarbons, unsaturated HFCs, also known as hydrofluoroolefins (HFOs) and hydrochlorofluoroolefins (HCFOs) (Montzka and Velders et al., 2018).

HFCs are also included in the Kyoto Protocol, established in 1997, within the United Nations Framework Convention on Climate Change (UNFCCC). The Kyoto Protocol committed developed countries to reducing their greenhouse gas emissions between 2008 and 2012. The focus was on the sum of emissions from all controlled greenhouse gases ( $\text{CO}_2$ ,  $\text{CH}_4$ ,  $\text{N}_2\text{O}$ , HFCs, PFCs,  $\text{SF}_6$  and  $\text{NF}_3$ ) and did not specifically limit HFCs or other compound groups. The Paris Agreement, established in 2015, is another international agreement to reduce greenhouse gas emissions, which follows on from the Kyoto Protocol but contains no binding commitments.

#### **1.6.5 Perfluorocarbons and other perfluorinated compounds**

Perfluorocarbons (PFCs) are compounds consisting of only fluorine and carbon. Perfluorinated compounds are other compounds that contain fluorine such as sulfur hexafluoride ( $\text{SF}_6$ ) and trifluoromethyl sulfur pentafluoride ( $\text{SF}_5\text{CF}_3$ ). These compounds do not deplete ozone as they do not contain chlorine or bromine, and are therefore not controlled by the Montreal Protocol. They have very long atmospheric lifetimes of the order of thousands of years (WMO, 2018). They are strong greenhouse gases, thousands of times stronger than  $\text{CO}_2$ , and are therefore included in the Kyoto Protocol and the Paris Agreement. Perfluorocarbons (PFCs) are used in a variety of applications such as

the electronics industry, semiconductor manufacturing, aluminium production and heat transfer fluids. The mixing ratios of PFCs are slowly increasing in the atmosphere (Engel and Rigby et al., 2018). Examples of PFCs are  $\text{CF}_4$ ,  $\text{C}_2\text{F}_6$ ,  $\text{C}_3\text{F}_8$ , *c*- $\text{C}_4\text{F}_8$ , *n*- $\text{C}_4\text{F}_{10}$ , *n*- $\text{C}_5\text{F}_{12}$ , *n*- $\text{C}_6\text{F}_{14}$  and *n*- $\text{C}_7\text{F}_{16}$ .  $\text{SF}_5\text{CF}_3$  was used in production of fluorosurfactants but its use has largely ceased and mixing ratios of  $\text{SF}_3\text{CF}_3$  have stabilised in the atmosphere (Sturges et al., 2012).  $\text{SF}_6$  is used primarily for electrical insulation (e.g. Ko et al., 1993) and its mixing ratios are still increasing in the atmosphere (Engel and Rigby et al., 2018).

### 1.6.6 Carbon tetrachloride

Carbon tetrachloride ( $\text{CCl}_4$ ) is an ozone-depleting substance and a greenhouse gas. It has an atmospheric lifetime of about 32 years and its atmospheric mixing ratios in 2016 were  $\sim 80$  ppt (Engel and Rigby et al., 2018). Its primary uses were as a feedstock for CFC production and as a solvent (Liang et al., 2016). It was phased out during the first stage of the Montreal Protocol with its production and consumption phased out by 1996 in developed countries and by 2010 in developing countries (Figure 1.3). For this reason,  $\text{CCl}_4$  mixing ratios are decreasing in the atmosphere, however, they are not decreasing as quickly as expected. This is mostly due to previously unrecognised large ongoing emissions of  $\text{CCl}_4$ , not controlled by the Montreal Protocol, from inadvertent by-product emissions of  $\text{CCl}_4$  from chloromethanes and perchloroethylene plants and fugitive emissions from the chlor-alkali process (Liang et al., 2016).

### 1.6.7 Methyl chloroform

Methyl chloroform ( $\text{CCl}_3\text{CH}_3$ ) is susceptible to hydroxyl radical attack due to its carbon-hydrogen bonds and so is mostly destroyed in the troposphere. Although, some methyl chloroform does reach the stratosphere and is photolysed so it is an ozone-depleting substance. Methyl chloroform is also a greenhouse gas. It was mainly used as a solvent for metal and electronic part cleaning. Methyl chloroform production and consumption was phased out under the Montreal Protocol by 1996 in developed countries and by 2015 in developing countries (Figure 1.3). Due to its relatively short lifetime ( $\sim 5$  years), the effects of the phase out were quickly seen in the atmosphere. The global abundance of methyl chloroform rapidly declined from its peak of 133 ppt in 1992 to 3 ppt in 2016 (Engel and Rigby et al., 2018).

### 1.6.8 Methyl halides

There are three methyl halide species – methyl chloride ( $\text{CH}_3\text{Cl}$ ), methyl bromide ( $\text{CH}_3\text{Br}$ ) and methyl iodide ( $\text{CH}_3\text{I}$ ), all of which are ozone-depleting substances, greenhouse gases and have relatively short atmospheric lifetimes. Methyl halides are mostly broken down in the troposphere, primarily through oxidation by hydroxyl radicals and so have only a small effect on stratospheric ozone.

The total global lifetime of CH<sub>3</sub>Cl is estimated to be about 0.9 years (Engel and Rigby et al., 2018). Sources of CH<sub>3</sub>Cl include biomass burning, the oceans, tropical and subtropical plants, mangroves, fungus, salt marshes, wetlands, rice paddies, shrublands and coal combustion (Engel and Rigby et al., 2018). Most emissions of CH<sub>3</sub>Cl come from natural sources and so CH<sub>3</sub>Cl is not controlled by the Montreal Protocol. CH<sub>3</sub>Cl mixing ratios have been mostly stable and were about 556 ppt in 2016 (Engel and Rigby et al., 2018).

The global total lifetime of CH<sub>3</sub>Br is estimated to be about 0.8 years (Engel and Rigby et al., 2018). CH<sub>3</sub>Br shares many of the same natural sources as CH<sub>3</sub>Cl but has additional anthropogenic sources and so is controlled under the Montreal Protocol. The anthropogenic source of CH<sub>3</sub>Br was primarily from its use as an agricultural fumigant. This application was phased out under the Montreal Protocol by 2005 in developed countries and by 2015 in developing countries with some essential use exemptions (Figure 1.3). Quarantine and pre-shipment (QPS) uses of CH<sub>3</sub>Br, mainly for pest control for the transport of agricultural products, are also exempt from the phase out. CH<sub>3</sub>Br mixing ratios have been mostly decreasing since the late-1990s and were about 6.8 ppt in 2016 (Engel and Rigby et al., 2018).

Methyl iodide has a short-atmospheric lifetime (~7 days) and is therefore a very short-lived ozone-depleting substance (see below). CH<sub>3</sub>I mostly comes from natural sources. As such, its impact on stratospheric ozone and climate change are thought to be small and CH<sub>3</sub>I is not regulated.

### **1.6.9 Very short-lived ozone-depleting substances**

Very short-lived ozone-depleting substances (VSLs) are compounds that contain chlorine and/or bromine and have atmospheric lifetimes of less than 6 months. VSLs are not regulated by the Montreal Protocol because they are mostly broken down before they reach the stratosphere, by hydroxyl radical oxidation in the troposphere.

The most abundant chlorinated VSL in the atmosphere is dichloromethane (CH<sub>2</sub>Cl<sub>2</sub>) with mixing ratios of 33-39 ppt in 2016 (Engel and Rigby et al., 2018). Other chlorinated VSLs include chloroform (CHCl<sub>3</sub>), perchloroethylene (PCE, CCl<sub>2</sub>CCl<sub>2</sub>), trichloroethene (C<sub>2</sub>HCl<sub>3</sub>) and 1,2-dichloroethane (CH<sub>2</sub>ClCH<sub>2</sub>Cl).

The most abundant brominated VSL in the atmosphere is bromoform (CHBr<sub>3</sub>) with mixing ratios of 0.4-4.0 ppt in the marine boundary layer (Engel and Rigby et al., 2018). Other brominated VSLs include dibromomethane (CH<sub>2</sub>Br<sub>2</sub>), bromochloromethane (CH<sub>2</sub>BrCl), dibromochloromethane (CHBr<sub>2</sub>Cl), and bromodichloromethane (CHBrCl<sub>2</sub>).

Brominated VSLs are predominantly of natural marine origin, while for chlorinated VSLs industrial emissions dominate over natural sources. Overall levels of chlorinated

VSLs have been increasing in the atmosphere whereas there is no clear evidence of a trend in brominated VSLs.

## 1.7 Aims and rationale

Due to the success of the Montreal Protocol, excellent progress has been made in reducing mixing ratios of ozone-depleting substances and protecting the ozone layer. Mixing ratios of most of the major ozone-depleting substances are decreasing in the atmosphere and the ozone layer is starting to show signs of recovery (WMO, 2018). In order to maintain the success of the Montreal Protocol and ozone layer recovery, continued monitoring is needed to verify ongoing compliance with the Protocol and identify and investigate future threats to the ozone layer.

There are a number of areas of interest that may influence stratospheric ozone in the future:

- Tropospheric chlorine decreased more slowly between 2012 and 2016 than between 2008 and 2012. During the period 2008-2012, the overall decrease in tropospheric chlorine was  $11.8 \pm 6.9$  ppt Cl yr<sup>-1</sup>, while the rate of decline during the period 2012-2016 was  $4.4 \pm 4.1$  ppt Cl yr<sup>-1</sup> (Engel and Rigby et al., 2018). This was mostly due to an increase in methyl chloride and VSLs, predominately dichloromethane, which are substances not controlled by the Montreal Protocol. As the mixing ratios of substances controlled by the Montreal Protocol decrease, the relative contribution of ozone-depleting substances not controlled by the Montreal Protocol is increasing. Chlorinated VSLs in and above the Asian summer monsoon are investigated in Chapter 3.
- Persistent emissions of low abundance (< 20 ppt) CFCs (CFC-13, CFC-113a, CFC-114, CFC-114a & CFC-115) (Laube et al., 2014; Vollmer et al., 2018). Mixing ratios and emissions of CFC-113a are investigated in Chapter 4.
- A recent study found a slowdown in the rate of decrease of CFC-11 mixing ratios in the atmosphere caused by an increase in global CFC-11 emissions (Montzka et al., 2018). This increase in emissions is counter to the intentions of the Montreal Protocol and may indicate illegal production of CFC-11. If emissions of CFC-11 continue in the future this could delay the recovery of the ozone layer (Carpenter and Daniel et al., 2018; Dameris et al., 2019; Dhomse et al., 2019; Keeble et al., 2020). CFC-11 in East Asia is investigated in Chapter 5.

Other areas that are not studied in this thesis but are also of interest include:

- Emissions of some ozone-depleting substances continue from exempt-use items and banks.
- Ozone-depleting substances are still used in some applications for which there is limited availability of non-ozone-depleting alternatives.
- The phase out schedule for HCFCs is taking place between 2019 and 2040.

- Carbon tetrachloride mixing ratios are decreasing more slowly than projected due to previously unaccounted for ongoing substantial emissions (Section 1.6.6; Liang et al., 2016).
- An increase in emissions of ozone-depleting substances from natural sources such as methyl chloride and methyl bromide due to the effects of climate change (Fang et al., 2019).
- Uncertainties in future levels of greenhouse gases (CO<sub>2</sub>, CH<sub>4</sub> & N<sub>2</sub>O) and climate change will have a large impact on future ozone recovery due to cooling of the stratosphere and changes in atmospheric circulation (Carpenter and Daniel et al., 2018).
- Most of the actions that can significantly hasten ozone layer recovery have already been taken, which means future options are more limited.

This study focuses on new threats to the ozone layer with a focus on East Asia. East Asia is a region that plays a key role in the global production and transport of ozone-depleting substances. The region has recently undergone rapid development and industrialisation. Consequently, there are increasing emissions of many halocarbons and halogenated species from East Asia. In addition to this East Asia is a region that has the potential for very rapid transport of emissions into the tropical tropopause layer and the lower stratosphere.

Chapter 3 discusses aircraft-based observations of ozone-depleting substances in the upper troposphere and lower stratosphere in and above the Asian summer monsoon. The Asian summer monsoon anticyclone provides an effective pathway to rapidly uplift air masses from the boundary layer into the upper troposphere and lower stratosphere on the time scale of a few days to a few weeks. Therefore, very short-lived substances could reach the stratosphere before they are removed to insignificant levels and they can therefore contribute to ozone depletion. The measurements in this study are used to estimate the equivalent effective stratospheric chlorine transported into the lower stratosphere and the relative importance of mixing ratios of very short-lived ozone-depleting substances under these conditions.

Chapter 4 investigates the ozone-depleting substance CFC-113a (CCl<sub>3</sub>CF<sub>3</sub>). Mixing ratios of this compound are increasing in the atmosphere (Laube et al., 2014) despite almost all production of CFCs being globally banned by the Montreal Protocol. Measurements of air samples collected at multiple sites worldwide, with a focus on samples collected in Taiwan, were used to investigate CFC-113a mixing ratios, emissions and potential source regions to better understand what may be responsible for the increasing mixing ratios of CFC-113a.

Chapter 5 investigates CFC-11 (CCl<sub>3</sub>F) using atmospheric observations in Taiwan. Global CFC-11 emissions were recently found to have increased in the atmosphere (Montzka et al., 2018). This increase in emissions has been attributed in part to eastern

China (Rigby et al., 2019). The aims of this study were to estimate CFC-11 emissions in East Asia and their contribution to global emissions; and investigate the potential source regions and emission sectors that could have CFC-11 emissions.

Chapter 2 describes the analytical techniques that were used to conduct this study. Chapter 6 summaries the key conclusions and suggests directions for further research. It is hoped that the findings of this thesis will ultimately provide some guidance for policymakers when determining the best approach to ensure stratospheric ozone recovery.

## References

- Andrady, A. L., Hamid, H. and Torikai, A.: Effects of solar UV and climate change on materials, *Photochem. Photobiol. Sci.*, 10(2), 292, doi:10.1039/c0pp90038a, 2011.
- Braesicke, P., Neu, J., (Lead Authors), Fioletov, V., Godin-Beekmann, S., Hubert, D., Petropavlovskikh, I., Shiotani, M. and Sinnhuber, B.-M.: Chapter 3 Update on Global Ozone: Past, Present, and Future, in *Scientific Assessment of Ozone Depletion: 2018, Global Ozone Research and Monitoring Project–Report No. 58*, World Meteorological Organization, Geneva, Switzerland., 2018.
- Carpenter, L. J., Daniel, J. S., (Lead Authors), Fleming, E. L., Hanaoka, T., Hu, J., Ravishankara, A. R., Ross, M. N., Tilmes, S., Wallington, T. J. and Wuebbles, D. J.: Chapter 6 Scenarios and Information for Policymakers, in *Scientific Assessment of Ozone Depletion: 2018, Global Ozone Research and Monitoring Project–Report No. 58*, World Meteorological Organization, Geneva, Switzerland., 2018.
- Chapman, S.: A theory of upper-atmospheric ozone, *Memoirs of the Royal Meteorological Society*, 3, 26, 103–125, 1930.
- Chubachi, S.: Preliminary result of ozone observations at Syowa Station from February, 1982 to January, 1983, *Mem. Natl. Inst. Polar Res. Jpn. Spec. Issue*, 34, 13-20, 1984.
- Dameris, M., Jöckel, P. and Nützel, M.: Possible implications of enhanced chlorofluorocarbon-11 concentrations on ozone, *Atmos. Chem. Phys.*, 19(22), 13759–13771, doi:10.5194/acp-19-13759-2019, 2019.
- Daniel, J. S., Velders, G. J. M., (Lead Authors), Douglass, A. R., Forster, P. M. D., Hauglustaine, D. A., Isaksen, I. S. A., Kuijpers, L. J. M., McCulloch, A. and Wallington, T. J.: Chapter 8 Halocarbon Scenarios, Ozone Depletion Potentials, and Global Warming Potentials, in *Scientific Assessment of Ozone Depletion: 2006, Global Ozone Research and Monitoring Project-Report No. 50*, World Meteorological Organization, Geneva, Switzerland., 2007.
- Daniel, J.S., and G.J.M. Velders (Lead Authors), H. Akiyoshi, A.F. Bais, E.L. Fleming, C.H. Jackman, L.J.M. Kuijpers, M. McFarland, S.A. Montzka, O. Morgenstern, M.N. Ross, S. Tilmes, D.W. Toohey, M.B. Tully, T.J. Wallington, and D.J. Wuebbles, A Focus on Information and Options for Policymakers, Chapter 5 in *Scientific Assessment of Ozone Depletion: 2010, Global Ozone Research and Monitoring Project–Report No. 52*, World Meteorological Organization, Geneva, Switzerland, 2011.
- Daniel, J.S., S. Solomon, and D.L. Albritton, On the evaluation of halocarbon radiative forcing and global warming potentials, *J. Geophys. Res. Atmos.*, 100(D1), 1271–1285, doi:10.1029/94JD02516, 1995.

- Daniel, J. S., Solomon, S., Portmann, R. W. and Garcia, R. R.: Stratospheric ozone destruction: The importance of bromine relative to chlorine, *J. Geophys. Res. Atmos.*, 104(D19), 23871–23880, doi:10.1029/1999JD900381, 1999.
- Dhomse, S. S., Feng, W., Montzka, S. A., Hossaini, R., Keeble, J., Pyle, J. A., Daniel, J. S. and Chipperfield, M. P.: Delay in recovery of the Antarctic ozone hole from unexpected CFC-11 emissions, *Nat. Commun.*, 10(1), 1–12, doi:10.1038/s41467-019-13717-x, 2019.
- Engel, A., Rigby, M., (Lead Authors), Burkholder, J. B., Fernandez, R. P., Froidevaux, L., Hall, B. D., Hossaini, R., Saito, T., Vollmer, M. K. and Yao, B.: Chapter 1 Update on Ozone-Depleting Substances (ODSs) and Other Gases of Interest to the Montreal Protocol, in *Scientific Assessment of Ozone Depletion: 2018, Global Ozone Research and Monitoring Project–Report No. 58*, World Meteorological Organization, Geneva, Switzerland., 2018.
- Fang, X., Pyle, J. A., Chipperfield, M. P., Daniel, J. S., Park, S. and Prinn, R. G.: Challenges for the recovery of the ozone layer, *Nat. Geosci.*, 12(8), 592–596, doi:10.1038/s41561-019-0422-7, 2019.
- Farman, J. C., Gardiner, B. G. and Shanklin, J. D.: Large losses of total ozone in Antarctica reveal seasonal ClO<sub>x</sub>/NO<sub>x</sub> interaction, *Nature*, 315, 207–210, doi:10.1038/315207a0, 1985.
- Halons Technical Options Committee (HTOC): United Nations Environment Programme (UNEP), Assessment Report 2018. [online] Available from: [https://ozone.unep.org/sites/default/files/2019-04/HTOC\\_assessment\\_2018.pdf](https://ozone.unep.org/sites/default/files/2019-04/HTOC_assessment_2018.pdf) (Accessed 10 February 2020), 2018.
- Holloway, A. M. and Wayne, R. P.: *Atmospheric Chemistry*, 1st ed., Royal Society of Chemistry, Cambridge, UK., ISBN 9781847558077, 2010.
- Keeble, J., Abraham, N. L., Archibald, A. T., Chipperfield, M. P., Dhomse, S., Griffiths, P. T. and Pyle, J. A.: Modelling the potential impacts of the recent, unexpected increase in CFC-11 emissions on total column ozone recovery, *Atmos. Chem. Phys.*, 20(12), 7153–7166, doi:10.5194/acp-20-7153-2020, 2020.
- Kim, K. H., Shon, Z. H., Nguyen, H. T. and Jeon, E. C.: A review of major chlorofluorocarbons and their halocarbon alternatives in the air, *Atmos. Environ.*, 45(7), 1369–1382, doi:10.1016/j.atmosenv.2010.12.029, 2011.
- Ko, M. K. W., Newman, P. A., Reimann, S., and Strahan, S. E. (Eds.): *SPARC Report on Lifetimes of Stratospheric Ozone-Depleting Substances, Their Replacements, and Related Species*, SPARC Report No. 6, WCRP-15/2013, SPARC Office. [online] Available from: <http://www.sparc-climate.org/publications/sparc-reports/sparc-report-no-6/> (Accessed 28 March 2018), 2013.

Ko, M.K.W., N.D. Sze, W.C. Wang, G. Shia, A. Goldman, F.J. Murcray, D.G. Murcray, and C.P. Rinsland, Atmospheric sulfur hexafluoride: Sources, sinks and greenhouse warming, *J. Geophys. Res. Atmos.*, 98(D6), 10499–10507, doi:10.1029/93JD00228, 1993.

Laube, J. C., Newland, M. J., Hogan, C., Brenninkmeijer, C. A. M., Fraser, P. J., Martinerie, P., Oram, D. E., Reeves, C. E., Röckmann, T., Schwander, J., Witrant, E. and Sturges, W. T.: Newly detected ozone-depleting substances in the atmosphere, *Nat. Geosci.*, 7(March), 10–13, doi:10.1038/NCEO2109, 2014.

Liang, Q., S. Reimann, and P.A. Newman, SPARC Report on the Mystery of Carbon Tetrachloride, SPARC, Volume 7, doi:10.3929/ethz-a-01069-0647, 2016.

Mackenzie, R.: Chapter 8. Stratospheric chemistry and ozone depletion, in: Hewitt, C.N. and Jackson, A.V., *Atmospheric Science for Environmental Scientists*, John Wiley & Sons, West Sussex, UK., 2009.

Molina, M. J. and Rowland, F. S.: Stratospheric sink for chlorofluoromethanes: chlorine atom-catalysed destruction of ozone, *Nature*, 249, 810–812, doi:10.1038/249810a0, 1974.

Montzka, S. A., Velders, G. J. M., (Lead Authors), Krummel, P. B., Mühle, J., Orkin, V. L., Park, S., Shah, N. and Walter-Terrinoni, H.: Chapter 2 Hydrofluorocarbons (HFCs), in *Scientific Assessment of Ozone Depletion: 2018, Global Ozone Research and Monitoring Project–Report No. 58*, World Meteorological Organization, Geneva, Switzerland., 2018.

Montzka, S. A., Dutton, G. S., Yu, P., Ray, E., Portmann, R. W., Daniel, J. S., Kuijpers, L., Hall, B. D., Mondeel, D., Siso, C., Nance, J. D., Rigby, M., Manning, A. J., Hu, L., Moore, F., Miller, B. R. and Elkins, J. W.: An unexpected and persistent increase in global emissions of ozone-depleting CFC-11, *Nature*, 557, 413–417, doi:10.1038/s41586-018-0106-2, 2018.

Multilateral Fund (MLF) for the Implementation of the Montreal Protocol: Welcome to the Multilateral Fund for the Implementation of the Montreal Protocol, [online] Available from: <http://www.multilateralfund.org/default.aspx> (Accessed 10 February 2020), 2020.

Ravishankara, A. R., Turnipseed, A. A., Jensen, N. R., Barone, S., Mills, M., Howard, C. J. and Solomon, S.: Do hydrofluorocarbons destroy stratospheric ozone?, *Science.*, 263(5143), 71–75, doi:10.1126/science.263.5143.71, 1994.

Rigby, M., Park, S., Saito, T., Western, L. M., Redington, A. L., Fang, X., Henne, S., Manning, A. J., Prinn, R. G., Dutton, G. S., Fraser, P. J., Ganesan, A. L., Hall, B. D., Harth, C. M., Kim, J., Kim, K.-R., Krummel, P. B., Lee, T., Li, S., Liang, Q., Lunt, M. F., Montzka, S. A., Mühle, J., O'Doherty, S., Park, M.-K., Reimann, S., Salameh, P. K., Simmonds, P., Tunnicliffe, R. L., Weiss, R. F., Yokouchi, Y. and Young, D.: Increase

in CFC-11 emissions from eastern China based on atmospheric observations, *Nature*, 569(7757), 546–550, doi:10.1038/s41586-019-1193-4, 2019.

Salawitch, R. J., (Lead Author), Fahey, D. W., Hegglin, M. I., McBride, L. A., Tribett, W. R. and Doherty, S. J.: *Twenty Questions and Answers About the Ozone Layer: 2018*, 84 pp., Update, *Scientific Assessment of Ozone Depletion: 2018*, Geneva, Switzerland., 2019.

Solomon, S., Ivy, D. J., Kinnson, D., Mills, M. J., Neely III, R. R. and Schmidt, A.: Emergence of healing in the Antarctic ozone layer, *Science.*, 353(6296), 269–274, doi:10.1126/science.aae0061, 2016.

Sturges, W. T., Oram, D. E., Laube, J. C., Reeves, C. E., Newland, M. J., Hogan, C., Martinerie, P., Witrant, E., Brenninkmeijer, C. A. M., Schuck, T. J. and Fraser, P. J.: Emissions halted of the potent greenhouse gas SF<sub>5</sub>CF<sub>3</sub>, *Atmos. Chem. Phys.*, 12(8), 3653–3658, doi:10.5194/acp-12-3653-2012, 2012.

United Nations Environment Programme (UNEP): *Handbook for the Montreal Protocol on Substances that Deplete the Ozone Layer Thirteenth edition (2019)*, ISBN: 978-9966-076-59-5, 2019.

Velders, G.J.M., S.O. Andersen, J.S. Daniel, D.W. Fahey, and M. McFarland, The Importance of the Montreal Protocol in protecting climate, *Proc. Natl. Acad. Sci.*, 104 (12), 4814–4819, doi:10.1073/pnas.0610328104, 2007.

Vollmer, M. K., Young, D., Trudinger, C. M., Mühle, J., Henne, S., Rigby, M., Park, S., Li, S., Guillevic, M., Mitrevski, B., Harth, C. M., Miller, B. R., Reimann, S., Yao, B., Steele, L. P., Wyss, S. A., Lunder, C. R., Arduini, J., Mcculloch, A., Wu, S., Rhee, T. S., Wang, R. H. J., Salameh, P. K., Hermansen, O., Hill, M., Langenfelds, R. L., Ivy, D., O'Doherty, S., Krummel, P. B., Maione, M., Etheridge, D. M., Zhou, L., Fraser, P. J., Prinn, R. G., Weiss, R. F. and Simmonds, P. G.: Atmospheric histories and emissions of chlorofluorocarbons CFC-13 (CClF<sub>3</sub>), ΣCFC-114 (C<sub>2</sub>Cl<sub>2</sub>F<sub>4</sub>), and CFC-115 (C<sub>2</sub>ClF<sub>5</sub>), *Atmos. Chem. Phys.*, 18, 979–1002, doi:10.5194/acp-18-979-2018, 2018.

Wallington, T. J., Schneider, W. F., Sehested, J. and Nielsen, O. J.: Hydrofluorocarbons and stratospheric ozone, *Faraday Discuss.*, 100, 55–64, doi:10.1039/FD9950000055, 1995.

WMO (World Meteorological Organization): *Scientific Assessment of Ozone Depletion: 2018 World Meteorological Organization Global Ozone Research and Monitoring Project—Report No. 58.*, ISBN: 978-1-7329317-1-8, 2018.

## Chapter 2: Methods

---

The data from this study come from measurements of air samples made using a gas chromatograph - mass spectrometer (GC-MS) (Section 2.1). Air samples were collected at locations of interest by pumping air into gas canisters (Section 2.2). The gas canisters were then transported to the UEA for analysis on an AutoSpec GC-MS where they were typically measured for 30-50 trace gases such as CFCs, HCFCs, HFCs, SF<sub>6</sub>, CCl<sub>4</sub>, CH<sub>3</sub>Cl, CH<sub>2</sub>Cl<sub>2</sub>, etc. The canisters were connected to an inlet system that prepares the samples for analysis (Section 2.3). The separation of compounds then takes place in the gas chromatograph column and the ionisation, deflection and detection of the compounds takes place in the mass spectrometer (Sections 2.4–2.5). These raw data are then processed and compared to the compound's mixing ratios in the standard to calculate the mixing ratios of the compounds in the samples (Section 2.6). The compound's mixing ratios in the standards are repeatedly compared to mixing ratios in other standards to ensure their accuracy (Section 2.8). Some of the data in this study come from measurements made using another GC-MS called the Entech instrument (Section 2.7).

The methodology for the analysis of halogenated trace gases in air samples is well established at UEA (e.g. Lee et al., 1995; Oram et al., 1996; Sturges et al., 2000; Laube et al., 2010a; 2016). I measured air samples collected in Taiwan, 31 samples in 2017 and 28 samples in 2018. These samples were measured twice, using two different gas chromatograph columns and the measurements were used in Chapter 5. I also measured 103 air samples collected on-board the Geophysica aircraft during the StratoClim campaign in 2017. 30 of these samples were measured again using a second gas chromatograph column. These measurements were used in Chapter 3. In addition, I did more measurements to continue the internal standard intercomparisons and did integrations and data processing for some of the measurements made by others. These measurements are discussed later in this chapter. The measurements of the other datasets discussed in this thesis were made by others using the same or similar methods.

### 2.1 Gas chromatography - mass spectrometry (GC-MS)

The basic principle of gas chromatography - mass spectrometry (GC-MS) involves the coupling of a gas chromatograph to a mass spectrometer (Figure 2.1). Gas chromatography involves the separation of compounds in an air sample by passing the sample through a gas chromatograph column, which is a long thin coiled tube. The column or column packing contains a stationary phase. The sample is transported through the GC column by a carrier gas, here helium, which is termed the mobile phase.

Different compounds interact differently with the stationary and mobile phases. The strength with which they bind determines the time they take to travel through the GC column therefore separating out different compounds. The time when the compound

elutes at the other end of the GC column is used to identify the compound. However, on its own a gas chromatograph cannot always confidently determine the presence of a compound because the time a compound takes to travel through the column may vary under different conditions and multiple compounds can elute out of the end of the column at the same time. Therefore, a GC system is often combined with a mass spectrometry system.

After the samples have been separated by the GC column, they are transported into the ionisation source of the mass spectrometer where they are bombarded with electrons. The molecule gains a high energy electron and produces the molecular ion. If there is sufficient excess energy the charged molecular ions may undergo further fragmentation into a wide range of ion fragments. These ions are then accelerated and subjected to an electric and/or magnetic field in order to deflect them, i.e. change the direction the ions are travelling. The amount of deflection depends on the ion's mass to charge ratio ( $m/z$ ) so assuming all the ions have the same charge, heavier ions will deflect less. The electric/magnetic field is manipulated to let certain ions pass through and this separates out the ions.

These ions will then strike the detector at the other end of the instrument and the current induced is recorded, showing relative abundance against  $m/z$  ratio. The detector will usually amplify the signal to make it easier to identify. The spectra is used to identify the compound and the relative abundance indicates how much of the compound is present in the sample.

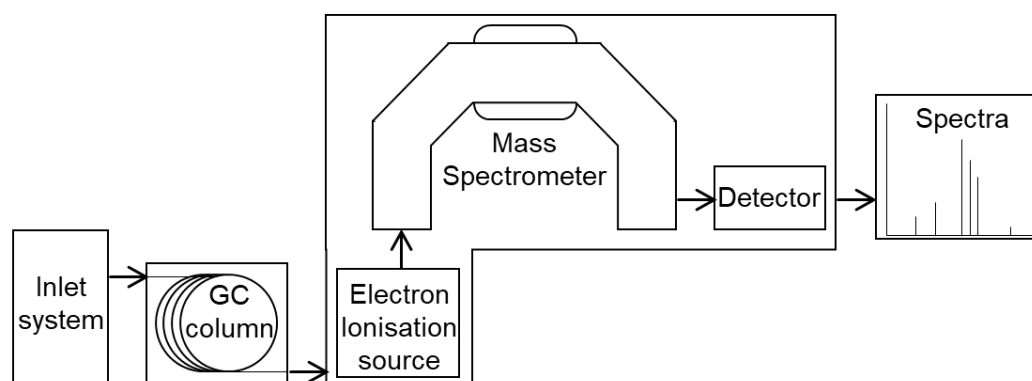


Figure 2.1: Components of the AutoSpec GC-MS system

## 2.2 Sample collection

Air samples from Taiwan were collected in 3-litre Silco-treated stainless-steel canisters (Restek) using a small 12 VDC diaphragm pump (Air Dimensions, model B161). Prior to sampling the canisters were evacuated six times to  $< 0.01$  mbar and pressurized, to 3.5–4.0 bar, with ultra-pure nitrogen (BOC research grade) whilst being heated to  $130$  °C, then they were evacuated one final time. During sampling they were filled and vented at least 3 times before being filled to a final pressure of  $\sim 2$  bar which takes a few minutes.

Air samples from the StratoClim campaign were collected with the whole air sampler (WAS) of Utrecht University operated on board the Geophysica research aircraft (Kaiser et al., 2006; Cairo et al., 2010; Laube et al., 2010b). Ambient air was compressed into evacuated stainless-steel canisters (2 litre) using a metal bellows pump that has been previously shown to not impact trace gas mixing ratios (Laube et al., 2010b). The internal surfaces of some of the canisters were passivated using a common passivation technique ('Silco<sup>TM</sup>-treatment') to minimise the breakdown of more reactive gases in the canisters between collection and analysis.

A number of studies have shown that long-lived and short-lived halocarbons can be stored in stainless-steel canisters for extended periods without significant changes in their mixing ratios (Fraser et al., 1999; Muhle et al., 2010; Oram et al., 2012; Sturges et al., 2012; Laube et al., 2012; Newland et al., 2013; Laube et al., 2014; Leedham Elvidge et al., 2015) (Section 2.8).

### **2.3 Sample preparation – the inlet system**

Before air samples were injected onto the GC column of the AutoSpec GC-MS instrument the trace gases were cryogenically extracted and pre-concentrated. A schematic of the manual inlet system is shown in Figure 2.2. The components of the inlet system are connected with 1/16th" and 1/8th" stainless-steel tubing and individual sections of the system are isolated with stainless steel diaphragm valves with a polyimide seat, Swagelok part no. 6LVV-DPVS4, ⊗. The whole inlet system is evacuated down to a pressure of  $\sim 10^{-2}$  Torr with an XDS 10 scroll pump from Edwards Ltd.

Sample preparation occurs as follows. The gas canister containing the air sample is connected to the inlet system. The high pressure side of the inlet system is flushed and evacuated three times with the sample. The higher pressure in the sample canister forces the sample through the inlet system. Samples are passed through a glass tube containing hygroscopic magnesium perchlorate ( $\text{Mg}(\text{ClO}_4)_2$ ) to remove any water from the samples. Samples can also be passed through an optional Ascarite (NaOH-coated silica) filter if one wants to remove carbon dioxide.

Approximately 200-250 ml of the dried sample is passed through a sample loop filled with an adsorbent (Hayesep D, 80/100 mesh) and immersed in an ethanol and dry ice ( $-78$  °C) mixture to cryogenically trap and pre-concentrate the compounds of interest. The bulk of the air sample, primarily oxygen, nitrogen and the more volatile noble gases pass through the sample loop and into a 6 litre reference volume. This separation prevents a large injection of nitrogen and oxygen which can overload the GC column at low temperatures and can trip and/or damage the MS. It also increases the sensitivity of the analytical procedure as a larger amount of the trace gases are injected and measured at the same time. The 6 L reference volume serves not only to prevent back diffusion of

lab air into the system but also to accurately measure the volume of air trapped using a Baratron pressure sensor to record the pressure change. The flow rate of a sample through the pre-concentration trap is controlled by adjusting two needle valves. The rate of increasing pressure is monitored on the Baratron to maintain a constant flow into the reference volume and the sample loop.

Once the desired sample volume is collected the sample loop is isolated from the sample flow. Then the sample is injected onto the GC column using a six-port gas sampling valve (Valco). The valve has two positions, one to fill the sample loop and the other to inject the contents of the loop onto the column. When the valve is switched the carrier gas flow is diverted through the loop, thereby sweeping a known volume of sample rapidly onto the column. Immediately after the injection the dry ice and ethanol mixture is replaced with boiling water ( $\sim 100\text{ }^{\circ}\text{C}$ ) and the trapped gases are released. The boiling water is removed from the sample loop 15 minutes after the injection. After sample injection the whole of the inlet system including the reference volume is evacuated ready for the next sample, a second connection between the vacuum pump and the reference volume is used to facilitate this process. This sample preparation procedure gives highly reproducible final mixing ratios on the GC-MS. The reproducibility is different for different compounds. See Table 3.1 for an example of typical reproducibilities.

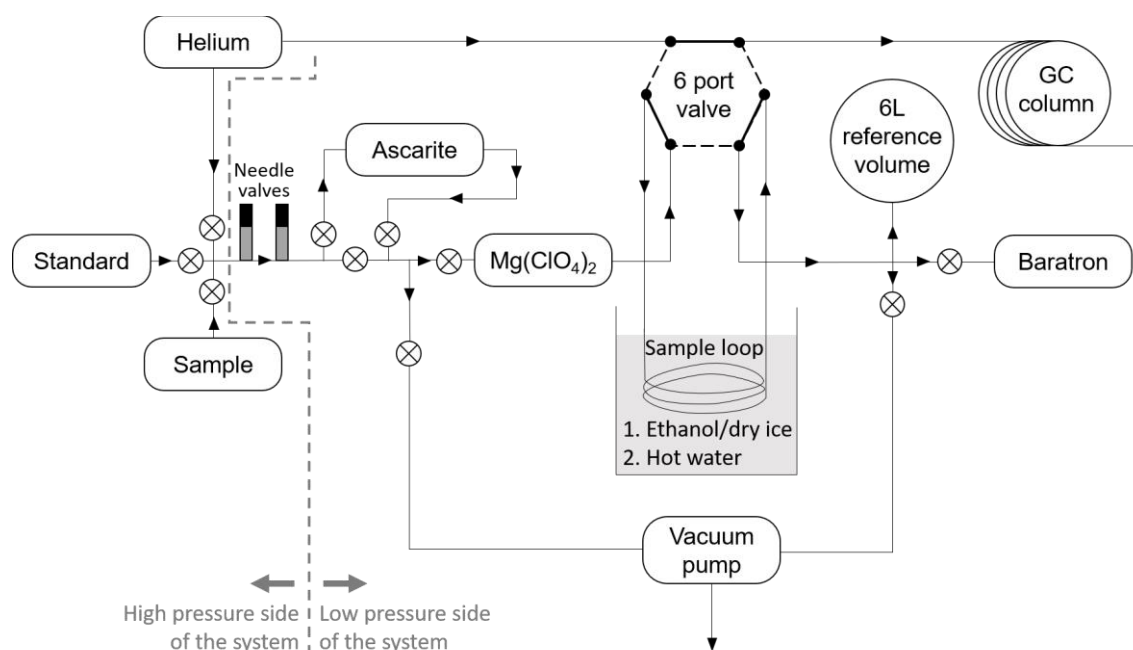


Figure 2.2: Schematic diagram of the manual inlet system for the AutoSpec GC-MS instrument.  $\otimes$  represents a valve.

## 2.4 The AutoSpec system

The majority of the measurements in this study were performed using an Agilent 6890 gas chromatograph coupled to a high-sensitivity Waters AutoSpec tri-sector mass spectrometer (GC-MS) (Figure 2.1).

Two gas chromatograph capillary PLOT (porous layer open tubular) columns were used during this analysis: an Agilent GS GasPro column (length ~50 m, ID 0.32 mm) and an Agilent KCl-passivated Al<sub>2</sub>O<sub>3</sub>-PLOT column (length: 50 m, ID 0.32 mm), (Laube et al., 2016). These two GC columns are used separately, depending on which compounds we want to measure in the samples. The GasPro column has silica i.e. silicon dioxide as the stationary phase. The AIPLOT column has aluminium oxide (Al<sub>2</sub>O<sub>3</sub>) deactivated by potassium chloride as the stationary phase. The AIPLOT column uses polarities and boiling points to separate compounds and therefore enables isomeric separation not possible with the GasPro column. During analysis on the AIPLOT column, an Ascarite (NaOH-coated silica) trap was used to remove carbon dioxide (Section 2.3), as the AIPLOT column produces carbon dioxide and has a stronger affinity for carbon dioxide than the GasPro column. Although, the ascarite trap can distort or reduce the signal of a number of compounds, in particular those that contain both a hydrogen and a chlorine atom as it can remove an HCl molecule from those.

During analysis the column was contained within a GC oven which was cooled to -10 °C using liquid CO<sub>2</sub> before injection. After 2 minutes, the temperature was ramped up. The temperature programme produced consistent retention times for the compounds of interest and enabled analysis of compounds with both low boiling points and high boiling points, for example, from C<sub>2</sub>F<sub>6</sub> (-78 °C) to CH<sub>2</sub>ClCH<sub>2</sub>Cl (83 °C).

The carrier gas, i.e. the mobile phase, used in this study was research grade helium, cleaned with an extra purifier cartridge. The optimal flow rate of the carrier gas is a balance between speed and separation efficiency. In this study the inlet pressure increases during the run to maintain a constant outlet flow rate of 2.0 ml min<sup>-1</sup> as the oven temperature increases.

After the sample passes through the GC column the compounds are ionised by electron ionisation. A heated metal filament (tungsten) thermoelectrically emits a beam of high-energy electrons. The electrons are accelerated by a potential difference of 70 electron volts (eV). These electrons enter the source through a slit and bombard molecules of the sample gas to form positively charged molecular ions and ion fragments. Uncharged fragments and negatively charged ions can also be formed but they cannot be detected. The fragmentation pattern of a compound should be similar between instruments providing the energy of the electrons is the same.

The AutoSpec instrument is an EBE tri-sector mass spectrometer, meaning ions pass through an electric sector, then a magnetic sector, then another electric sector. The

magnetic sector deflects ions based on their mass to charge ratio ( $m/z$ ) and the electric sectors reflect ions based on their kinetic energies. The idea behind combining magnetic sectors and electric sectors is that the dispersion that occurs in one sector is corrected for by the focusing in the next sector. The second electric sector also filters out metastable ions. This improves the sensitivity and resolution of the instrument. The magnitude and frequency of the electric fields are varied to selectively allow only ions with very specific  $m/z$  ratios to reach the detector while any other ions collide with the internal surfaces. Therefore, the AutoSpec can operate at a very high mass resolution or, if the mass resolution is reduced, while still being high, the AutoSpec can operate at a very high sensitivity. The source and the analyser are kept under vacuum using three diffusion pumps inside the AutoSpec, and using scroll pumps as forepumps, to prevent air molecules from reacting with or deflecting the sample ions.

The detector on the AutoSpec instrument is a dual conversion dynode configuration. It is an off-axis detector which reduces background noise by preventing neutral ions from striking the detector. A dynode is a metal surface that releases multiple electrons when it is struck by a fast moving ion. In the AutoSpec detector these electrons then collide with a phosphor screen which results in the emission of photons. The photons then enter a photomultiplier tube which amplifies the signal and results in a secondary emission of electrons through the photoelectric effect, where photons impacting a surface releases electrons. The induced current is then recorded by the computer as peaks in the detector signal (Figures 2.3 & 2.4). The AutoSpec instrument is used to make high precision measurements of trace gases in small air samples and typically has a detection limit of  $<0.1$  femtomole per mole of air ( $10^{-16}$ ).

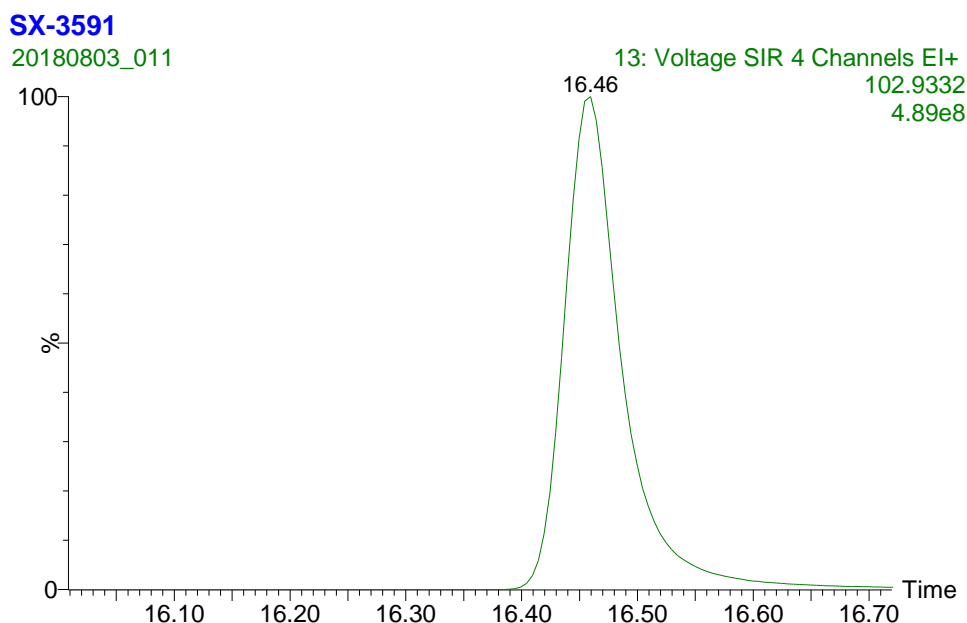


Figure 2.3: Example chromatogram of CFC-11, mass fragment  $\text{CF}^{35}\text{Cl}^{37}\text{Cl}^+$ ,  $m/z$  102.9332, in the SX-3591 working standard, on function 13 of the single ion monitoring method, measured in August 2018 on the GasPro column.

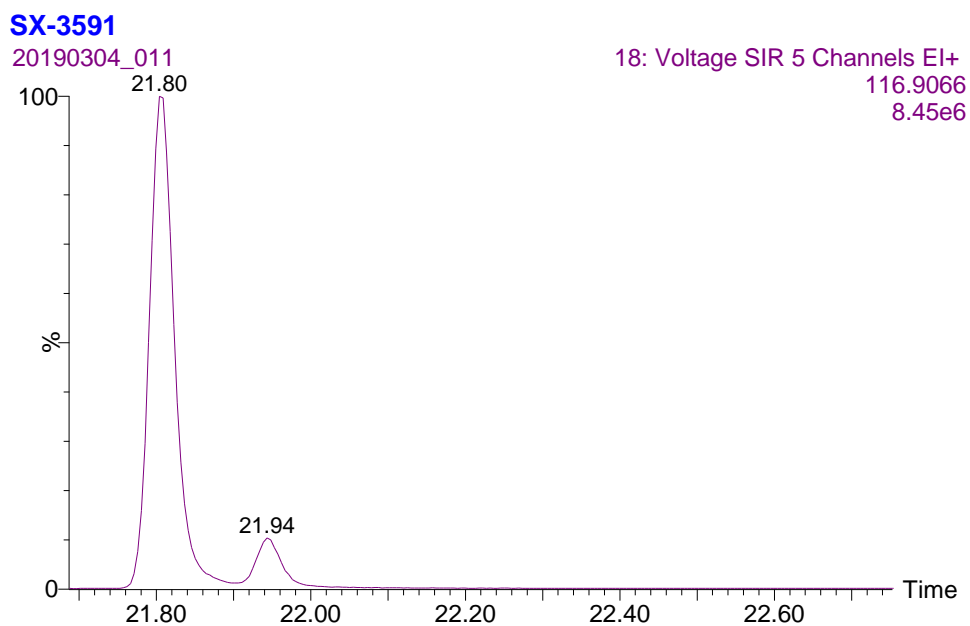


Figure 2.4: Example chromatogram of CFC-113 (21.80 minutes) and CFC-113a (21.94 minutes),  $m/z$  116.9066 in the SX-3591 working standard, on function 18 of the single ion monitoring method, measured in March 2019 on the AIPLOT column.

## 2.5 Instrument setup

The AutoSpec can be operated in one of two modes: scan mode and single ion monitoring (SIM) mode. Scan mode and SIM mode both have trade-offs between the number of mass to charge ( $m/z$ ) ratios monitored and sensitivity. Scan mode is often used for preliminary compound identification and is where the AutoSpec scans across a range of  $m/z$  values in each window of time. The sensitivity of the AutoSpec is proportional to the time spent acquiring ion counts on each ion. Therefore, in scan mode sensitivity is greatly reduced as a large number of ions are measured and so the time spent acquiring them is limited. Single ion monitoring (SIM) mode, on the other hand, is where a small number of  $m/z$  ratios are monitored in each window of time and therefore this mode has much higher sensitivity and so works well for measuring compounds with low mixing ratios. As the ions being measured and the times over which they are measured need to be decided in advanced SIM mode requires more pre-analysis preparation than scan mode and the retention windows need to be repeatedly adjusted as the elution of compounds shifts over time.

The software package ‘MassLynx’, provided by Waters®, is used to control the instrument setup. During this study, the mass spectrometer was operated using electron ionisation and single ion monitoring (SIM) mode, also termed EI-SIR (Electron Impact-Selected Ion Recording) mode, with a mass resolution of  $\sim 1000$  at 5 % peak height determined using the internal reference compound (see below).

The selected ion recording mode is split into functions, which are windows of time when a selection of  $m/z$  values are monitored corresponding to the elution times of

compounds of interest and their ionisation products (Table 2.1). The ions selected to measure a compound are based on a number of factors. Firstly, the size of the peaks need to be large enough to be detected but not so large that they saturate the detector. Secondly, the range of  $m/z$  values being scanned in each window needs to be kept as small as possible or sensitivity may decrease. Typically, the largest  $m/z$  value in a function should not be more than 1.5 times the smallest  $m/z$  value. Thirdly, the  $m/z$  value is selected to avoid interference from other co-eluting compounds. The same compound is often measured on more than one  $m/z$  value.

Table 2.1: A typical single ion monitoring method used on the AutoSpec instrument during this study with the retention windows of the functions, the retention times of the compounds and the ions measured. This example is from August 2018 when the Taiwan 2018 air samples were being analysed using the GasPro column.

Function	Name	Formula	Retention Time (min)	Retention Window (min)	Ions (m/z)		
1	C <sub>2</sub> F <sub>6</sub>	C <sub>2</sub> F <sub>6</sub>	7.78	7.45 - 8.25	118.992		
	SF <sub>6</sub>	SF <sub>6</sub>	8.01		126.9641		
2	HFC-23	CHF <sub>3</sub>	8.37	8.25 - 9.50	51.0046	68.9952	
3	COS	COS	9.91	9.50 - 10.10	59.97	60.9703	61.9628
4	HFC-32	CH <sub>2</sub> F <sub>2</sub>	10.34	10.10 - 10.50	51.0046	52.0125	
5	C <sub>3</sub> F <sub>8</sub>	C <sub>3</sub> F <sub>8</sub>	10.69	10.50 - 11.00	168.9888		
6	CFC-115	CF <sub>3</sub> CClF <sub>2</sub>	11.32	11.00 - 11.50	86.9627	84.9657	
7	HFC-125	CF <sub>3</sub> CHF <sub>2</sub>	11.63	11.50 - 11.98	101.0014		
	SF <sub>5</sub> CF <sub>3</sub>	SF <sub>5</sub> CF <sub>3</sub>	11.68		88.9673		
	HFC-143a	CH <sub>3</sub> CF <sub>3</sub>	11.87		65.0203		
8	CFC-12	CCl <sub>2</sub> F <sub>2</sub>	12.13	11.98 - 13.20	100.9361	102.9332	104.9302
	HCFC-22	CHClF <sub>2</sub>	12.1		66.9751		
9	Methyl Chloride	CH <sub>3</sub> Cl	13.54	13.20 - 13.97	49.9923	50.9957	51.9894
	HFC-134a	CH <sub>2</sub> FCF <sub>3</sub>	13.39		51.0046	50.9957	
10	C <sub>2</sub> H <sub>3</sub> Cl	C <sub>2</sub> H <sub>3</sub> Cl	14.11	13.97 - 14.55	61.9923	63.9894	
	HCFC-31	CH <sub>2</sub> ClF <sub>2</sub>	14.25		67.9829	69.98	
11	HFC-227ea	CF <sub>3</sub> CHFCF <sub>3</sub>	14.8	14.55 - 15.10	150.9982	101.0014	
12	Methyl Bromide	CH <sub>3</sub> Br	15.47	15.10 - 16.00	93.9418	95.9398	
	HCFC-142b	CH <sub>3</sub> CClF <sub>2</sub>	15.5		65.0203		
	HCFC-124	CClF <sub>2</sub> CHF <sub>2</sub>	15.36		66.9751		
13	HCFC-21	CHCl <sub>2</sub> F	16.23	16.00 - 16.65	101.9439		
	CFC-11	CCl <sub>3</sub> F	16.47		102.9332	101.9439	
	HFC-365mfc	CF <sub>3</sub> CH <sub>2</sub> CF <sub>2</sub> CH <sub>3</sub>	16.19		133.0077		
14	HCFC-133a	CH <sub>2</sub> ClCF <sub>3</sub>	16.89	16.65 - 17.40	119.9768	117.9797	
	CH <sub>2</sub> CCl <sub>2</sub>	CH <sub>2</sub> CCl <sub>2</sub>	17.14		95.9534	97.9504	
15	C <sub>2</sub> H <sub>5</sub> Cl	C <sub>2</sub> H <sub>5</sub> Cl	17.58	17.40 - 17.90	64.008	66.005	
16	Dichloromethane	CH <sub>2</sub> Cl <sub>2</sub>	18.07	17.90 - 18.60	82.9455	84.9426	
	cis-CHClCHCl	CHClCHCl	18.25		95.9534	97.9504	
17	HCFC-141b	CH <sub>3</sub> CCl <sub>2</sub> F	18.89	18.60 - 19.80	102.9332		
	CFC-113	CCl <sub>3</sub> CF <sub>3</sub>	19.2		102.9332	116.9066	
	CFC-113a	CCl <sub>3</sub> CF <sub>3</sub>	19.1		116.9066		
	C <sub>2</sub> H <sub>5</sub> Br	C <sub>2</sub> H <sub>5</sub> Br	19.32		107.9575		
	HCFC-123	CF <sub>3</sub> CHCl <sub>2</sub>	19.32		132.9423		
18	Chloroform	CHCl <sub>3</sub>	20.06	19.80 - 21.20	116.9066	118.9036	
	Carbon Tetrachloride	CCl <sub>4</sub>	20.55		116.9066	118.9036	
19	Halothane	CF <sub>3</sub> CHFClBr	21.4	21.20 - 21.60	195.8902		
20	Isoflurane	CF <sub>2</sub> OCF <sub>2</sub> CHFCl	22.27	21.60 - 23.40	114.9762		
	Methyl Chloroform	CH <sub>3</sub> CCl <sub>3</sub>	22.47		116.9066		
	Dibromomethane	CH <sub>2</sub> Br <sub>2</sub>	22.31		92.934	94.9319	
21	1,2-dichloroethane	CH <sub>2</sub> ClCH <sub>2</sub> Cl	23.99	23.40 - 24.50	63.9894	61.9923	

Hexadecane,  $C_{16}H_{34}$ , is used as an internal reference compound and is continuously injected into the ionisation source of the mass spectrometer. The hexadecane gas is contained in a glass vessel which is attached to a movable stainless-steel tube. The flow of the hexadecane is changed by using a valve and changing the distance from the hexadecane to the ion source. Hexadecane is used because it breaks down into a wide range of fragments ions ( $m/z$  29 to 226) that are in a similar range to the fragment ions of the compounds of interest.

The hexadecane is also used for tuning and mass calibration at the beginning of every measurement day. To tune the instrument the ion repeller and focusing lenses are adjusted whilst observing the hexadecane peak on  $C_4H_9^+$   $m/z$  57.0704, the most abundant hexadecane mass, to produce a large symmetric peak. Then mass calibration is completed, the accelerating voltage is scanned over the selected mass range in each function and peaks are matched with known hexadecane fragment ions. In each function a hexadecane lock-mass is included, that has a  $m/z$  value close to those of the other ions being measured. The software then tracks the position of the lock-mass peaks during the day so that small peak position changes caused by slight fluctuations in the magnetic field can be automatically corrected for.

### **2.5.1 Typical measurement day**

On a typical day, after the instrument has been tuned and mass calibrated, the working standard is analysed twice to allow for the instrument to settle down. In this study two working standards, AAL-071170 and SX-3591, were used. They are both background air samples that have 'known' mixing ratios of the compounds of interest (Section 2.8). After this a helium blank is measured.

A helium blank is when 200-300 ml of the helium carrier gas is cryogenically trapped, pre-concentrated and analysed as if it were an air sample. Any peaks detected during this run are due to contamination within the system and the size of the helium peaks is subtracted from the peaks in all the other runs on that day. For almost all compounds of interest the size of the peak in the helium blank is <1 % the size of the peak in the average sample response. Another reason for analysing a helium blank at the beginning of every day is that unexpectedly large peaks in the helium blank may be an indication of a leak in the system.

After the helium blank is measured three duplicate measurements are made of the same sample bracketed by measurements of the working standard. The repeat measurements of the sample are used to calculate part of the analytical uncertainty (see below). For the remainder of the day two samples are measured, followed by another measurement of the working standard. This procedure means usually five to seven samples are analysed each day as it takes approximately 45 minutes to measure a sample, standard or helium blank. The working standard is measured multiple times during the day in order to

calculate the mixing ratios in the samples and to correct for any change in the detector response during the day, i.e. instrument drift (see below).

1. Standard
2. Standard
3. Helium Blank
4. Standard
5. Sample 1
6. Sample 1
7. Sample 1
8. Standard
9. Sample 2
10. Sample 3
11. Standard
12. Sample 4
13. Sample 5
14. Standard
15. Sample 6
16. Sample 7
17. Standard

## 2.6 Data processing

After analysis, the area under each of the peaks is integrated and normalised according to the exact air volume injected. Then the peak areas in the samples are compared to the equivalent peak areas in the surrounding standards. The first standard measured at the beginning of the measurement day is excluded from the data processing. In order to correct for instrument drift, which can cause variations in the peak areas, the standards are weighted according to their temporal proximity to the sample. A combined standard value is then used to calculate a sample-to-standard ratio. The ratio of the helium blank to the standard is then removed from each of the sample-to-standard ratios using Equation 2.1.

$$\frac{\text{Sample ratio} - \text{Helium ratio}}{1 - \text{Helium ratio}} = \text{blank corrected sample-to-standard ratio} \quad (2.1)$$

This ratio is then multiplied by the 'known' mixing ratio in the standard to calculate the mixing ratio in the sample. In some cases, the peak heights are used instead of the peak areas. For samples that are measured multiple times the measurements are averaged together to calculate a mixing ratio.

The analytical precision is calculated the same way for all the measurements and represents the  $1\sigma$  standard deviation. The uncertainty is based on the square root of the sum of squares of the standard deviation of the standards measured throughout the day

and the standard deviation of the three repeat measurements of a sample on that day (Equation 2.2).

$$\text{Total uncertainty} = \sqrt{SD_{\text{sample}}^2 + SD_{\text{standard}}^2} \quad (2.2)$$

## 2.7 Entech instrument

The air samples collected in Taiwan were also measured on the Entech-Agilent GC-MS system. Some of these data in this thesis comes from these measurements and it is explained in Chapters 4 and 5 when this is the case. The analysis using this system was carried out and the data generously provided by David Oram. For more detail about the 'Entech' instrument system see Leedham-Elvidge et al. (2015).

Briefly, 800 ml – 1000 ml of air are typically trapped using a commercial, fully automated, three-stage cryogenic pre-concentration system (Entech Instruments, model 7100). The gas chromatograph is an Agilent 6890 with a GasPro capillary column (30 m × 320 μm, Agilent Technologies) and the carrier gas is research grade helium. The mass spectrometer is a 5973 quadrupole, operated in electron ionisation at 70 eV and single ion monitoring mode. Mixing ratios were determined by comparison with measurements of a working standard, SX-0706070 or SX-3580.

## 2.8 Stability of substances in standards

### 2.8.1 Purpose of a working standard

A working standard is a gas cylinder of air that is measured multiple times per day, in this case, on the AutoSpec GC-MS. As mentioned previously the working standard serves multiple purposes. Firstly, recording and later correcting for drift in the instrument response during the measurement day. Secondly, calculating the mixing ratios, for the compounds of interest, in the samples by comparing the relative response, i.e. the size of the peak, in the sample to the size of the peak in the standard (Section 2.6). It is assumed that we know what the mixing ratio of the compound in the standard is. An additional purpose of a standard is to enable the comparison of measurements made at different times using the same instrument, measurements made with the instrument using different set-ups, and measurements made using different instruments. These comparisons can be used to identify issues if the mixing ratios of a compound are found to differ when using different measurement methods.

### 2.8.2 Purpose of intercomparison measurements

During the course of this research, two primary working standards were used on the AutoSpec GC-MS. Firstly the AAL-071170 that was the working standard from 2008 to 2017 and then on 17-Aug-2017 the standard was replaced with the SX-3591 that became the new working standard. It is necessary to change the working standard after a

number of years because the pressure decreases in standards as the air is used up. Also, mixing ratios of many compounds in the atmosphere increase or decrease over time and therefore the compound's mixing ratios in an older standard may no longer be comparable to modern day air samples.

Mixing ratios of compounds in standards can drift over time. The mixing ratio of a compound may slowly increase or decrease over time due to chemical reactions taking place inside the cylinder. In order to check for drifts in the standards, intercomparison days were performed regularly. Intercomparison days involve measuring at least one other standard, two or three times, as if it were a sample, in addition to the working standard on the AutoSpec GC-MS instrument. This study includes intercomparisons done between 2008 and 2018 and is an update to a previous intercomparison done in 2015 by Johannes Laube.

### **2.8.3 Description of standards**

For intercomparisons it is necessary to compare multiple standards to decrease the chance of concurrent drift making the standards incorrectly appear stable. In this study, five standards were compared: ALM-39753, AAL-071170, SX-0706077, SX-3580 and SX-3591. ALM-39753 was the working standard on a different AutoSpec instrument at the UEA from 1998 to 2008. Both ALM-39753 and AAL-071170 are Aculife-treated aluminium gas cylinders. All the SX canisters are electro-polished stainless-steel canisters from 'Essex Industries'.

All the working standards are real air samples collected at Niwot Ridge, Colorado, USA and are representative of northern hemispheric background mixing ratios: ALM-39753 (filled 1993), AAL-071170 (filled 2006), SX-0706077 (filled 2009), SX-3580 (filled 2013) and SX-3591 (filled 2016). The standards were collected, initially calibrated and supplied by the Global Monitoring Division of the Earth System Research Laboratory of the National Oceanic and Atmospheric Administration (NOAA-ESRL-GMD) in Boulder, Colorado, USA.

Table 2.2: Intercomparison measurement days on the AutoSpec instrument between 2008 and 2018 and the standards measured on each day.

Measurement date	ALM-39753	AAL-071170	SX-0706077	SX-3580	SX-3591
17-Dec-2008	✓	✓			
03-Sep-2009	✓	✓			
08-Sep-2009	✓	✓			
12-May-2010	✓	✓	✓		
13-May-2010	✓	✓	✓		
07-Jun-2013	✓	✓	✓		
21-May-2014		✓	✓		
29-May-2014	✓	✓			
02-Jun-2014		✓	✓	✓	
04-Jun-2014		✓	✓	✓	
24-Sep-2014	✓	✓			
15-Sep-2015		✓	✓	✓	
22-Jul-2016		✓		✓	
21-Mar-2017	✓	✓	✓		
28-Mar-2017	✓	✓			
30-Mar-2017		✓	✓		✓
05-Apr-2017		✓			✓
15-Aug-2017		✓	✓		✓
17-Aug-2017	✓	✓			✓
24-Aug-2017		✓			✓
21-Sep-2017		✓			✓
23-Nov-2017	✓	✓	✓		✓
13-Mar-2018		✓			✓
20-Aug-2018	✓	✓			✓
22-Aug-2018			✓		✓
07-Sep-2018		✓			✓

#### 2.8.4 Intercomparison methodology

In total, this study included 26 intercomparison days spread across 11 years (Table 2.2). All the standards were measured against AAL-071170 as the working standard from 17-Dec-2008 to 15-Aug-2017 and then from 17-Aug-2017 all the standards were measured against SX-3591 as the working standard. The relative response of the standard against the working standard and the analytical uncertainty within each measurement day were calculated as explained in Section 2.6. The only differences with the intercomparison days is that every standard is measured multiple times and instead of a sample-to-standard ratio it is a standard-to-standard ratio.

The standard-to-standard ratio was used to investigate the stability of the compound mixing ratios in the standards. As most of the measurements were made relative to AAL-071170, any measurements that were made using a different working standard were converted to make them relative to AAL-071170 so that all the measurements could be compared.

For example when both ALM-39753 & AAL-071170 were measured against SX-3591 as the working standard, the relative response of ALM-39753 against SX-3591 was divided by the relative response of AAL-071170 against SX-3591 to calculate the relative response of ALM-39753 against AAL-071170.

$$\frac{ALM-39753}{SX-3591} \div \frac{AAL-071170}{SX-3591} = \frac{ALM-39753}{AAL-071170}$$

Then to work out the relative response of SX-3591 against AAL-071170, one divided by the relative response of AAL-071170 against SX-3591 was taken.

$$\frac{SX-3591}{SX-3591} \div \frac{AAL-071170}{SX-3591} = \frac{SX-3591}{AAL-071170}$$

$$\frac{SX-3591}{SX-3591} = 1$$

This leads to the relative response of the AAL-071170 standard always being one and everything else being compared to it. So if a compound in one of the other standards had a mixing ratio higher than the mixing ratio in AAL-071170 then the number would be greater than one. If the mixing ratio was lower than in AAL-071170 the number would be less than one.

If the mixing ratios of a compound in a standard are stable over time then the standard-to-standard ratio, i.e. the relative response should stay the same within uncertainties even over several years. If there is a trend in the relative response over time this means the mixing ratio of the compound in one (or possibly both) of the standards is either increasing or decreasing. The average and the 3 sigma standard deviation of all the measurements for all the intercomparison days is calculated. This is plotted in Figure 2.5 as a larger data point with error bars. The trend line of the relative responses over time was used to calculate relative responses for the first and last intercomparison days for which the standard was measured. It was then determined if these two values agreed within 1 sigma, 2 sigma or 3 sigma standard deviation. If the relative responses did not agree within 3 sigma standard deviation then it is determined that there is a significant drift.

In this study, a selection of 29 halogenated trace gases were investigated. Other compounds such as most PFCs and some HFCs listed in Table 2.1 were also measured but were not the focus of this thesis. See Table 2.3 for a complete list of the compounds investigated and the agreement of their relative responses in the standards. Four examples, methyl bromide, CFC-11, dichloromethane and COS are included in Figure 2.5. The plots for the other 25 compounds are included in the Appendix.

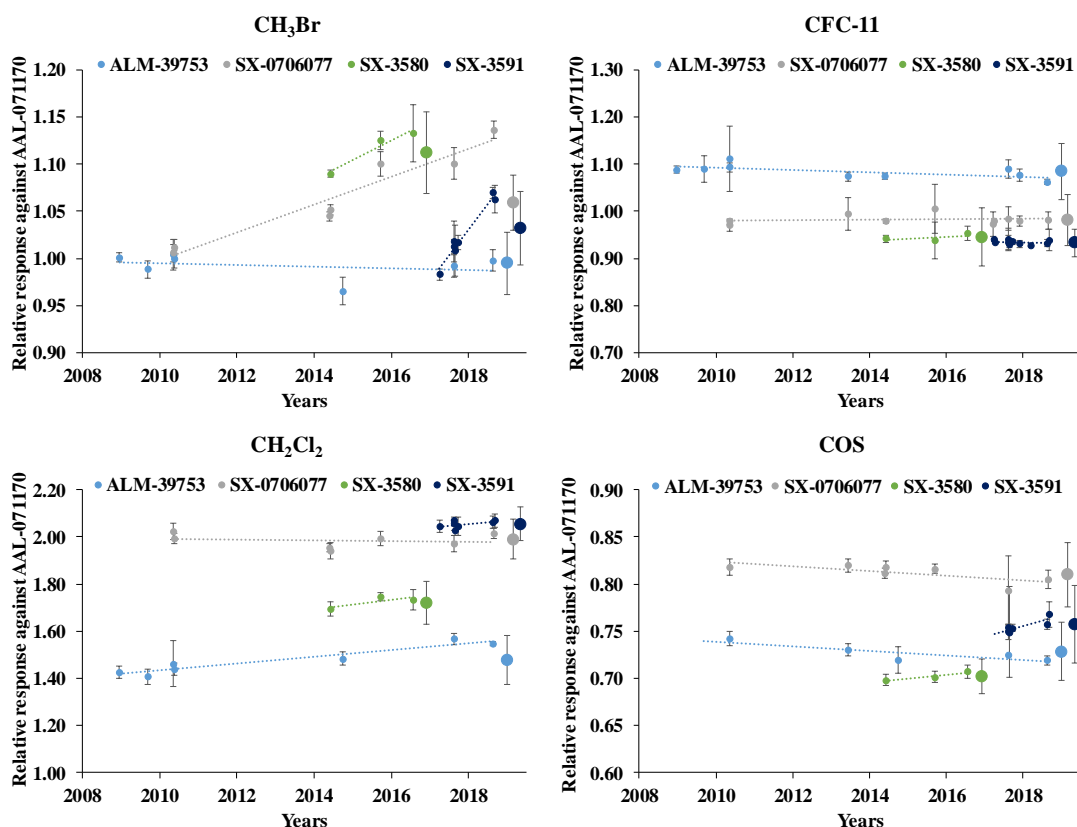


Figure 2.5: Relative responses of the standards against AAL-071170 for CH<sub>3</sub>Br, CFC-11, CH<sub>2</sub>Cl<sub>2</sub>, and COS.

### 2.8.5 Intercomparison results

The relative responses of the other standards against AAL-071170 for most of the compounds investigated remained mostly the same between 2008 and 2018 within either 1 sigma or 2 sigma. There are only five examples of agreement within only 3 sigma (Table 2.3). In general, the compounds that are long-lived in the atmosphere were more stable in the standards than the compounds that are short-lived in the atmosphere.

There were some examples of compounds for some standards not agreeing within 3 sigma. In ALM-39753 dichloromethane and chloroform were found to be drifting. Dichloromethane was previously found to be drifting in the ALM-39753 standard (Leedham Elvidge et al., 2015). Fortunately, ALM-39753 is no-longer being used for measurements and in all the other standards dichloromethane and chloroform show no evidence of drift. Also, 1,2-dichloroethane agrees within 1 sigma with ALM-39753 and agrees within 2 sigma with SX-3591 but does not agree within 3 sigma with SX-0706077 or SX-3580. It is believed that 1,2-dichloroethane is actually drifting in the AAL-071170 standard and that ALM-39753 is co-drifting with it. As the two working standards used in this study, SX-3591 and AAL-071170, still agree within 2 sigma no drift correction was done. The standards stored in aluminium cylinders might not be stable long-term for the very short-lived chlorine compounds, CH<sub>2</sub>Cl<sub>2</sub>, CHCl<sub>3</sub>, and CH<sub>2</sub>ClCH<sub>2</sub>Cl. In the future, 1,2-dichloroethane, dichloromethane and chloroform in ALM-39753 and AAL-071170 will need to continue being monitored.

The SX-3580 standard was only included in four intercomparison days and not all the compounds were analysed for every day so in some cases the relative responses of compounds in SX-3580 against AAL-071170 are only available for one or two days. For compounds that were only measured once it was not possible to investigate the variation of those compounds in SX-3580. For compounds that were measured twice a trend line was calculated but should be treated with caution. The relative responses of CFC-13, CH<sub>3</sub>CCl<sub>3</sub> and CH<sub>2</sub>ClCH<sub>2</sub>Cl in SX-3580 against AAL-071170 do not agree within 3 sigma but they are all based on only two measurements. CFC-13 and CH<sub>3</sub>CCl<sub>3</sub> agree in the other standards and it is hypothesised that additional measurements of SX-3580 would likely improve the agreement.

Table 2.3: The agreement of the relative responses of the standards against AAL-071170. ✓ whether they agree within 1σ, 2σ or 3σ standard deviation of the daily measurement uncertainty. ✗ they don't agree within 3σ. NA - Not Available, the compound was only measured once and so it is not possible to investigate drift over time.

Compounds	ALM-39753			SX-0706077			SX-3580			SX-3591		
	1σ	2σ	3σ	1σ	2σ	3σ	1σ	2σ	3σ	1σ	2σ	3σ
C <sub>2</sub> H <sub>5</sub> Br	✓				✓				✓		✓	
C <sub>3</sub> F <sub>8</sub>		✓		✓			✓				✓	
CFC-11		✓		✓			✓			✓		
CFC-113	✓			✓				✓		✓		
CFC-115	✓			✓				✓		✓		
CFC-12		✓		✓			NA				✓	
CFC-13	✓				✓		✗				✓	
COS			✓		✓			✓			✓	
CH <sub>2</sub> Cl <sub>2</sub>		✗		✓				✓		✓		
CH <sub>2</sub> Br <sub>2</sub>	✓				✓				✓			✓
CH <sub>2</sub> ClCH <sub>2</sub> Cl	✓			✗			✗				✓	
Halon-1211		✓		✓			NA			✓		
Halon-2402	✓			✓			NA			✓		
HCFC-133a	✓					✓		✓		✓		
HCFC-142b	✓			✓			✓			✓		
HFC-125	✓			✓			✓			✓		
HCFC-141b		✓			✓		✓			✓		
HFC-143a	✓			✓			✓			✓		
HCFC-22	✓			✓			✓				✓	
HFC-23		✓		✓			✓				✓	
CH <sub>3</sub> CCl <sub>3</sub>	✓			✓			✗			✓		
CH <sub>3</sub> Br	✓			✗			✗			✗		
CH <sub>3</sub> Cl		✓		✓			✓			✓		
SF <sub>6</sub>	✓			✓			✓			✓		
CCl <sub>4</sub>	✓			✓			✓			✓		
CHCl <sub>3</sub>		✗		✓			✓			✓		
CFC-113a		✓			✓		✓				✓	
HFC-32	✓			✓			✓				✓	
Halon-1301		✓			✓		NA			✓		

## 2.8.6 Drift correction

There is evidence to suggest that the mixing ratios of methyl bromide (CH<sub>3</sub>Br) are changing in some of the standards. The responses of methyl bromide in SX-3580, SX-0706077 and SX-3591 relative to AAL-071170 do not agree within 3 sigma (Table 2.3). The response in ALM-39753 agrees within 1 sigma possibly because ALM-39753 and

AAL-071170 are co-drifting. The slope of the trend for SX-3591 against AAL-071170 is relatively large and could suggest that methyl bromide is drifting in both of these standards (Figure 2.5). Overall, it is believed that methyl bromide mixing ratios are decreasing in AAL-071170 and ALM-39753 and increasing in SX-3591.

Methyl bromide was therefore drift corrected. This correction was done by taking the original NOAA supplied methyl bromide mixing ratio in the AAL-071170 (8.8 ppt in 2006). Then calculating the mixing ratios of methyl bromide in the AAL-071170 at different points in time using the relative response of the AAL-071170 against the other standards on the intercomparison days and the original NOAA supplied methyl bromide mixing ratios in the other standards. The assumption behind this is that the original NOAA supplied mixing ratios of the standards are still valid when measured shortly after their delivery as there has not been very much time for drifting. When AAL-071170 was the working standard its relative response was calculated using the method shown above, (i.e. 1 divided by the relative response of the other standard). Intercomparisons with ALM-39753 were excluded because it is likely ALM-39753 is also drifting.

These mixing ratios of methyl bromide in the AAL-071170 were then plotted (Figure 2.6) and a linear trend line calculated,  $y=mx+c$ , where  $y$  is the mixing ratio of methyl bromide in the sample and  $x$  is the date it was measured as a decimal date. To calculate the methyl bromide mixing ratio in a sample, take the date of the measurement and the equation of the trend line, to calculate what the mixing ratio of methyl bromide was in the AAL-071170 on that day. Then multiply this number by the relative response of the sample to calculate the methyl bromide mixing ratio in the sample. This drift correction was initially done in 2017, it was only after it was repeated in 2018 that it became apparent that methyl bromide mixing ratios were also likely drifting in SX-3591. However, the only methyl bromide measurements used in this study are from before 2018, i.e. very shortly after the initial filling and calibration of SX-3591 by NOAA, so the drift correction should still be acceptable for these measurements.

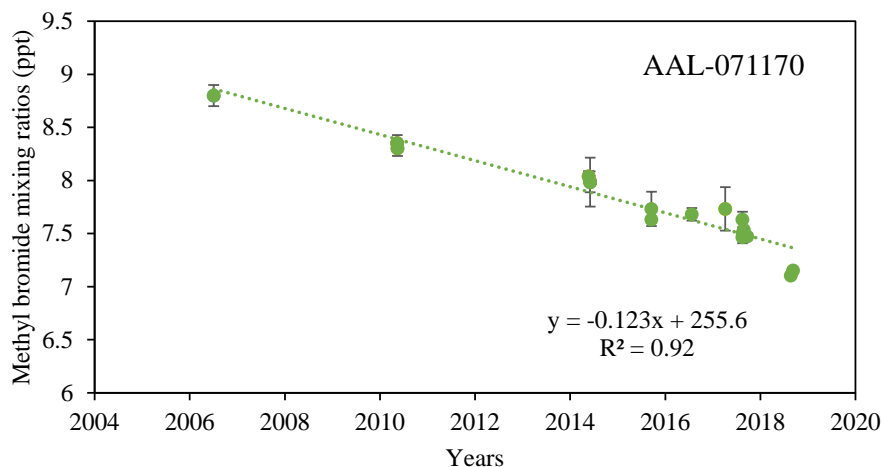


Figure 2.6: Methyl bromide mixing ratios in AAL-071170 between 2006 and 2018.

### 2.8.7 Calculating the mixing ratios in the standards

SX-3591 became the working standard on the AutoSpec instrument at the UEA on 17-Aug-2017. The standard is a background northern hemispheric air sample collected in Colorado in the summer of 2016 by NOAA-ESRL-GMD. It was calibrated by NOAA for some of the most important trace gases but not for all of the compounds measured at the UEA. Mixing ratios for the compounds in the SX-3591 were calculated using the mixing ratio in AAL-071170 and the ratio of the relative response of AAL-071170 against SX-3591.

$$SX\text{-}3591 \text{ mixing ratio} = \frac{AAL\text{-}071170 \text{ mixing ratio}}{\text{average response of AAL-071170 relative to SX-3591}}$$

Mixing ratios calculated for compounds in SX-3591 were then compared to the mixing ratios provided by NOAA, where it was possible, to investigate whether they agreed within the uncertainties (Table 2.4). For the 13 compounds that were compared the calculated SX-3591 mixing ratios agreed with the SX-3591 NOAA mixing ratios within 1 sigma standard deviation for all the compounds except for COS, HCFC-141b, CH<sub>3</sub>Br and CH<sub>3</sub>Cl. The mixing ratios of HCFC-141b and CH<sub>3</sub>Cl agreed within 2 sigma standard deviation. The CH<sub>3</sub>Br mixing ratio calculated in this study is lower than the CH<sub>3</sub>Br mixing ratio provided by NOAA. This is because, as previously mentioned, CH<sub>3</sub>Br is drifting, after it was drift corrected, it agreed within 1 sigma. The COS mixing ratio calculated in this study is higher than the NOAA mixing ratio. COS is not an ozone-depleting substance and it was not a focus of this study. Therefore, this disagreement was not investigated further, and COS measurements were excluded from further analysis.

Table 2.4: SX-3591 mixing ratios calculated with AAL-071170 mixing ratios and relative responses of AAL-071170 against SX-3591 compared to SX-3591 mixing ratios provided by NOAA. ✓ indicates that the mixing ratios agree within the uncertainties. ✗ indicates that the mixing ratios do not agree within the uncertainties.

Compounds	AAL-071170			SX-3591		SX-3591 NOAA		SX-3591 mixing ratios agree	
	Mixing ratio (ppt)	Uncertainty (ppt)	Calibration scale	Mixing ratio (ppt)	Uncertainty (ppt)	Mixing ratio (ppt)	Uncertainty (ppt)	Within 1σ	Within 2σ
<b>C<sub>2</sub>H<sub>5</sub>Br</b>	0.122	0.013	UEA 2015	0.106	0.008				
<b>C<sub>3</sub>F<sub>8</sub></b>	0.451	0.023	UEA 2015	0.635	0.012				
<b>CFC-11</b>	248.4		NOAA 2016 GC-ECD	232.071	1.203	231.8	0.9	✓	✓
<b>CFC-113</b>	79.8	0.3	NOAA 2002 GC-ECD	72.345	0.434	72.8	0.4	✓	✓
<b>CFC-115</b>	8.309		UEA 1994	8.494	0.050				
<b>CFC-12</b>	539.894	2.352	NOAA 2008 GC-ECD	510.907	2.752	511.3	1.2	✓	✓
<b>CFC-13</b>	2.943		UEA 1994	3.135	0.052				
<b>COS</b>	685.8	5.3	NOAA 2002 GC-MS	518.949	4.646	504.3	1.0	✗	✗
<b>CH<sub>2</sub>Cl<sub>2</sub></b>	32.538	0.390	NOAA 2003 GC-MS	66.880	0.639	66.5	0.2	✓	✓
<b>CH<sub>2</sub>Br<sub>2</sub></b>	2.46	0.1	NOAA 2003 GC-MS	0.819	0.077	0.83	0.02	✓	✓
<b>CH<sub>2</sub>ClCH<sub>2</sub>Cl</b>	5.67	0.10	UEA 2012	10.209	0.467				
<b>Halon-1211</b>	4.40	0.01	NOAA 2006 GC-ECD	3.556	0.019	3.56	0.02	✓	✓
<b>Halon-2402</b>	0.428	0.002	UEA 2015	0.370	0.005				
<b>HCFC-133a</b>	0.294	0.012	UEA 2012	0.489	0.006				
<b>HCFC-142b</b>	16.7	0.1	NOAA 1994 GC-MS	24.356	0.435	24.5	0.1	✓	✓
<b>HCFC-141b</b>	18.7	0.1	NOAA 1994 GC-MS	26.597	0.232	26.1	0.1	✗	✓
<b>HFC-143a</b>	5.617	0.283	UEA 2015	18.531	0.242				
<b>HCFC-22</b>	178.9	0.6	NOAA 2006 GC-MS	251.250	2.321				
<b>HFC-23</b>	115.44	6.14	UEA 2015	47.789	0.901				
<b>CH<sub>3</sub>CCl<sub>3</sub></b>	16.6	0.2	NOAA 2003 GC-ECD	2.424	0.088	2.4	0.1	✓	✓
<b>CH<sub>3</sub>Br</b>	8.8	0.1	NOAA 2003 GC-MS	5.116	0.654	7.6	0.1	✗	✗
<b>CH<sub>3</sub>Cl</b>	588.4	1.9	NOAA 2003 GC-MS	543.964	5.234	552.3	0.5	✗	✓
<b>SF<sub>6</sub></b>	5.95	0.04	NOAA 2006 GC-ECD	9.521	0.146				
<b>CCl<sub>4</sub></b>	93.9	0.2	NOAA 2002 GC-ECD	82.739	2.457	81.7	0.5	✓	✓
<b>CHCl<sub>3</sub></b>	9.3	0.2	NOAA 1992 GC-MS	15.362	0.270				
<b>CFC-113a</b>	0.375	0.009	UEA 2012	0.726	0.020				
<b>Halon-1301</b>	3.078	0.036	NOAA 2006 GC-ECD	3.297	0.028				
<b>HFC-32</b>	1.59		SIO-2007	15.419	0.410				
<b>HFC-125</b>	4.977		UB-98	24.742	0.199				

## 2.9 Atmospheric models

The focus of this study was on atmospheric observations but during the study the output from three different models was used in combination with the observations to aid investigation.

1. The Numerical Atmospheric Modelling Environment (NAME) Lagrangian particle dispersion model was used in Chapter 4 and Chapter 5. The output from the NAME model was not generated by myself but was generously provided by others: Norfazrin Mohd Hanif (Universiti Kebangsaan Malaysia), Matthew Ashfold (University of Nottingham), Marios Panagi (University of Leicester) and Zoe Fleming (University of Leicester). The NAME model is a three-dimensional model that was originally developed by the UK Meteorology Office to model the dispersion of radioactive clouds after a nuclear accident (Maryon et al., 1991). Since then, NAME has been continuously developed and used in a wide range of atmospheric dispersion research (Jones et al., 2007; Manning et al., 2011; Fleming et al., 2012).

In this study NAME was run in backwards trajectory mode to simulate the history of air sampled during campaigns in Taiwan and Malaysia to investigate source regions of CFC-113a and CFC-11 emissions in East Asia. In Chapter 5 the output from the NAME model was divided into 15 regions to investigate the influence of air masses from each region on mixing ratios of CFC-11 in Taiwan. The output from the NAME model was also combined with emission inventories of carbon monoxide (CO) to investigate the possible emission sectors of CFC-11 emissions in East Asia. For further information see Chapter 4 and Chapter 5.

2. The Chemical Lagrangian Model of the Stratosphere (CLaMS) was used in Chapter 3. The output from the CLaMS model was not generated by myself but was generously provided by Bärbel Vogel (Forschungszentrum Jülich). 15-day backward trajectories were calculated with the trajectory module of the CLaMS model, driven by horizontal winds from ERA-5 reanalysis (Hersbach and Dee, 2016). Backward trajectories were run for some of the air samples collected during the StratoClim research aircraft campaign in summer 2017. The trajectories were used to investigate transport times and source regions of air masses in and above the Asian summer monsoon and their influence on mixing ratios of very short-lived ozone-depleting substances in the upper tropopause and lower stratosphere. For further information see Chapter 3.
3. A two-dimensional atmospheric chemistry-transport model was used in Chapter 4. The model contains 12 horizontal layers each representing 2 km of the atmosphere and 24 equal-area zonally averaged latitudinal bands, making a total of 288 grid boxes. The model was first developed by Hough (1989) and has since then has been used to investigate the global emissions of long-lived trace gases in multiple other

studies e.g. Newland et al., (2013); Laube et al., (2014); Laube et al., (2016). In this study I modified the model to estimate top-down, global annual emissions of CFC-113a and CFC-113. The global emissions rate was iteratively adjusted until the modelled mixing ratios matched as closely as possible to observations in Cape Grim, Tasmania. For further information see Chapter 4.

## References

- Cairo, F., Pommereau, J. P., Law, K. S., Schlager, H., Garnier, A., Fierli, F., Ern, M., Streibel, M., Arabas, S., Borrmann, S., Berthelmer, J. J., Blom, C., Christensen, T., D'Amato, F., Di Donfrancesco, G., Deshler, T., Diedhiou, A., Durry, G., Engelsen, O., Goutail, F., Harris, N. R. P., Kerstel, E. R. T., Khaykin, S., Konopka, P., Kylling, A., Larsen, N., Lebel, T., Liu, X., MacKenzie, A. R., Nielsen, J., Oulanowski, A., Parker, D. J., Pelon, J., Polcher, J., Pyle, J. A., Ravegnani, F., Rivière, E. D., Robinson, A. D., Röckmann, T., Schiller, C., Simões, F., Stefanutti, L., Stroh, F., Some, L., Siegmund, P., Sitnikov, N., Vernier, J. P., Volk, C. M., Voigt, C., Von Hobe, M., Viciani, S. and Yushkov, V.: An introduction to the SCOUT-AMMA stratospheric aircraft, balloons and sondes campaign in West Africa, August 2006: Rationale and roadmap, *Atmos. Chem. Phys.*, 10(5), 2237–2256, doi:10.5194/acp-10-2237-2010, 2010.
- Fleming, Z. L., Monks, P. S. and Manning, A. J.: Review: Untangling the influence of air-mass history in interpreting observed atmospheric composition, *Atmos. Res.*, 104–105, 1–39, doi:10.1016/j.atmosres.2011.09.009, 2012.
- Fraser, P., Oram, D., Reeves, C., Penkett, S. and McCulloch, A.: Southern Hemisphere halon trends (1978-1998) and global halon emissions, *J. Geophys. Res.*, 104(D13), 15985–15999, doi:10.1029/1999JD900113, 1999.
- Hersbach, H. and Dee, D.: ERA5 reanalysis is in production, *ECMWF Newsletter*, Vol. 147, p.7, 2016.
- Hough, A. M.: The development of a two-dimensional global tropospheric model-1. The model transport, *Atmospheric Environment* (1967), 23, 6, 1235-1261, doi:10.1016/0004-6981(89)90150-9, 1989.
- Jones, A., Thomson, D., Hort, M. and Devenish, B.: The U.K. Met Office's Next-Generation Atmospheric Dispersion Model, NAME III, in *Air Pollution Modeling and Its Application XVII*, edited by C. Borrego and A.-L. Norman, pp. 580–589, Boston, MA, Springer US., 2007.
- Kaiser, J., Engel, A., Borchers, R. and Röckmann, T.: Probing stratospheric transport and chemistry with new balloon and aircraft observations of the meridional and vertical N<sub>2</sub>O isotope distribution, *Atmos. Chem. Phys.*, 6(11), 3535–3556, doi:10.5194/acp-6-3535-2006, 2006.

Laube, J. C., Martinerie, P., Witrant, E., Blunier, T., Schwander, J., Brenninkmeijer, C. A. M., Schuck, T. J., Bolder, M., Röckmann, T., Van Der Veen, C., Bönisch, H., Engel, A., Mills, G. P., Newland, M. J., Oram, D. E., Reeves, C. E. and Sturges, W. T.: Accelerating growth of HFC-227ea (1,1,1,2,3,3,3- heptafluoropropane) in the atmosphere, *Atmos. Chem. Phys.*, 10(13), 5903–5910, doi:10.5194/acp-10-5903-2010, 2010a.

Laube, J. C., Engel, A., Bönisch, H., Möbius, T., Sturges, W. T., Braß, M. and Röckmann, T.: Fractional release factors of long-lived halogenated organic compounds in the tropical stratosphere, *Atmos. Chem. Phys.*, 10(3), 1093–1103, doi:10.5194/acp-10-1093-2010, 2010b.

Laube, J. C., Hogan, C., Newland, M. J., Mani, F. S., Fraser, P. J., Brenninkmeijer, C. A. M., Martinerie, P., Oram, D. E., Röckmann, T., Schwander, J., Witrant, E., Mills, G. P., Reeves, C. E. and Sturges, W. T.: Distributions, long term trends and emissions of four perfluorocarbons in remote parts of the atmosphere and firn air, *Atmos. Chem. Phys.*, 12(9), 4081–4090, doi:10.5194/acp-12-4081-2012, 2012.

Laube, J. C., Newland, M. J., Hogan, C., Brenninkmeijer, C. A. M., Fraser, P. J., Martinerie, P., Oram, D. E., Reeves, C. E., Röckmann, T., Schwander, J., Witrant, E. and Sturges, W. T.: Newly detected ozone-depleting substances in the atmosphere, *Nature Geoscience*, 7, 4, 266-269, 10.1038/ngeo2109, 2014.

Laube, J. C., Mohd Hanif, N., Martinerie, P., Gallacher, E., Fraser, P. J., Langenfelds, R., Brenninkmeijer, C. A. M., Schwander, J., Witrant, E., Wang, J.-L., Ou-Yang, C.-F., Gooch, L. J., Reeves, C. E., Sturges, W. T. and Oram, D. E.: Tropospheric observations of CFC-114 and CFC-114a with a focus on long-term trends and emissions, *Atmos. Chem. Phys.*, 16(23), 15347–15358, doi:10.5194/acp-16-15347-2016, 2016.

Lee, J. M., Sturges, W. T., Penkett, S. A., Oram, D. E., Schmidt, U., Engel, A. and Bauer, R.: Observed stratospheric profiles and stratospheric lifetimes of HCFC-141b and HCFC-142b, *Geophys. Res. Lett.*, 22(11), 1369–1372, doi:10.1029/95GL01313, 1995.

Leedham Elvidge, E. C., Oram, D. E., Laube, J. C., Baker, A. K., Montzka, S. A., Humphrey, S., O’Sullivan, D. A. and Brenninkmeijer, C. A. M.: Increasing concentrations of dichloromethane, CH<sub>2</sub>Cl<sub>2</sub>, inferred from CARIBIC air samples collected 1998-2012, *Atmos. Chem. Phys.*, 15(4), 1939–1958, doi:10.5194/acp-15-1939-2015, 2015.

Manning, A. J., O’Doherty, S., Jones, A. R., Simmonds, P. G. and Derwent, R. G.: Estimating UK methane and nitrous oxide emissions from 1990 to 2007 using an inversion modeling approach, *J. Geophys. Res. Atmos.*, 116(D02305), 1–19, doi:10.1029/2010JD014763, 2011.

Maryon, R. H., Smith, F. B., Conway, B. J. and Goddard, D. M.: The U.K. nuclear accident model, *Prog. Nucl. Energy*, 26(2), 85–104, doi:10.1016/0149-1970(91)90043-O, 1991.

Mühle, J., Ganesan, A. L., Miller, B. R., Salameh, P. K., Harth, C. M., Grealley, B. R., Rigby, M., Porter, L. W., Steele, L. P., Trudinger, C. M., Krummel, P. B., O’Doherty, S., Fraser, P. J., Simmonds, P. G., Prinn, R. G. and Weiss, R. F.: Perfluorocarbons in the global atmosphere: tetrafluoromethane, hexafluoroethane, and octafluoropropane, *Atmos. Chem. Phys.*, 10(11), 5145–5164, doi:10.5194/acp-10-5145-2010, 2010.

Newland, M. J., Reeves, C. E., Oram, D. E., Laube, J. C., Sturges, W. T., Hogan, C., Begley, P. and Fraser, P. J.: Southern hemispheric halon trends and global halon emissions, 1978-2011, *Atmospheric Chemistry and Physics*, 13, 11, 5551- 5565, 10.5194/acp-13-5551-2013, 2013.

Oram, D. E., Reeves, C. E., Sturges, W. T., Penkett, S. A., Fraser, P. J. and Langenfelds, R. L.: Recent tropospheric growth rate and distribution of HFC-134a (CF<sub>3</sub>CH<sub>2</sub>F), *Geophys. Res. Lett.*, 23(15), 1949–1952, doi:10.1029/96GL01862, 1996.

Oram, D. E., Mani, F. S., Laube, J. C., Newland, M. J., Reeves, C. E., Sturges, W. T., Penkett, S. A., Brenninkmeijer, C. A. M., Röckmann, T. and Fraser, P. J.: Long-term tropospheric trend of octafluorocyclobutane (c-C<sub>4</sub>F<sub>8</sub> or PFC-318), *Atmos. Chem. Phys.*, 12(1), 261–269, doi:10.5194/acp-12-261-2012, 2012.

Sturges, W. T., Wallington, T. J., Hurley, M. D., Shine, K. P., Sihra, K., Engel, A., Oram, D. E., Penkett, S. A., Mulvaney, R. and Brenninkmeijer, C. A. M.: A potent greenhouse gas identified in the atmosphere: SF<sub>5</sub>CF<sub>3</sub>, *Science*, 289(5479), 611–613, doi:10.1126/science.289.5479.611, 2000.

Sturges, W. T., Oram, D. E., Laube, J. C., Reeves, C. E., Newland, M. J., Hogan, C., Martinerie, P., Witrant, E., Brenninkmeijer, C. A. M., Schuck, T. J. and Fraser, P. J.: Emissions halted of the potent greenhouse gas SF<sub>5</sub>CF<sub>3</sub>, *Atmos. Chem. Phys.*, 12(8), 3653–3658, doi:10.5194/acp-12-3653-2012, 2012.

# **Chapter 3: Aircraft-based observations of ozone-depleting substances in the upper troposphere and lower stratosphere in and above the Asian summer monsoon**

---

The work in this chapter was originally prepared for a publication in the *Journal of Geophysical Research (JGR)* and has been recently submitted. Due to this there are some cases where sentences are written in the first-person plural i.e. “we decided to use our measurements ...”. I wrote the article and did most of the data analysis, but the co-authors of the article also contributed to the work. Bärbel Vogel produced the output from the CLaMS chemistry-transport model, which I then compared to the atmospheric observations. Geoffrey Lee, Johannes Laube, and I measured and analysed the air samples used in this study. Additionally, Johannes Laube and I worked together to calculate the Fractional Release Factors, Equivalent Chlorine and Equivalent Effective Stratospheric Chlorine. Johannes Laube, David Oram and William Sturges are my PhD supervisors. Johannes Laube and William Sturges arranged for the University of East Anglia (UEA) to measure air samples collected during the StratoClim aircraft campaigns. Johannes Laube and David Oram organised the collection of sub-samples from Cape Grim Baseline Air Pollution Station. Paul Fraser and Ray Langenfelds work at the Cape Grim Baseline Air Pollution Station. Bradley Hall and Stephen Montzka were involved in producing the NOAA atmospheric observations that were used in this study. Fred Stroh coordinated the Geophysica aircraft campaigns as part of the StratoClim Project. Thomas Röckmann and Carina van der Veen used a whole air sampler on the Geophysica research aircraft to collect the air samples used in this study. In addition, many of the co-authors contributed comments and suggestions for editing this work.

Adcock, K. E., Fraser, P. J., Hall, B. D., Langenfelds, R. L., Lee, G., Montzka, S. A., Oram, D. E., Röckmann, T., Stroh, F., Sturges, W. T., van der Veen, C., Vogel, B. and Laube, J. C.: Aircraft-based observations of ozone-depleting substances in the upper troposphere and lower stratosphere in and above the Asian summer monsoon, *J. Geophys. Res. Atmos.*, submitted 2020.

## Abstract

Recent studies show that the Asian summer monsoon transports emissions from the rapidly industrialising nations in East and South Asia into the tropical upper troposphere. Here we present a unique set of measurements on over 100 air samples collected on multiple flights of the M55 Geophysica high altitude research aircraft over the Mediterranean, Nepal and northern India during the summers of 2016 and 2017 as part of the EU project StratoClim. These air samples were measured for 27 ozone-depleting substances (ODSs), many of which were enhanced above expected levels, including the very short-lived chlorine-containing compounds, dichloromethane ( $\text{CH}_2\text{Cl}_2$ ), 1,2-dichloroethane ( $\text{CH}_2\text{ClCH}_2\text{Cl}$ ) and chloroform ( $\text{CHCl}_3$ ). Backward trajectories, calculated with the trajectory module of the chemistry-transport model CLaMS and driven by horizontal winds from the ERA-5 reanalysis, indicated fast transport times and source regions of the air masses in South Asia. We derived the total Equivalent Chlorine (ECI), and Equivalent Effective Stratospheric Chlorine (EESC) and found that these quantities were higher than other estimates in the literature. Our findings show that the Asian monsoon is transporting larger than expected mixing ratios of very short-lived ODSs into the upper troposphere and lower stratosphere, likely leading to stratospheric ozone depletion. We also derived fractional release factors for the long-lived compounds and found these to agree relatively well with results from previous aircraft campaigns in different stratospheric regions.

## 3.1 Introduction

The Asian summer monsoon occurs during the boreal summer (July, August & September) over East and South Asia. It is a major meteorological system characterised by deep convection and anticyclonic flow in the upper troposphere and lower stratosphere (UTLS) that is subject to strong dynamical variability (e.g. Li et al., 2005; Randel and Park, 2006; Park et al., 2007, 2008, 2009; Garny and Randel, 2013; Vogel et al., 2015). In the region of the Asian monsoon air masses are rapidly uplifted from the boundary layer into the UTLS (e.g. Park et al., 2009; Randel et al., 2010; Brunamonti et al., 2018).

In this study, we investigate whether the Asian summer monsoon convection transports elevated levels of ozone-depleting substances (ODSs) including very short-lived substances (VSLs) into the lower stratosphere. VSLs are defined here as having atmospheric lifetimes of 6 months or less (Engel and Rigby et al., 2018). They are not included in the Montreal Protocol on Substances that Deplete the Ozone Layer and it was, until relatively recently, thought that they are largely removed in the troposphere before they reach the stratosphere and therefore contribute relatively little to ozone depletion. However, the Asian summer monsoon anticyclone provides an effective pathway to transport air containing tropospheric trace gases from the surface into the lower stratosphere on the time scale of a few days to a few weeks and so even the VSLs could be able to reach the stratosphere at significantly elevated mixing ratios

(e.g. Brioude et al., 2010; Vogel et al., 2014, 2019; Orbe et al., 2015; Hossaini et al., 2016; Tissier and Legras, 2016).

The Asian summer monsoon may therefore be impacting the Northern Hemisphere lower stratosphere. Convection uplifts air over polluted regions, such as the Indian subcontinent and South East Asia and this air is then horizontally confined in the UTLS by the anticyclonic winds (e.g. Park et al., 2007; Ploeger et al., 2015; Vogel et al., 2015). Then air in the Asian summer monsoon is transported either vertically towards the tropical stratosphere or quasi-horizontally into the Northern Hemisphere extra-tropical lower stratosphere (e.g. Orbe et al., 2015; Garny and Randel, 2016; Vogel et al., 2016, 2019; Ploeger et al., 2017). The tropics are the main input region into the stratosphere and the Asian monsoon is a secondary input region (Engel and Rigby et al., 2018). Using the model-based results of Ploeger et al. (2017) it can be estimated that, on an annual average basis, air from the Asian summer monsoon contributes about 5 % of the air in the Northern Hemisphere extra-tropical stratosphere (at a potential temperature level of 380 K), whereas in the tropical stratosphere the contribution is about 2 % in the tropical pipe (at 460 K) and in the Southern Hemisphere extra-tropical stratosphere less than 0.5 % (at 380 K, Ploeger et al., 2017). The transport of ODSs from the Asian monsoon region into the Northern Hemisphere extra-tropical lower stratosphere therefore has the potential to change the chemical composition of this part of the atmosphere. In addition, it has recently been found that ozone at mid-latitudes in the lower stratosphere is still decreasing, and although this is an ongoing discussion, it has been suggested that VSLs may be one of the factors contributing to this (Hossaini et al., 2015a; Ball et al., 2018; Chipperfield et al., 2018).

Background mixing ratios of chlorine-containing VSLs have been increasing recently by  $\sim 4.3 \pm 4.9$  ppt Cl yr<sup>-1</sup> (2012-2016; Engel and Rigby et al., 2018) and they could continue to increase in the future (Hossaini et al., 2015b, 2019; Leedham Elvidge et al., 2015; McCulloch, 2017; Oram et al., 2017; Fang et al., 2019). Total atmospheric chlorine from ODSs has been decreasing in recent years due to the Montreal Protocol. However, this rate of decrease is slowing down which is due, in part, to increasing mixing ratios of VSLs - in particular in East and South East Asia. This could undermine some of the progress made by the Montreal Protocol and its amendments and further offset the reduction in emissions of long-lived ODSs.

The three major chlorine-containing VSLs are dichloromethane (CH<sub>2</sub>Cl<sub>2</sub>), 1,2-dichloroethane (CH<sub>2</sub>ClCH<sub>2</sub>Cl) and chloroform (trichloromethane, CHCl<sub>3</sub>) (Engel and Rigby et al., 2018). CHCl<sub>3</sub> and CH<sub>2</sub>Cl<sub>2</sub> are usually co-produced industrially (McCulloch, 2017). CH<sub>2</sub>Cl<sub>2</sub> has an atmospheric lifetime of about 6 months and its global atmospheric abundances are believed to be at least 90 % anthropogenic in origin (Engel and Rigby et al., 2018). It has a wide range of industrial applications in chemical and pharmaceutical processes and in the production of HFC-32 (McCulloch, 2017). CHCl<sub>3</sub> has an atmospheric lifetime of about 6 months and is estimated to be about 50 % anthropogenic in origin (Engel and Rigby et al., 2018). The principal use for CHCl<sub>3</sub> is as a chemical feedstock for the production of HCFC-22 (Oram et al., 2017).

$\text{CH}_2\text{ClCH}_2\text{Cl}$  has an atmospheric lifetime of about 3 months and it is likely fully anthropogenic in origin (Engel and Rigby et al., 2018). Its primary use is in the manufacture of vinyl chloride, the precursor to polyvinyl chloride (PVC), and other chlorinated solvents (Oram et al., 2017). It is likely that there are major source regions of these chlorine-containing VSLs in China and India (Oram et al., 2017; Fang et al., 2019; Say et al., 2019).

Recent studies, using air samples collected at ground-based measurement sites and on board a commercial aircraft at altitudes of 10-12 km as part of the CARIBIC project, found enhancements of VSLs in the South East Asian region, both at the surface and in the upper troposphere (Leedham Elvidge et al., 2015; Oram et al., 2017). Upper tropospheric levels of these VSLs are likely to ascend into the lower stratosphere. Our study investigates this hypothesis with air samples collected via a high-altitude research aircraft in this region but at higher altitudes (up to 20 km), i.e. within the lower stratosphere where no *in situ* data exists for many ODSs.

## 3.2 Methods

### 3.2.1 Aircraft campaigns

Air samples were collected during two campaigns of the M55 Geophysica high-altitude research aircraft that were part of the StratoClim EU project ([www.stratoclim.org](http://www.stratoclim.org)).

The first campaign took place over the Mediterranean in September 2016. The aim of this campaign was to measure the composition of the outflow from the Asian summer monsoon anticyclone. The monsoon circulation system has a large variability in its spatial extent and can reach from East Asia to the Mediterranean and North-East Africa (Annamalai and Slingo, 2001; Garny and Randel, 2013; Vogel et al., 2015; Pan et al., 2016). This campaign is referred to as AMO-16 (the Asian Monsoon Outflow 2016 campaign). During AMO-16, 24 air samples were collected during two flights (1<sup>st</sup> and 6<sup>th</sup> September 2016). The aircraft operated from Kalamata, Greece (37.1°, 22.0°) and samples were collected in the region of 33°- 41° N, 23° - 31° E, 10 - 20 km altitude (Figure 3.1).

The second campaign took place over the Indian subcontinent in July-August 2017. The aim of this campaign was to measure the composition of the upper part of the Asian summer monsoon anticyclone. This campaign is referred to as AMA-17 (the Asian Monsoon Anticyclone 2017 campaign). During AMA-17, 94 samples were collected during 6 flights (27-Jul-2017, 29-Jul-2017, 31-Jul-17, 02-Aug-2017, 04-Aug-2017, and 06-Aug-2017). The campaign base was Tribhuvan International Airport at Kathmandu, Nepal (27.7°, 85.4°) and samples were collected in the region of 21°- 29° N, 79° - 91° E, 10 - 20 km altitude (Figure 3.1). In addition to the flight samples, 9 air samples were collected at ground level, 2 samples at Kathmandu University and the rest at Kathmandu airport. Kathmandu is situated at an elevation of about 1400 m.

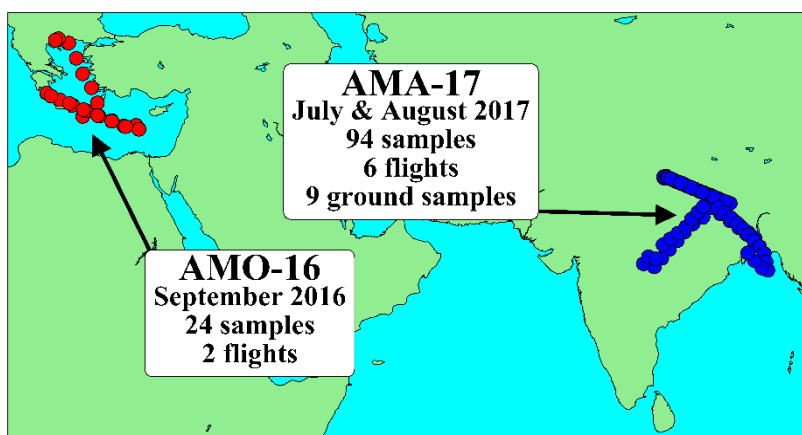


Figure 3.1: The latitude and longitude locations where air samples were collected on board the Geophysica research aircraft during the AMO-16 (red) and AMA-17 (blue) campaigns.

### 3.2.2 Analytical technique

Air samples were collected with the whole air sampler (WAS) of Utrecht University operated on board the Geophysica research aircraft (Kaiser et al., 2006; Cairo et al., 2010; Laube et al., 2010b). Ambient air was compressed into evacuated stainless-steel canisters (2 litre) using a metal bellows pump that has been previously shown to not impact trace gas mixing ratios (Laube et al., 2010b). In addition, for AMA-17 the internal surfaces of 30 canisters were passivated using a common passivation technique ('Silco<sup>TM</sup>-treatment') to minimise the breakdown of more reactive gases in the canisters between collection and analysis (25 filled on board the aircraft and 5 at ground level).

The samples were transported to the University of East Anglia (UEA) for analysis on a high sensitivity gas chromatograph - tri-sector mass spectrometer system (Waters AutoSpec GC-MS). A full description of this system can be found in Chapter 2. The trace gases were cryogenically extracted and pre-concentrated. The different compounds were separated on a GS-GasPro column (length ~ 50 m; ID: 0.32 mm). Additionally, all of the AMO-16 and some of the AMA-17 samples were reanalysed on a KCl-passivated CP-PLOT Al<sub>2</sub>O<sub>3</sub> column (length: 50 m; ID: 0.32 mm) (Laube et al., 2016). During analysis on the Al<sub>2</sub>O<sub>3</sub> column, an Ascarite (NaOH-coated silica) trap was used to remove carbon dioxide, which can distort or reduce the signal of a number of compounds. A full list of measured species and their calibration scales can be found in Table 3.1.

All samples were bracketed by measurements of a working standard (in AMO-16: AAL-071170, and in AMA-17: SX-3591). Calibrations of our target compounds in these working standards were in part provided by the Global Monitoring Division of the Earth System Research Laboratories at the National Oceanic and Atmospheric Administration (GMD, NOAA-ESRL) in Boulder, USA and complemented by UEA internal calibrations for some gases. UEA intercomparisons of these working standards

with three other working standards, two of which had internal surfaces of passivated aluminium, were used to ensure that results were consistent over time and in relation to long-term tropospheric trends (Section 2.8). It was confirmed that the mixing ratios of all compounds presented here remained constant in the two primary working standards within 3 standard deviations during the 2008-2018 period, except for methyl bromide (CH<sub>3</sub>Br) in the SX-3591 standard. This is likely to be due to loss (absorption and/or breakdown) of CH<sub>3</sub>Br on the internal walls of the cylinders and CH<sub>3</sub>Br mixing ratios for SX-3591 were drift-corrected accordingly (Section 2.8). The dry-air mole fractions (mixing ratios) were measured for 27 ODSs (Table 3.1), and the unit, parts per trillion (ppt), is used in this study as an equivalent to picomole per mole. Some additional non-ODSs were measured that are good tracers for stratospheric mean age-of-air calculations and can be used to derive tropospheric emissions, including sulfur hexafluoride (SF<sub>6</sub>), perfluoroethane (C<sub>2</sub>F<sub>6</sub>), HFC-125 (CHF<sub>2</sub>CF<sub>3</sub>) and HFC-32 (CH<sub>2</sub>F<sub>2</sub>).

Table 3.1: NOAA, UEA Cape Grim and WMO 2018 mixing ratios used to calculate the global estimate of equivalent chlorine (ECl) and their calibration scales (Section 3.3.4). The average precision of the measurements in the samples analysed in this study. The measurement precisions are based on the uncertainties from sample repeats and repeated measurements of the working standard on the same day.

<b>Compound</b>	<b>Summer 2017 tropical upper tropospheric mixing ratios (ppt)<sup>1</sup></b>	<b>Average precision (% , 1<math>\sigma</math>)<sup>2</sup></b>	<b>Source<sup>3</sup></b>	<b>Calibration scale</b>
CCl <sub>4</sub>	80.2	0.9 %	NOAA global	NOAA 2008 GC-ECD
CFC-11	229	0.8 %	NOAA global	NOAA 2016 GC-ECD
CFC-113	70.7	0.9 %	NOAA global	NOAA 2002 GC-ECD
CFC-113a	0.72	2.1 %	UEA Cape Grim shifted	UEA 2012
CFC-114	14.7	0.6 %	UEA Cape Grim shifted	UEA 2014
CFC-114a	1.06	0.5 %	UEA Cape Grim shifted	UEA 2014
CFC-115	8.86	0.7 %	UEA Cape Grim shifted	UEA 1994
CFC-12	508	0.6 %	NOAA global	NOAA 2008 GC-ECD
CFC-13	4.01	1.3 %	UEA Cape Grim shifted	UEA 1994
CH <sub>3</sub> Br	6.45-6.82	0.8 %	NOAA MLO & SMO	NOAA 2003 GC-MS
CH <sub>3</sub> CCl <sub>3</sub>	2.18	1.4 %	NOAA global	NOAA 2003 GC-ECD
CH <sub>3</sub> Cl	558-586	0.6 %	NOAA MLO & SMO	NOAA 2003 GC-MS
Halon-1202	0.01	2.3 %	UEA Cape Grim shifted	UEA 1998
Halon-1211	3.42	0.8 %	NOAA global	NOAA 2006 GC-ECD
Halon-1301	3.25	1.0 %	UEA Cape Grim shifted	NOAA 2006 GC-ECD
HCFC-133a	0.40	1.3 %	UEA Cape Grim shifted	UEA 2012
HCFC-141b	24.2	1.0 %	NOAA average	NOAA 1994 GC-MS
HCFC-142b	21.9	0.8 %	NOAA average	NOAA 1994 GC-MS
HCFC-22	239	0.6 %	NOAA average	NOAA 2006 GC-MS
C <sub>2</sub> F <sub>6</sub>	4.12	0.8 %	UEA Cape Grim shifted	UEA 1994
HFC-125	23.1	0.8 %	UEA Cape Grim shifted	UB-98
HFC-32	12.0	0.8 %	UEA Cape Grim shifted	SIO-2007

SF <sub>6</sub>	9.28	0.6 %	NOAA global	NOAA 2014 GC-ECD
CH <sub>2</sub> Cl <sub>2</sub>	29.6-44.3	0.9 %	WMO 2018 Table 1-4 LZRH	NOAA 2003 GC-MS
CHCl <sub>3</sub>	6.4-8.0	1.5 %	WMO 2018 Table 1-4 LZRH	NOAA 1992 GC-MS
CH <sub>2</sub> ClCH <sub>2</sub> Cl	5.2-9.5	2.0 %	WMO 2018 Table 1-4 LZRH	UEA 2012
CH <sub>2</sub> Br <sub>2</sub>	0.59-0.98	1.5 %	WMO 2018 Table 1-4 LZRH	NOAA 2004 GC-MS
Halon-2402*	0.42	—	WMO 2018 Table 1-1 2016 NOAA flask	—
CFC-112*	0.42	—	WMO 2018 Table 1-1 UEA Cape Grim early-2016	—
CFC-112a*	0.067	—	WMO 2018 Table 1-1 UEA Cape Grim early-2016	—
CHClCCl <sub>2</sub> *	0.00–0.16	—	WMO 2018 Table 1-4 LZRH	—
CCl <sub>2</sub> CCl <sub>2</sub> *	0.49–0.95	—	WMO 2018 Table 1-4 LZRH	—
CHBr <sub>3</sub> *	0.05–0.72	—	WMO 2018 Table 1-4 LZRH	—
CH <sub>2</sub> BrCl*	0.08–0.20	—	WMO 2018 Table 1-4 LZRH	—
CHBr <sub>2</sub> Cl*	0.04–0.19	—	WMO 2018 Table 1-4 LZRH	—
CHBrCl <sub>2</sub> *	0.08–0.49	—	WMO 2018 Table 1-4 LZRH	—
HCFC-124*	1.3	—	WMO 2014 Table 1-1 2012 AGAGE, in situ	—

<sup>1</sup>These are not the mixing ratios measured in this study but are the mixing ratios drawn from other sources to compare to the measurements in this study.

<sup>2</sup>The average precision is the average precision of the measurements in this study not the mixing ratios in the second column.

<sup>3</sup>“NOAA global” is referring to global monthly means from the NOAA/ESRL halocarbons program  
“UEA Cape Grim shifted” are mixing ratios measured by University of East Anglia in air samples collected at the Cape Grim station in early 2018 and shifted back in time by 6 months to allow for the transport time from the tropics to Cape Grim

“NOAA MLO & SMO” is the range of mixing ratios observed at the NOAA stations at Mauna Loa and American Samoa

“NOAA average” is the average of the mixing ratios observed at Mauna Loa and American Samoa

\* Compounds that were not measured in this study

GC-ECD: gas chromatography with electron capture detection

GC-MS: gas chromatography with mass selective detection

Due to potential loss during storage for some of the compounds of interest, the time between collection and measurement was kept as short as possible. During AMO-16, the time between collection and measurement was 14-19 days. During AMA-17, the time between collection and measurement was more variable between 2-8 weeks/16-54 days. Only CCl<sub>4</sub> (carbon tetrachloride, tetrachloromethane) and CH<sub>3</sub>Cl (methyl chloride, chloromethane) were affected by the longer time delay in AMA-17. When plotted against CFC-11 there were some samples with mixing ratios that did not match the generally positive linear trend of increasing mixing ratios with increasing CFC-11 mixing ratios (Figures 3.2 & 3.3). For some samples CCl<sub>4</sub> mixing ratios were much lower than the rest of the samples indicating loss inside the canisters (Figure 3.2). CCl<sub>4</sub> has previously been found to be unstable in stainless steel air sampling canisters over long periods (Laube et al., 2008, 2013). Additionally, CH<sub>3</sub>Cl mixing ratios in some samples were higher than the rest of the samples and did not match the trend (Figure

3.3). This indicates production of CH<sub>3</sub>Cl inside the canisters. Samples collected in Silco<sup>TM</sup>-treated canisters did not appear to be effected by the time delay i.e. none of those samples had CH<sub>3</sub>Cl or CCl<sub>4</sub> mixing ratios that did not match the linear trend (Figures 3.2 & 3.3) suggesting that the treatment effectively prevented these reactions inside the canisters. Therefore, none of the Silco<sup>TM</sup>-treated canisters were excluded.

For the other canisters, these data were filtered for both these compounds to only use samples with a shorter time between collection and measurement. The number of days between collection and measurement was decreased one day at a time and the samples that were measured after that number of days were removed from the plot. This was continued until all the samples that clearly did not follow the linear trend were removed. For CCl<sub>4</sub>, samples with a delay of 19 days or more were excluded, this left 30 samples (Figure 3.2). For CH<sub>3</sub>Cl, samples with a delay of 44 days or more were excluded, this left 87 samples (Figure 3.3). In summary, the CH<sub>3</sub>Cl and CCl<sub>4</sub> mixing ratios in samples that were measured later and were not stored in Silco<sup>TM</sup>-treated canisters have been removed from the analysis.

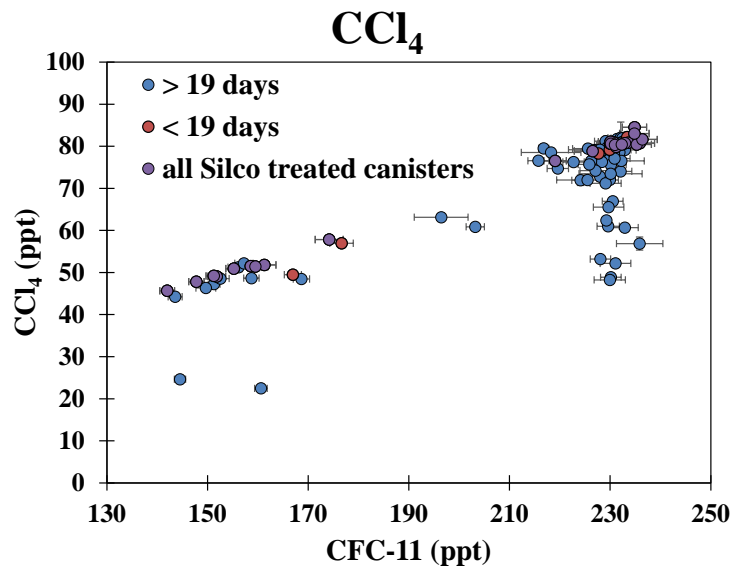


Figure 3.2: CCl<sub>4</sub> mixing ratios against CFC-11 mixing ratios from the AMA-17 campaign. Silco treated canisters, canisters where there was less than 19 days between collection and measurement and canisters where there were more than 19 days between collection and measurement.

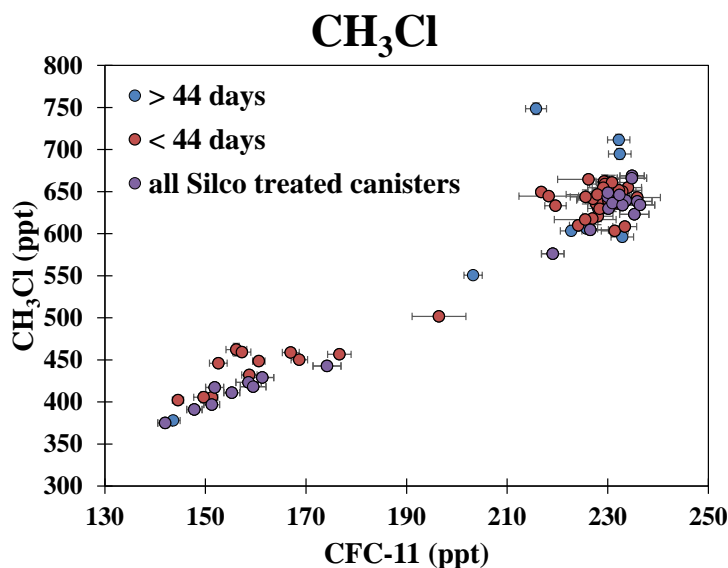


Figure 3.3:  $\text{CH}_3\text{Cl}$  mixing ratios against CFC-11 mixing ratios from the AMA-17 campaign. Silco treated canisters, canisters where there was less than 44 days between collection and measurement and canisters where there were more than 44 days between collection and measurement.

### 3.2.3 CLaMS backward air mass trajectories

There are multiple factors that influence the mixing ratios of VSLs in the UTLS: the mixing ratios of the compounds near the surface, the time it takes for the air to be transported from the surface to the UTLS, and the mixing processes in the troposphere and the stratosphere. In order to investigate these factors, 15-day backward trajectories were run for each sample collected during AMA-17 using the trajectory module of the Chemical Lagrangian Model of the Stratosphere (CLaMS; McKenna, 2002; Konopka et al., 2012; Pommrich et al., 2014 and references therein). This was not done for AMO-16 due to the longer transport time scales and the further diluted source signal as trajectories tend to become more unreliable the further they are run back in time.

The CLaMS backward trajectory calculations are driven by horizontal winds from the high-resolution ERA-5 reanalysis (Hersbach and Dee, 2016) recently released by the European Centre for Medium-Range Weather Forecasts (ECMWF). ERA-5 provides data on a  $0.3^\circ \times 0.3^\circ$  horizontal grid every hour on 137 hybrid levels from the surface to 0.01 hPa. In general, this results in a much better representation of convective updrafts and tropical cyclones in ERA-5 (Hoffmann et al., 2019) compared with the earlier ERA-Interim re-analysis (Dee et al., 2011). In the region of the Asian summer monsoon, CLaMS trajectory calculations driven by ERA-5, that were used for analysing balloon-borne measurements in Kunming, China, yield more reliable upward transport in tropical cyclones compared to trajectories driven by ERA-Interim (Li et al., 2020).

For the vertical velocities, the diabatic approach was applied using diabatic heating rates to derive the vertical velocities including latent heat release (for details, see Ploeger et al., 2010). Further, CLaMS employs a hybrid vertical coordinate ( $\zeta$ ), which transforms from a strictly isentropic coordinate  $\theta$  in the stratosphere to a pressure-based coordinate system below a certain reference level (in this study 300 hPa) in the troposphere (for more details, see Konopka et al., 2012; Pommrich et al., 2014).

The CLaMS model trajectory calculations were used to find the last location the air parcel was above the model boundary layer (trajectory end point). The model boundary layer was set to  $\approx 2$ -3 km above the surface following orography ( $\zeta < 120$  K) (see Vogel et al., 2015). This location provides an indication of the regions where surface sources last influenced the mixing ratios in the air samples. Additionally, the number of days since the air sample was last in the model boundary layer allows investigation of the influence of transport time on their mixing ratios. Only samples measured at potential temperatures less than 390 K were used for backward trajectory calculations as deeper in the stratosphere transport times are much slower leading to a much less reliable trajectory analysis. To assess the uncertainty of a certain backward trajectory, ERA-5-based CLaMS backward trajectories were calculated every second for the entire time interval over which an air sample was collected during the flight. The variability of trajectory end points reflects mixing of air parcels with different origins contributing to the chemical composition of the measured air sample.

### **3.2.4 Equivalent Chlorine (ECI)**

Equivalent chlorine (ECI) is the sum of the mixing ratios of chlorine and bromine atoms from all halogen source gases; the bromine mixing ratios are multiplied by a weighting factor of 60 (Engel and Rigby et al., 2018) as bromine is about 60-65 times more effective at depleting ozone than chlorine in the mid-latitudes. The ECI calculation was used to investigate the impact of ODSs in the tropopause region of the Asian summer monsoon anticyclone in comparison to estimates of ECI based on measurements in other atmospheric regions.

### **3.2.5 Equivalent Effective Stratospheric Chlorine (EESC)**

The Equivalent Effective Stratospheric Chlorine (EESC) is defined as the “chlorine-equivalent sum of chlorine and bromine derived from ODS tropospheric abundances, weighted to reflect their expected depletion of stratospheric ozone.” (Engel and Rigby et al., 2018). EESC – like the ECI – takes into account the sum of the mixing ratios of chlorine and bromine atoms from all halogen source gases with bromine multiplied by 60. However, EESC – in contrast to ECI – takes into account the effects of stratospheric transport and chemistry on the amount of chlorine and bromine present at a given location.

As stratospheric circulation is slow, air sampled in the stratosphere may have entered it several years ago. The ‘mean age-of-air’ is defined as the average amount of time an air parcel has spent in the stratosphere. Inert compounds can be used as ‘age-of-air tracers’

to calculate the ‘mean age-of-air’ of the air sampled in the stratosphere provided that there are a) long-term measurements of their global tropospheric mixing ratios and b) these mixing ratios have been monotonously increasing over time at sufficient rates. Our mean age calculation also takes into account the underlying transit time distribution (the “age spectrum”) using the parameterisation introduced by Engel et al. (2002).

The mean ages-of-air were calculated using ground-level background mixing ratio trends of selected gases from 1978 to January 2018 from air samples collected at the Cape Grim, Tasmania (40.7°S, 144.7°E) Station and analysed at the UEA (Laube et al., 2010a, 2013). These mixing ratio trends were shifted backwards in time by 6 months. This has been proven to be a good proxy for air entering the stratosphere via the upper troposphere in the tropics, provided the gas is inert enough in the troposphere, (i.e. no significant decomposition on tropospheric transport time scales, Leedham Elvidge et al., 2018). Commonly used age-of-air tracers include sulfur hexafluoride (SF<sub>6</sub>) and carbon dioxide (CO<sub>2</sub>) (e.g. Volk et al., 1997; Andrews et al., 2001; Engel et al., 2002). However, recent research has introduced other potential age tracers (Leedham Elvidge et al., 2018). We compared three different age-of-air tracers: SF<sub>6</sub>, C<sub>2</sub>F<sub>6</sub>, and HFC-125 in air samples collected during AMO-16 and AMA-17. The mean ages-of-air were then calculated using the same methods described in Leedham Elvidge et al. (2018).

For trace gases with stratospheric sinks such as ODSs, at mid-latitudes a mean age of 3 years is generally used as a reference to estimate the EESC in that region (Engel and Rigby et al., 2018). The mixing ratios of ODSs measured in the stratosphere at a mean age-of-air of 3 years, for example, would be roughly similar to their mixing ratios in the upper troposphere 3 years earlier, assuming no decomposition. As ODSs are at least partly broken down by strong UV radiation and/or reaction with OH radicals and O(<sup>1</sup>D) in the stratosphere, the mixing ratios of these compounds are however impacted not just by the age of the air but also by different reactions and reaction rates.

For long-lived ODSs, similarly time-shifted tropospheric trends from Cape Grim were propagated into the stratosphere and mixing ratios assuming no decomposition were calculated for the mean ages-of-air, with the latter based on the measured age-of-air tracers. However, for these ODSs decomposition did take place so the actual mixing ratios measured in the samples were lower. We used the difference between the expected mixing ratios (given a particular mean age-of-air and assuming no decomposition) and the measured mixing ratios in AMO-16 and AMA-17 to calculate the fraction of the ECI that had already been released. These measures are known as Fractional Release Factors (FRFs). The more long-lived a compound, the less decomposition takes place and the smaller their fractional release factor is at the same mean age-of-air. Importantly, we also used an improved method of FRF calculation (Ostermüller et al., 2017), which takes into account the dependency of the FRFs on the lifetime of an ODS. The FRF uncertainties were calculated using the uncertainties in the stratospheric measurements, the uncertainty in the tropospheric measurements and the interhemispheric gradient in the troposphere.

For some of the FRF-mean-age correlations, the FRF was negative around mean ages-of-air of zero years. This was because our samples were collected above a polluted continental region so in some cases the mixing ratios of the remote tropospheric monitoring stations were lower than the mixing ratios observed in the Asian monsoon anticyclone tropopause region. This would cause our FRFs to have a low bias. Therefore, FRFs at a mean age-of-air of zero years were calculated from the respective FRF-mean age correlations (using a second order polynomial fit function) and when significantly different from zero, they were subtracted from the FRFs to calculate adjusted FRFs. The FRFs of CFC-115, CFC-114a, HCFC-133a, CH<sub>3</sub>CCl<sub>3</sub>, Halon-1202, CH<sub>3</sub>Cl, and CH<sub>3</sub>Br were shifted in this way. This correction method relies on the assumption that the trace gases measured in 3-year old air originated from a similarly polluted air mass below the tropopause, whereas it could in principal have come from somewhere else. The fact that we do observe continuity throughout the profile gives some confidence, but we note that this introduces an additional uncertainty to these FRFs, which we therefore refer to as regional FRFs.

For the VSLs, it was not possible to use tropospheric trends at background stations to calculate FRFs because of significant loss and variability in the troposphere and the wide range of mixing ratios observed near the tropopause. Therefore, simplified FRFs were calculated by comparing the highest and lowest measured mixing ratios in the tropopause region (355 K – 375 K) to the measured mixing ratios above 375 K in the campaigns.

For AMA-17, measurements of CFC-114, CFC-114a, CFC-13, CH<sub>3</sub>Cl, Halon-1202 and CCl<sub>4</sub> mixing ratios were only available for some of the samples. Therefore, the correlations of the available mixing ratios and FRFs with those of CFC-11 were used to estimate the values for the missing samples. Some compounds were not measured or exhibited poor quality and were therefore excluded from the EESC estimate: CHClCCl<sub>2</sub>, CCl<sub>2</sub>CCl<sub>2</sub>, CHBr<sub>3</sub>, CH<sub>2</sub>BrCl, CHBr<sub>2</sub>Cl, CHBrCl<sub>2</sub>, CFC-112, CFC-112a, HCFC-124, and Halon-2402.

To summarise, EESC depends on three factors: the mixing ratios of ODSs in the troposphere, the transport from the troposphere to the stratosphere (mean age-of-air) and breakdown of ODSs in the stratosphere (FRFs). The EESC was calculated and compared to other estimates in the literature in order to assess the overall impact on stratospheric ozone from ODSs in both campaigns.

### 3.3 Results and discussion

#### 3.3.1 Well mixed ozone-depleting substances

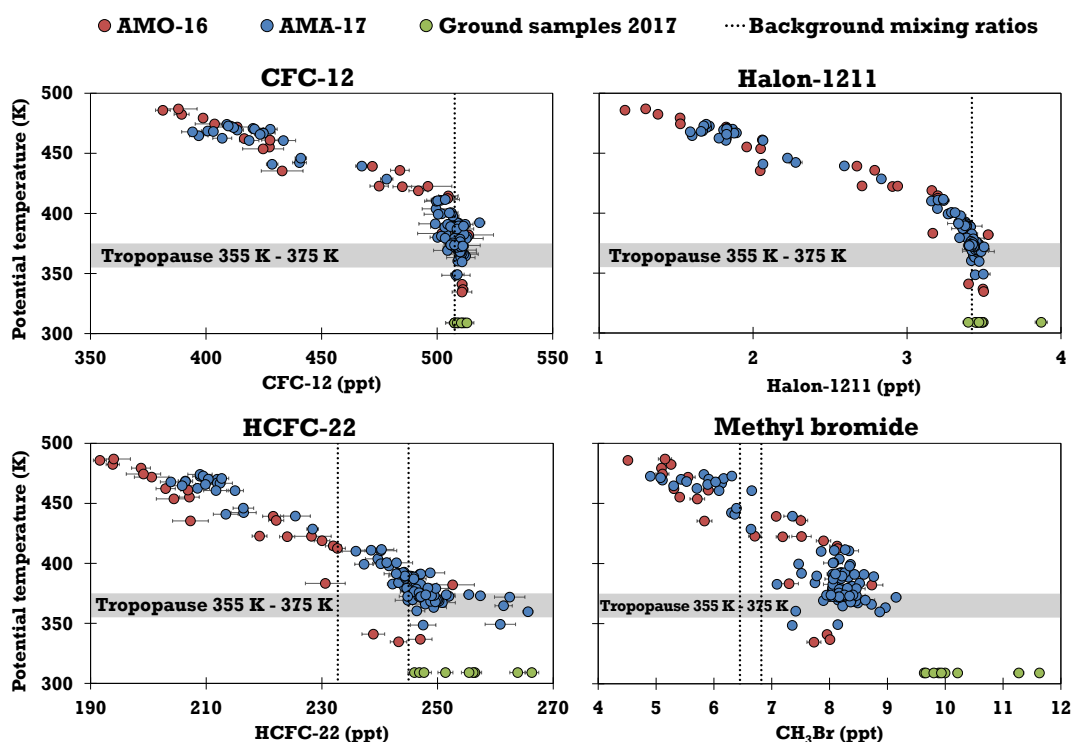


Figure 3.4: Mixing ratios of CFC-12, Halon-1211, HCFC-22 and methyl bromide ( $\text{CH}_3\text{Br}$ ) as a function of potential temperature (a pseudo-vertical coordinate) for AMO-16, AMA-17 and the ground samples collected during AMA-17. The dotted vertical line indicates the globally averaged background mixing ratios of CFC-12 and Halon-1211 for July-August 2017 from NOAA ground-based data (Table 3.1). Two background levels are indicated for HCFC-22 and  $\text{CH}_3\text{Br}$ , the lower one is from measurements at American Samoa ( $14.2^\circ\text{S}$ ,  $170.6^\circ\text{W}$ ) and the higher one from Mauna Loa ( $19.5^\circ\text{N}$ ,  $155.6^\circ\text{W}$ ) (Table 3.1).

CFC-12 and Halon-1211 in Figure 3.4 illustrate the observed distributions of long-lived ODSs that have been phased out under the Montreal Protocol. These two gases have only relatively small emission sources to the atmosphere in the monsoon input region and therefore their mixing ratios in the tropopause are not very variable. The ground-based AMA-17 samples and the lower aircraft measurements generally agree with the expected low variability as well as the NOAA background mixing ratios (Figure 3.4, top). At higher potential temperatures (i.e. altitude), in the stratosphere, the mixing ratios decrease due to photochemical degradation and mixing with other stratospheric air masses (Figure 3.4). This pattern is similar to what is found for many other long-lived ODSs in this study. Conversely, HCFC-22 and  $\text{CH}_3\text{Br}$  are enhanced above expected background mixing ratios (Figure 3.4, bottom). Similar enhancements are

observed for HCFC-141b and CH<sub>3</sub>Cl (Appendix). These enhancements indicate continued large emissions of these compounds in the monsoon input region.

Among long-lived gases, Halon-1211 has a relatively short stratospheric lifetime of about 25 years, so it breaks down relatively quickly in the stratosphere (Figure 3.4). The beginning of the decreasing curve in Halon-1211 mixing ratios, therefore, indicates that air has entered the lower stratosphere and suggests the location of the chemical tropopause. Other data (Brunamonti et al., 2018; Vogel et al., 2019) indicate that there is a transition region between the troposphere and the stratosphere at the top of the anticyclone. For our purposes using the ODS-based one is most appropriate as we are looking at similar gases. In this study, we define the location of the chemical transition layer between the troposphere and stratosphere to be the region of 355 K – 375 K (i.e. just below the level at which Halon-1211 mixing ratios start to decrease) which is represented by the horizontal grey bar in Figure 3.4. The location of the tropopause region is important because the slow ascent rates represent a transport barrier, that limits particularly the contribution of VSLs to ozone depletion in the stratosphere due to their quicker chemical decomposition.

### 3.3.2 Very short-lived ozone-depleting substances

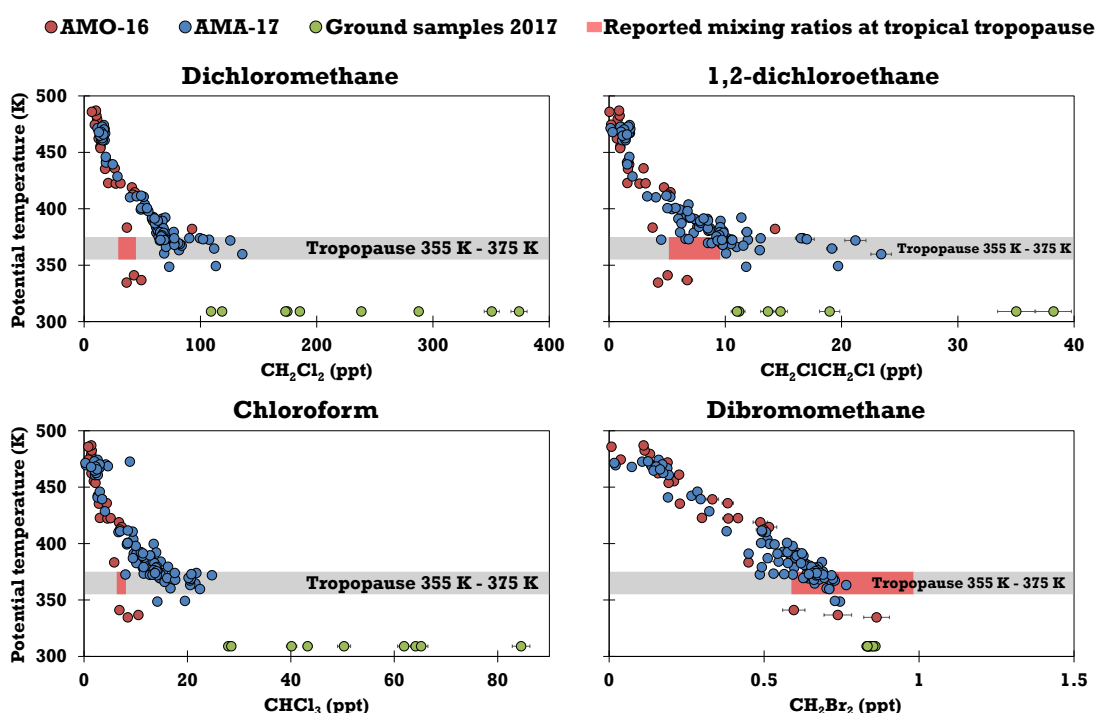


Figure 3.5: Mixing ratios for dichloromethane, 1,2-dichloroethane, chloroform and dibromomethane (CH<sub>2</sub>Br<sub>2</sub>) as a function of potential temperature for AMO-16, AMA-17 and the AMA-17 ground samples. The red shaded region indicates the estimated mixing ratios at the Level of Zero Radiative Heating (LZRH) from the WMO 2018 report (Engel and Rigby et al., 2018; Table 3.1).

The mixing ratios of the three major chlorine-containing VSLs, dichloromethane ( $\text{CH}_2\text{Cl}_2$ ), 1,2-dichloroethane ( $\text{CH}_2\text{ClCH}_2\text{Cl}$ ) and chloroform ( $\text{CHCl}_3$ ), and one bromine-containing VSL, dibromomethane ( $\text{CH}_2\text{Br}_2$ ) are shown in Figure 3.5 as a function of potential temperature. The chlorinated compounds show a large range of mixing ratios both in the ground-based samples and in the tropopause region indicating continued large emissions, which reach the tropopause (Figure 3.5). At higher potential temperatures, their mixing ratios decrease rapidly as in the stratosphere they are broken down, predominantly by UV radiation (Figure 3.5).

From WMO 2018 (Engel and Rigby et al., 2018), estimated mixing ratios of these compounds in the tropopause region (as derived from multiple sources such as various aircraft campaigns) are represented by the red-shaded areas indicated at the tropopause levels (Table 3.1, Figure 3.5). For the chlorine-containing VSLs, almost all the AMA-17 samples collected near the tropopause have higher mixing ratios (Figure 3.5) than the WMO estimates. They are still enhanced above these data presented in WMO 2018 until about 400 K potential temperature, indicating that the Asian summer monsoon transports enhanced levels of chlorine-containing VSLs into the lower stratosphere. Dibromomethane, in contrast to the three chlorine-containing VSLs, has mostly natural oceanic sources, and its mixing ratios measured near the tropopause agree within the range of these data presented in WMO 2018 (Figure 3.5).

Samples collected during AMO-16 often have lower mixing ratios for the chlorine-containing VSLs than the samples from AMA-17 in the aircraft measurements at lower levels of potential temperature. This is possibly because during AMO-16 in general two different types of air masses were sampled: mid-latitude extra-tropical air with lower mixing ratios and monsoon outflow influenced air with higher mixing ratios, but not necessarily Asian sources.

Mixing ratios of these three chlorine-containing VSLs are well correlated, even in the more source-influenced upper tropospheric region. For AMA-17, the three aircraft samples with the highest  $\text{CH}_2\text{Cl}_2$  mixing ratios are also the samples with the three highest  $\text{CH}_2\text{ClCH}_2\text{Cl}$  and  $\text{CHCl}_3$  mixing ratios. For AMO-16, the sample with the highest  $\text{CH}_2\text{Cl}_2$  mixing ratio also has the highest  $\text{CH}_2\text{ClCH}_2\text{Cl}$  and  $\text{CHCl}_3$  mixing ratios. There is one outlier in AMA-17 which has high  $\text{CH}_2\text{Cl}_2$  mixing ratios but is not particularly enhanced for the other compounds ( $\text{CH}_2\text{Cl}_2$  107 ppt, 305 K, Figure 3.6). This suggests that the enhanced  $\text{CH}_2\text{Cl}_2$  in this sample originates from a different source. In addition, an influence from the tropospheric trends could play a role in these correlations as both  $\text{CHCl}_3$  and  $\text{CH}_2\text{Cl}_2$  have been increasing in recent years (Fang et al., 2019; Claxton et al., 2020). Given that the samples with high mixing ratios of these three VSLs are all at low altitudes and contain relatively young air this influence can however be neglected here.

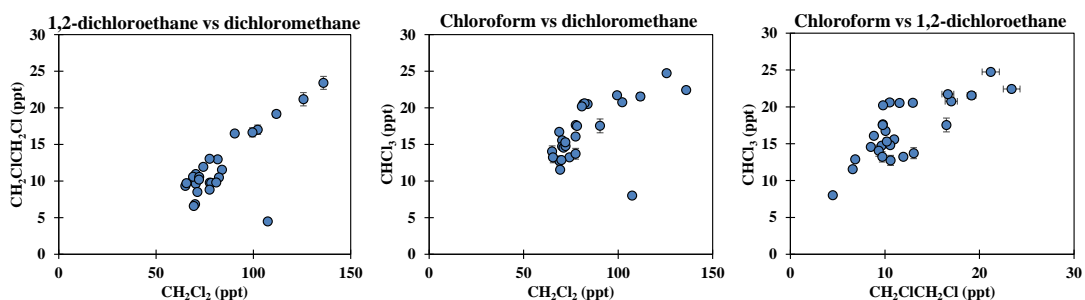


Figure 3.6: Dichloromethane, 1,2-dichloroethane and chloroform mixing ratios correlations in the tropopause region (355 K – 375 K) for the AMA-17 campaign. The outlier sample with comparatively high dichloromethane mixing ratios was excluded from some of the analysis.

In addition to having strong correlations with each other, the chlorine-containing VSLs are also correlated with other compounds (Figure 3.7). When investigating only the samples in the tropopause region using Spearman correlations (i.e. assuming a monotonic but not necessarily linear relationship) and excluding the outlier sample,  $\text{CH}_2\text{Cl}_2$  has the strongest Spearman's correlation coefficients with  $\text{CHCl}_3$  ( $R = 0.87$ ), HFC-32 ( $R = 0.87$ ), HCFC-22 ( $R = 0.87$ ),  $\text{CH}_2\text{ClCH}_2\text{Cl}$  ( $R = 0.75$ ) and HFC-125 ( $R = 0.74$ ).  $\text{CH}_2\text{ClCH}_2\text{Cl}$  has the strongest positive Spearman's correlations with  $\text{CH}_2\text{Cl}_2$  ( $R = 0.75$ ), HCFC-133a ( $R = 0.71$ ),  $\text{CHCl}_3$  ( $R = 0.70$ ),  $\text{CCl}_4$  ( $R = 0.66$ ) and HFC-23 ( $R = 0.66$ ). The compounds that are well correlated with  $\text{CHCl}_3$  are  $\text{CH}_2\text{Cl}_2$  ( $R = 0.87$ ), HFC-32 ( $R = 0.82$ ), HFC-125 ( $R = 0.72$ ),  $\text{SF}_6$  ( $R = 0.71$ ) and  $\text{CH}_2\text{ClCH}_2\text{Cl}$  ( $R = 0.70$ ). These correlations are all significant ( $p < 0.01$ ) and all of the compounds have known strong industrial emissions in East and South-East Asia (Kim et al., 2010; Vollmer et al., 2015; Fang et al., 2018, 2019; Lunt et al., 2018); suggesting the sources of the halogenated compounds in these air samples are from continental industrial areas and indicating that they are either emitted from co-located sources or co-produced. The strongest correlation is between  $\text{CH}_2\text{Cl}_2$  and  $\text{CHCl}_3$  and these two compounds are known to be co-produced in large quantities in East Asia (Oram et al., 2017).

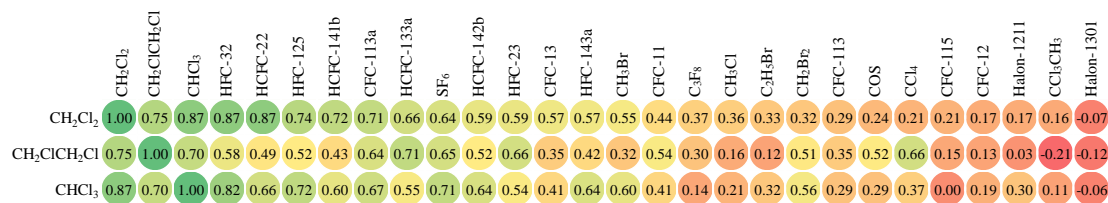


Figure 3.7: Spearman's correlation coefficients ( $R$ ) of dichloromethane, 1,2-dichloroethane and chloroform with a range of halogenated trace gases in the tropopause in the AMA-17 campaign. The outlier sample in Figure 3.6 is excluded from these correlations.

### 3.3.3 CLaMS backward trajectories

The influence of the source location, transport time and mixing of different air parcels on VSLs in the AMA-17 air samples were investigated using 15-day backward trajectories from the CLaMS model. Due to the longer transport timescales at higher altitudes only samples measured at potential temperatures less than 390 K were used for backward trajectory calculations, i.e. 53 out of 94 samples. On average there were about 160 trajectories run for each sample. 32 samples had at least one trajectory that reached the model boundary layer within 15 days with the remainder ending in the free troposphere and stratosphere.

Figure 3.8 shows the location where the air was last in the model boundary layer i.e. 2-3 km above the surface ( $\zeta = 120$  K) based on the CLaMS trajectories. This was used to investigate the location of the sources influencing the mixing ratios of the VSLs in the air samples. The source locations for most of the air samples are found in South-East Asia, mostly around southern China, close to longitudes and latitudes at which the samples were collected (Figure 3.1) with less frequent sources in the rest of South-East Asia (Figure 3.8). This agrees with previous research that air is mostly confined within the Asian summer monsoon anticyclone and subsequently transported from the anticyclone to the lower stratosphere (Ploeger et al., 2017; Vogel et al., 2019). The diversity of trajectory source regions found even for a single air sample, limits the discussion of the origins of the high mixing ratios (Figure 3.8).

As potential temperature increases,  $\text{CH}_2\text{Cl}_2$  mixing ratios decrease and transport times increase because it takes longer to reach higher potential temperatures and this allows more time for  $\text{CH}_2\text{Cl}_2$  to break down. It might be assumed that samples with shorter transport times would also generally have higher  $\text{CH}_2\text{Cl}_2$  mixing ratios. There is, however, not a significant correlation between transport time and  $\text{CH}_2\text{Cl}_2$  mixing ratios. This does not necessarily mean that there is not a relationship, just that other factors have a large impact, for example, mixing of different air parcels and the spatial-temporal distribution at the tropopause, caused by uplift from the boundary layer.

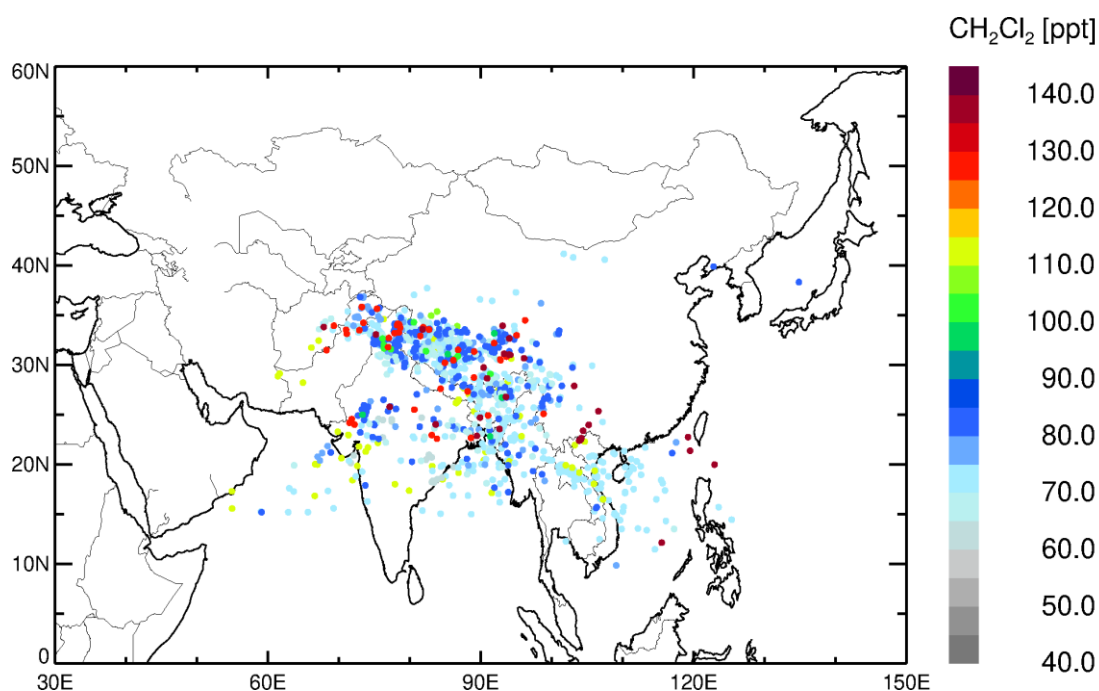


Figure 3.8: CLaMS model 15-day backward trajectories for each sample collected during AMA-17. The colour of these data points indicates the  $\text{CH}_2\text{Cl}_2$  mixing ratios in the air sample. The location of these data points shows the last location where the air was in the model boundary layer i.e. 2-3 km, ( $\zeta = 120$  K).

### 3.3.4 Equivalent Chlorine (ECI)

After analysing the individual VSLs, their contribution to the total equivalent chlorine (ECI) in the tropopause region was investigated. Table 3.2 shows two estimates of ECI, one estimate derived using a similar methodology to that used in the WMO 2018 report (Engel and Rigby et al., 2018) and the other estimate based on the air samples from AMA-17.

In the first method for calculating ECI, the tropospheric reference mixing ratios of the long-lived compounds were taken from NOAA (<https://www.esrl.noaa.gov/gmd/dv/ftpdata.html>). Similar to previous approaches (Laube et al., 2010b, 2013) either global mixing ratios were used, or in the case of compounds with significant tropospheric sinks such as HCFCs and methyl halides, data from the NOAA ground-based measurement sites at Mauna Loa (19.5°N, 155.6°W) and American Samoa (14.2°S, 170.6°W) in July-August 2017, the same time period as AMA-17, were used (Table 3.1). UEA measurements of air samples collected at Cape Grim, Tasmania, in early 2018 and shifted back in time by 6 months were used to complement this approach (Table 3.1). For the VSLs that are broken down rapidly in the troposphere and for which it is therefore much harder to estimate the proportion transported to the tropopause, the global estimates of tropospheric reference mixing ratios come from the WMO 2018 report for the Level of Zero Radiative Heating (LZRH) (Engel and Rigby et al., 2018)(Table 3.1). These mixing ratios of VSLs in the WMO 2018 report were based on results from the CAST, CONTRAST and ATTREX

aircraft campaigns that took place in the tropics in 2013 and 2014 (Engel and Rigby et al., 2018). They were used to investigate the differences between the tropics and the Asian monsoon input of VSLs in the lower stratosphere. It should be noted that some of the reported values were on different calibration scales to the measurements in this study which may cause small differences.

There are some ODSs that were considered in Engel and Rigby et al. (2018) but were not available from the AMA-17 samples:  $\text{CHClCCl}_2$ ,  $\text{CCl}_2\text{CCl}_2$ ,  $\text{CHBr}_3$ ,  $\text{CH}_2\text{BrCl}$ ,  $\text{CHBr}_2\text{Cl}$ ,  $\text{CHBrCl}_2$ , CFC-112, CFC-112a, HCFC-124, and Halon-2402. For these compounds, we used the same mixing ratios from Engel and Rigby et al. (2018) in both estimates to make them comparable (Table 3.1). The mixing ratio ranges provided by Engel and Rigby et al. (2018) were multiplied by the number of chlorine and bromine atoms in each compound, with the mixing ratios of the brominated compounds also multiplied by 60. In total, these compounds contribute 79-253 ppt to ECl.

For the global estimates of ECl, a potential temperature range of 355-365 K was used. This is the range of the tropical tropopause layer or the LZRH in the WMO 2018 report (Engel and Rigby et al., 2018). Air at this altitude is likely to continue to ascend into the lower tropical stratosphere by radiative heating. Some studies have suggested that the LZRH may be pushed upwards by the Asian summer monsoon as air from the troposphere rises, creating an elevated tropopause (e.g. Dunkerton, 1995; Highwood and Hoskins, 1998; Dethof et al., 1999; Ploeger et al., 2017). To take this into account, we used an increased potential temperature range of 355-375 K for estimates based on the AMA-17 air samples, which is also in agreement with the tropopause location indicated by our observations of gases with exclusively stratospheric sinks such as Halon-1211 (Figure 3.4). There were 27 samples collected in this range during AMA-17 and these were used to estimate the ECl. An ECl estimate for AMO-16 was not calculated as no air samples were collected in the tropopause region in this campaign (and far fewer samples were collected in general). Note that we did not consider ECl contributions from the breakdown products of VSLs in this study, so our ECl can be considered a lower limit of the total chlorine and bromine entering the stratosphere via the Asian summer monsoon anticyclone.

Table 3.2 shows that the total ECl from the monsoon aircraft campaign is higher than the total ECl from the global estimates based on Cape Grim, NOAA and WMO mixing ratios. However, the AMA-17-based ECl also has a wider range and the lower end of the range overlaps with the higher end of the range for the global estimate (Table 3.2). So there is not a significant difference between the overall ECl range estimates. This is due to many of our samples in the tropopause having higher mixing ratios of ODSs than in the previous global estimates while some samples also show mixing ratios in the range of the global estimates (Sections 3.3.1, 3.3.2).

The compounds contributing to the ECl were divided into four categories: very short-lived chlorine, very short-lived bromine, long-lived chlorine and long-lived bromine (Table 3.2). The estimates for the very short-lived bromine species both have a very large range but they mostly overlap. The long-lived chlorine in the AMA-17 samples is

slightly higher than the global estimate. This is because mixing ratios of the CFCs and carbon tetrachloride ( $\text{CCl}_4$ ) agree within our range, methyl chloroform ( $\text{CH}_3\text{CCl}_3$ ) is slightly smaller in the AMA-17 estimate, and HCFCs and methyl chloride ( $\text{CH}_3\text{Cl}$ ) are slightly larger. For the long-lived bromine species, the AMA-17 estimate is also slightly higher than the global estimate. Here, the halon mixing ratios agree with the AMA-17 estimate, so the higher long-lived bromine estimate for AMA-17 is almost completely due to methyl bromide ( $\text{CH}_3\text{Br}$ ) (6.5 - 6.8 ppt vs 7.4 - 9.1 ppt) indicating larger sources of methyl bromide in the monsoon input region.

Mixing ratios of very short-lived chlorine species are higher in the AMA-17 estimate than in the global estimate based on WMO 2018 mixing ratios at the LZRH. In the latter estimate very short-lived chlorine contributes about 2 to 3 % to the total ECl entering the stratosphere whereas in the AMA-17 estimate this is higher, 4 to 8 % of the total ECl. We note that the AMA-17 estimate is for a particular region and a particular time of year when there is likely to be a very high injection rate during the Asian monsoon (Leedham-Elvidge et al., 2015; Say et al., 2019). The WMO 2018 values are more representative of a global annual average and so the estimates based on this are lower. In both estimates very short-lived chlorine makes up a relatively small fraction of the total ECl in the tropopause region.

Using the results in Ploeger et al. (2017) we calculated that, averaged over the whole year, 5 % of the air in the Northern Hemispheric lower stratosphere comes from the Asian summer monsoon. If we assume that 5 % of the additional equivalent chlorine from the AMA-17 estimate ends up in the lower stratosphere of the Northern Hemisphere, this translated to an additional 0.3-34.9 ppt of ECl from all measured compounds, of which 1.6-15.2 ppt are from chlorinated VSLs. Total tropospheric chlorine from controlled substances has been decreasing by  $12.7 \pm 0.92$  ppt Cl yr<sup>-1</sup> and uncontrolled substances have been increasing by  $8.3 \pm 4.9$  ppt Cl yr<sup>-1</sup> leading to an overall decrease of  $4.4 \pm 4.1$  ppt Cl yr<sup>-1</sup> (Engel and Rigby et al., 2018). The decrease in chlorine has been partially offset by the increase in VSLs (Engel and Rigby et al., 2018). These current annual decreases are up to eight times smaller than the additional 0.3-34.9 ppt of equivalent chlorine we calculated. Although these elevated mixing ratios are only observed in one part of the atmosphere it indicates that the influence of the enhanced mixing ratios of the methyl halides as well as the very short-lived chlorine-containing ODSs is significant.

Table 3.2: Comparison of the global estimate of equivalent chlorine (ECI) based on Cape Grim, NOAA and WMO mixing ratios (see Table 3.1) and the regional estimate based on the air samples from AMA-17. <sup>1</sup>The percentage contribution of the very short-lived chlorine to the total ECI. <sup>2</sup>For the compounds that were not measured in this study the WMO 2018 reported values were used in both estimates. <sup>3</sup>ECI excluding compounds that were not measured in this study.

	<b>Global estimate ECI (ppt) 355 K – 365 K</b>	<b>AMA-17 ECI (ppt) 355 K – 375 K</b>
<b>Very short-lived chlorine</b>	<b>89-132 (2-3 %)<sup>1</sup></b>	<b>163-393 (4-8 %)<sup>1</sup></b>
CH <sub>2</sub> Cl <sub>2</sub>	59-89	130-272
CHCl <sub>3</sub>	19-24	24-74
CH <sub>2</sub> ClCH <sub>2</sub> Cl	10-19	9-47
<b>Very short-lived bromine</b>	<b>71-118</b>	<b>58-92</b>
CH <sub>2</sub> Br <sub>2</sub>	71-118	58-92
<b>Long-lived chlorine</b>	<b>3159-3186</b>	<b>3188-3356</b>
CFCs	1960	1939-1997
HCFCs	310	317-343
CH <sub>3</sub> CCl <sub>3</sub>	6.5	4.8-6.0
CCl <sub>4</sub>	321	321-338
CH <sub>3</sub> Cl	558-586	603-669
Halon-1211	3.4	3.4-3.5
<b>Long-lived bromine</b>	<b>789-811</b>	<b>842-963</b>
Halons	402	398-414
CH <sub>3</sub> Br	387-409	445-549
<b>Estimated (not measured)<sup>2</sup></b>	<b>79-253</b>	<b>79-253</b>
<b>Total Equivalent Chlorine (ECI)</b>	<b>4186-4499 (4107-4246)<sup>3</sup></b>	<b>4331-5057 (4252-4804)<sup>3</sup></b>

### 3.3.5 Mean age-of-air tracer comparison

The mean age-of-air derived from SF<sub>6</sub> measurements (henceforth SF<sub>6</sub> age) was compared to two other age-of-air tracers: C<sub>2</sub>F<sub>6</sub> and HFC-125. We found that SF<sub>6</sub> ages are generally older than C<sub>2</sub>F<sub>6</sub> and HFC-125 ages (Figure 3.9). C<sub>2</sub>F<sub>6</sub> and HFC-125 ages are similar and as these two compounds have very different tropospheric trends the good agreement supports the findings of Leedham Elvidge et al. (2018) that SF<sub>6</sub> age has a high bias and this bias increases with increasing mean age.

The extent of the bias was calculated by plotting the SF<sub>6</sub> ages against an average of the other two age-of-air tracers. For AMA-17 C<sub>2</sub>F<sub>6</sub> was only measured in 30 out of 94 samples so they were averaged with HFC-125 when available. Mean ages <-0.1 years

were excluded as significantly negative mean ages are considered to have substantial tropospheric influence and will bias the trend. For SF<sub>6</sub> ages on the x-axis and the two other tracers on the y-axis the AMO-16 linear regression was  $y = 0.818 (\pm 0.037) x - 0.069 (\pm 0.081)$  and the AMA-17 linear regression was  $y = 0.835 (\pm 0.024) x - 0.047 (\pm 0.047)$  (Figure 3.9) which is consistent with previous work (Leedham Elvidge et al., 2018). When calculating the EESC (Section 3.3.7) we used an adjusted SF<sub>6</sub> age average correction function of  $y = 0.817x + 0.092$  as the trend is based on a larger dataset and is within the slope uncertainty of our trend. The trend is based on a combination of polar and mid-latitude measurements from Leedham Elvidge et al. (2018) but excluding an aircraft campaign referred to as B34 as it took place more than 20 years ago and this study uses only recent data.

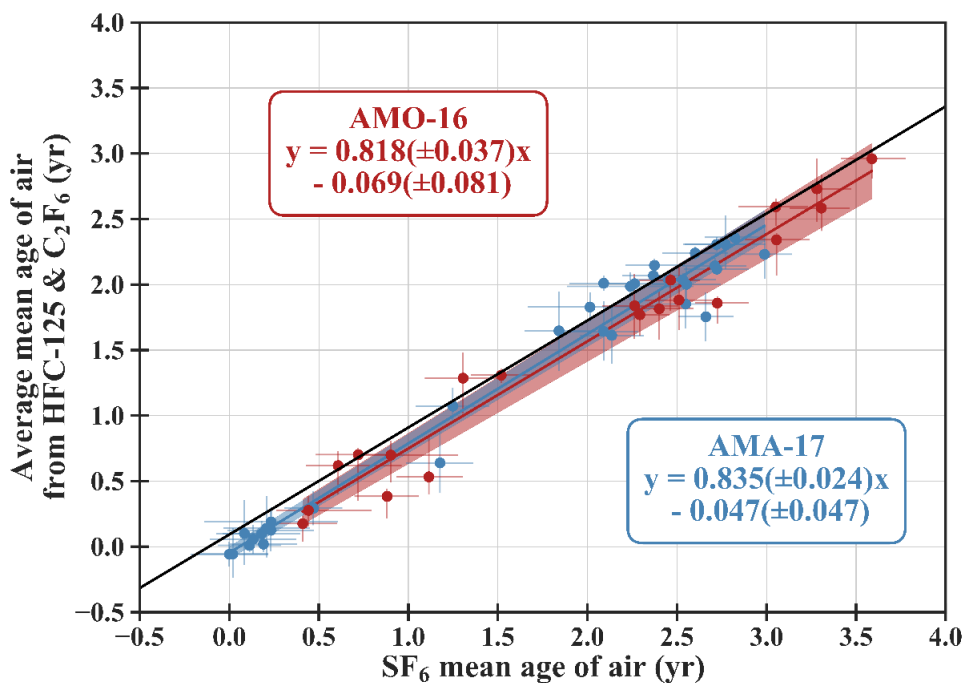


Figure 3.9: Comparison of mean age-of-air estimates with uncertainties from C<sub>2</sub>F<sub>6</sub>, HFC-125 and SF<sub>6</sub> for the AMO-16 and AMA-17 campaigns. Also shown is the trend line calculated for mid-latitudes using data from Leedham Elvidge et al. (2018) (black line).

### 3.3.6 Fractional Release Factors (FRFs)

Time-independent fractional release factors were calculated based on our aircraft samples. We used adjusted SF<sub>6</sub>-based mean ages-of-air calculated using the method in Leedham Elvidge et al. (2018) (Section 3.3.5). The highest mean age-of-air in AMA-17 was 2.4 years. Therefore FRFs were calculated for the AMO-16 and AMA-17 campaigns at 2.4 years and were compared to the FRFs for 2.4 years calculated from the FRF trends from mid-latitude stratospheric measurements in Leedham Elvidge et al. (2018) (Table 3.3). In AMO-16, the highest mean age-of-air was 3 years. Therefore,

FRFs were also calculated for this campaign at a mean age-of-air of 3 years and compared to other published FRFs at this more commonly used age (Table 3.3). FRFs for this study, Leedham Elvidge et al. (2018) and Engel et al. (2018) were calculated using the same method (Ostermüller et al., 2017). WMO 2014 and Laube et al. (2013) used a different method that did not take into account the dependence of the transit time distribution on the lifetime of the compound for which a FRF is calculated.

There is generally good agreement between the FRFs from the AMO-16 and AMA-17 campaigns and Leedham Elvidge et al. (2018). The FRFs for most of the compounds, except for  $\text{CCl}_4$  and  $\text{CH}_3\text{CCl}_3$ , agree within the uncertainties. The  $\text{CCl}_4$  FRFs in our study are lower than Leedham Elvidge et al. (2018) for both campaigns but the AMO-16  $\text{CCl}_4$  FRF mean age-of-air of 3 years does agree, within the uncertainties, with the  $\text{CCl}_4$  FRF in Engel et al. (2018). In the aircraft campaigns, the  $\text{CH}_3\text{CCl}_3$  FRF is lower than Leedham Elvidge et al. (2018), possibly due to influence from its rapidly decreasing tropospheric trend. There are now three datasets (this study, Leedham Elvidge et al. (2018) & Engel et al. (2018)) using a new method for FRFs and calculating time-independent fractional release factors. There is generally good agreement between their FRFs which supports the new method.

FRFs reported in Engel et al. (2018) are mostly very similar to the WMO 2014 FRFs. This is because Engel et al. (2018) used an equation to convert previously used FRFs from the WMO 2014 report into time-dependent FRFs which made very little difference to previous estimates as they were derived during a period with small tropospheric trends for most compounds (Engel et al., 2018). FRFs reported in Laube et al. (2013) are generally lower than those in the other studies, this is likely related to differences in the mean age estimates used (higher mean age from  $\text{SF}_6$  as has been shown in Leedham Elvidge et al., 2018).

Table 3.3: Comparison of FRFs at 2.4 years mean age-of-air and 3 years mean age-of-air between the AMO-16 campaign, the AMA-17 campaign, Leedham Elvidge et al. (2018), Engel et al. (2018), WMO 2014 and Laube et al. (2013). <sup>1</sup> The WMO 2018 report reported the same FRFs as the WMO 2014 report (Engel and Rigby et al., 2018). MLO/SMO: Calculated based on tropospheric trends from NOAA stations at Mauna Loa/American Samoa (Section 3.3.4).

	AMO-16	AMA-17	Leedham Elvidge et al. (2018)	AMO-16	Leedham Elvidge et al. (2018)	Engel et al. (2018)	WMO 2014 <sup>1</sup>	Laube et al. (2013)
Mean age-of-air	2.4	2.4	2.4	3	3	3	3	3
CCl <sub>4</sub>	0.44 (0.42-0.46)	0.45 (0.42-0.47)	0.57 (0.53-0.69)	0.58 (0.55-0.60)	0.76 (0.66-0.86)	0.56	0.56	0.42 (0.39-0.46)
CFC-11	0.36 (0.34-0.37)	0.38 (0.36-0.40)	0.36 (0.34-0.42)	0.48 (0.47-0.50)	0.47 (0.43-0.52)	0.47	0.47	0.35 (0.32-0.39)
CFC-113	0.23 (0.22-0.24)	0.26 (0.24-0.27)	0.22 (0.22-0.27)	0.32 (0.31-0.33)	0.3 (0.27-0.34)	0.3	0.29	0.22 (0.2-0.25)
CFC-113a	0.36 (0.24-0.48)	0.38 (0.27-0.48)		0.48 (0.36-0.60)				
CFC-115	0.04 (0.02-0.07)	0.04 (0.03-0.06)		0.06 (0.04-0.08)		0.07	0.04	
CFC-12	0.22 (0.21-0.23)	0.23 (0.22-0.23)	0.19 (0.18-0.24)	0.29 (0.28-0.30)	0.26 (0.23-0.3)	0.24	0.23	0.19 (0.16-0.21)
CH <sub>3</sub> Br (MLO)	0.41 (0.30-0.51)	0.39 (0.31-0.48)		0.52 (0.42-0.62)		0.6	0.6	
CH <sub>3</sub> Br (SMO)	0.43 (0.33-0.53)	0.41 (0.33-0.49)		0.56 (0.46-0.66)		0.6	0.6	
CH <sub>3</sub> CCl <sub>3</sub>	0.42 (0.39-0.45)	0.38 (0.35-0.42)	0.58 (0.51-0.6)	0.52 (0.49-0.55)	0.69 (0.64-0.75)	0.61	0.67	0.61 (0.56-0.65)
CH <sub>3</sub> Cl (MLO)	0.31 (0.25-0.38)	0.43 (0.38-0.48)		0.44 (0.38-0.50)		0.44	0.44	
CH <sub>3</sub> Cl (SMO)	0.31 (0.25-0.38)	0.42 (0.36-0.47)		0.44 (0.38-0.51)		0.44	0.44	
Halon-1211	0.53 (0.50-0.55)	0.56 (0.53-0.59)	0.53 (0.49-0.57)	0.68 (0.66-0.71)	0.66 (0.61-0.71)	0.65	0.62	0.52 (0.48-0.56)
Halon-1301	0.29 (0.27-0.31)	0.30 (0.28-0.33)	0.28 (0.28-0.34)	0.39 (0.37-0.41)	0.39 (0.35-0.43)	0.32	0.28	0.26 (0.24-0.29)
HCFC-133a	0.36 (0.23-0.49)	0.24 (0.11-0.37)		0.40 (0.27-0.53)				
HCFC-141b	0.26 (0.18-0.35)	0.27 (0.19-0.34)	0.22 (0.22-0.29)	0.35 (0.26-0.43)	0.31 (0.27-0.36)	0.34	0.34	0.17 (0.14-0.21)
HCFC-142b	0.11 (0.06-0.15)	0.10 (0.05-0.15)	0.1 (0.09-0.12)	0.14 (0.09-0.18)	0.13 (0.11-0.15)	0.17	0.17	0.05 (0.04-0.06)
HCFC-22	0.11 (0.04-0.18)	0.11 (0.05-0.17)	0.09 (0.09-0.12)	0.14 (0.07-0.21)	0.13 (0.11-0.15)	0.15	0.13	0.07 (0.05-0.08)
CFC-114	0.08 (0.07-0.09)	0.09 (0.07-0.10)		0.11 (0.10-0.12)		0.13	0.12	

CFC-114a	0.22 (0.20-0.23)	0.23 (0.21-0.24)		0.29 (0.28-0.30)				
CFC-13	0.04 (0.00-0.11)	0.04 (0.00-0.11)		0.06 (0.00-0.12)				
Halon-1202	0.57 (0.48-0.66)	0.57 (0.46-0.67)		0.69 (0.60-0.78)		0.67	0.62	

### 3.3.7 Equivalent Effective Stratospheric Chlorine (EESC)

EESC was calculated for a mean age-of-air of 3 years for AMO-16 as this is the mean age-of-air usually used in the literature to approximate mid-latitude ozone depletion. EESC was also calculated for a mean age-of-air of 2.4 years for both campaigns in order to compare the campaigns. The EESC was calculated using tropospheric trends from the same NOAA and Cape Grim data sets mentioned above (Section 3.3.4), an adjusted SF<sub>6</sub>-based mean age-of-air (Section 3.3.5) and mixing ratios from the aircraft samples to calculate time-independent FRFs (Section 3.3.6).

For both campaigns, EESC was calculated using both the ‘mean age EESC’ method used in Newman et al. (2007) and the ‘relevant age EESC’ method from Engel et al. (2018). This gives a total of four EESC estimates. Both methods were also used and compared in the WMO 2018 report (Engel and Rigby et al., 2018). The ‘relevant age EESC’ is a refinement in the calculation method of EESC. The mean age EESC assumes that the age spectrum for an inert species is representative of the age spectrum of a chemically reactive species. This is not the case as the average age-of-air for source gases that have been dissociated in the stratosphere is longer than the average age of inert tracers in the same stratospheric location (Plumb et al., 1999; Engel et al., 2018). Younger air contains more reactive species than older air so the organic fraction of a chemically active species is largely determined by the fraction of the air with shorter transit times (Plumb et al., 1999). To take into account the interaction between chemical loss and transit time, the relevant age EESC method uses new time-independent fractional release factors (Ostermüller et al., 2017) and an age spectrum weighted by chemical loss (Engel et al., 2018).

Additionally, each estimate has a range because of the relatively short lifetime of CH<sub>3</sub>Br and CH<sub>3</sub>Cl. The EESC contribution of these two compounds was calculated twice: again using tropospheric trends from Mauna Loa and American Samoa. The lower end of the range is based on Mauna Loa trends and the higher end of the range is based on American Samoa trends. Neither of these sites are ideal for estimates of the amount of shorter-lived ODSs reaching the tropical upper troposphere, but they are the closest ground-based approximations available and yield similar FRFs (Table 3.3).

The EESCs from this study were calculated using the same method used in Engel et al. (2018). However, there are some differences between our EESCs and the Engel et al. (2018) estimates:

1) The shifting of FRFs explained in Section 3.2.5 determined that for some species the mixing ratios observed near the tropopause were significantly lower (CFC-115, CH<sub>3</sub>CCl<sub>3</sub>) or higher (CFC-114a, HCFC-133a, Halon-1202, CH<sub>3</sub>Cl, CH<sub>3</sub>Br) than expected from surface-based trends. This is likely because the Asian monsoon region is different to the regions where the surface-based observations were made. Shifting the FRFs is necessary to make FRFs comparable with other values in the literature. The adjusted FRFs compare well with those from other studies (Section 3.3.6) in line with the expectation that they are dominated by common sinks and global tropospheric trends. The EESC, however, is calculated using the FRFs and the surface-based trends and so does not take into account that the actual amount found near the tropopause is different, which is important for deriving a regional EESC. Therefore, for the compounds that had their FRFs adjusted the difference was calculated using the amount that the FRF was shifted by multiplied by the mixing ratio at a mean age-of-air of zero years based on the tropospheric trends. These differences were then added to all our regional EESC estimates.

2) We included some minor compounds that Engel et al. (2018) did not include (CFC-113a, HCFC-133a and CFC-13). They also did not include CFC-114a but their CFC-114 mixing ratio is a combination of CFC-114 and CFC-114a. Therefore, to compare our EESC to Engel et al. (2018) we recalculated our EESC excluding CFC-113a, HCFC-133a and CFC-13. Including these species makes very little difference, it adds only ~1 ppt to the EESCs, well within the uncertainty of the estimate.

3) They included Halon-2402 and due to small contamination problems, this was not possible here. We determined the contribution of Halon-2402 to our EESC estimates using the 2017 mean tropospheric mixing ratio and the fractional release factor given in Engel et al. (2018), to arrive at an additional contribution of ~32 ppt from this molecule.

Table 3.4: Regional Equivalent Effective Stratospheric Chlorine (EESC) estimates from the AMO-16 and AMA-17 campaigns calculated using both the relevant age and the mean age. The numbers in brackets are the EESC without taking into account the difference in mixing ratios at the tropopause for long-lived compounds (see above). Also shown are global EESC estimates in previous literature (Velders and Daniel, 2014; Engel and Rigby et al., 2018).

Campaign	EESC <sup>a</sup>		EESC+VSLs <sup>b</sup>	
	relevant age	mean age	relevant age	mean age
<b>AMA-17</b> (age-of-air 2.4 years)	1630 – 1650 (1330 – 1350)	1685 – 1715 (1385 – 1415)	1804 – 2087 (1504 – 1787)	1859 – 2152 (1559 – 1852)
<b>AMO-16</b> (age-of-air 2.4 years)	1483 – 1495 (1267 – 1278)	1513 – 1528 (1297 – 1312)	1604 – 1692 (1387 – 1475)	1633 – 1725 (1417 – 1509)
<b>AMO-16</b> (age-of-air 3 years)	1861 – 1872 (1644 – 1655)	1903 – 1919 (1687 – 1703)	1988 – 2075 (1771 – 1859)	2030 – 2122 (1814 – 1906)
<b>Engel et al. (2018)</b> (age-of-air 3 years)	1646 (in 2017)	1602 (in 2017)	–	–
<b>Velders and Daniel, (2014)</b> (age-of-air 3 years)	–	1659 (1540-1790) (projection for 2016) 1647 (1527-1779) (projection for 2017)	–	–

<sup>a</sup> EESC including CFC-13, CFC-113a, HCFC-133a and Halon-2402.

<sup>b</sup> EESC+VSLs: EESC<sup>a</sup> with an additional contribution from very short-lived substances (VSLs).

At an age-of-air of 2.4 years both the relevant age-based EESC and the mean age-based EESC are more than 100 ppt lower in AMO-16 than in AMA-17. This is likely because during AMO-16 different types of air masses were sampled: outflow from the Asian monsoon and Northern Hemispheric extra-tropical air. It implies that, if it was measured, the EESC above the Asian monsoon at an age-of-air of 3 years may be much higher than the Engel et al. (2018) EESC estimate.

Engel et al. (2018) reported 2017 relevant age-based EESC for mid-latitudes as 1646 ppt and for mean age-based EESC as 1602 ppt. In Engel and Rigby et al. (2018) the reported early 2017 relevant age-based EESC for mid-latitudes was 1649 ppt and for mean age-based EESC was 1601 ppt. For AMO-16 the relevant age-based EESC is 12 % higher and the mean age-based EESC is 16 % higher than the Engel et al. (2018) estimates for air of the same age. We also compared the AMO-16 EESC to Velders and Daniels (2014) estimates for 2016 and 2017. These EESCs are calculated using the mean age-based EESC method so they are compared to our mean age-based AMO-16 estimate. The estimate is 13-14 % higher than the Velders and Daniels (2014) best estimate in 2016. Overall, the regional EESCs in our study are higher than EESCs in other studies.

Including the adjustment as explained above increases AMO-16 EESC by 216 ppt and AMA-17 by 300 ppt. If the adjustment is not included then the AMO-16 relevant age-based EESC agrees within our range with the Engel et al. (2018) estimate and the mean age-based EESC AMO-16 is 5-6 % higher than the Engel et al. (2018) estimate. Also, if the adjustment is not included then the mean age-based AMO-16 agrees within the uncertainties with the Velders and Daniels (2014) estimates, although, their best estimates are lower than our range (Table 3.4).

In both campaigns, using the relevant age gives a slightly lower EESC range than the mean age (Table 3.4). This is not the case in Engel et al. (2018) where the relevant age gives a higher EESC than the mean age in 2017. When using our measurements, the differences between relevant age-based EESC and mean age-based EESC are larger at higher potential temperatures. Above about 390 K the compounds that tend to be higher in the mean age-based EESC are CFC-11, CCl<sub>4</sub>, CFC-113, CFC-12, CH<sub>3</sub>Br, CH<sub>3</sub>CCl<sub>3</sub>, and Halon-1211. Whereas CFC-113a, CFC-115, Halon-1301, HCFC-133a, HCFC-141b, HCFC-142b, HCFC-22 and CFC-114a tend to be higher in the relevant age-based EESC. The compounds that contribute the most to EESC are CFC-11, CFC-12, CH<sub>3</sub>Cl, CH<sub>3</sub>Br, CCl<sub>4</sub> and Halon-1211. Together they account for more than half of the EESC. The compounds that are higher in the mean age-based EESC than in the relevant age-based EESC by the largest amount are CFC-11, CFC-12, CH<sub>3</sub>Br, CCl<sub>4</sub>, and Halon-1211.

Compounds with an increasing tropospheric trend tend to have a higher relevant age, while those with a decreasing tropospheric trend tend to have a higher mean age. One contributing factor to this is that relevant age assumes that younger air inside an air mass has more of an influence on total chlorine and bromine than older air in the air mass (Engel et al., 2018). This would shift compounds with a decreasing (increasing) tropospheric trend towards lower (higher) mixing ratios and therefore may explain the differences between this study and Engel et al. (2018). Engel et al. (2018) use tropospheric trends from Velders and Daniels (2014) which included projections into the future. In our study measured mixing ratios are used so there are some differences. Velders and Daniels (2014) use a larger increasing trend in HCFC-22, HCFC-141b and HCFC-142b tropospheric mixing ratios than in our study. This would make the relevant age of these HCFCs larger than the mean age, whereas our HCFCs relevant age is still larger than the mean age but not by as much. Also, the contribution of these HCFCs to total EESC will be larger in Velders and Daniels (2014) than in our study as they use higher HCFC mixing ratios.

Additionally, our CFC-11 and CCl<sub>4</sub> tropospheric mixing ratio trends are not decreasing as quickly as in Velders and Daniels (2014) so our relevant age CFC-11 and CCl<sub>4</sub> are still lower than the mean age but not by as much as in Engel et al. (2018). However, as Engel et al. (2018) use lower mixing ratios of CFC-11 and CCl<sub>4</sub>, the contributions of those compounds to the total EESC will be smaller in Engel et al. (2018) and will, therefore, have less impact on the difference between relevant age and mean age. These differences in tropospheric trends may explain why Engel et al. (2018) found mean age

lower than relevant age in 2017 but it swaps around in our study where the mean age is higher than the relevant age.

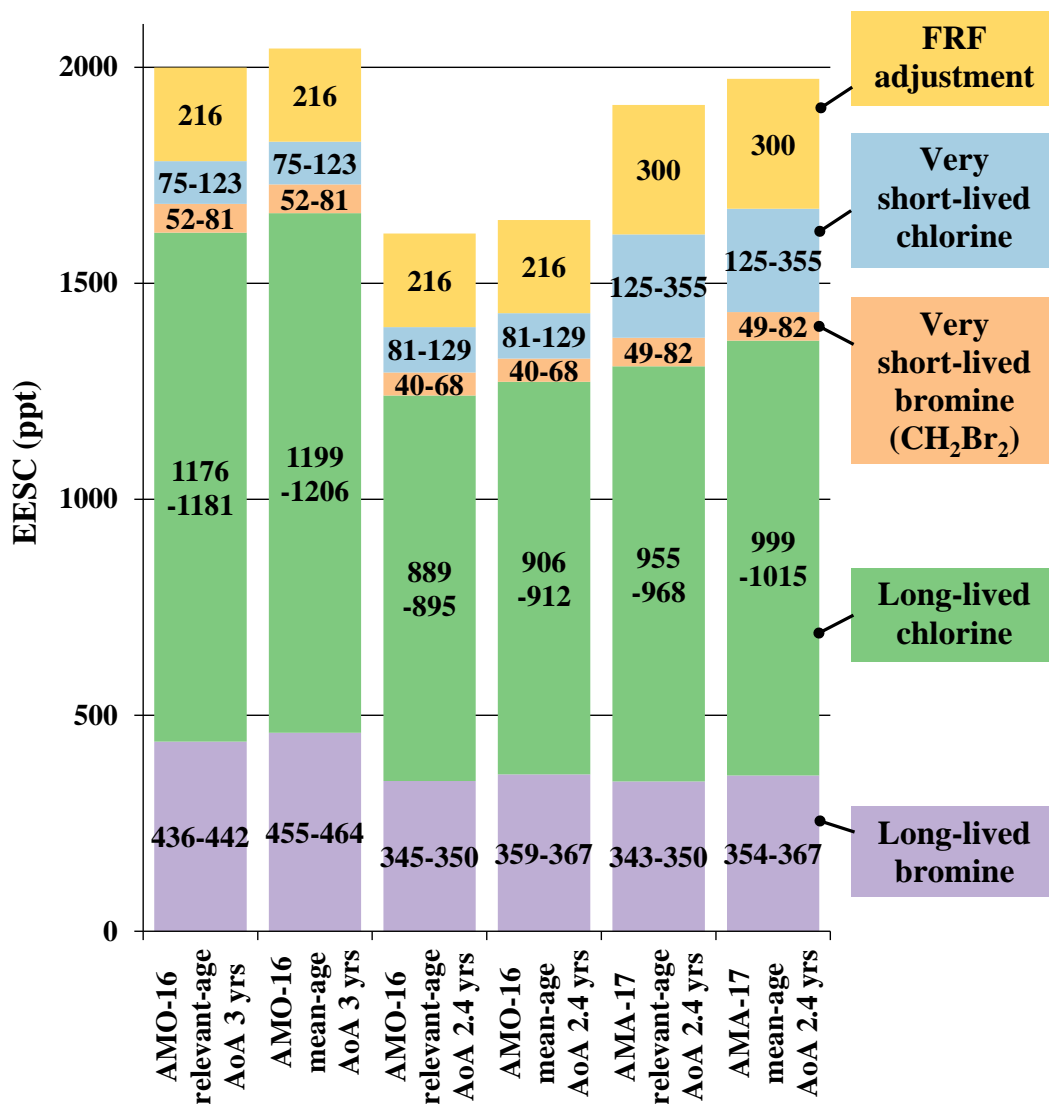


Figure 3.10: EESC at mean age-of-air of 2.4 years for the AMO-16 and AMA-17 campaigns and at mean age-of-air of 3 years for the AMO-16 campaign, calculated using relevant age and mean age, showing the contributions from long-lived (including FRF adjustments) and very short-lived chlorine and bromine. AoA = age-of-air.

To investigate the impact of VSLs on lower stratospheric ozone depletion, an EESC contribution for these substances was calculated. For the four VSLs we measured, the mixing ratios in the samples collected above 375 K were subtracted from the maximum and minimum mixing ratios below 375 K to approximate FRFs, which were then used to estimate the contribution of our VSLs to EESC. The EESC contribution at 2.4 years

mean age-of-air from our VSLs is between 121-197 ppt based on the air samples collected during AMO-16 and 174-437 ppt based on the air samples collected during AMA-17 (Figure 3.10). This is about 8-26 % of the EESC from long-lived compounds (Figure 3.10). When using the minimum VSLs contribution and the minimum of the long-lived EESC in AMO-16 the contribution is 8 % and when using the maximum VSLs contribution and the maximum of the long-lived EESC in AMA-17 the contribution is 26 %. This inclusion increases both the EESC and its range (Table 3.4) and indicates that the contribution of VSLs to ozone depletion is significant, especially in the northern hemispheric lower stratosphere where there is less fractional release of reactive chlorine from the longer-lived species. Moreover, the total EESC contribution from these VSLs may be higher than our estimate as some fraction of the halogenated ‘product gases’ from their tropospheric breakdown may also be injected in to the stratosphere (‘product gas injection’ is discussed in Engel and Rigby et al., 2018). There are also other VSLs not measured in this study that may contribute (e.g.  $\text{CHBr}_3$ ,  $\text{CH}_3(\text{CH}_2)_2\text{Br}$  and other anthropogenic chlorocarbons).

Assuming a linear trend, EESC at mid-latitudes has decreased by 14-16 ppt per year from its peak values to 2017 (Engel and Rigby et al., 2018). This shows that the contribution from VSLs observed in measurements from both campaigns is large compared to the size of the decreasing trend.

### 3.4 Conclusions

Air samples collected in the upper troposphere and lower stratosphere on board the high-altitude Geophysica research aircraft in the vicinity of and within the Asian monsoon anticyclone were found to have substantially elevated mixing ratios of very short-lived chlorine-containing ozone-depleting substances compared to WMO 2018 estimates for the year 2016 (Engel and Rigby et al., 2018). For example,  $\text{CH}_2\text{Cl}_2$  mixing ratios in the tropopause region are 30-44 ppt in the WMO 2018 report but 65-136 ppt in the AMA-17 samples. This is likely largely due to the rapid transport of emissions of these substances from South Asia to the UTLS via the Asian summer monsoon circulation and higher-than-global emission rates in this region. We show that VSLs are transported irreversibly from the Asian summer monsoon circulation system into the lower stratosphere where they will contribute to ozone depletion. The contribution of very short-lived chlorine-containing substances is significantly higher than that reported in the WMO Scientific Assessment of Ozone Depletion (Engel and Rigby et al., 2018) in terms of Equivalent Chlorine (ECl) in the tropopause region (89-132 ppt vs 169-393 ppt). These additional VSL contributions increase the estimate of Equivalent Effective Stratospheric Chlorine (EESC) in the lower stratosphere above the Asian summer monsoon region by 8-26 %.

Our estimates of ECl and EESC from long-lived species in the stratosphere in this region are generally larger than global average values. For example, EESC based on relevant age at 3 years in Engel et al. (2018) is 1646 ppt, whereas the AMO-16-based range is 1861-1872 ppt. ECl from long-lived species is 3947-3997 ppt in the global

estimate and 4031-4319 ppt in the AMA-17 estimate. The Asian monsoon region generally has large continental emissions and more input into the stratosphere than many other regions. This explains why the AMA-17 estimate is larger than the global average from WMO as it is impacted by regional chlorine-containing emissions to a larger degree than global mean estimates.

The tropics are the main entrance region to the stratosphere associated with the large-scale Brewer-Dobson circulation. Transport via the Asian summer monsoon circulation system provides an additional seasonal source into the stratosphere, especially the northern hemispheric lower stratosphere (Orbe et al., 2016; Ploeger et al., 2017), where ozone levels have not been recovering as expected (Ball et al., 2018). A previous study found similar enhanced mixing ratios of  $\text{CH}_2\text{Cl}_2$ ,  $\text{CH}_2\text{ClCH}_2\text{Cl}$  and  $\text{CHCl}_3$  in the upper tropopause region during boreal winter over South-East Asia, indicating that rapid upward transport also occurs in the winter monsoon (Oram et al., 2017). The additional input of chlorine into the stratosphere from these sources could delay the recovery of the ozone layer if emissions of VSLs persist in the future (Hossaini et al., 2015a). Since our observations are both spatially and temporally limited the quantification of this possible future impact is beyond the scope of this study.

However, when combining the differences between the global ECl estimate and our AMA-17-based ECl (Table 3.2) with the estimate from Ploeger et al. (2017) of the monsoon contributing an annual average of about 5 % to northern hemispheric lower stratospheric air, we derive a difference ranging from 0.3-34.9 ppt of ECl, from all measured compounds, much of it in the form of chlorinated VSLs. Depending on the inter-annual monsoon variability as well as how much ECl enters this part of the stratosphere via the tropical west pacific and through extratropical isentropic transport, the available levels of chlorine and bromine might thus be substantially higher than the global average derived from global ground-based measurements. Independent evidence pointing in the direction of such a possibility has most recently been found by Harrison et al. (2019) who, based on satellite observations, reported unusually high levels of phosgene ( $\text{COCl}_2$ ) in the stratosphere, a product gas of the photochemical decomposition of  $\text{CH}_2\text{Cl}_2$ ,  $\text{CHCl}_3$  and other gases. In summary, this work highlights the importance of both the Asian monsoon anticyclone as a fast transport mechanism in an important ODS emission region, and the role of chlorinated VSLs for stratospheric ozone.

### **Acknowledgements**

We are grateful for the contributions of Michel Bolder and the Geophysica team (sample collection and campaign organisation), Guus Velders and Andreas Engel (EESC comparisons), Elinor Tuffnell (data processing) and the NOAA Global Monitoring Division (surface halocarbon data). We thank the staff at the Cape Grim station and at CSIRO GASLAB Aspendale for collecting and maintaining the Cape Grim air archive and preparing the UEA flasks and sub-samples. We also acknowledge CSIRO and the Bureau of Meteorology for funding these activities. The StratoClim

flights were funded by the European Commission (FP7 project StratoClim-603557, [www.stratoclim.org](http://www.stratoclim.org)). This work was supported by the Natural Environment Research Council through the EnvEast Doctoral Training Partnership (grant number NE/L002582/1) as well as the ERC project EXC<sup>3</sup>ITE (EXC3ITE-678904-ERC-2015-STG). Johannes C. Laube received funding from the UK Natural Environment Research Council (Research Fellowship NE/I021918/1).

## References

- Andrews, A. E., Boering, K. A., Daube, B. C., Wofsy, S. C., Loewenstein, M., Jost, H., Podolske, J. R., Webster, C. R., Herman, R. L., Scott, D. C., Flesch, G. J., Moyer, E. J., Elkins, J. W., Dutton, G. S., Hurst, D. F., Moore, F. L., Ray, E. A., Romashkin, P. A. and Strahan, S. E.: Mean ages of stratospheric air derived from in situ observations of CO<sub>2</sub>, CH<sub>4</sub>, and N<sub>2</sub>O, *J. Geophys. Res. Atmos.*, 106(D23), 32295–32314, doi:10.1029/2001JD000465, 2001.
- Annamalai, H. and Slingo, J. M.: Active / break cycles: diagnosis of the intraseasonal variability of the Asian Summer Monsoon, *Clim. Dyn.*, 18(1–2), 85–102, doi:10.1007/s003820100161, 2001.
- Ball, W. T., Alsing, J., Mortlock, D. J., Staehelin, J., Haigh, J. D., Peter, T., Tummon, F., Stübi, R., Stenke, A., Anderson, J., Bourassa, A., Davis, S. M., Degenstein, D., Frith, S., Froidevaux, L., Roth, C., Sofieva, V., Wang, R., Wild, J., Yu, P., Ziemke, J. R. and Rozanov, E. V: Evidence for a continuous decline in lower stratospheric ozone offsetting ozone layer recovery, *Atmos. Chem. Phys.*, 18(2), 1379–1394, doi:10.5194/acp-18-1379-2018, 2018.
- Brioude, J., Portmann, R. W., Daniel, J. S., Cooper, O. R., Frost, G. J., Rosenlof, K. H., Granier, C., Ravishankara, A. R., Montzka, S. A. and Stohl, A.: Variations in ozone depletion potentials of very short-lived substances with season and emission region, *Geophys. Res. Lett.*, 37(19), 3–7, doi:10.1029/2010GL044856, 2010.
- Brunamonti, S., Jorge, T., Oelsner, P., Hanumanthu, S., Singh, B. B., Kumar, K. R., Sonbawne, S., Meier, S., Singh, D., Wienhold, F. G., Luo, B. P., Böettcher, M., Poltera, Y., Jauhiainen, H., Kayastha, R., Karmacharya, J., Dirksen, R., Naja, M., Rex, M., Fadnavis, S., and Peter, T.: Balloon-borne measurements of temperature, water vapor, ozone and aerosol backscatter on the southern slopes of the Himalayas during StratoClim 2016–2017, *Atmos. Chem. Phys.*, 18, 15937–15957, doi:10.5194/acp-18-15937-2018, 2018.
- Cairo, F., Pommereau, J. P., Law, K. S., Schlager, H., Garnier, A., Fierli, F., Ern, M., Streibel, M., Arabas, S., Borrmann, S., Berthelmer, J. J., Blom, C., Christensen, T., D’Amato, F., Di Donfrancesco, G., Deshler, T., Diedhiou, A., Durr, G., Engelsen, O., Goutail, F., Harris, N. R. P., Kerstel, E. R. T., Khaykin, S., Konopka, P., Kylling, A., Larsen, N., Lebel, T., Liu, X., MacKenzie, A. R., Nielsen, J., Oulanowski, A., Parker,

D. J., Pelon, J., Polcher, J., Pyle, J. A., Ravegnani, F., Rivi re, E. D., Robinson, A. D., R ckmann, T., Schiller, C., Sim es, F., Stefanutti, L., Stroh, F., Some, L., Siegmund, P., Sitnikov, N., Vernier, J. P., Volk, C. M., Voigt, C., Von Hobe, M., Viciani, S. and Yushkov, V.: An introduction to the SCOUT-AMMA stratospheric aircraft, balloons and sondes campaign in West Africa, August 2006: Rationale and roadmap, *Atmos. Chem. Phys.*, 10(5), 2237–2256, doi:10.5194/acp-10-2237-2010, 2010.

Chipperfield, M. P., Dhomse, S., Hossaini, R., Feng, W., Santee, M. L., Weber, M., Burrows, J. P., Wild, J. D., Loyola, D. and Coldewey-Egbers, M.: On the Cause of Recent Variations in Lower Stratospheric Ozone, *Geophys. Res. Lett.*, 45(11), 5718–5726, doi:10.1029/2018GL078071, 2018.

Claxton, T., Hossaini, R., Wilson, C., Montzka, S. A., Chipperfield, M. P., Wild, O., Bednarz, E. M., Carpenter, L. J., Andrews, S. J., Hackenberg, S. C., M hle, J., Oram, D., Park, S., Park, M. K., Atlas, E., Navarro, M., Schauffler, S., Sherry, D., Vollmer, M., Schuck, T., Engel, A., Krummel, P. B., Maione, M., Arduini, J., Saito, T., Yokouchi, Y., O’Doherty, S., Young, D. and Lunder, C.: A Synthesis Inversion to Constrain Global Emissions of Two Very Short Lived Chlorocarbons: Dichloromethane, and Perchloroethylene, *J. Geophys. Res. Atmos.*, 125(12), doi:10.1029/2019JD031818, 2020.

Dee, D. P., Uppala, S. M., Simmons, A. J., Berrisford, P., Poli, P., Kobayashi, S., Andrae, U., Balmaseda, M. A., Balsamo, G., Bauer, P., Bechtold, P., Beljaars, A. C. M., van de Berg, L., Bidlot, J., Bormann, N., Delsol, C., Dragani, R., Fuentes, M., Geer, A. J., Haimberger, L., Healy, S. B., Hersbach, H., H lm, E. V., Isaksen, L., K llberg, P., K hler, M., Matricardi, M., McNally, A. P., Monge-Sanz, B. M., Morcrette, J.-J., Park, B.-K., Peubey, C., de Rosnay, P., Tavolato, C., Th paut, J.-N. and Vitart, F.: The ERA-Interim reanalysis: configuration and performance of the data assimilation system, *Q. J. R. Meteorol. Soc.*, 137(656), 553–597, doi:10.1002/qj.828, 2011.

Dethof, A., O’Neill, A., Slingo, J. M. and Smit, H. G. J.: A mechanism for moistening the lower stratosphere involving the Asian summer monsoon, *Q. J. R. Meteorol. Soc.*, 125(556), 1079–1106, doi:10.1002/qj.1999.49712555602, 1999.

Dunkerton, T. J.: Evidence of meridional motion in the summer lower stratosphere adjacent to monsoon regions, *J. Geophys. Res.*, 100(D8), 16675–16688, doi:10.1029/95JD01263, 1995.

Engel, A., Strunk, M., M ller, M., Haase, H., Poss, C., Levin, I. and Schmidt, U.: Temporal development of total chlorine in the high-latitude stratosphere based on reference distributions of mean age derived from CO<sub>2</sub> and SF<sub>6</sub>, *J. Geophys. Res.*, 107(D12), ACH 1-1-ACH 1-11, doi:10.1029/2001JD000584, 2002.

Engel, A., B nisch, H., Osterm ller, J., Chipperfield, M. P., Dhomse, S. and J ckel, P.: A refined method for calculating equivalent effective stratospheric chlorine, *Atmos. Chem. Phys.*, 18(2), 601–619, doi:10.5194/acp-18-601-2018, 2018.

Engel, A., Rigby, M., (Lead Authors), Burkholder, J. B., Fernandez, R. P., Froidevaux,

- L., Hall, B. D., Hossaini, R., Saito, T., Vollmer, M. K. and Yao, B.: Chapter 1 Update on Ozone-Depleting Substances (ODSs) and Other Gases of Interest to the Montreal Protocol, in *Scientific Assessment of Ozone Depletion: 2018*, Global Ozone Research and Monitoring Project–Report No. 58, World Meteorological Organization, Geneva, Switzerland., 2018.
- Fang, X., Ravishankara, A. R., Velders, G. J. M., Molina, M. J., Su, S., Zhang, J., Hu, J. and Prinn, R. G.: Changes in Emissions of Ozone-Depleting Substances from China Due to Implementation of the Montreal Protocol, *Environ. Sci. Technol.*, 52(19), 11359–11366, doi:10.1021/acs.est.8b01280, 2018.
- Fang, X., Park, S., Saito, T., Tunnicliffe, R., Ganesan, A. L., Rigby, M., Li, S., Yokouchi, Y., Fraser, P. J., Harth, C. M., Krummel, P. B., Mühle, J., O’Doherty, S., Salameh, P. K., Simmonds, P. G., Weiss, R. F., Young, D., Lunt, M. F., Manning, A. J., Gressent, A. and Prinn, R. G.: Rapid increase in ozone-depleting chloroform emissions from China, *Nat. Geosci.*, 12(2), 89–93, doi:10.1038/s41561-018-0278-2, 2019.
- Garny, H. and Randel, W. J.: Dynamic variability of the Asian monsoon anticyclone observed in potential vorticity and correlations with tracer distributions, *J. Geophys. Res. Atmos.*, 118(24), 13421–13433, doi:10.1002/2013JD020908, 2013.
- Garny, H. and Randel, W. J.: Transport pathways from the Asian monsoon anticyclone to the stratosphere, *Atmos. Chem. Phys.*, 16, 2703–2718, doi:10.5194/acp-16-2703-2016, 2016.
- Harrison, J. J., Chipperfield, M. P., Hossaini, R., Boone, C. D., Dhomse, S., Feng, W. and Bernath, P. F.: Phosgene in the Upper Troposphere and Lower Stratosphere: A Marker for Product Gas Injection Due to Chlorine-Containing Very Short Lived Substances, *Geophys. Res. Lett.*, 46(2), 1032–1039, doi:10.1029/2018GL079784, 2019.
- Hersbach, H. and Dee, D.: ERA5 reanalysis is in production, *ECMWF Newsletter*, Vol. 147, p.7, 2016.
- Highwood, E. J. and Hoskins, B. J.: The tropical tropopause, *Q. J. R. Meteorol. Soc.*, 124(549), 1579–1604, doi:10.1002/qj.49712454911, 1998.
- Hoffmann, L., Günther, G., Li, D., Stein, O., Wu, X., Griessbach, S., Heng, Y., Konopka, P., Müller, R., Vogel, B. and Wright, J. S.: From ERA-Interim to ERA5: The considerable impact of ECMWF’s next-generation reanalysis on Lagrangian transport simulations, *Atmos. Chem. Phys.*, 19(5), 3097–3214, doi:10.5194/acp-19-3097-2019, 2019.
- Hossaini, R., Chipperfield, M. P., Montzka, S. A., Rap, A., Dhomse, S. and Feng, W.: Efficiency of short-lived halogens at influencing climate through depletion of stratospheric ozone, *Nat. Geosci.*, 8(3), 186–190, doi:10.1038/NGEO2363, 2015a.
- Hossaini, R., Chipperfield, M. P., Saiz-Lopez, A., Harrison, J. J., Von Glasow, R., Sommariva, R., Atlas, E., Navarro, M., Montzka, S. A., Feng, W., Dhomse, S., Harth, C., Mühle, J., Lunder, C., O’Doherty, S., Young, D., Reimann, S., Vollmer, M. K.,

- Krummel, P. B. and Bernath, P. F.: Growth in stratospheric chlorine from short-lived chemicals not controlled by the Montreal Protocol, *Geophys. Res. Lett.*, 42(11), 4573–4580, doi:10.1002/2015GL063783, 2015b.
- Hossaini, R., Patra, P. K., Leeson, A. A., Kryzstofiak, G., Abraham, N. L., Andrews, S. J., Archibald, A. T., Aschmann, J., Lidster, T., Wilson, C., Ziska, F. and Hossaini, R.: A multi-model intercomparison of halogenated very short-lived substances (TransCom-VSLS): linking oceanic emissions and tropospheric transport for a reconciled estimate of the stratospheric source gas injection of bromine, *Atmos. Chem. Phys.*, 16, 9163–9187, doi:10.5194/acp-16-9163-2016, 2016.
- Hossaini, R., Atlas, E., Dhomse, S. S., Chipperfield, M. P., Bernath, P. F., Fernando, A. M., Mühle, J., Leeson, A. A., Montzka, S. A., Feng, W., Harrison, J. J., Krummel, P., Vollmer, M. K., Reimann, S., O'Doherty, S., Young, D., Maione, M., Arduini, J. and Lunder, C. R.: Recent Trends in Stratospheric Chlorine from Very Short-Lived Substances, *J. Geophys. Res. Atmos.*, doi:10.1029/2018JD029400, 2019.
- Kaiser, J., Engel, A., Borchers, R. and Röckmann, T.: Probing stratospheric transport and chemistry with new balloon and aircraft observations of the meridional and vertical N<sub>2</sub>O isotope distribution, *Atmos. Chem. Phys.*, 6(11), 3535–3556, doi:10.5194/acp-6-3535-2006, 2006.
- Kim, J., Li, S., Kim, K. R., Stohl, A., Mühle, J., Kim, S. K., Park, M. K., Kang, D. J., Lee, G., Harth, C. M., Salameh, P. K. and Weiss, R. F.: Regional atmospheric emissions determined from measurements at Jeju Island, Korea: Halogenated compounds from China, *Geophys. Res. Lett.*, 37(12), 2007–2011, doi:10.1029/2010GL043263, 2010.
- Konopka, P., Ploeger, F. and Müller, R.: Entropy-based and static stability based Lagrangian model grids, in: *Lagrangian Modeling of the Atmosphere*, Geophysical Monograph Series, 200, AGU Chapman Conference on Advances in Lagrangian Modeling of the Atmosphere, Grindelwald, Switzerland, 9–14 Octo., 2012.
- Laube, J. C., Engel, A., Bönisch, H., Möbius, T., Worton, D. R., Sturges, W. T., Grunow, K. and Schmidt, U.: Contribution of very short-lived organic substances to stratospheric chlorine and bromine in the tropics – a case study, *Atmos. Chem. Phys.*, 8(23), 7325–7334, doi:10.5194/acp-8-7325-2008, 2008.
- Laube, J. C., Martinerie, P., Witrant, E., Blunier, T., Schwander, J., Brenninkmeijer, C. A. M., Schuck, T. J., Bolder, M., Röckmann, T., Van Der Veen, C., Bönisch, H., Engel, A., Mills, G. P., Newland, M. J., Oram, D. E., Reeves, C. E. and Sturges, W. T.: Accelerating growth of HFC-227ea (1,1,1,2,3,3,3- heptafluoropropane) in the atmosphere, *Atmos. Chem. Phys.*, 10(13), 5903–5910, doi:10.5194/acp-10-5903-2010, 2010a.
- Laube, J. C., Engel, A., Bönisch, H., Möbius, T., Sturges, W. T., Braß, M. and Röckmann, T.: Fractional release factors of long-lived halogenated organic compounds in the tropical stratosphere, *Atmos. Chem. Phys.*, 10(3), 1093–1103, doi:10.5194/acp-10-1093-2010, 2010b.

- Laube, J. C., Keil, A., Bönisch, H., Engel, A., Röckmann, T., Volk, C. M. and Sturges, W. T.: Observation-based assessment of stratospheric fractional release, lifetimes, and ozone depletion potentials of ten important source gases, *Atmos. Chem. Phys.*, 13(5), 2779–2791, doi:10.5194/acp-13-2779-2013, 2013.
- Laube, J. C., Mohd Hanif, N., Martinerie, P., Gallacher, E., Fraser, P. J., Langenfelds, R., Brenninkmeijer, C. A. M., Schwander, J., Witrant, E., Wang, J.-L., Ou-Yang, C.-F., Gooch, L. J., Reeves, C. E., Sturges, W. T. and Oram, D. E.: Tropospheric observations of CFC-114 and CFC-114a with a focus on long-term trends and emissions, *Atmos. Chem. Phys.*, 16(23), 15347–15358, doi:10.5194/acp-16-15347-2016, 2016.
- Leedham Elvidge, E. C., Oram, D. E., Laube, J. C., Baker, A. K., Montzka, S. A., Humphrey, S., O’Sullivan, D. A. and Brenninkmeijer, C. A. M.: Increasing concentrations of dichloromethane, CH<sub>2</sub>Cl<sub>2</sub>, inferred from CARIBIC air samples collected 1998-2012, *Atmos. Chem. Phys.*, 15(4), 1939–1958, doi:10.5194/acp-15-1939-2015, 2015.
- Leedham Elvidge, E., Bönisch, H., Brenninkmeijer, C. A. M., Engel, A., Fraser, P. J., Gallacher, E., Langenfelds, R., Mühle, J., Oram, D. E., Ray, E. A., Ridley, A. R., Röckmann, T., Sturges, W. T., Weiss, R. F. and Laube, J. C.: Evaluation of stratospheric age of air from CF<sub>4</sub>, C<sub>2</sub>F<sub>6</sub>, C<sub>3</sub>F<sub>8</sub>, CHF<sub>3</sub>, HFC-125, HFC-227ea and SF<sub>6</sub>; implications for the calculations of halocarbon lifetimes, fractional release factor, *Atmos. Chem. Phys.*, 18(5), 3369–3385, doi:10.5194/acp-18-3369-2018, 2018.
- Li, D., Vogel, B., Müller, R., Bian, J., Günther, G., Plöger, F., Li, Q., Zhang, J., Bai, Z. and Riese, M.: Dehydration and low ozone in the tropopause layer over the Asian monsoon caused by tropical cyclones: Lagrangian transport calculations using ERA-Interim and ERA5 reanalyses data, *Atmos. Chem. Phys.*, 20, 4133–4152, doi:10.5194/acp-20-4133-2020, 2020.
- Li, Q., Jiang, J. H., Wu, D. L., Read, W. G., Livesey, N. J., Waters, J. W., Zhang, Y., Wang, B., Filipiak, M. J., Davis, C. P., Turquety, S., Wu, S., Park, R. J., Yantosca, R. M. and Jacob, D. J.: Convective outflow of South Asian pollution: A global CTM simulation compared with EOS MLS observations, *Geophys. Res. Lett.*, 32(14), 1–4, doi:10.1029/2005GL022762, 2005.
- Lunt, M. F., Park, S., Li, S., Henne, S., Manning, A. J., Ganesan, A. L., Simpson, I. J., Blake, D. R., Liang, Q., O’Doherty, S., Harth, C. M., Mühle, J., Salameh, P. K., Weiss, R. F., Krummel, P. B., Fraser, P. J., Prinn, R. G., Reimann, S. and Rigby, M.: Continued Emissions of the Ozone-Depleting Substance Carbon Tetrachloride From Eastern Asia, *Geophys. Res. Lett.*, 45(20), 11,423-11,430, doi:10.1029/2018GL079500, 2018.
- McCulloch, A.: Dichloromethane in the environment, A note prepared for the European Chlorinated Solvents Association (ECSA) and the Halogenated Solvents Industry Alliance (HSIA), 9th November 2017. [online] Available from: [http://www.chlorinated-solvents.eu/images/Documents/Newsroom/Dichloromethane paper.pdf](http://www.chlorinated-solvents.eu/images/Documents/Newsroom/Dichloromethane%20paper.pdf) (Accessed 19 February 2018), 2017.

- McKenna, D. S.: A new Chemical Lagrangian Model of the Stratosphere (CLaMS) 1. Formulation of advection and mixing, *J. Geophys. Res.*, 107(D16), Pages ACH 15-1-ACH 15-15, doi:10.1029/2000JD000114, 2002.
- Newman, P. A., Daniel, J. S., Waugh, D. W. and Nash, E. R.: A new formulation of equivalent effective stratospheric chlorine (EESC), *Atmos. Chem. Phys.*, 7(17), 4537–4552, doi:10.5194/acp-7-4537-2007, 2007.
- Oram, D. E., Ashfold, M. J., Laube, J. C., Gooch, L. J., Humphrey, S., Sturges, W. T., Leedham-Elvidge, E., Forster, G. L., Harris, N. R. P., Mead, M. I., Samah, A. A., Phang, S. M., Ou-Yang, C.-F., Lin, N.-H., Wang, J.-L., Baker, A. K., Brenninkmeijer, C. A. M. and Sherry, D.: A growing threat to the ozone layer from short-lived anthropogenic chlorocarbons, *Atmos. Chem. Phys.*, 17(19), 11929–11941, doi:10.5194/acp-17-11929-2017, 2017.
- Orbe, C., Waugh, D. W. and Newman, P. A.: Air-mass origin in the tropical lower stratosphere: The influence of Asian boundary layer air, *Geophys. Res. Lett.*, 42(10), 4240–4248, doi:10.1002/2015GL063937, 2015.
- Orbe, C., Waugh, D. W., Newman, P. A. and Steenrod, S.: The transit-time distribution from the northern hemisphere midlatitude surface, *J. Atmos. Sci.*, 73(10), 3785–3802, doi:10.1175/JAS-D-15-0289.1, 2016.
- Ostermüller, J., Bönisch, H., Jöckel, P. and Engel, A.: A new time-independent formulation of fractional release, *Atmos. Chem. Phys.*, 17(6), 3785–3797, doi:10.5194/acp-17-3785-2017, 2017.
- Pan, L. L., Honomichl, S. B., Kinnison, D. E., Abalos, M., Randel, W. J., Bergman, J. W. and Bian, J.: Transport of chemical tracers from the boundary layer to stratosphere associated with the dynamics of the asian summer monsoon, *J. Geophys. Res. Atmos.*, 121(23), 14,159-14,174, doi:10.1002/2016JD025616, 2016.
- Park, M., Randel, W. J., Gettelman, A., Massie, S. T. and Jiang, J. H.: Transport above the Asian summer monsoon anticyclone inferred from Aura Microwave Limb Sounder tracers, *J. Geophys. Res. Atmos.*, 112(D16), 1–13, doi:10.1029/2006JD008294, 2007.
- Park, M., Randel, W. J., Emmons, L. K., Bernath, P. F., Walker, K. A. and Boone, C. D.: Chemical isolation in the Asian monsoon anticyclone observed in Atmospheric Chemistry Experiment (ACE-FTS) data, *Atmos. Chem. Phys.*, 8(3), 757–764, doi:10.5194/acp-8-757-2008, 2008.
- Park, M., Randel, W. J., Emmons, L. K. and Livesey, N. J.: Transport pathways of carbon monoxide in the Asian summer monsoon diagnosed from Model of Ozone and Related Tracers (MOZART), *J. Geophys. Res. Atmos.*, 114(D8), 1–11, doi:10.1029/2008JD010621, 2009.
- Ploeger, F., Konopka, P., Günther, G., Groß, J.-U. and Müller, R.: Impact of the vertical velocity scheme on modeling transport in the tropical tropopause layer, *J. Geophys. Res.*, 115(D3), 1–14, doi:10.1029/2009JD012023, 2010.

- Ploeger, F., Gottschling, C., Griessbach, S., Groß, J.-U., Guenther, G., Konopka, P., Müller, R., Riese, M., Stroh, F., Tao, M., Ungermann, J., Vogel, B. and von Hobe, M.: A potential vorticity-based determination of the transport barrier in the Asian summer monsoon anticyclone, *Atmos. Chem. Phys.*, 15(22), 13145–13159, doi:10.5194/acp-15-13145-2015, 2015.
- Ploeger, F., Konopka, P., Walker, K. and Riese, M.: Quantifying pollution transport from the Asian monsoon anticyclone into the lower stratosphere, *Atmos. Chem. Phys.*, 17(11), 7055–7066, doi:10.5194/acp-17-7055-2017, 2017.
- Plumb, I. C., Vohralik, P. F. and Ryan, K. R.: Normalization of correlations for atmospheric species with chemical loss, *J. Geophys. Res. Atmos.*, 104(D9), 11723–11732, doi:10.1029/1999JD900014, 1999.
- Pommrich, R., Müller, R., Groß, J.-U., Konopka, P., Ploeger, F., Vogel, B., Tao, M., Hoppe, C. M., Günther, G., Spelten, N., Hoffmann, L., Pumphrey, H.-C., Viciani, S., D’amato, F., Volk, C. M., Hoor, P., Schlager, H. and Riese, M.: Tropical troposphere to stratosphere transport of carbon monoxide and long-lived trace species in the Chemical Lagrangian Model of the Stratosphere (CLaMS), *Geosci. Model Dev.*, 7, 2895–2916, doi:10.5194/gmd-7-2895-2014, 2014.
- Randel, W. J. and Park, M.: Deep convective influence on the Asian summer monsoon anticyclone and associated tracer variability observed with Atmospheric Infrared Sounder (AIRS), *J. Geophys. Res. Atmos.*, 111(12), 1–13, doi:10.1029/2005JD006490, 2006.
- Randel, W. J., Park, M., Emmons, L., Kinnison, D., Bernath, P., Walker, K. A., Boone, C. and Pumphrey, H.: Asian monsoon transport of pollution to the stratosphere, *Science.*, 328(5978), 611–613, doi:10.1126/science.1182274, 2010.
- Say, D., Ganesan, A. L., Lunt, M. F., Rigby, M., O’Doherty, S., Harth, C., Manning, A. J., Krummel, P. B. and Bauguitte, S.: Emissions of halocarbons from India inferred through atmospheric measurements, *Atmos. Chem. Phys.*, 19(15), 9865–9885, doi:10.5194/acp-19-9865-2019, 2019.
- Tissier, A.-S. and Legras, B.: Convective sources of trajectories traversing the tropical tropopause layer, *Atmos. Chem. Phys.*, 16, 3383–3398, doi:10.5194/acp-16-3383-2016, 2016.
- Velders, G. J. M. and Daniel, J. S.: Uncertainty analysis of projections of ozone-depleting substances: Mixing ratios, EESC, ODPs, and GWPs, *Atmos. Chem. Phys.*, 14(6), 2757–2776, doi:10.5194/acp-14-2757-2014, 2014.
- Vogel, B., Günther, G., Müller, R., Groß, J.-U., Hoor, P., Krämer, M., Müller, S., Zahn, A. and Riese, M.: Fast transport from Southeast Asia boundary layer sources to northern Europe: rapid uplift in typhoons and eastward eddy shedding of the Asian monsoon anticyclone, *Atmos. Chem. Phys.*, 14(23), 12745–12762, doi:10.5194/acp-14-12745-2014, 2014.

Vogel, B., Günther, G., Müller, R., Groß, J.-U. and Riese, M.: Impact of different Asian source regions on the composition of the Asian monsoon anticyclone and of the extratropical lowermost stratosphere, *Atmos. Chem. Phys.*, 15(23), 13699–13716, doi:10.5194/acp-15-13699-2015, 2015.

Vogel, B., Günther, G., Müller, R., Groß, J.-U., Afchine, A., Bozem, H., Hoor, P., Krämer, M., Müller, S., Riese, M., Rolf, C., Spelten, N., Stiller, G. P., Ungermann, J. and Zahn, A.: Long-range transport pathways of tropospheric source gases originating in Asia into the northern lower stratosphere during the Asian monsoon season 2012, *Atmos. Chem. Phys.*, 16(23), 15301–15325, doi:10.5194/acp-16-15301-2016, 2016.

Vogel, B., Müller, R., Günther, G., Spang, R., Hanumanthu, S., Li, D., Riese, M. and Stiller, G. P.: Lagrangian simulations of the transport of young air masses to the top of the Asian monsoon anticyclone and into the tropical pipe, *Atmos. Chem. Phys.*, 19, 6007–6034, doi:10.5194/acp-19-6007-2019, 2019.

Volk, C. M., Elkins, J. W., Fahey, D. W., Dutton, G. S., Gilligan, J. M., Loewenstein, M., Podolske, J. R., Chan, K. R. and Gunson, M. R.: Evaluation of source gas lifetimes from stratospheric observations, *J. Geophys. Res. Atmos.*, 102(D21), 25543–25564, doi:10.1029/97JD02215, 1997.

Vollmer, M. K., Rigby, M., Laube, J. C., Henne, S., Siek, T., Gooch, L. J., Wenger, A., Young, D., Steele, L. P., Langenfelds, L., Brenninkmeijer, C. A. M., Wang, J., Wyss, S. A., Hill, M., Oram, D. E., Krummel, P. B., Schoenenberger, F., Zellweger, C., Fraser, P. J., William, T., O'Doherty, S. and Reimann, S.: Abrupt reversal in emissions and atmospheric abundance of HCFC-133a (CF<sub>3</sub>CH<sub>2</sub>Cl), *Geophys. Res. Lett.*, 42, 8702–8710, doi:10.1002/2015GL065846, 2015.

# **Chapter 4: Continued increase of CFC-113a (CCl<sub>3</sub>CF<sub>3</sub>) mixing ratios in the global atmosphere: emissions, occurrence and potential sources**

---

The work in this chapter was originally prepared for a publication in Atmospheric Chemistry and Physics (ACP) and was published in 2018. Due to this there are some cases where sentences are written in the first-person plural i.e. “we decided to use our measurements ...”. I wrote the article and did most of the data analysis, but the co-authors of the article also contributed to the work. Matthew Ashfold and Norfazrin Mohd Hanif produced the output from the NAME particle dispersion model, which I then compared to the atmospheric observations. Claire Reeves taught me how to use the atmospheric chemistry transport model and helped me estimate the emissions of CFC-113 and CFC-113a. Johannes Laube, David Oram, Lauren Gooch and Emma Leedham Elvidge were all involved in measuring and analysing the air samples used in this study. Johannes Laube, William Sturges, David Oram and Emma Leedham Elvidge were also involved in organising the University of East Anglia’s (UEA) contributions to the sampling campaigns included in this study. Emma Leedham Elvidge also recalculated the atmospheric lifetime of CFC-113a. In this chapter, data are gathered together from multiple measurement sites and sampling campaigns. Therefore, many of the co-authors are included because of their involvement in the collection of these samples: Charles C-K Chou and Chang-Feng Ou-Yang (Taiwan campaign), Carl A. M. Brenninkmeijer (CARIBIC project), Paul Fraser and Ray Langenfelds (Cape Grim Baseline Air Pollution Station), Siew Moi Phang and Azizan Abu Samah (Bachok Marine Research Station), Thomas Röckmann (Geophysica research aircraft campaigns), and Simon O’Doherty (Tacolneston Tall Tower). In addition, many of the co-authors and the reviewers contributed comments and suggestions for editing this work to prepare it for publication.

Adcock, K. E., Reeves, C. E., Gooch, L. J., Leedham Elvidge, E., Ashfold, M. J., Brenninkmeijer, C. A. M., Chou, C., Fraser, P. J., Langenfelds, R. L., Mohd Hanif, N., O’Doherty, S., Oram, D. E., Ou-Yang, C.-F., Moi Phang, S., Abu Samah, A., Röckmann, T., Sturges, W. T. and Laube, J. C.: Continued increase of CFC-113a (CCl<sub>3</sub>CF<sub>3</sub>) mixing ratios in the global atmosphere: emissions, occurrence and potential sources, *Atmos. Chem. Phys.*, 18(7), 4737–4751, doi:10.5194/acp-18-4737-2018, 2018.

## Abstract

Atmospheric measurements of the ozone-depleting substance CFC-113a ( $\text{CCl}_3\text{CF}_3$ ) are reported from ground-based stations in Australia, Taiwan, Malaysia and the United Kingdom, together with aircraft-based data for the upper troposphere and lower stratosphere. Building on previous work we find that, since the gas first appeared in the atmosphere in the 1960s, global CFC-113a mixing ratios have been increasing monotonically to the present day. Mixing ratios of CFC-113a have increased by 40 % (percent) from 0.50 to 0.70 ppt (parts per trillion) in the Southern Hemisphere between the end of the previously published record in December 2012 and February 2017. We derive updated global emissions of  $1.7 \text{ Gg yr}^{-1}$  ( $1.3\text{-}2.4 \text{ Gg yr}^{-1}$ ) (gigagrams per year) on average between 2012 and 2016 using a two-dimensional model. We compare the long-term trends and emissions of CFC-113a to those of its structural isomer, CFC-113 ( $\text{CClF}_2\text{CCl}_2\text{F}$ ), which still has much higher mixing ratios than CFC-113a, despite its mixing ratios and emissions decreasing since the 1990s. The continued presence of Northern Hemispheric emissions of CFC-113a is confirmed by our measurements of a persistent interhemispheric gradient in its mixing ratios, with higher mixing ratios in the Northern Hemisphere. The sources of CFC-113a are still unclear, but we present evidence that indicates large emissions in East Asia, most likely due to its use as a chemical involved in the production of hydrofluorocarbons. Our aircraft data confirm the interhemispheric gradient as well as showing mixing ratios consistent with ground-based observations and the relatively long atmospheric lifetime of CFC-113a.

## 4.1 Introduction

Recently, mixing ratios of CFC-113a ( $\text{CCl}_3\text{CF}_3$ ), the structural isomer of the well-known ozone-depleting substance CFC-113 ( $\text{CF}_2\text{ClCFCl}_2$ ), were found to still be increasing in the atmosphere up until 2012 (Laube et al., 2014). The previously published evidence for increasing mixing ratios of CFC-113a comes from air samples collected at Cape Grim, Tasmania ( $41^\circ \text{ S}$ ) and firn air data collected in Greenland ( $77^\circ \text{ N}$ ) in 2008 (NEEM project) (Buizert et al., 2012; Laube et al., 2014). The firn air depth profile data, when combined with inverse modelling, provide smoothed time series of compound mixing ratios going back almost one century (Buizert et al., 2012; Laube et al., 2012). CFC-113a became detectable in the atmosphere in the 1960s (Laube et al., 2014). Cape Grim is a clean-air measurement site located in Tasmania, Australia, with air sampling/analysis activities since 1976 and the CFC-113a record derived from the Cape Grim Air Archive (1978 onwards) shows mixing ratios increasing over time with a sharp acceleration starting around 2010 (Laube et al., 2014). Global annual emissions of CFC-113a were estimated using a two-dimensional atmospheric chemistry-transport model, showing increases since the 1960s and more than doubling between 2010 and 2012, reaching  $2.0 \text{ Gg yr}^{-1}$  in 2012 (Laube et al., 2014). In addition, measurements of aircraft samples from the CARIBIC-IAGOS observatory identified an interhemispheric gradient with mixing ratios increasing from the Southern Hemisphere to the Northern Hemisphere; and the atmospheric lifetime of CFC-113a was estimated at 51 years from stratospheric research aircraft flights in late 2009 and early 2010 (Laube et al., 2014).

The origin of the emissions that cause this increase in CFC-113a mixing ratios is as yet undetermined. Some evidence of a potential connection with hydrofluorocarbon (HFC) production has been found (Laube et al., 2014) and here we use additional data to investigate this possibility further. Laube et al. (2014) reported data until 2012. This study uses data that have become available since 2012 to provide an update on its global trend and emissions and to assess these in terms of our understanding of the sources of this gas and its potential impact on ozone.

## 4.2 Methods

### 4.2.1 Analytical technique

Air samples from all the campaigns discussed in this study were collected in electropolished and/or silco-treated stainless steel gas cylinders, except for the CARIBIC observatory, for which samples were collected using glass-bottle based samplers (Brenninkmeijer et al., 2007). Various pumps were used for the different sampling activities, all of which have been thoroughly tested for a large range of trace gases (Brenninkmeijer et al., 2007; Laube et al., 2010; Allin et al., 2015 and Oram et al., 2017).

After collection, the samples were transported to the University of East Anglia (UEA) to be analysed on a high-sensitivity gas chromatograph coupled to a Waters AutoSpec magnetic sector mass spectrometer (GC-MS). A full description of this system can be found in Chapter 2. The trace gases were cryogenically extracted and pre-concentrated. Analysis was partly carried out using a GS GasPro column (length ~50 m, ID 0.32 mm) and partly with a KCl-passivated Al<sub>2</sub>O<sub>3</sub>-PLOT column (length: 50 m, ID 0.32 mm). During analysis on the Al<sub>2</sub>O<sub>3</sub>-PLOT column, an Ascarite (NaOH-coated silica) filter was used to remove carbon dioxide.

Several tests and comparisons ensured that no significant differences in CFC-113 and CFC-113a mixing ratios were obtained regardless of the column or filter used. A possible interference could arise when measuring CFC-113a on the GS GasPro column using m/z 116.91 if mixing ratios of the nearby eluting HCFC-123 are high. This was the case for a small number of samples analysed for this work and those measurements were either a) repeated using the interference-free m/z 120.90, b) replaced with measurements on the KCl-passivated Al<sub>2</sub>O<sub>3</sub>-PLOT column, or c) excluded. The KCl-passivated Al<sub>2</sub>O<sub>3</sub>-PLOT column separated CFC-113 and CFC-113a well, no interferences were observed and m/z 116.91 was used for quantification.

All the samples are compared to the same NOAA standard (AAL-071170) and there were routine measurements of multiple standards to exclude the possibility of mixing ratio changes in the standard over time (Section 2.8). The HCFC-133a, HFC-125 and HFC-134a mixing ratios from Taiwan in 2013 were measured on the Entech-Agilent GC-MS system operating in electron ionisation (EI) mode. This consists of a preconcentration unit (Entech model 7100) connected to an Agilent 6890 GC and 5973 quadrupole MS (Section 2.7). The calibration scale used for CFC-113a is the UEA

calibration scale and for CFC-113 is the NOAA 2002 calibration scale. On a typical day, the working standard is measured five to eight times, between every two or three samples. The sample peak sizes are measured relative to the standards measured just before and after them. The working standard is used to correct for small changes in instrument response over the course of a day. The dry air mole fraction (mixing ratio) is measured and the unit, parts per trillion (ppt) is used in this study as an equivalent to picomole per mole. The measurement uncertainties are calculated the same way for all measurements and represent one sigma standard deviation. They are based on the square root of the sum of the squared uncertainties from sample repeats and repeated measurements of the air standard on the same day.

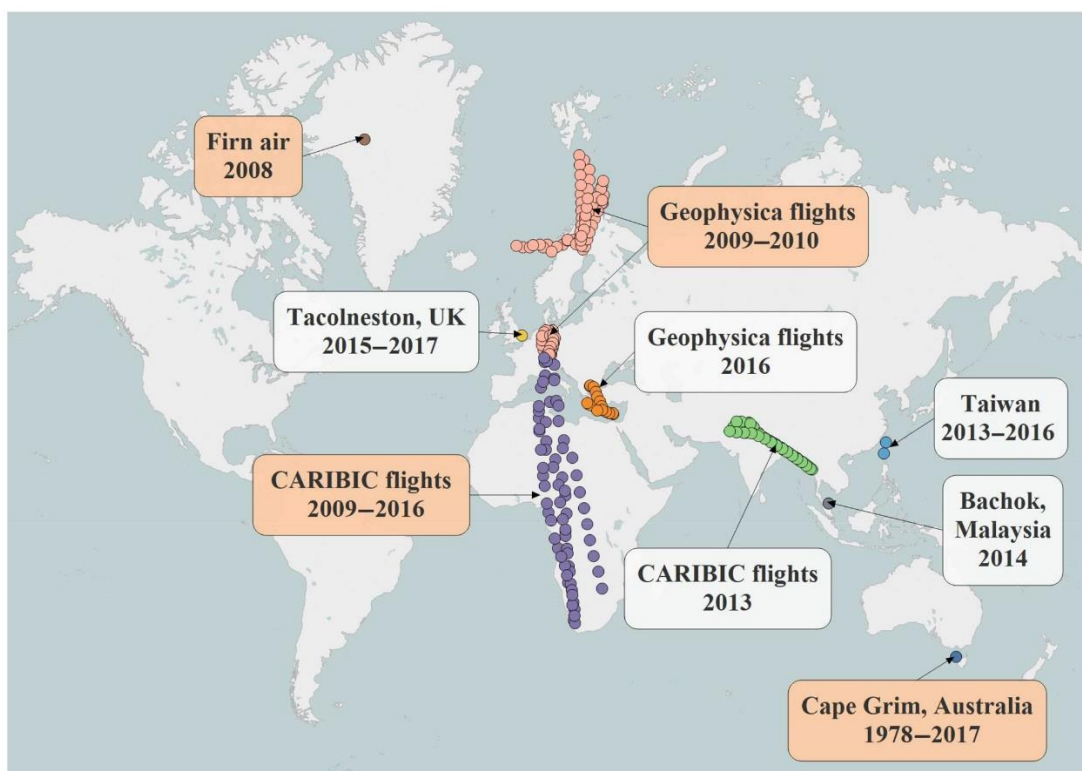


Figure 4.1: Sampling locations used in this study. Those locations that have been added since Laube et al. (2014) are in white. Those with orange labels featured in, or have been extended since, Laube et al. (2014).

#### 4.2.2 Sampling

The following new data are presented in this study (see also Figure 4.1 and Table 4.1):

1. Laube et al. (2014) reported CFC-113a measurements from Cape Grim, Tasmania from 1978 to 2012. We now report four more years of CFC-113a measurements from Cape Grim, up to February 2017. From 2013 to 2017, 20 samples were collected at Cape Grim at irregular intervals of between one to five months apart. The CFC-113 mixing ratios (1978-2017) from analyses of archived air samples collected at Cape Grim, Tasmania and analysed at the UEA, together with NOAA

- flask data, and AGAGE *in situ* data are also included to compare the two isomers. CFC-113 stability in the Cape Grim Air Archive has been demonstrated in the AGAGE program for periods up to 15 years and longer (Fraser et al., 1996; CSIRO unpublished data). Most of the CFC-113 UEA Cape Grim data set was previously published in Laube et al. (2013). Some of the earlier samples from Laube et al. (2013) and Laube et al. (2014) were reanalysed on the KCl-passivated Al<sub>2</sub>O<sub>3</sub>-PLOT column (length: 50 m, ID 0.32 mm). They showed very good agreement with the previous GasPro column-based measurement with comparable precisions and no detectable offset. The Cape Grim air samples were collected under background conditions with winds from the south-west, marine sector, so that sampled air masses were not influenced by nearby terrestrial sources and are representative of the extra-tropical Southern Hemisphere. Details of the sampling procedure have been reported in previous publications (e.g. Fraser et al., 1999; Laube et al., 2013).
2. Tacolneston tower is a measurement site in Norfolk (Ganesan et al., 2015), and is part of the UK Tall Tower Network. Air samples were collected on a near-biweekly basis between July 2015 and March 2017 using an air inlet at 185 m.
  3. Ground-based samples were collected from Bachok Marine Research Station on the northeast coast of Peninsular Malaysia in January and February 2014.
  4. During the StratoClim campaign (<http://www.stratoclim.org/>), air samples were collected during two flights by the Geophysica high altitude research aircraft, as described in Kaiser et al. (2006), in the upper troposphere and lower stratosphere (10-20 km) over the Mediterranean on 01-Sep-2016 and 06-Sep-2016.
  5. Air samples were collected at regular intervals at altitudes of 10-12 km during long distance flights on a commercial Lufthansa aircraft from 2009 to 2016 (Brenninkmeijer et al., 2007) on four flights between Frankfurt, Germany and Bangkok, Thailand; five flights between Frankfurt, Germany and Cape Town, South Africa; and one flight between Frankfurt, Germany and Johannesburg, South Africa; including the four flights referred to in Laube et al. (2014) (CARIBIC project, [www.caribic-atmospheric.com](http://www.caribic-atmospheric.com)).
  6. Four ground-based air sampling campaigns took place in Taiwan from 2013 to 2016. Between 19 and 33 air samples were collected in March and April each year. In 2013 and 2015 samples were collected from a site on the southern coast of Taiwan (Hengchun) and in 2014 and 2016 samples were collected from a site on the northern coast of Taiwan (Cape Fuguei). See also Vollmer et al. (2015), Laube et al. (2016) and Oram et al. (2017).

Table 4.1: Air sampling campaigns from which atmospheric CFC-113a mixing ratios were measured, including the data published in Laube et al. (2014).

Sampling campaign	Location	Longitude and Latitude	Dates	No. of samples	Nature of data
<b>NEEM</b>	Greenland	77.445° N, 51.066° W 2484m a.s.l.	14-Jul-2008– 30-Jul-2008	3 closest to the surface	Firn air surface data
<b>Cape Grim</b>	Tasmania, Australia	40.683° S, 144.690° E	(07-Jul-1978) 14-Mar-2013– 23-Feb-2017	66 total, 20 new	Southern Hemisphere ground-based site
<b>Taiwan</b>	East Asia	Hengchun, 22.0547° N, 120.6995° E, (2013, 2015) Cape Fuguei, 25.297° N, 121.538° E, (2014, 2016)	2013–2016	2013: 19 2014: 24 2015: 23 2016: 33	Northern Hemisphere ground-based sites
<b>Tacolneston Tower</b>	Norfolk, United Kingdom	52.3104° N, 1.0820° E	13-Jul-2015– 16-Mar-2017	47	Northern Hemisphere tall tower site
<b>Bachok Marine Research Station</b>	Bachok, Malaysia	6.009° N, 102.425° E	20-Jan-2014– 03-Feb-2014	16	Tropical ground- based site
<b>Geophysica flights 2009-2010</b>	North Sea	76-48° N, 28-0° E	30-Oct-2009– 02-Feb-2010	98	Research aircraft
<b>Geophysica flights 2016</b>	Mediterranean Sea	33-41° N, 22-32° E	01-Sep-2016 06-Sep-2016	23	Research aircraft
<b>CARIBIC flights</b>	Germany to South Africa	48° N-30° S, 6-19° E	27-Oct-2009 28-Oct-2009 14-Nov-2010 20-Mar-2011 10-Feb-2015 13-Jan-2016	14 7 13 14 15 7	Commercial aircraft
<b>CARIBIC flights</b>	Germany to Thailand	32-17° N, 70-97° E	21-Feb-2013 21-Mar-2013 09-Nov-2013 05-Dec-2013	14 7 14 14	Commercial aircraft

#### 4.2.3 Emission modelling

A two-dimensional atmospheric chemistry-transport model was used to estimate, top-down, global annual emissions of CFC-113a and CFC-113 for the purpose of comparing the emissions of the two isomers. The model contains 12 horizontal layers each representing 2 km of the atmosphere and 24 equal-area zonally averaged latitudinal

bands (288 grid boxes). For more details about the model see Newland et al. (2013); and Laube et al. (2016).

This model was previously used to estimate the global annual emissions of CFC-113a (Laube et al., 2014). We now update the CFC-113a emission estimates using an additional four years of Cape Grim measurements. The CFC-113 emissions are estimated using CFC-113 mixing ratios at Cape Grim for 1978-2017 from the UEA Cape Grim dataset and compared with bottom-up emissions estimates from the Alternative Fluorocarbons Environmental Acceptability Study (AFEAS, <https://agage.mit.edu/data/afeas-data>). The modelled mixing ratios for the latitude band that Cape Grim is located within (35.7° S–41.8° S) were matched as closely as possible to the observations at Cape Grim (40.7° S) by iteratively adjusting the global annual emissions rate until the differences between the modelled mixing ratios and the observations were minimised.

The model was run for 84 years from 1934 to 2017. It begins in 1934 because that was considered early enough to be before emissions of CFC-113a and CFC-113 began. Using the corrections in Leedham Elvidge et al. (2018) we calculated the atmospheric lifetime of CFC-113a to be 51 years (30-148 years) based on an updated and improved mean age-of-air estimate. The atmospheric lifetime of CFC-113 is currently estimated to be 93 years with a ‘likely’ range of 82-109 years (Ko et al., 2013). The photolysis rates are calculated for each grid box as a function of seasonally varying temperature and the absorption spectra for the wavelengths 200–400 nm. For CFC-113a the absorption spectrum is taken from Davis et al. (2016) and for CFC-113 it is taken from Burkholder et al. (2015). For the reaction with O(<sup>1</sup>D) the rate coefficients used are  $2.61 \times 10^{-10} \text{ cm}^3 \text{ molecule}^{-1} \text{ s}^{-1}$  and  $2.33 \times 10^{-10} \text{ cm}^3 \text{ molecule}^{-1} \text{ s}^{-1}$  for CFC-113a and CFC-113 respectively (Baasandorj et al., 2011). The diffusive loss of gases out of the top of the model is controlled by making the mixing ratios immediately above the model a constant fraction ( $F$ ) of the mixing ratios in the top layer of the model (22-24 km). Nearly all the loss of both compounds is above the model and so the atmospheric lifetimes are almost completely controlled by varying the  $F$  factor. The values of  $F$  were set to 0.6250 (0.0001-0.9854) for steady-state lifetimes of 51 years (30 years-148 years) for CFC-113a and to 0.8254 (0.7888-0.8618) for lifetimes of 93 years (82 years-109 years) for CFC-113. The minimum lifetime of 30 years for CFC-113a could not be achieved by adjusting the  $F$  value alone so was simulated by choosing a very small value for  $F$  of 0.0001 and by increasing the photolysis rate inside the model domain by a factor of 5.24. This is likely because the data used to determine the range (30-148 years) do not provide adequate constraint rather than implying that there may be unknown sinks.

A latitudinal distribution of emissions, with 95 % of emissions originating in the Northern Hemisphere, was assumed for both compounds. As Cape Grim is a remote Southern Hemispheric site the emission distribution within the Northern Hemisphere has almost no effect on the modelled mixing ratios in the latitudinal band of Cape Grim. The emission distribution used for CFC-113 was assumed to be constant for the whole

of the model run and has been used in previous studies for similar compounds (McCulloch et al., 1994; Reeves et al., 2005; Laube et al., 2014, 2016). For CFC-113a we decided to select an emission distribution based on how well the modelled mixing ratios in the latitude band 48.6-56.4° N agreed with the observations at Tacolneston for the later part of the trend. Tacolneston can be considered to be representative of Northern Hemisphere background mixing ratios of CFC-113a for that latitude as there are no significant enhancements in mixing ratios (Figure 4.2). The emission distribution used in the CFC-113a model is the same as CFC-113 for the first 60 years (1934-1993) and then gradually shifts over the next 10 years from more northerly latitudes (36-57° N) to more southerly latitudes (19-36° N). It then remains at more southerly latitudes until the end of the run in 2017. This distribution shift is based on the assumption that CFC-113a emissions are predominantly from Europe and North America at the beginning of the model run and then shift to be coming predominantly from East Asia towards the end of the model run. There are significant enhancements in CFC-113a mixing ratios in our measurements from Taiwan indicating continued emissions in this region (Section 4.3.2.1) which is consistent with emissions in this latitude band in the model. The latter is also consistent with previous work that has found emissions of ozone-depleting substances shifted from more northerly Northern Hemisphere latitudes to more southerly Northern Hemisphere latitudes (Reeves et al., 2005; Montzka et al., 2009). This is likely due to developing countries, which are mostly located further south, having more time to phase out the use of many ODSs than developed countries (Newland et al., 2013; CTOC, 2014; Fang et al., 2016). With this emissions distribution, the modelled CFC-113a mixing ratios at Tacolneston matched closely to the observations (Figure 4.2). It should be noted that while there is evidence that supports the emission distribution used here, there might be alternative distributions that result in equally good fits to the trends, particularly in the earlier part of the record.

The upper and lower emission uncertainties for CFC-113a and CFC-113 were calculated by combining five different components together.

The first component is the uncertainty in the model transport. CFC-11 and CFC-12 are long-lived gases with reasonably well-known emissions and atmospheric mixing ratios. When using this model, the difference between modelled mixing ratios and observed mixing ratios of CFC-11 and CFC-12 at Cape Grim is about 5 % (Reeves et al., 2005). This difference, 5 %, is taken to represent the uncertainty in the model transport.

The second component, is the average measurement uncertainty, which is calculated using the mean of the one sigma standard deviations derived as the square root of the sum of the squared uncertainties in sample repeats and repeated measurements of an air standard on the same day. In other words, the average size of the error bars in Figure 4.3 and Figure 4.5. A more detailed explanation for how the error bars were calculated can be found in Section 2.6. The average measurement uncertainty is calculated to be 0.8 % for CFC-113 and 3.9 % for CFC-113a.

The third component is the model fit uncertainty, which is the mean percentage difference between the ‘best fit’ modelled mixing ratios and the observations. The model fit uncertainty is 1.0 % for CFC-113 and 2.6 % for CFC-113a.

The fourth component is the calibration uncertainty, which for CFC-113a is 3.8 % (Laube et al., 2014) and for CFC-113 is 0.5 % (Brad Hall, personal communication). The CFC-113 uncertainty is the uncertainty in the NOAA calibration scale. We do not have the full calibration uncertainty for CFC-113 as the content of CFC-113a is currently unknown for the NOAA ‘CFC-113’ calibration as the two isomers are hard to separate from each other.

The fifth component is the uncertainty in the atmospheric lifetimes. The ‘best fit’ (minimum-maximum) steady-state lifetimes used in this study are 51 years (30 years-148 years) for CFC-113a and 93 years (82 years-109 years) for CFC-113 (Ko et al., 2013; Leedham Elvidge et al., 2018).

These five components were then combined together. Firstly, we calculated the square root of the sum of squares of the uncertainties in model transport, measurements and model fit, after which the calibration uncertainty was then added (Equation 4.1). Combining these uncertainties as described above gives overall uncertainties of  $\pm 5.7$  % for CFC-113 and  $\pm 10.6$  % for CFC-113a.

$$\text{Overall uncertainty} = \sqrt{\frac{\text{model transport}^2}{\text{uncertainty}} + \frac{\text{measurement}^2}{\text{uncertainty}} + \frac{\text{model fit}^2}{\text{uncertainty}} + \text{calibration uncertainty}} \quad (4.1)$$

The observed mixing ratios were then adjusted by these overall uncertainties and the model was re-run and the emissions varied to reproduce these new adjusted mixing ratios. The atmospheric lifetimes were also adjusted at the same time to estimate the upper and lower bounds of the emissions. The upper bound is estimated using the lowest lifetime and the highest mixing ratios and the lower bound is estimated using the highest lifetime and the lowest mixing ratios.

Estimating the upper (lower) bound of the emissions in this way assumes that the influence of the five uncertainties would all be acting to increase (decrease) the emissions. However, it is likely that to some extent the influence of the uncertainties will be counteracting each other. Therefore, the upper and lower bounds as presented are likely to be an overestimate of the true uncertainty.

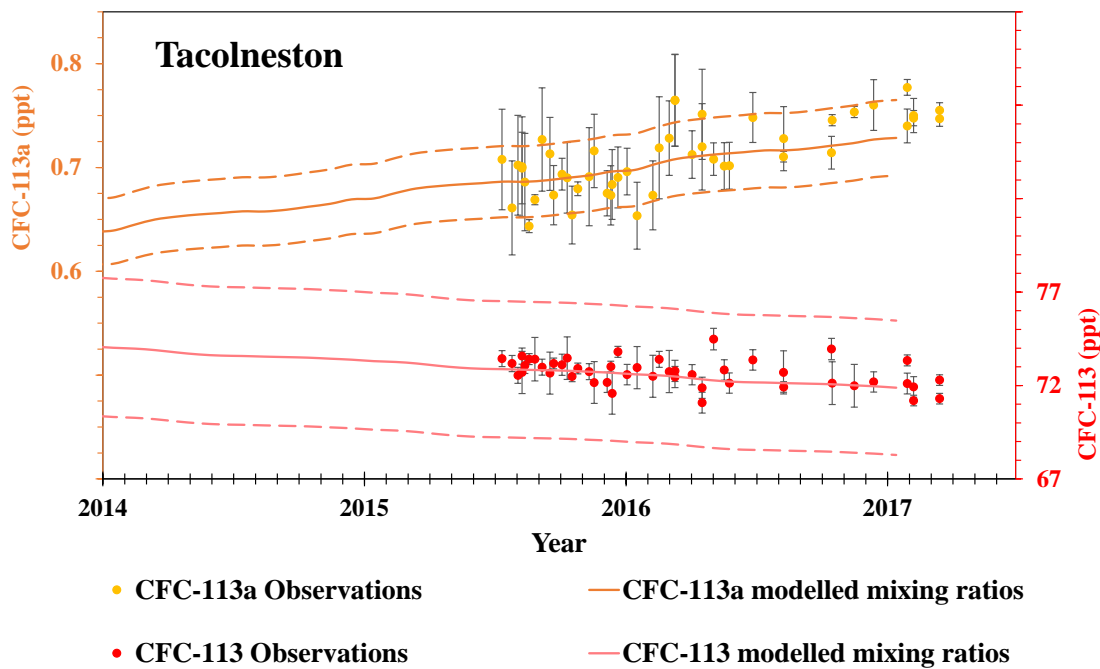


Figure 4.2: CFC-113a and CFC-113 modelled and observed mixing ratios at Tacolneston. The error bars represent the  $1\sigma$  standard deviation. The modelled uncertainties are 5 % and are based on the model reproducing the reported mixing ratios of CFC-11 and CFC-12 at Cape Grim to within 5 % uncertainty (Reeves et al., 2005).

#### 4.2.4 Dispersion modelling

The UK Met Office’s Numerical Atmospheric Modelling Environment (NAME, Jones et al., 2007), a Lagrangian particle dispersion model, was used to produce footprints of where the air sampled during the Taiwan and Malaysia campaigns (Table 4.1) had previously been close to the Earth’s surface. The model setup related to samples collected in Taiwan in 2016 was slightly different to the setup for simulations in 2013–2015; hereafter those differences are noted in parentheses, though they have no practical implications for our findings. The footprints were calculated over 12 days by releasing batches of 60,000 (30,000 in 2016) inert backward trajectories over a 3-hour period encompassing each sample. Over the course of the 12 day travel time the location of all trajectories within the lowest 100 m of the model atmosphere was recorded every 15 minutes on a grid with a resolution of  $0.5625^\circ$  longitude and  $0.375^\circ$  latitude ( $0.25^\circ$  by  $0.25^\circ$  in 2016). The trajectories were calculated using three-dimensional meteorological fields produced by the UK Met Office’s Numerical Weather Prediction tool, the Unified Model (UM) (Cullen 1993). These fields have a horizontal grid resolution of  $0.35^\circ$  longitude by  $0.23^\circ$  latitude for the 2013 and 2014 simulations, and  $0.23^\circ$  longitude by  $0.16^\circ$  latitude for the 2015 and 2016 simulations. In all cases the meteorological fields have 59 vertical levels below  $\sim 30$  km. Dates in the NAME footprint maps are presented in the format yyyy-mm-dd and use UTC time.

## 4.3 Results

### 4.3.1 Long-term atmospheric trends and estimated global annual emissions of CFC-113a and CFC-113

CFC-113a mixing ratios at Cape Grim were previously found to have been increasing from 1978-2012 (Laube et al., 2014, Figure 4.3). Since 2012, they have continued to increase from 0.50 ppt in December 2012 to 0.70 ppt in February 2017 (Figure 4.3). Between 1978 and 2009 the average rate of increase was  $0.012 \text{ ppt yr}^{-1}$ ; between 2010 and 2017 the rate has risen threefold to about  $0.037 \text{ ppt yr}^{-1}$ .

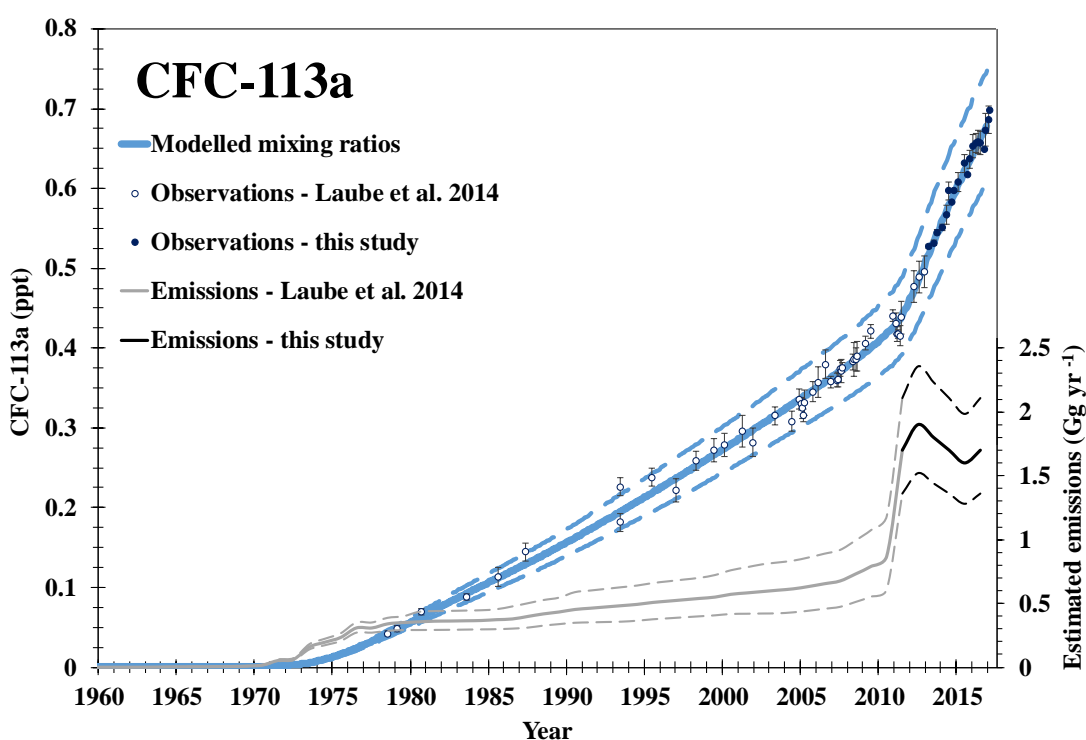


Figure 4.3: CFC-113a modelled and observed mixing ratios at Cape Grim 1960-2017 and estimated global annual emissions of CFC-113a. The observations are from July 1978-February 2017 with  $1\sigma$  standard deviations as error bars. Data prior to 04-Dec-2012 is from Laube et al. (2014). The blue solid line represents the modelled mixing ratios with uncertainties (dashed blue line). The black and grey lines represent the modelled ‘best fit’ emissions with uncertainties (dashed). The grey lines are the emission estimates that were reported in Laube et al. (2014) and the black lines are the extension of the emission trends in this study.

Measurements at Tacolneston were only made for a short time period in comparison to measurements at Cape Grim (20 months), but it also experienced an increase in CFC-113a mixing ratios of  $0.03 \text{ ppt yr}^{-1}$  over the period July 2015 to March 2017, based on start and end points (Figure 4.2). Furthermore, for the CARIBIC flights the mean mixing ratios of CFC-113a increased on average, by  $0.04 \text{ ppt yr}^{-1}$  between 2009 and

2016 (Figure 4.4). Overall, there is a consistent picture of a continued global increase in background mixing ratios of CFC-113a. Its atmospheric burden has been increasing since the 1960s (Laube et al., 2014) and this has continued until early 2017, implying that ongoing emissions of CFC-113a exceed its rate of removal.

The modelled global annual CFC-113a emissions began in the 1960s and increased steadily at an average rate of  $0.02 \text{ Gg yr}^{-1} \text{ yr}^{-1}$  until they reached  $0.9 \text{ Gg yr}^{-1}$  ( $0.6\text{-}1.2 \text{ Gg yr}^{-1}$ ) in 2010 followed by a sharp increase to  $0.52 \text{ Gg yr}^{-1} \text{ yr}^{-1}$  from 2010 to 2012 when emissions were  $1.9 \text{ Gg yr}^{-1}$  ( $1.5\text{-}2.4 \text{ Gg yr}^{-1}$ ) (Figure 4.3). We find that between 2012 and 2016, modelled emissions were on average  $1.7 \text{ Gg yr}^{-1}$ . The best model fit (minimum-maximum) suggests some minor and statistically non-significant variability between  $1.6 \text{ Gg yr}^{-1}$  ( $1.3\text{-}2.0 \text{ Gg yr}^{-1}$ ) in 2015 and  $1.9 \text{ Gg yr}^{-1}$  ( $1.5\text{-}2.4 \text{ Gg yr}^{-1}$ ) in 2012.

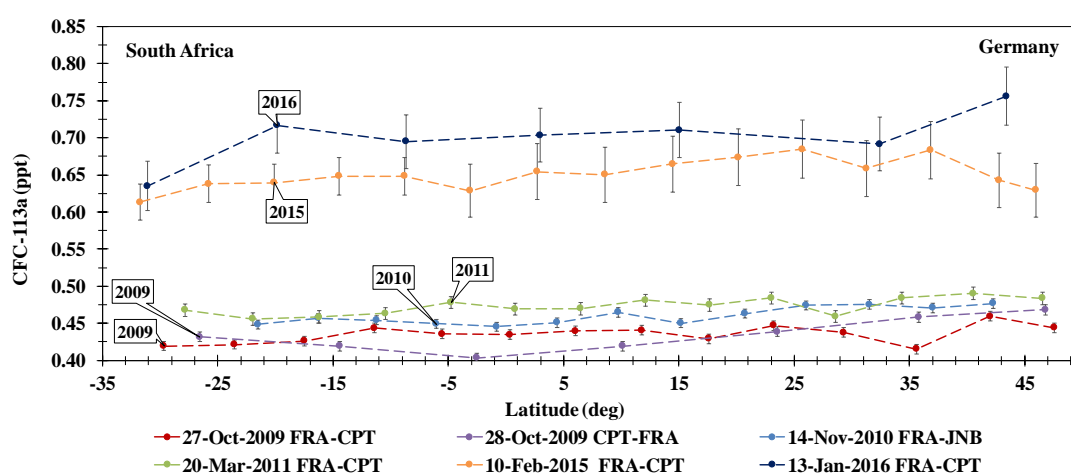


Figure 4.4: CFC-113a mixing ratios from samples collected during CARIBIC aircraft campaign flights from 2009 to 2016 for each flight from Frankfurt, Germany (FRA) to Cape Town, South Africa (CPT) and Johannesburg, South Africa (JNB), with  $1\sigma$  standard deviations as error bars.

It is instructive to look at CFC-113 to learn more about CFC-113a. The atmospheric trends of CFC-113 at Cape Grim (Figure 4.5) and estimated emissions are very different from those of CFC-113a. Mixing ratios of both compounds increased at the beginning of the record, but then the CFC-113 mixing ratios stabilised in the early 1990s and started to decrease (Figure 4.5), consistent with previous observations (Fraser et al., 1996; Montzka et al., 1999; Rigby et al., 2013; Carpenter and Reimann et al., 2014). This trend is similar to those of many other CFCs in the atmosphere (for example CFC-11 and CFC-12, Rigby et al., 2013), but in contrast to the increasing mixing ratios of CFC-113a. Note that CFC-113a mixing ratios are still much lower than those of CFC-113 even at the end of our current record in early 2017. CFC-113 is the third most abundant CFC in the atmosphere (Carpenter and Reimann et al., 2014) and mixing ratios of CFC-113a are only about 1 % of CFC-113 mixing ratios in 2017. CFC-113 mixing ratios at Cape Grim measured by NOAA (<https://www.esrl.noaa.gov/gmd/dv/ftpdata.html>) and AGAGE (Prinn et al., 2018;

[http://agage.eas.gatech.edu/data\\_archive/agage/](http://agage.eas.gatech.edu/data_archive/agage/)) are also included in Fig. 4.5. The NOAA and AGAGE measurement techniques do not enable the separation of the isomers so their reported CFC-113 mixing ratios are the sum of CFC-113 and CFC-113a. It is assumed that the influence of this is small as CFC-113a mixing ratios are small in comparison to the CFC-113 mixing ratios but this does create an additional uncertainty in our comparisons. There is a small offset of 2 % between the NOAA data and the current UEA Cape Grim dataset, with the UEA Cape Grim dataset being slightly higher, similar to the offset reported previously (Laube et al., 2013).

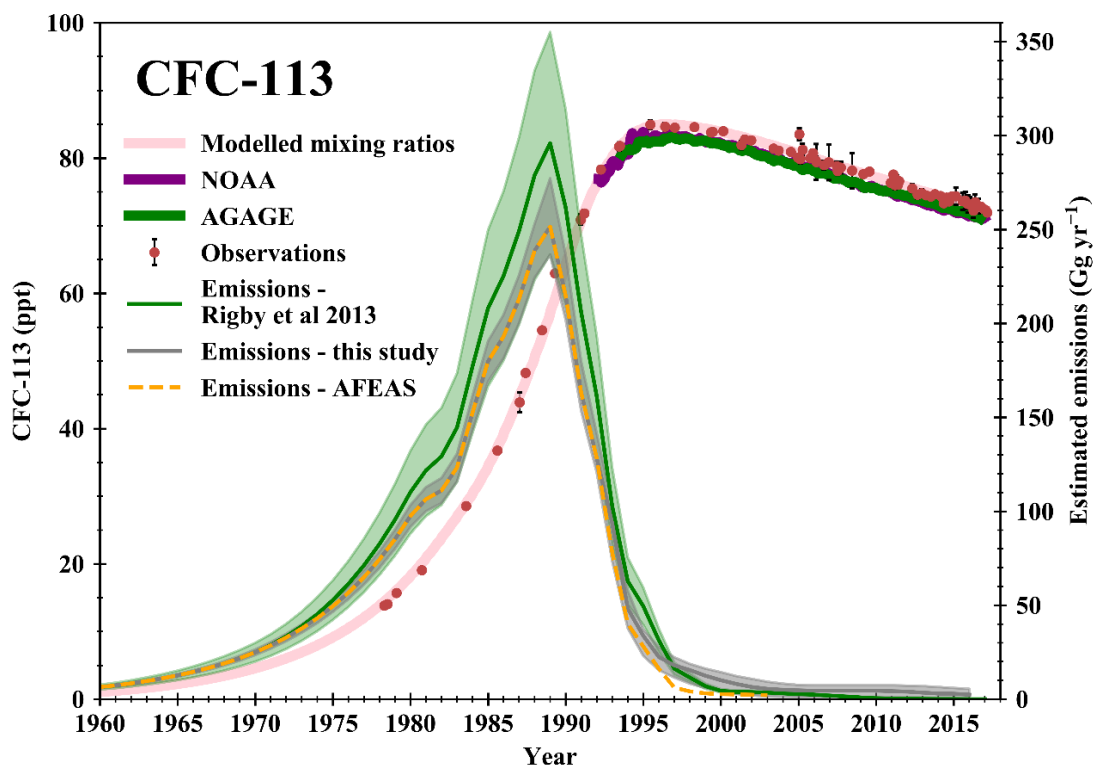


Figure 4.5: CFC-113 modelled and observed mixing ratios at Cape Grim 1960-2017 and estimated global annual ‘best fit’ emissions of CFC-113 with uncertainties. The observations are from Cape Grim, Tasmania, July 1978-February 2017 with  $1\sigma$  standard deviations as error bars. Also, for comparison are the NOAA and AGAGE CFC-113 mixing ratios at Cape Grim and previous emissions estimates from AFEAS and Rigby et al. (2013) (based on AGAGE in situ data) with ‘likely’ uncertainties. The NOAA and AGAGE reported CFC-113 mixing ratios are the sum of CFC-113 and CFC-113a mixing ratios.

The CFC-113 model derived emissions begin in the 1940s and rapidly increase until they peak in 1989 at  $252 \text{ Gg yr}^{-1}$ , after which they decrease to  $2.4 \text{ Gg yr}^{-1}$  in 2016 (Figure 4.5). This sharp decline witnesses the success of the Montreal Protocol, which came into force in 1989 and phased out the production of CFCs by 1996 in developed countries and 2010 in developing countries (UNEP, 2016a). The total cumulative

emissions of CFC-113, up to the end of 2016, are 3164 Gg while the cumulative emissions of CFC-113a are 29 Gg, making the total cumulative emissions of CFC-113a less than 1 % of its isomer CFC-113. Alternatively, in the last decade, 2007-2016, cumulative emissions of CFC-113 are 38 Gg, while for CFC-113a they are 13 Gg, or a third of the CFC-113 cumulative emissions. Current CFC-113a emissions are similar to those of CFC-113 and could even surpass them if the trends continue (Figure 4.6).

Up until 1992, the CFC-113 emissions used in the model are the bottom-up emissions estimates from AFEAS. In the model, these emissions lead to a best-fit match to the CFC-113 observations. This shows that in the first part of the record, AFEAS report data accurately reflecting global CFC-113 emissions. However, after 1992 the AFEAS emissions lead to lower modelled mixing ratios than the observations indicating that AFEAS was missing some emissions after 1992. Therefore, the emissions used in our study here are the AFEAS emissions up until 1992. From 1992 onwards they are based on the best model fit to the UEA Cape Grim observations. CFC-113 emissions were also derived in another study using a range of emission inventories and estimates (Rigby et al., 2013). Those emissions mostly agree with ours within the uncertainties.

It should be noted that CFC-113 is not the focus of this study, but we do find that emissions of it persist until 2017, which leaves room for the possibility that some of the recent emissions of CFC-113a are related to CFC-113 emissions, possibly through HFC production or agrochemical production (Section 4.4) similar to findings for other isomeric CFCs (Laube et al., 2016).

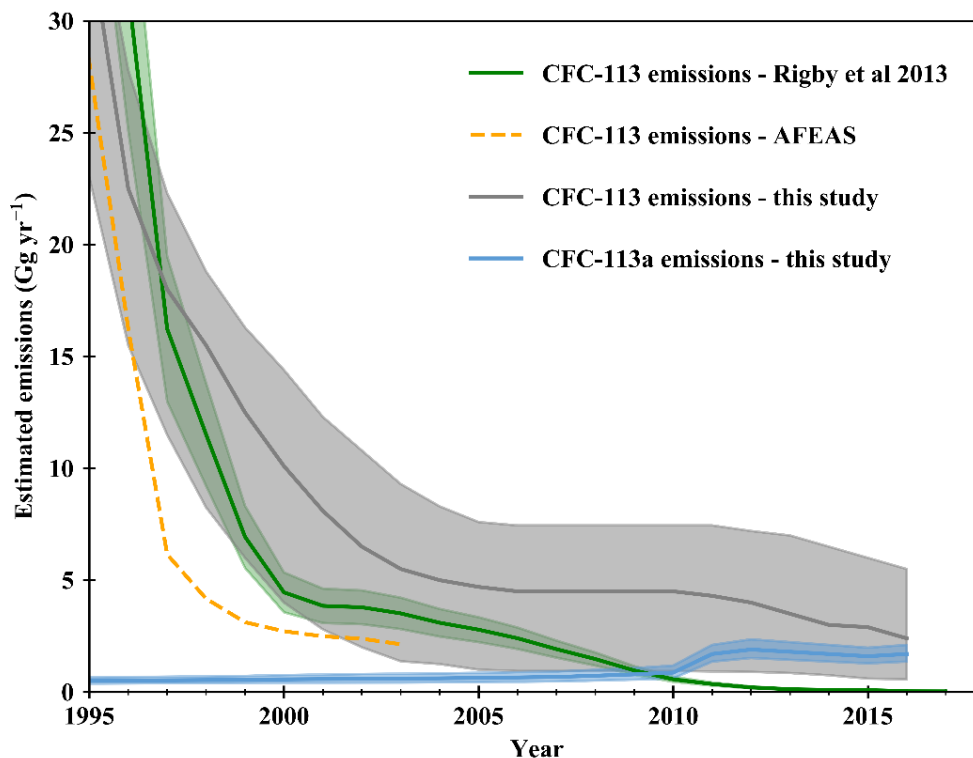


Figure 4.6: CFC-113 emissions from this study, AFEAS and Rigby et al. (2013) and CFC-113a emissions from this study 1995-2016 with uncertainties.

The upper and lower bounds of the CFC-113 emissions in this study are derived using the ‘likely’ range in the CFC-113 lifetime given by SPARC of 82-109 years (Ko et al., 2013). The ‘possible’ range of 69-138 years was also estimated by Ko et al. (2013), however using a lifetime of 138 years the modelled mixing ratios did not decrease sufficiently rapidly after 1990 to match the observed downwards trend in CFC-113 even in the absence of emissions. During the period from 2003 onwards we calculate very small emissions for CFC-113 suggesting that the rate of change is dominated by its atmospheric lifetime. We can use the observed decrease in CFC-113 mixing ratios from 2003 onwards to calculate a decay time (lifetime at zero emissions). For long lived gases with stratospheric sinks, such as CFC-113, the decay time and steady state lifetime are very similar differing by no more than 2 % (Ko et al., 2013). Setting the emissions to zero from 2003 onwards and adjusting the lifetime so that the model reproduces the CFC-113 mixing ratios at Cape Grim, suggests the lifetime for CFC-113 is 110 years. By assuming zero emissions, this lifetime is a maximum value, since any source of CFC-113 would have to be balanced by a shorter lifetime. Combining the measurement and model errors as described in Section 4.2.3 gives an error of 5.7 %. Accounting for the 2 % error introduced by assuming the decay time is the same as the steady state lifetime gives an overall error of 6 %. Applying this to the lifetime gives a maximum lifetime of  $110 \pm 7$  years.

For comparison, we also calculated the maximum lifetime from the observed rate of decrease in CFC-113 mixing ratios at Cape Grim between 2003 and 2017 using a rearrangement of the chemical continuity equation and assuming no sources of CFC-113:

$$\tau = -\frac{\Delta t}{\ln\left(\frac{C_{t+\Delta t}}{C_t}\right)} \quad (4.2)$$

where  $\tau$  is the lifetime,  $C_t$  is the mixing ratio at time  $t$ , and  $C_{t+\Delta t}$  is the mixing ratio at time  $t+\Delta t$  where  $\Delta t$  is the time interval between the two mixing ratios. To account for the measurement variability, the lifetime was calculated five times using the annual mean observed mixing ratios separated by a running 10-year interval (i.e. 2003 to 2013, 2004 to 2014 etc up to 2007 to 2017). The resulting lifetime of  $113 \pm 4$  years is then the mean  $\pm$  the standard deviation of these five values. Accounting for the possible 2 % difference between the decay time and steady state lifetime gives an overall range of  $113 \pm 5$  years. This is in good agreement with the maximum lifetime of  $110 \pm 7$  years calculated using the model. It has been suggested that changing atmospheric dynamics, due to climate change, could lead to atmospheric lifetimes changing over time (Douglass et al., 2008). Additionally, it is possible that climate change could lead to changes in boundary layer height which may influence the observed mixing ratios at ground-based measurement sites (Aulagnier et al., 2010). These possible changes are not taken into account in this study.

## 4.3.2 Global distributions of CFC-113a

### 4.3.2.1 Enhancement above background mixing ratios

Many of the CFC-113a mixing ratios observed in Taiwan (light blue stars, Figure 4.7) are significantly higher than at the other locations considered in this study. The background mixing ratios consistently increase through this period from about 0.4 to about 0.7 ppt whereas the highest Taiwan samples have mixing ratios of up to 3 ppt. These enhancements in mixing ratios in all four years of the Taiwan campaigns indicate continued emissions in this region, most likely continental East Asia.

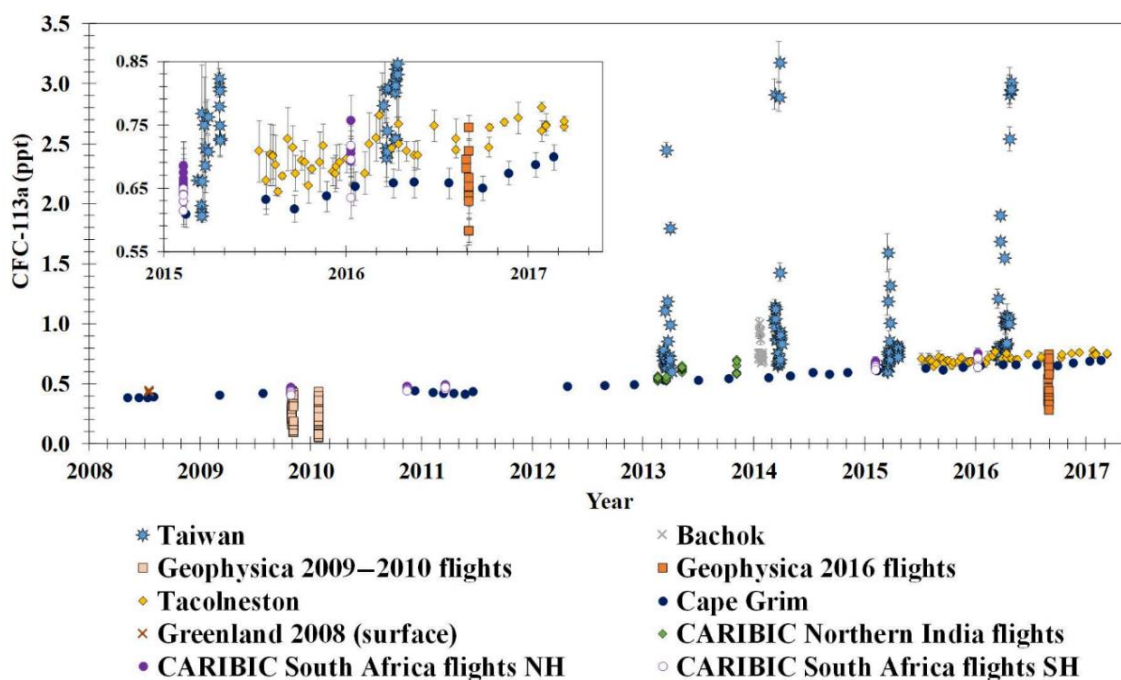


Figure 4.7: CFC-113a mixing ratios 2008-2017 from all the sources presented in this study with an inset of the period 2015-2017 to give an enlarged view of the Tacolneston data. The error bars represent the  $1\sigma$  standard deviation.

To determine the region(s) of emissions more accurately NAME footprints were used (Figure 4.8a-g, Appendix). In general, when there are enhancements in CFC-113a mixing ratios the NAME footprints usually show the air most likely came from the boundary layer over eastern China or the Korean Peninsula as shown in (a), (c), (d), and (g) for example (Figures 4.8 & 4.9). In contrast, the footprints in (b), (e) and (f) are examples of samples with lower CFC-113a mixing ratios and correspondingly there is very little influence from eastern China or the Korean Peninsula. However, we recognise the limitations of our relatively sparse dataset which prevents us from pinpointing the source region(s) further.

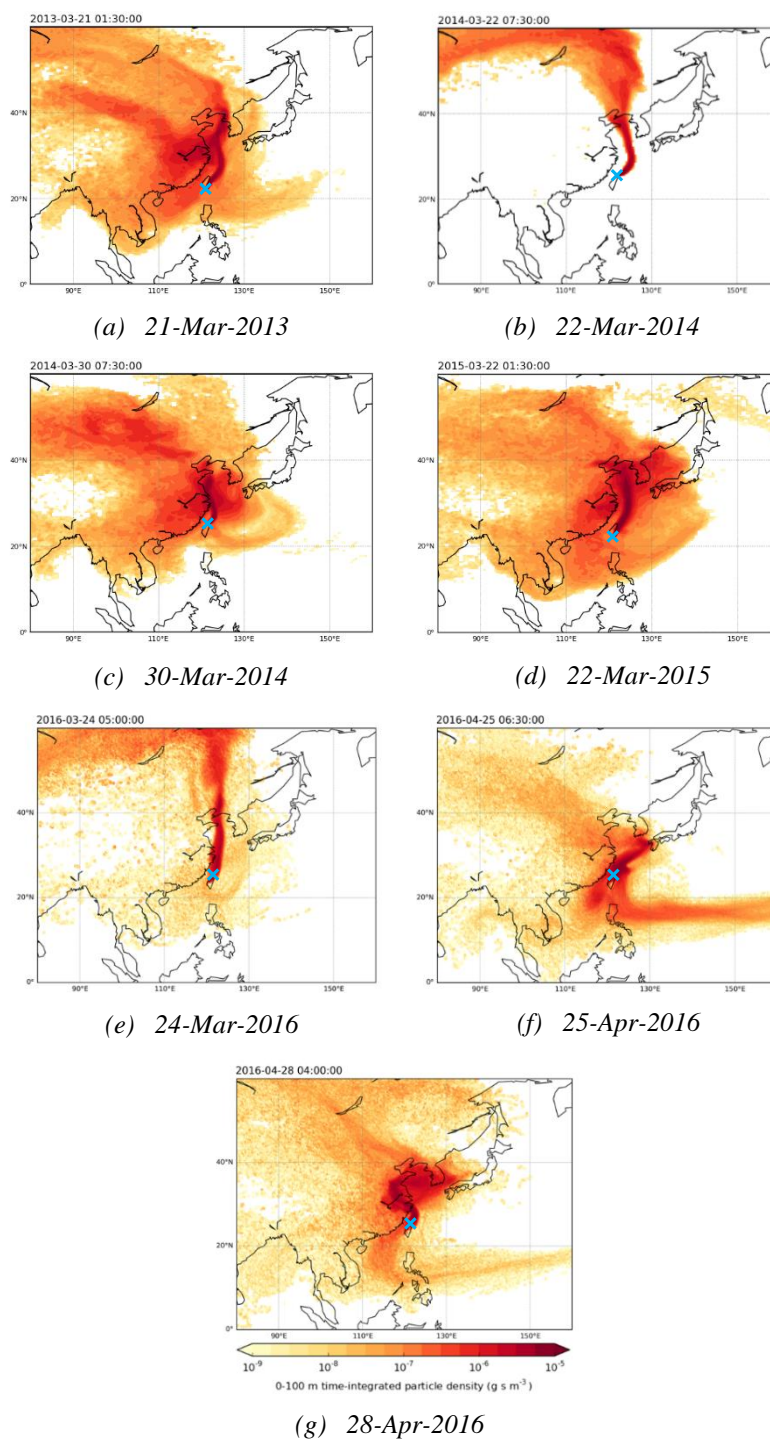


Figure 4.8: NAME footprints derived from 12-day backward simulations and showing the time integrated density of particles below 100 m altitude for the approximate times when samples were collected during the Taiwan campaign. Each sampling site is denoted by a blue cross. (a), (c), (d) and (g) are the samples with the highest CFC-113a mixing ratios measured in each year. (f) is the sample taken just before (g) when the air was coming from a different direction and the mixing ratio of CFC-113a was much lower. (b) and (e) are also examples of samples with lower CFC-113a mixing ratios. Arrows in Fig. 4.9 show the mixing ratios of CFC-113a for these NAME footprints. For the rest of the NAME footprints see the Appendix.

The mixing ratios in Taiwan are very variable indicating nearby source region(s) whereas Cape Grim and Tacolneston mixing ratios are much less variable. Therefore, the Taiwan measurements are better suited to investigate correlations that might shed further light on potential sources. After investigating correlations of CFC-113a with over 50 other halocarbons in samples from Taiwan we found CFC-113a mixing ratios correlate well ( $R^2 > 0.750$ ) in multiple years with those of CFC-113 and HCFC-133a ( $\text{CH}_2\text{ClCF}_3$ ) indicating a possible link between the sources of these compounds (Table 4.2). CFC-113a correlates well with CFC-113 in 2013 and 2014 but shows almost no correlation in 2015 and a slightly decreased correlation coefficient in 2016 (Table 4.2, Figure 4.9). In contrast, HCFC-133a strongly correlates with CFC-113a in the first three years (Table 4.2). The tropospheric lifetime of HCFC-133a is 4-5 years (McGillen et al., 2015) and its mixing ratios have varied in recent years. They increased in 2012/2013 and decreased in 2014/2015 (Vollmer et al., 2015). Large changes in emissions are needed to produce such a variable trend but the causes of these changes are still unclear (Vollmer et al., 2015). According to our latest data from Cape Grim, in 2016 they began increasing again.

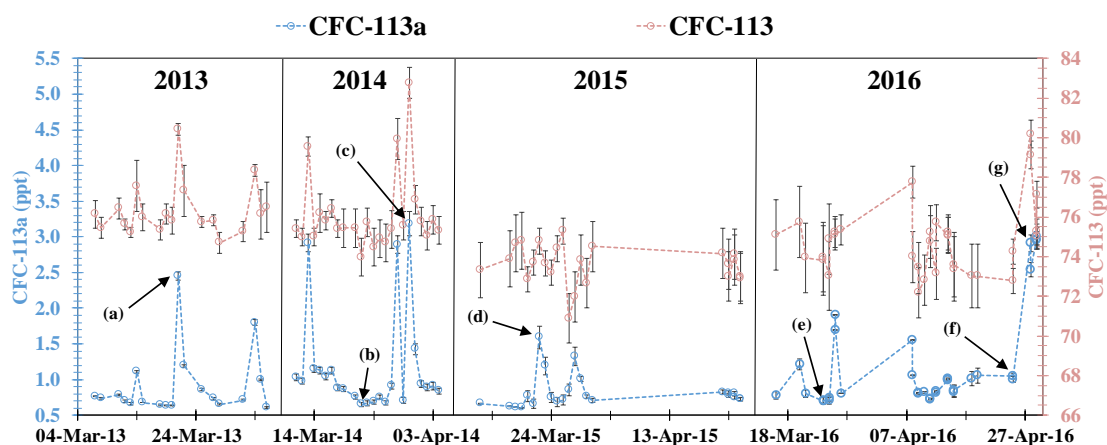


Figure 4.9: CFC-113a and CFC-113 mixing ratios observed in Taiwan in March and April 2013-2016. Arrows show the mixing ratios of CFC-113a that relate to the NAME footprints shown in Fig. 4.8. The error bars represent the  $1\sigma$  standard deviation.

Table 4.2: Squared Pearson correlations ( $R^2$ ) of CFC-113a mixing ratios with other compounds in Taiwan 2013-2016.

	2013	2014	2015	2016
<b>CFC-113</b>	0.866	0.909	0.013	0.429
<b>HCFC-133a</b>	0.923	0.923	0.891	0.637
<b>HFC-134a</b>	0.001	0.055	0.010	–
<b>HFC-125</b>	0.319	0.219	0.016	0.850
<b>CFC-114a</b>	–	–	0.754	0.386
<b>HCFC-123</b>	–	0.013	0.217	0.202
<b>HCFC-124</b>	–	0.537	0.833	0.078
<b>No. of data points</b>	19	24	23	33

CFC-113a mixing ratios in many of the samples collected at Bachok, Malaysia (grey crosses, Figure 4.7) are also enhanced above background levels although not to the same degree as the Taiwan samples, they range from 0.68 ppt to 1.00 ppt. The higher mixing ratios also have their origin in East Asian air masses being transported rapidly to the tropics by the East Asian winter monsoon circulation (Ashfold et al., 2015; Oram et al., 2017). Figure 4.10 shows an example NAME footprint from a sample collected in January 2014 that is representative for many other events.

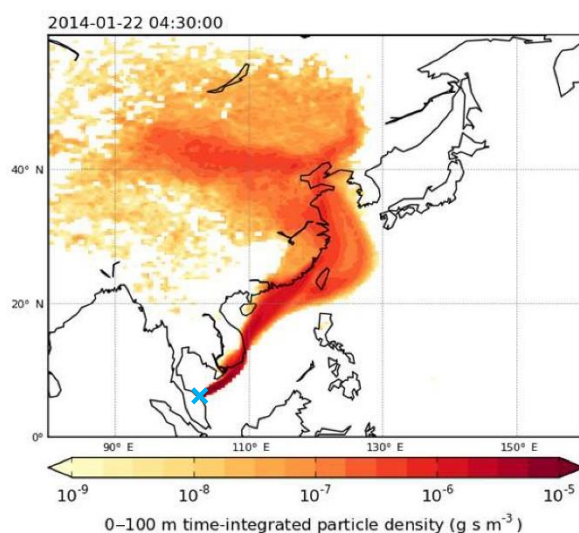


Figure 4.10: NAME footprint derived from 12-day backward simulation and showing the time integrated density of particles below 100 m altitude on 22-Jan-2014 during a period of elevated CFC-113a mixing ratios at Bachok, Malaysia. The sampling site is denoted by a blue cross.

The Tacolneston samples (yellow diamonds, Figure 4.7) show no significant enhancements in CFC-113a mixing ratios. This indicates the absence of sources in North-West Europe. Due to this and the relatively long lifetime of CFC-113a Tacolneston can be considered to be representative of Northern Hemisphere background mixing ratios of CFC-113a for that latitude. Both sites in Taiwan and also Tacolneston are Northern Hemisphere sites and although the Taiwan sites have many enhancements in CFC-113a mixing ratios there are some samples with background mixing ratios (Figure 4.7). For example, in spring 2016, the only period for which these datasets overlap, the lowest CFC-113a mixing ratio in Taiwan is 0.70 ppt on 24-Mar-2016 (Figure 4.8e). The closest Tacolneston sample to this is on 04-Apr-2016 with a CFC-113a mixing ratio of 0.71 ppt. This shows that Taiwan can encounter mixing ratios at background levels of CFC-113a. However, many of the air samples collected in Taiwan show mixing ratios of CFC-113a above background levels, indicating that enhanced levels of CFC-113a are generally widespread across this region.

#### **4.3.2.2 Interhemispheric gradient of CFC-113a**

For the period when measurements were made at both Cape Grim and Tacolneston (from July 2015 to February 2017), the Tacolneston mixing ratios were almost exclusively higher (though often indistinguishable within uncertainties) than the Cape Grim mixing ratios (Figure 4.7-inset). On average Cape Grim mixing ratios are  $0.055 \pm 0.024$  ppt lower than Tacolneston mixing ratios. This shows that there is an interhemispheric gradient with higher CFC-113a mixing ratios in the Northern Hemisphere as would be expected for a compound emitted primarily in the Northern Hemisphere. This gradient is further supported by data from the six CARIBIC flights between Germany and South Africa for 2009-2016 (Figures 4.4 & 4.7). The CARIBIC samples (purple circles, Figure 4.7) from the 2016 flight coincide temporally with the Tacolneston and the Cape Grim samples in Fig. 4.7 and confirm the observation of higher mixing ratios in the Northern Hemisphere (filled purple circles) and lower mixing ratios in the Southern Hemisphere (unfilled purple circles).

Laube et al. (2014) already found an interhemispheric gradient in CFC-113a using four of these CARIBIC flights 2009-2011 and furthermore discovered that the increasing trend of CFC-113a at Cape Grim, lagged behind the increasing trend inferred from the firn air samples, collected to a depth of 76 metres, from Greenland, in the Northern Hemisphere. As the firn air measurements in the Laube et al. (2014) study were collected in Greenland between 14-30 July 2008, the surface measurements will be representative of atmospheric mixing ratios at that time. They will also be representative of background Northern Hemispheric CFC-113a mixing ratios for that latitude as the Greenland firn air location was isolated from any large industrial areas with potential sources of CFC-113a. Figure 4.7 includes the three measurements closest to the surface (brown crosses) although they are so close together that they appear to be one cross in the Figure and the average mixing ratio of the three samples is  $0.44 \pm 0.01$  ppt.

Overall, these measurements demonstrate that there is an interhemispheric gradient in CFC-113a with higher mixing ratios in the Northern Hemisphere. This persistent interhemispheric difference indicates ongoing emissions of CFC-113a in the Northern Hemisphere with higher emissions in the Northern Hemisphere compared to the Southern Hemisphere. Similar interhemispheric gradients have been found for other CFCs (Engel and Rigby et al., 2018), as CFCs are almost exclusively produced by industrial processes and most industrial production (and consumption) takes place in the Northern Hemisphere.

#### 4.3.2.3 Measurements of CFC-113a in the stratosphere

Nearly all air samples collected during CARIBIC flights represent cruising altitudes of 10-12 km, which for samples over northern India, during four flights going from Germany to Thailand (green diamonds, Figure 4.7) would be near the tropopause. Their mixing ratios should be representative for air masses prior to entering the tropical tropopause region which is the main entrance region to the stratosphere (Fueglistaler et al., 2009). For the flight on 9-Nov-2013, there is some enhancement above background mixing ratios over South-East Asia (Figures 4.7, 4.11). We speculate that this is likely due to air being transported from East Asia into the tropics via cold surges and then being transported up into the upper troposphere via convection (Oram et al., 2017). This means that the uplift mechanism in this region could potentially enhance mixing ratios of long-lived ODSs entering the stratosphere as compared to the ‘background’ clean air ground-based abundances that are normally used to derive such inputs (Carpenter and Reimann et al., 2014). The mechanism has already been proven to exist for shorter-lived gases (Oram et al., 2017) and we see very similar patterns transporting elevated mixing ratios of CFC-113a to the tropics very rapidly (within days) during a time of increased convective uplift.

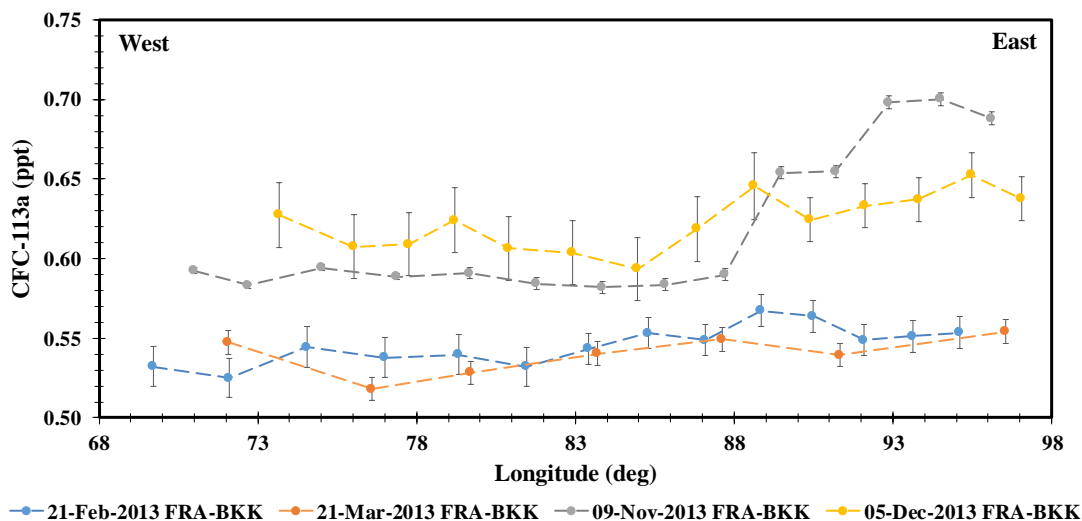


Figure 4.11: CFC-113a mixing ratios from samples collected over northern India during CARIBIC aircraft flights in 2013 going from Frankfurt, Germany (FRA) to Bangkok, Thailand, (BKK), with  $1\sigma$  standard deviations as error bars.

The Geophysica flights reach altitudes of 20 km and so sample lower stratospheric air. The Geophysica 2009-2010 flights (pink squares) and the Geophysica 2016 flights (orange squares) begin at background mixing ratios and then decrease (Figure 4.7, Figure 4.12). The Geophysica 2016 highest CFC-113a mixing ratio was  $0.75 \pm 0.02$  ppt. The Tacolneston mixing ratio at this time was  $0.72 \pm 0.01$  ppt. In 2009-2010 the Geophysica highest mixing ratio was  $0.44 \pm 0.01$  ppt and at this time the Cape Grim mixing ratio was  $0.43 \pm 0.01$  ppt. The highest mixing ratios observed in both campaigns agree quite well (within uncertainties) with tropospheric background mixing ratios at the time and can therefore be considered as representative of stratospheric entrance mixing ratios. In general, mixing ratios decrease as the aircraft ascends, mainly because air at higher altitudes will have taken longer to travel there and therefore is older and CFC-113a at higher altitudes has experienced photolytic decomposition.

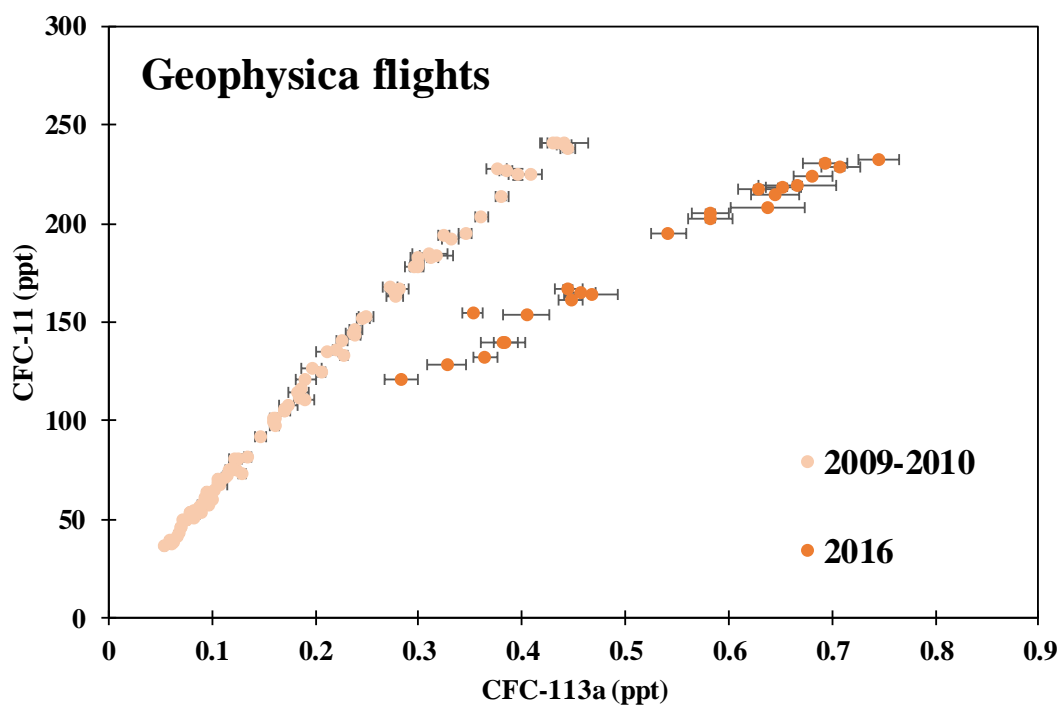


Figure 4.12: CFC-113a mixing ratios against CFC-11 mixing ratios from Geophysica research aircraft flights into the stratosphere in late 2009 and early 2010 published in Laube et al. (2014) and additional Geophysica research aircraft flights in 2016 in Kalamata (StratoClim project). The error bars represent the  $1\sigma$  standard deviation.

Mixing ratios of CFC-11 also decrease with increasing altitude and they can be used to interpret the changes in CFC-113a mixing ratios. Given that CFC-11 mixing ratios have declined over the last 25 years older air will have entered the stratosphere with higher mixing ratios and will also have undergone more chemical processing. In addition, as the stratospheric lifetime of CFC-11 is shorter than its global lifetime, its mixing ratios will decline more rapidly in the stratosphere than in the troposphere. However, its vertical profile is a function of how its photolysis changes with altitude and the rate of vertical transport. If photochemical loss were the main factor determining the vertical profile of both these CFCs, there would be a straight-line correlation, particularly since

both have very similar lifetimes which should also lead to the intercept being very close to zero, which is seen for the 2009/10 flights (Figure 4.12). The intercept for the 2016 data does not look like it will be near zero, but if samples were collected at higher altitudes the mixing ratios trend might curve closer towards zero (Figure 4.12). If the tropospheric trends of these CFCs are different then this can lead to curvature of the line. For example, as the tropospheric mixing ratio of CFC-11 is declining whilst it is increasing for CFC-113a, this should cause the line to curve towards higher CFC-113a mixing ratios which is apparent in the 2009/10 flights (Figure 4.12). Moreover, later profiles should have shallower gradients, which is what we see with the 2016 data compared to the 2009/10 data (Figure 4.12).

#### **4.4 Possible sources of CFC-113a**

CFCs are entirely anthropogenic in origin. This means that there are processes either producing or involving CFC-113a that lead to continuing emissions of substantial amounts of this compound, especially in East Asia. Whilst the Montreal Protocol has banned the production and consumption of CFCs, there are exemptions including the use of ODSs as chemical feedstocks, chemical intermediates and fugitive emissions (UNEP, 2016a). As the Montreal Protocol does not require isomers to be reported separately, CFC-113 and CFC-113a may be reported together.

The strong correlations of CFC-113a with CFC-113 and HCFC-133a in Taiwan (Section 4.3.2.1) suggest that they are involved in the same production pathways or that their production facilities are co-located. There is an absence of a correlation between CFC-113a and CFC-113 in 2015 in Taiwan and in addition, the overall mixing ratios in 2015 appear to be lower than in the other years and have fewer large enhancements (Figure 4.9). This could be because in general less air was arriving from China/Korea in 2015, which is indicated by the NAME footprints (Appendix). Regions in China and Korea were found to be the most likely locations of CFC-113a emissions. Alternatively, the varying correlations in different years between CFC-113a and CFC-113 could be an indication of two or more independent sources of CFC-113a. CFC-113 feedstock use, for production of polymers, trifluoroacetic acid, pesticides and HFCs, decreased by over 50 % in 2015 due to one producer, which is also a user choosing not to produce CFC-113 in 2015 and reducing in-house inventories instead (Maranion et al., 2017). If this were the process leading to correlated emissions of CFC-113a and CFC-113 it may explain their lack of correlation in 2015.

One possible source of CFC-113a is from HFC production, specifically, of HFC-134a ( $\text{CH}_2\text{FCF}_3$ ) and HFC-125 ( $\text{CF}_3\text{CHF}_2$ ), as both may involve CFC-113a in their production process. One of the pathways for production of HFC-134a begins with CFC-113 being isomerised to form CFC-113a, which is then fluorinated to produce CFC-114a ( $\text{CF}_3\text{CCl}_2\text{F}$ ), the latter is then hydrogenated to produce HFC-134a (Manzer, 1990; Rao et al., 1992; Bozorgzadeh et al., 2001; Maranion et al., 2017). Another production method involves the reaction of hydrogen fluoride with trichloroethylene to form HCFC-133a and HFC-134a (Manzer, 1990; McCulloch and Lindley, 2003;

Shanthan Rao et al., 2015). The process for manufacturing HFC-125 involves the starting materials of either HCFC-123 or HCFC-124. CFC-113a, CFC-113 and HCFC-133a can be formed as by-products when HCFC-123 and HCFC-124 are fluorinated and recycled during the process that forms HFC-125 (Kono et al., 2002; Takahashi et al., 2002).

If there were leaks in the system or venting of gases was practiced during these processes, this could lead to enhanced mixing ratios of CFC-113a and strong correlations with its isomer CFC-113 and HCFC-133a. HFC production should be contained and not involve fugitive emissions to the atmosphere. However, the Chemicals Technical Options Committee (CTOC) 2014 report suggests there may be small leaks, depending on the quality of the system, ranging between 0.1 % and 5 % of the feedstock used. The CTOC reported that a leak rate of about 1.6 % would be needed if all CFC-113a and HCFC-133a in the atmosphere had come from their use as feedstock in the production of HFC-134a, HFC-125 and HFC-143a, which is within the previous range (CTOC, 2014). HFC-143a is produced using HCFC-133a so it was included in the CTOC estimate but CFC-113a is not involved in its production so it is not included in this study (CTOC, 2014).

HFC-134a and HFC-125 mixing ratios are not well correlated with those of CFC-113a, CFC-113 or HCFC-133a, except for HFC-125 in 2016 that has a good correlation with CFC-113a (Table 4.2). We would not necessarily expect them to be well correlated as most of the emissions of the HFCs are usually related to their uses rather than their production. CFC-114a is also part of the production process of HFC-134a (Manzer, 1990), and can be another by-product during HFC-125 production (Kono et al., 2002; Takahashi et al., 2002). CFC-114a was only measured in 2015 and 2016 in Taiwan and was strongly correlated with CFC-113a in 2015 but not in 2016. This inconsistent correlation does not help to define further the source of CFC-113a. Furthermore HCFC-123 mixing ratios are not well correlated with CFC-113a, CFC-113 or HCFC-133a in any year in Taiwan but HCFC-124 mixing ratios are well correlated in 2015 with CFC-113a ( $R^2=0.833$ , Table 4.2) and with HCFC-133a ( $R^2=0.791$ ). This strong correlation with HCFC-124 points to HFC-125 production being the dominant source in 2015.

As discussed above, eastern China and/or the Korean Peninsula are the most likely source regions for the elevated mixing ratios of CFC-113a observed in Taiwan, and the HFC industry in China has been growing rapidly in recent years (Fang et al., 2016). In China in 2013, productions of  $118 \text{ Gg yr}^{-1}$  of HFC-134a and  $78 \text{ Gg yr}^{-1}$  of HFC-125 were reported (Fang et al., 2016). Most industry in China is located on the eastern coast and the majority of HFC manufacturers are in the three eastern provinces of Shanghai, Zhejiang and Jiangsu. There are also HFC-134a and HFC-125 production plants in Japan, South Korea and Taiwan but the majority are located in China. The HFC production plants located in Taiwan could influence the mixing ratios at both the sites in Taiwan which introduces an additional uncertainty.

Alternatively, there is an official exemption in the Montreal Protocol for the use of CFC-113a as an “agrochemical intermediate for the manufacture of synthetic

pyrethroids”, (UNEP, 2003) probably because it is used to make the insecticides cyhalothrin and tefluthrin (Brown et al., 1994; Jackson et al., 2001; Cuzzato and Bragante, 2002). In addition, CFC-113 is a feedstock used to make trifluoroacetic acid (TFA) and pesticides (Maranion et al., 2017). CFC-113a is an intermediate in this process and these production processes are used in India and China and so this could also be a source in this region (Maranion et al., 2017). Furthermore, HCFC-133a is also used to manufacture TFA and agrochemicals although the process involving HCFC-133a is not related to the process involving CFC-113a (Rüdiger et al., 2002; Maranion et al., 2017).

Furthermore, CFC-113a is potentially present as an impurity in CFC-113 and the emissions of CFC-113a could be from CFC-113 banks. We saw in Section 4.3.1 that estimated emissions of CFC-113a began in the 1960s and HFC production did not become a large-scale industry until much later, so there must have been another source of CFC-113a during that earlier part of the record. In Section 4.3.1 we concluded that there was possibly a small amount of continued emissions of CFC-113 to maintain the observed atmospheric mixing ratios. This would be consistent with either a source from banks and/or release in conjunction with CFC-113a.

To summarise we have identified four possible sources of CFC-113a: agrochemical production, HFC-134a production, HFC-125 production and an impurity in CFC-113. The correlations indicate that HFC production is the dominant source in the East Asian region; however, there is currently insufficient data available to conclude this with high confidence. Overall, the sources of CFC-113a emissions are still uncertain and further evidence is needed to quantify and pinpoint them. However, the likely sources we have found do not necessarily indicate non-compliance with the Montreal Protocol as the use of CFCs as intermediates in the production of other compounds are permitted under the Montreal Protocol.

## **4.5 Conclusions**

There is a continued global increasing trend in CFC-113a mixing ratios based on a number of globally distributed sampling activities giving a consistent picture. CFC-113a mixing ratios at Cape Grim, Tasmania increased since the previous study from 0.50 ppt in December 2012 to 0.70 ppt in February 2017. The derived emissions were still significantly above 2010 levels and were on average  $1.7 \text{ Gg yr}^{-1}$  ( $1.3\text{-}2.4 \text{ Gg yr}^{-1}$ ) between 2012 and 2016. Additionally, CFC-113a mixing ratios vary globally and our findings confirm an interhemispheric gradient with mixing ratios decreasing from the Northern Hemisphere to the Southern Hemisphere. No significant emissions of CFC-113a occur in the UK but strong sources exist in East Asia. There are multiple possible sources of CFC-113a emissions and correlation analysis suggests the emissions might be associated with the production of HFC-134a and HFC-125.

The background abundances of CFC-113a reported here are currently small ( $<1.0$  ppt) in comparison to the most common CFC, CFC-12 which had declining atmospheric mixing ratios of  $\sim 510$  ppt in 2017 (NOAA, 2017). Therefore, the contribution of CFC-

113a to stratospheric ozone depletion is comparably small and is not a cause for concern. While its increase in recent years has been considerable in percentage terms, it would have to continue increasing at this rate for several centuries before it reaches the atmospheric mixing ratios of the major CFCs in the 1990s. For example, a constant emission of  $2 \text{ Gg yr}^{-1}$  for CFC-113a yields a steady-state global mixing ratio of about 3.2 ppt. In 2016, HFCs were added to the Montreal Protocol and under the new amendment HFC consumption will be phased down in the coming decades (UNEP, 2016b). Therefore, if this phase down schedule is successful and the main source of CFC-113a is indeed from HFC production, then CFC-113a atmospheric mixing ratios should stop increasing in the future. However, whilst it seems likely, it is still not clear whether HFC production is actually the main source of global CFC-113a emissions and whilst CFC-113a emissions have appeared to be stable in recent years this does not mean that they will not increase in the future. Further investigation and continued monitoring is needed to assess future changes and ensure the continued effectiveness of the Montreal Protocol. When continuous measurements of CFC-113a in the East Asia region become available the magnitude and origins of East Asian CFC-113a emissions can be quantified.

In the past, it was assumed that isomers of CFCs had similar uses, sources and trends and therefore it was not necessary to report them separately. However, in this study, we have found that the isomers CFC-113a and CFC-113 continue to have different trends in the atmosphere and in their emissions. Recently CFC-114a ( $\text{CF}_3\text{CCl}_2\text{F}$ ) and CFC-114 ( $\text{CClF}_2\text{CClF}_2$ ) were also found to have different trends and sources (Laube et al., 2016). If policy-makers wish to limit the impacts of individual isomers, then atmospheric observational data on individual CFC isomers should be reported to UNEP wherever possible. In addition, the increase in CFC-113a demonstrates that the use of ODSs as chemical feedstock or intermediates is becoming relatively more important as the use of ODSs for direct applications decreases. If policy-makers target zero emissions of CFCs, then they might consider regulating these uses of ODSs.

## **Acknowledgements**

We are grateful for the work of the Geophysica team, the CARIBIC team (CARIBIC-IAGOS), the staff at the Cape Grim Baseline Air Pollution Station, the NOAA Global Monitoring Division, and the AGAGE network. The StratoClim flights were funded by the European Commission (FP7 project Stratoclim-603557, [www.stratoclim.org](http://www.stratoclim.org)). The collection and curation of the Cape Grim Air Archive is jointly funded by CSIRO, the Bureau of Meteorology (BoM) and Refrigerant Reclaim Australia.; BoM/CGBAPS staff at Cape Grim were/are largely responsible for the collection of archive samples and UEA flask air samples; the original (mid-1990s) subsampling of the archive for UEA was funded by AFEAS and CSIRO, ongoing subsampling by CSIRO. K. E. Adcock was supported by the UK Natural Environment Research Council (PhD studentship NE/L002582/1). J. C. Laube received funding from the UK Natural Environment Research Council (Research Fellowship NE/I021918/1). Norfazrin Mohd Hanif has been funded through PhD studentship by the Ministry of Education Malaysia (MOE)

and Universiti Kebangsaan Malaysia (UKM). We acknowledge use of the NAME atmospheric dispersion model and associated NWP meteorological data sets made available to us by the UK Met Office. We also acknowledge the significant storage resources and analysis facilities made available to us on JASMIN by STFC CEDA along with the corresponding support teams.

## References

Allin, S. J., Laube, J. C., Witrant, E., Kaiser, J., McKenna, E., Dennis, P., Mulvaney, R., Capron, E., Martinerie, P., Röckmann, T., Blunier, T., Schwander, J., Fraser, P. J., Langenfelds, R. L. and Sturges, W. T.: Chlorine isotope composition in chlorofluorocarbons CFC-11, CFC-12 and CFC-113 in firn, stratospheric and tropospheric air, *Atmos. Chem. Phys.*, 15(12), 6867–6877, doi:10.5194/acp-15-6867-2015, 2015.

Ashfold, M. J., Pyle, J. A., Robinson, A. D., Meneguz, E., Nadzir, M., Phang, S. M., Samah, A. A., Ong, S., Ung, H. E., Peng, L. K., Yong, S. E., Harris, N. R. P. and Ashfold, M.: Rapid transport of East Asian pollution to the deep tropics, *Atmos. Chem. Phys.*, 15, 3565–3573, doi:10.5194/acp-15-3565-2015, 2015.

Aulagnier, C., Rayner, P., Ciais, P., Vautard, R., Rivier, L. and Ramonet, M.: Is the recent build-up of atmospheric CO<sub>2</sub> over Europe reproduced by models. Part 2: An overview with the atmospheric mesoscale transport model CHIMERE, *Tellus, Ser. B Chem. Phys. Meteorol.*, 62(1), 14–25, doi:10.1111/j.1600-0889.2009.00443.x, 2010.

Baasandorj, M., Feierabend, K. J. and Burkholder, J. B.: Rate Coefficients and ClO Radical Yields in the Reaction of O(<sup>1</sup>D) with CClF<sub>2</sub>CCl<sub>2</sub>F, CCl<sub>3</sub>CF<sub>3</sub>, CClF<sub>2</sub>CClF<sub>2</sub>, and CCl<sub>2</sub>FCF<sub>3</sub>, *Int. J. Chem. Kinet.*, 41(1987), 498–506, doi:10.1002/kin, 2011.

Bozorgzadeh, H., Kemnitz, E., Nickkho-Amiry, M., Skapin, T. and Winfield, J. M.: Conversion of 1,1,2-trichlorotrifluoroethane to 1,1,1-trichlorotrifluoroethane and 1,1-dichlorotetrafluoroethane over aluminium-based catalysts, *J. Fluor. Chem.*, 107, 45–52 [online] Available from: [http://ac.els-cdn.com/S002211390000350X/1-s2.0-S002211390000350X-main.pdf?\\_tid=3845707e-7053-11e7-a009-00000aacb360&acdnat=1500889019\\_2ab62e1f092b19b11e78f0a630956a69](http://ac.els-cdn.com/S002211390000350X/1-s2.0-S002211390000350X-main.pdf?_tid=3845707e-7053-11e7-a009-00000aacb360&acdnat=1500889019_2ab62e1f092b19b11e78f0a630956a69) (Accessed 24 July 2017), 2001.

Brenninkmeijer, C. A. M., Crutzen, P., Boumard, F., Dauer, T., Dix, B., Ebinghaus, R., Filippi, D., Fischer, H., Franke, H., Frieß, U., Heintzenberg, J., Helleis, F., Hermann, M., Kock, H. H., Koepfel, C., Lelieveld, J., Leuenberger, M., Martinsson, B. G., Miemczyk, S., Moret, H. P., Nguyen, H. N., Nyfeler, P., Oram, D., O'sullivan, D., Penkett, S., Platt, U., Püpeck, M., Ramonet, M., Randa, B., Reichelt, M., Rhee, T. S., Rohwer, J., Rosenfeld, K., Scharffe, D., Schlager, H., Schumann, U., Slemr, F., Sprung, D., Stock, P., Thaler, R., Valentino, F., Van Velthoven, P., Waibel, A., Wandel, A., Waschitschek, K., Wiedensohler, A., Xueref-Remy, I., Zahn, A., Zech, U. and Ziereis, H.: Civil Aircraft for the regular investigation of the atmosphere based on an instrumented container: The new CARIBIC system, *Atmos. Chem. Phys.*, 7, 4953–4976, doi:10.5194/acp-7-4953-2007, 2007.

Brown, S. M., Glass, J. C. and Sheldrake, G. N.: Preparation of

1,1,1, trichlorotrifluoroethane, UK Patent Application, GB2269381A, [online] Available from: <https://patents.google.com/patent/GB2269381A/en?q=%22CFC-113a%22,trichlorotrifluoroethane,CCl3CF3&q=cylhalothrin,Lambda-cylhalothrin,C23H19ClF3NO3&q=tefluthrin,C17H14ClF7O2&q=C07C17%2F10> (Accessed 24 July 2017), 1994.

Buizert, C., Martinerie, P., Petrenko, V. V., Severinghaus, J. P., Trudinger, C. M., Witrant, E., Rosen, J. L., Orsi, A. J., Rubino, M., Etheridge, D. M., Steele, L. P., Hogan, C., Laube, J. C., Sturges, W. T., Levchenko, V. A., Smith, A. M., Levin, I., Conway, T. J., Dlugokencky, E. J., Lang, P. M., Kawamura, K., Jenk, T. M., White, J. W. C., Sowers, T., Schwander, J. and Blunier, T.: Gas transport in firn: Multiple-tracer characterisation and model intercomparison for NEEM, Northern Greenland, *Atmos. Chem. Phys.*, 12, 4259–4277, doi:10.5194/acp-12-4259-2012, 2012.

Burkholder, J. B., Sander, S. P., Abbatt, J. P. D., Barker, J. R., Huie, R. E., Kolb, C. E., Kurylo, M. J., Orkin, V. L., Wilmouth, D. M. and Wine, P. H.: Chemical Kinetics and Photochemical Data for Use in Atmospheric Studies Evaluation Number 18 NASA Panel for Data Evaluation. [online] Available from: [https://jpldataeval.jpl.nasa.gov/pdf/JPL\\_Publication\\_15-10.pdf](https://jpldataeval.jpl.nasa.gov/pdf/JPL_Publication_15-10.pdf) (Accessed 26 May 2017), 2015.

Carpenter, L. J., Reimann, S., (Lead Authors), Burkholder, J. B., Clerbaux, C., Hall, B. D., Hossaini, R., Laube, J. C. and Yvon-Lewis, S. A.: Chapter 1: Update on Ozone-Depleting Substances (ODSs) and Other Gases of Interest to the Montreal Protocol, in *Scientific Assessment of Ozone Depletion: 2014, Global Ozone Research and Monitoring Project – Report No. 55*, World Meteorological Organization, Geneva, Switzerland., 2014.

Chemicals Technical Options Committee (CTOC): Montreal Protocol on Substances that Deplete the Ozone Layer Report of the Chemicals Technical Options Committee 2014 Assessment Report. [online] Available from: <http://ozone.unep.org/en/ctoc-assessment-report-2014> (Accessed 28 March 2018), ISBN: 978-9966-076-13-7, 2014.

Cullen, M. J. P.: Unified-Forecast/ Climate-Model, *Meteorol. Mag.*, 122, 81–94, 1993.

Cuzzato, P. and Bragante, L.: Process to obtain CFC-113a from CFC-113, United States Patent, US Patent 6,791,001 B2, [online] Available from: <https://patentimages.storage.googleapis.com/pdfs/164b296774fb119c06f0/US20020151755A1.pdf> (Accessed 9 March 2017), 2002.

Davis, M. E., Bernard, F., McGillen, M. R., Fleming, E. L. and Burkholder, J. B.: UV and infrared absorption spectra, atmospheric lifetimes, and ozone depletion and global warming potentials for CCl<sub>2</sub>FCCl<sub>2</sub>F (CFC-112), CCl<sub>3</sub>CClF<sub>2</sub> (CFC-112a), CCl<sub>3</sub>CF<sub>3</sub> (CFC-113a), and CCl<sub>2</sub>FCF<sub>3</sub> (CFC-114a), *Atmos. Chem. Phys.*, 16(12), 8043–8052, doi:10.5194/acp-16-8043-2016, 2016.

Douglass, A. R., Stolarski, R. S., Schoeberl, M. R., Jackman, C. H., Gupta, M. L., Newman, P. A., Nielsen, J. E. and Fleming, E. L.: Relationship of loss, mean age of air and the distribution of CFCs to stratospheric circulation and implications for atmospheric lifetimes, *J. Geophys. Res. Atmos.*, 113(14), 1–14,

doi:10.1029/2007JD009575, 2008.

Engel, A., Rigby, M., (Lead Authors), Burkholder, J. B., Fernandez, R. P., Froidevaux, L., Hall, B. D., Hossaini, R., Saito, T., Vollmer, M. K. and Yao, B.: Chapter 1 Update on Ozone-Depleting Substances (ODSs) and Other Gases of Interest to the Montreal Protocol, in *Scientific Assessment of Ozone Depletion: 2018, Global Ozone Research and Monitoring Project–Report No. 58*, World Meteorological Organization, Geneva, Switzerland., 2018.

Fang, X., Velders, G. J. M., Ravishankara, A. R., Molina, M. J., Hu, J. and Prinn, R. G.: Hydrofluorocarbon (HFC) Emissions in China: An Inventory for 2005-2013 and Projections to 2050, *Environ. Sci. Technol.*, 50(4), 2027–2034, doi:10.1021/acs.est.5b04376, 2016.

Fraser, P., Cunnold, D., Alyea, F., Weiss, R., Prinn, R., Simmonds, P., Miller, B. and Langenfelds, R.: Lifetime and emission estimates of 1,1,2-trichlorotrifluorethane (CFC-113) from daily global background observations June 1982-June 1994, *J. Geophys. Res.*, 101(D7), 12585–12599, 1996.

Fraser, P., Oram, D., Reeves, C., Penkett, S. and McCulloch, A.: Southern Hemisphere halon trends (1978-1998) and global halon emissions, *J. Geophys. Res.*, 104(D13), 15985–15999, doi:10.1029/1999JD900113, 1999.

Fueglistaler, S., Dessler, A. E., Dunkerton, T. J., Folkins, I., Fu, Q. and Mote, P. W.: Tropical Tropopause Layer, *Rev. Geophys.*, 47, RG1004, doi:10.1029/2008RG000267, 2009.

Ganesan, A. L., Manning, A. J., Grant, A., Young, D., Oram, D. E., Sturges, W. T., Moncrieff, J. B. and O’Doherty, S.: Quantifying methane and nitrous oxide emissions from the UK and Ireland using a national-scale monitoring network, *Atmos. Chem. Phys.*, 15, 6393–6406, doi:10.5194/acp-15-6393-2015, 2015.

Jackson, A. R., Doyle, S. J., Moorhouse, K. and Gray, T.: Chlorination Process, United States Patent, US Patent 6,229,057 B1, [online] Available from: <https://patentimages.storage.googleapis.com/00/8d/59/58d47ee41c4baf/US6229057.pdf> (Accessed 24 July 2017), 2001.

Jones, A., Thomson, D., Hort, M. and Devenish, B.: The U.K. Met Office’s Next-Generation Atmospheric Dispersion Model, NAME III, in *Air Pollution Modeling and Its Application XVII*, edited by C. Borrego and A.-L. Norman, pp. 580–589, Boston, MA, Springer US., 2007.

Kaiser, J., Engel, A., Borchers, R. and Röckmann, T.: Probing stratospheric transport and chemistry with new balloon and aircraft observations of the meridional and vertical N<sub>2</sub>O isotope distribution, *Atmos. Chem. Phys.*, 6(11), 3535–3556, doi:10.5194/acp-6-3535-2006, 2006.

Ko, M. K. W., Newman, P. A., Reimann, S., and Strahan, S. E. (Eds.): *SPARC Report on Lifetimes of Stratospheric Ozone-Depleting Substances, Their Replacements, and Related Species*, SPARC Report No. 6, WCRP-15/2013, SPARC Office. [online]

Available from: <http://www.sparc-climate.org/publications/sparc-reports/sparc-report-no-6/> (Accessed 28 March 2018), 2013.

Kono, S., Yoshimura, T. and Shibamura, T.: Process for producing 1,1,1,2,2-pentafluoroethane, United States Patent, US Patent 6,392,106 B1, [online] Available from: <https://patentimages.storage.googleapis.com/96/18/bb/1942c2e2d57286/US6392106.pdf> (Accessed 5 September 2017), 2002.

Laube, J. C., Engel, A., Bönisch, H., Möbius, T., Sturges, W. T., Braß, M. and Röckmann, T.: Fractional release factors of long-lived halogenated organic compounds in the tropical stratosphere, *Atmos. Chem. Phys.*, 10, 1093–1103, doi:10.5194/acp-10-1093-2010, 2010.

Laube, J. C., Hogan, C., Newland, M. J., Mani, F. S., Fraser, P. J., Brenninkmeijer, C. A. M., Martinerie, P., Oram, D. E., Röckmann, T., Schwander, J., Witrant, E., Mills, G. P., Reeves, C. E. and Sturges, W. T.: Distributions, long term trends and emissions of four perfluorocarbons in remote parts of the atmosphere and firn air, *Atmos. Chem. Phys.*, 12(9), 4081–4090, doi:10.5194/acp-12-4081-2012, 2012.

Laube, J. C., Keil, A., Bönisch, H., Engel, A., Röckmann, T., Volk, C. M. and Sturges, W. T.: Observation-based assessment of stratospheric fractional release, lifetimes, and ozone depletion potentials of ten important source gases, *Atmos. Chem. Phys.*, 13, 2779–2791, doi:10.5194/acp-13-2779-2013, 2013.

Laube, J. C., Newland, M. J., Hogan, C., Brenninkmeijer, C. A. M., Fraser, P. J., Martinerie, P., Oram, D. E., Reeves, C. E., Röckmann, T., Schwander, J., Witrant, E. and Sturges, W. T.: Newly detected ozone-depleting substances in the atmosphere, *Nat. Geosci.*, 7(March), 10–13, doi:10.1038/NNGEO2109, 2014.

Laube, J. C., Hanif, N. M., Martinerie, P., Gallacher, E., Fraser, P. J., Langenfelds, R., Brenninkmeijer, C. A. M., Schwander, J., Witrant, E., Wang, J.-L., Ou-Yang, C.-F., Gooch, L. J., Reeves, C. E., Sturges, W. T. and Oram, D. E.: Tropospheric observations of CFC-114 and CFC-114a with a focus on long-term trends and emissions, *Atmos. Chem. Phys.*, 16, 15347–15358, doi:10.5194/acp-16-15347-2016, 2016.

Leedham Elvidge, E. C., Oram, D. E., Laube, J. C., Baker, A. K., Montzka, S. A., Humphrey, S., O’Sullivan, D. A. and Brenninkmeijer, C. A. M.: Increasing concentrations of dichloromethane, CH<sub>2</sub>Cl<sub>2</sub>, inferred from CARIBIC air samples collected 1998-2012, *Atmos. Chem. Phys.*, 15(4), 1939–1958, doi:10.5194/acp-15-1939-2015, 2015.

Leedham Elvidge, E. C., Bönisch, H., Brenninkmeijer, C. A. M., Engel, A., Fraser, P. J., Gallacher, E., Langenfelds, R., Mühle, J., Oram, D. E., Ray, E. A., Ridley, A. R., Röckmann, T., Sturges, W. T., Weiss, R. F. and Laube, J. C.: Evaluation of stratospheric age-of-air from CF<sub>4</sub>, C<sub>2</sub>F<sub>6</sub>, C<sub>3</sub>F<sub>8</sub>, CHF<sub>3</sub>, HFC-125, HFC-227ea and SF<sub>6</sub>; implications for the calculations of halocarbon lifetimes, fractional release factors and ozone depletion potentials, *Atmos. Chem. Phys.*, 18(5), 3369–3385, doi:10.5194/acp-18-3369-2018, 2018.

Manzer, L. E.: The CFC-Ozone Issue: Progress on the Development of Alternatives to

- CFCs, *Science.*, 249(4964), 31–35, doi:10.1126/science.249.4964.31, 1990.
- Maranian, B., Pizano, M. and Woodcock, A.: Montreal Protocol on Substances that Deplete the Ozone Layer, Report of the UNEP Technology and Economic Assessment Panel, Volume 1, Progress Report, May 2017, Nairobi, Kenya. [online] Available from: <http://conf.montreal-protocol.org/meeting/oewg/oewg-39/presession/Background-Documents/TEAP-Progress-Report-May2017.pdf> (Accessed 19 September 2017), 2017.
- McCulloch, A., Midgley, P. M. and Fisher, D. A.: Distribution of emissions of chlorofluorocarbons (CFCs) 11, 12, 113, 114 and 115 among reporting and non-reporting countries in 1986, *Atmos. Environ.*, 28(16), 2567–2582, doi:10.1016/1352-2310(94)90431-6, 1994.
- McCulloch, A. and Lindley, A. A.: From mine to refrigeration: A life cycle inventory analysis of the production of HFC-134a, *Int. J. Refrig.*, 26, 865–872, doi:10.1016/S0140-7007(03)00095-1, 2003.
- McGillen, M. R., Bernard, F., Fleming, E. L. and Burkholder, J. B.: HCFC-133a (CF<sub>3</sub>CH<sub>2</sub>Cl): OH rate coefficient, UV and infrared absorption spectra, and atmospheric implications, *Geophys. Res. Lett.*, 42(14), 6098–6105, doi:10.1002/2015GL064939, 2015.
- Montzka, S. A., Butler, J. H., Elkins, J. W., Thompson, T. M., Clarke, A. D. and Lock, L. T.: Present and future trends in the atmospheric burden of ozone-depleting halogens, *Nature*, 398(6729), 690–694, doi:10.1038/19499, 1999.
- Montzka, S. A., Hall, B. D. and Elkins, J. W.: Accelerated increases observed for hydrochlorofluorocarbons since 2004 in the global atmosphere, *Geophys. Res. Lett.*, 36(3), 1–5, doi:10.1029/2008GL036475, 2009.
- National Oceanic and Atmospheric Administration (NOAA): GMD Data Archive, [online] Available from: [ftp://ftp.cmdl.noaa.gov/hats/cfcs/cfc12/combined/HATS\\_global\\_F12.txt](ftp://ftp.cmdl.noaa.gov/hats/cfcs/cfc12/combined/HATS_global_F12.txt) (Accessed 24 April 2017), 2017.
- Newland, M. J., Reeves, C. E., Oram, D. E., Laube, J. C., Sturges, W. T., Hogan, C., Begley, P. and Fraser, P. J.: Southern hemispheric halon trends and global halon emissions, 1978-2011, *Atmos. Chem. Phys.*, 13(11), 5551–5565, doi:10.5194/acp-13-5551-2013, 2013.
- Oram, D. E., Ashfold, M. J., Laube, J. C., Gooch, L. J., Humphrey, S., Sturges, W. T., Leedham-Elvidge, E., Forster, G. L., Harris, N. R. P., Mead, M. I., Samah, A. A., Phang, S. M., Ou-Yang, C.-F., Lin, N.-H., Wang, J.-L., Baker, A. K., Brenninkmeijer, C. A. M. and Sherry, D.: A growing threat to the ozone layer from short-lived anthropogenic chlorocarbons, *Atmos. Chem. Phys.*, 175194, 11929–11941, doi:10.5194/acp-17-11929-2017, 2017.
- Prinn, R. G., Weiss, R. F., Arduini, J., Arnold, T., Langley Dewitt, H., Fraser, P. J., Ganesan, A. L., Gasore, J., Harth, C. M., Hermansen, O., Kim, J., Krummel, P. B., Li, S., Loh, Z. M., Lunder, C. R., Maione, M., Manning, A. J., Miller, B. R., Mitrevski, B., Mühle, J., O’Doherty, S., Park, S., Reimann, S., Rigby, M., Saito, T., Salameh, P. K.,

Schmidt, R., Simmonds, P. G., Paul Steele, L., Vollmer, M. K., Wang, R. H., Yao, B., Yokouchi, Y., Young, D. and Zhou, L.: History of chemically and radiatively important atmospheric gases from the Advanced Global Atmospheric Gases Experiment (AGAGE), *Earth Syst. Sci. Data*, 10(2), 985–1018, doi:10.5194/essd-10-985-2018, 2018.

Rao, M. V. N., Weigert, F. J. and Manzer, L. E.: Catalytic Process for Producing  $\text{CCl}_3\text{CF}_3$ , United States Patent, US Patent 5,120,883, [online] Available from: <https://patentimages.storage.googleapis.com/07/5c/92/7117da778942ae/US5120883.pdf>, 1992.

Reeves, C. E., Sturges, W. T., Sturrock, G. A., Preston, K., Oram, D. E., Schwander, J., Mulvaney, R., Barnola, J.-M. and Chappellaz, J.: Trends of halon gases in polar firn air: implications for their emission distributions, *Atmos. Chem. Phys*, 5, 2055–2064, doi:10.5194/acp-5-2055-2005, 2005.

Rigby, M., Prinn, R. G., Montzka, S. A., McCulloch, A., Harth, C. M., Mühle, J., Salameh, P. K., Weiss, R. F., Young, D., Simmonds, P. G., Hall, B. D., Dutton, G. S., Nance, D., Mondeel, D. J., Elkins, J. W., Krummel, P. B., Steele, L. P. and Fraser, P. J.: Re-evaluation of the lifetimes of the major CFCs and  $\text{CH}_3\text{CCl}_3$  using atmospheric trends, *Atmos. Chem. Phys*, 13, 2691–2702, doi:10.5194/acp-13-2691-2013, 2013.

Rüdiger, S., Gross, U., Shekar, S. C., Rao, V. V., Sateesh, M. and Kemnitz, E.: Studies on the conversion of 1,1,1-trichlorotrifluoroethane, chloro-2,2,2-trifluoroethane, and 1,1,1-trifluoroethane by catalytic oxidation, hydrolysis and ammonolysis, *Green Chem.*, 4(6), 541–545, doi:10.1039/B206098C, 2002.

Shanthan Rao, P., Narsaiah, B., Rambabu, Y., Sridhar, M. and Raghavan, K. V.: Catalytic processes for fluorochemicals: Sustainable alternatives, in *Industrial Catalysis and Separations: Innovations for Process Intensification*, edited by K. V Raghavan and B. M. Reddy, pp. 407–435, Apple Academic Press, Toronto., 2015.

Takahashi, K., Kono, S. and Shibnuma, T.: Manufacturing method for fluorine-containing ethane, United States Patent, US Patent 6,455,745 B1, [online] Available from: <https://patentimages.storage.googleapis.com/pdfs/945d53805f1b12c0c1e5/US6455745.pdf> (Accessed 9 March 2017), 2002.

United Nations Environment Programme (UNEP): Fifteenth Meeting of the Parties to the Montreal Protocol on Substances that Deplete the Ozone Layer, Nairobi, 10-14 November 2003, New Ozone-Depleting Substances that have been Reported by the Parties, UNEP/OzL.Pro.15/INF/2, [online] Available from: [http://www.42functions.eu/new\\_site/en/meetings/mop/mop15-index.php](http://www.42functions.eu/new_site/en/meetings/mop/mop15-index.php) (Accessed 18 October 2017), 2003.

United Nations Environment Programme (UNEP): Twenty-Eighth Meeting of the Parties to the Montreal Protocol on Substances that Deplete the Ozone Layer, Kigali, 10–14 October 2016, Decision XXVIII/1 Further Amendment of the Montreal Protocol. [online] Available from: <http://ozone.unep.org/sites/ozone/files/Publications/Handbooks/Montreal-Protocol->

English.pdf (Accessed 21 July 2017), 2016a.

United Nations Environment Programme (UNEP): Amendment to the Montreal Protocol on Substances that Deplete the Ozone Layer Decision XXVII/1, UNEP/OzL.Pro.28/CRP/10. [online] Available from: [http://conf.montreal-protocol.org/meeting/mop/mop-28/final-report/English/Kigali\\_Amendment-English.pdf](http://conf.montreal-protocol.org/meeting/mop/mop-28/final-report/English/Kigali_Amendment-English.pdf) (Accessed 18 July 2017), 2016b.

Vollmer, M. K., Rigby, M., Laube, J. C., Henne, S., Siek, T., Gooch, L. J., Wenger, A., Young, D., Steele, L. P., Langenfelds, L., Brenninkmeijer, C. A. M., Wang, J., Wyss, S. A., Hill, M., Oram, D. E., Krummel, P. B., Schoenenberger, F., Zellweger, C., Fraser, P. J., William, T., O'Doherty, S. and Reimann, S.: Abrupt reversal in emissions and atmospheric abundance of HCFC-133a (CF<sub>3</sub>CH<sub>2</sub>Cl), *Geophys. Res. Lett.*, 42, 8702–8710, doi:10.1002/2015GL065846, 2015.

## **Chapter 5: Investigation of East Asian emissions of CFC-11 using atmospheric observations in Taiwan**

---

The work in this chapter was originally prepared for a publication in *Environmental Sciences and Technology (ES&T)* and was published in 2020. Due to this there are some cases where sentences are written in the first-person plural i.e. “we decided to use our measurements ...”. I wrote the article and did most of the data analysis, but the co-authors of the article also contributed to the work. Matthew Ashfold, Marios Panagi and Norfazrin Mohd Hanif were all involved in producing the output from the NAME particle dispersion model. Norfazrin Mohd Hanif combined the output from the NAME model with carbon monoxide emission inventories from the Representative Concentration Pathway. I compared these results to the atmospheric observations. Claire Reeves helped me calculate the interspecies ratios and the CFC-11 emission estimates. Charles C-K Chou and Chang-Feng Ou-Yang were involved in the collaboration between Academia Sinica and National Central University in Taiwan, and the University of East Anglia (UEA), and Charles collected the air samples in Taiwan. Johannes Laube, David Oram and William Sturges in addition to being my supervisors were also involved in the collaboration between the UEA and Taiwan. Lauren Gooch was a PhD student at the UEA before me and measured and processed these data for the samples collected in Taiwan in 2014 and 2015. She also measured the samples collected in Taiwan in 2016. Then I did the data processing for these samples and measured and did the data processing for the Taiwan samples collected in 2017 and 2018. David Oram also did some of the measurements for the samples collected in Taiwan in 2014. Many of the co-authors and the reviewers contributed comments and suggestions for editing this work to prepare it for publication.

Adcock, K. E., Ashfold, M. J., Chou, C. C.-K., Gooch, L. J., Mohd Hanif, N., Laube, J. C., Oram, D. E., Ou-Yang, C.-F., Panagi, M., Sturges, W. T. and Reeves, C. E.: Investigation of East Asian Emissions of CFC-11 Using Atmospheric Observations in Taiwan, *Environ. Sci. Technol.*, 54(7), 3814–3822, doi:10.1021/acs.est.9b06433, 2020.

## Abstract

Recent findings of an unexpected slowdown in the decline of CFC-11 mixing ratios in the atmosphere have led to the conclusion that global CFC-11 emissions have increased over the last decade and have been attributed in part to eastern China. This study independently assesses these findings by evaluating enhancements of CFC-11 mixing ratios in air samples collected in Taiwan between 2014 and 2018. Using the NAME (Numerical Atmospheric Modelling Environment) particle dispersion model we find the likely source of the enhanced CFC-11 observed in Taiwan to be East China. Other halogenated trace gases were also measured and there were positive interspecies correlations between CFC-11 and  $\text{CHCl}_3$ ,  $\text{CCl}_4$ , HCFC-141b, HCFC-142b,  $\text{CH}_2\text{Cl}_2$  and HCFC-22, indicating co-location of the emissions of these compounds. These correlations in combination with published emission estimates of  $\text{CH}_2\text{Cl}_2$  and HCFC-22 from China, and of  $\text{CHCl}_3$  and  $\text{CCl}_4$  from eastern China, are used to estimate CFC-11 emissions. Within the uncertainties, these estimates do not differ for eastern China and the whole of China, so we combine them to derive a mean estimate which we refer to as being from '(eastern) China'. For 2014-2018 we estimate an emission of  $19 \pm 5 \text{ Gg yr}^{-1}$  (gigagrams per year) of CFC-11 from (eastern) China, approximately one quarter of global emissions. Comparing this to previously reported CFC-11 emissions estimated for earlier years we estimate CFC-11 emissions from (eastern) China to have increased by  $7 \pm 5 \text{ Gg yr}^{-1}$  from the 2008-2011 average to the 2014-2018 average, which is  $50 \pm 40 \%$  of the estimated increase in global CFC-11 emissions and is consistent with the emission increases attributed to this region in an earlier study.

## 5.1 Introduction

CFC-11 (trichlorofluoromethane,  $\text{CCl}_3\text{F}$ ) is presently the second most abundant chlorofluorocarbon in the atmosphere with average global mixing ratios of 231-234 parts per trillion (ppt) in 2018 (NOAA 2019). It is a long-lived ozone-depleting substance (atmospheric lifetime of 52 years) that is controlled under the Montreal Protocol on Substances that Deplete the Ozone Layer (Engel and Rigby et al., 2018). The Montreal Protocol phased out production and consumption of CFCs (including CFC-11) by 1996 in developed countries and by 2010 in developing countries, with a few 'essential' use exceptions (UNEP 2019a). CFC-11 was used primarily as a foam-blowing agent, as an aerosol propellant and as a refrigerant (UNEP 2019b). CFC-11 global emissions peaked at about  $350 \text{ Gg yr}^{-1}$  in the late 1980s and its tropospheric mixing ratios peaked in the early 1990s at about 270 ppt, after which both began to decline (Engel and Rigby et al., 2018).

Excluding 'essential' uses, assuming no new production, there should only be CFC-11 emissions from equipment and products filled with CFC-11 before the ban, referred to as a 'bank' e.g. foam cells in building insulation. CFC-11 emissions are expected to be slowly released from the bank and to decrease over time as the bank diminishes. However, a recent study found an unexpected slowdown in the rate of decline of CFC-

11 mixing ratios and an increase in global CFC-11 emissions of  $13 \pm 5 \text{ Gg yr}^{-1}$  from  $54 \pm 3 \text{ Gg yr}^{-1}$  in 2002-2012 to  $67 \pm 3 \text{ Gg yr}^{-1}$  in 2014-2016 based on NOAA observations (Montzka et al., 2018). Another study also recently found an increase in global CFC-11 emissions of  $17 \pm 3 \text{ Gg yr}^{-1}$  based on NOAA observations or  $11 \pm 3 \text{ Gg yr}^{-1}$  based on AGAGE observations between 2008-2012 and 2014-2017 (Rigby et al., 2019). The NOAA-derived CFC-11 emissions in Rigby et al. (2019) differ from the NOAA-derived Montzka et al. (2018) CFC-11 emissions because Rigby et al. (2019) includes an additional year (2017). Note that a different lifetime was also used (57 years in Montzka, 52 years in Rigby), although this has a small effect on the magnitude of the rise.

There are multiple possible origins of these additional emissions: an increase in the emissions rate from CFC-11 banks; a change in exempt uses of CFC-11; changes in atmospheric dynamics; or from illegal production. It is unlikely that there would be a large enough increase in emissions from banks (Montzka et al., 2018; Harris et al., 2019; UNEP 2019b) or exempt uses of CFC-11 (UNEP 2019b) to explain the change in CFC-11 emissions and changes in atmospheric dynamics can likely only explain part of the increase in emissions (Montzka et al., 2018).

Therefore, it is likely that since at least 2012 there has been an additional source of CFC-11 from production not allowed under the Montreal Protocol. East Asia (Montzka et al., 2018), specifically eastern mainland China (Rigby et al., 2019), has been identified as a likely source of these new CFC-11 emissions. The ‘eastern mainland China’ region contains the provinces of Anhui, Beijing, Hebei, Jiangsu, Liaoning, Shandong, Shanghai, Tianjin and Zhejiang. CFC-11 emissions from eastern mainland China were estimated to be  $13.4 \pm 1.7 \text{ Gg yr}^{-1}$  in 2014-2017, this is  $7.0 \pm 3.0 \text{ Gg yr}^{-1}$  higher than in 2008-2012 (Rigby et al., 2019).

Where the remaining CFC-11 emissions are coming from is not well known. Previous studies found relatively small CFC-11 emissions elsewhere:  $\sim 9 \text{ Gg yr}^{-1}$  in western Europe in 1995-2000 (Manning et al., 2003);  $\sim 4 \text{ Gg yr}^{-1}$  in eastern Europe in 2009 (Keller et al., 2012);  $\sim 0.9 \text{ Gg yr}^{-1}$  in southern China in 2010 (Wu et al., 2014);  $\sim 0.5 \text{ Gg yr}^{-1}$  in Australia in 2013 (Fraser et al., 2015);  $\sim 4.5 \text{ Gg yr}^{-1}$  in the USA in 2014 (Hu et al., 2017);  $\sim 1.7 \text{ Gg yr}^{-1}$  in India in 2016 (Say et al., 2019).

The reasons for a potential increase in the illegal production of CFC-11 are a subject of speculation. It has been suggested that reduced availability of HCFC-141b and increased demand for foams in building insulation may have driven demand for new production of CFC-11 for rigid polyurethane foams (UNEP 2018a; EIA, 2018; UNEP 2019b). During the foaming process for rigid foams approximately 4 % (e.g. appliance foams) to 25 % (e.g. spray foams) of the blowing agent is immediately released to the atmosphere (UNEP 2018a; UNEP 2019b). Therefore, if CFC-11 was being used for this then that may account for at least some of the recent increase in atmospheric levels of CFC-11. Furthermore, a large amount of the CFC-11 will remain in the foams, thereby

increasing the size of the CFC-11 bank and the potential for further emissions of CFC-11 in the future (UNEP 2018b; UNEP 2019b). Continued emissions of the ozone-depleting substance CFC-11 could undermine the success of the Montreal Protocol and delay the recovery of the ozone layer (Carpenter and Daniel et al., 2018; Dameris et al., 2019; Dhomse et al., 2019; Keeble et al., 2020). It was reported, at the 31<sup>st</sup> Meeting of the Parties to the Montreal Protocol in November 2019, that preliminary evidence indicated CFC-11 emissions declined in 2018 and 2019 (UNEP, 2019c). Possibly due to increased enforcement efforts by the Chinese authorities in response to the reports about CFC-11 (UNEP, 2019d).

## 5.2 Methods

In this study we measured multiple halogenated organic trace gases, including CFC-11, in air samples collected in Taiwan, using gas chromatography coupled with mass spectrometry (GC-MS). Five ground-based air sampling campaigns took place in Taiwan from 2014 to 2018. The samples were collected on the coast, well away from any local sources of pollution, when the wind direction was from the sea. Between 20 and 33 air samples were collected in the spring of each year (mostly March – April; including May and early June in 2017-18) with a total of 135 samples collected altogether (Table 5.1). In 2015, samples were collected from a site on the southern coast of Taiwan (Hengchun, 22.0547 °N, 120.6995 °E). In all other years samples were collected at the Cape Fuguei (CAFE) Research Station, operated by Academia Sinica, on the northern coast of Taiwan (25.297 °N, 121.538 °E). Both sampling sites are well located to study the East Asian outflow. During the springtime, Taiwan is typically influenced by strong continental outflow from East Asia, particularly from China (Adcock et al., 2018; Mohd Hanif, 2019).

### 5.2.1 Analytical technique

Air samples were collected in 3-litre silco-treated stainless-steel canisters (Restek). The samples were then transported to the University of East Anglia (UEA) and analysed for about 50 trace gases including CFC-11. The samples were analysed on an Agilent 6890 gas chromatograph coupled to a high-sensitivity Waters AutoSpec magnetic sector mass spectrometer (GC-MS) using an Agilent GS-GasPro column (length ~50 m; ID: 0.32 mm). CFC-11 was measured using the mass fragment  $\text{CF}^{35}\text{Cl}^{37}\text{Cl}^+$  ( $m/z$  102.9332). The average precision of the CFC-11 measurements was 1.4 %. For more information see Chapter 2. The samples in 2014 were also measured on a second GC-MS system (Entech-Agilent GC-MS) operating in electron ionization (EI) mode. This consists of a preconcentration unit (Entech model 7100) connected to an Agilent 6890GC and 5973 quadrupole MS (Section 2.7). In this study the CFC-11,  $\text{CCl}_4$ ,  $\text{CHCl}_3$ , HCFC-22, HCFC-141b, and HCFC-142b mixing ratios in 2014 come from the Entech GC-MS measurements as these compounds were not measured on the AutoSpec GC-MS in 2014. The mixing ratios in all other years (2015-2018) come from the measurements on the AutoSpec GC-MS. The  $\text{CH}_2\text{Cl}_2$  mixing ratios come from measurements made on the AutoSpec GC-MS for all five years (2014-2018).

The samples were measured against several clean air standards filled and calibrated by the Global Monitoring Division (GMD) of the National Oceanic and Atmospheric Administration (NOAA) in Boulder, Colorado. Multiple internal comparisons carried out over more than 10 years ensured the reliability and accuracy of the mixing ratios of all trace gases reported here (Section 2.8) and previous comparisons with NOAA measurements have shown excellent agreement (Laube et al., 2013). All CFC-11 results were transferred on to the recent NOAA 2016 GC-ECD calibration scale ([https://www.esrl.noaa.gov/gmd/cc1/CFC11\\_scale.html](https://www.esrl.noaa.gov/gmd/cc1/CFC11_scale.html)). The dry-air mole fraction in picomole per mole was measured, and we here report mixing ratios, in parts per trillion (ppt), as an equivalent to the dry-air mole fraction. The uncertainties are calculated the same way for all measurements and represent  $1\sigma$  standard deviations. They are based on the square root of the sum of the squared uncertainties from sample repeats and repeated measurements of the air standard on the same day (Section 2.6).

### **5.2.2 Identification of CFC-11 source regions**

The history of air arriving at the sampling sites has been investigated with the Met Office's NAME (Numerical Atmospheric Modelling Environment) Lagrangian particle dispersion model (Jones et al., 2007). These histories (hereafter footprints) were calculated by releasing batches of 30000 inert particles over a three-hour period encompassing the collection time of each sample. Over the course of the 12-day travel time, the locations of all particles within the lowest 100 m of the model atmosphere were recorded every 15 minutes on a grid with a resolution of  $0.25^\circ$  longitude and  $0.25^\circ$  latitude. The trajectories of the particles were calculated using three-dimensional meteorological fields produced by the Met Office's Numerical Weather Prediction tool, the Unified Model (UM). These fields have a horizontal grid resolution of  $0.23^\circ$  longitude by  $0.16^\circ$  latitude and 59 vertical levels below  $\sim 30$  km.

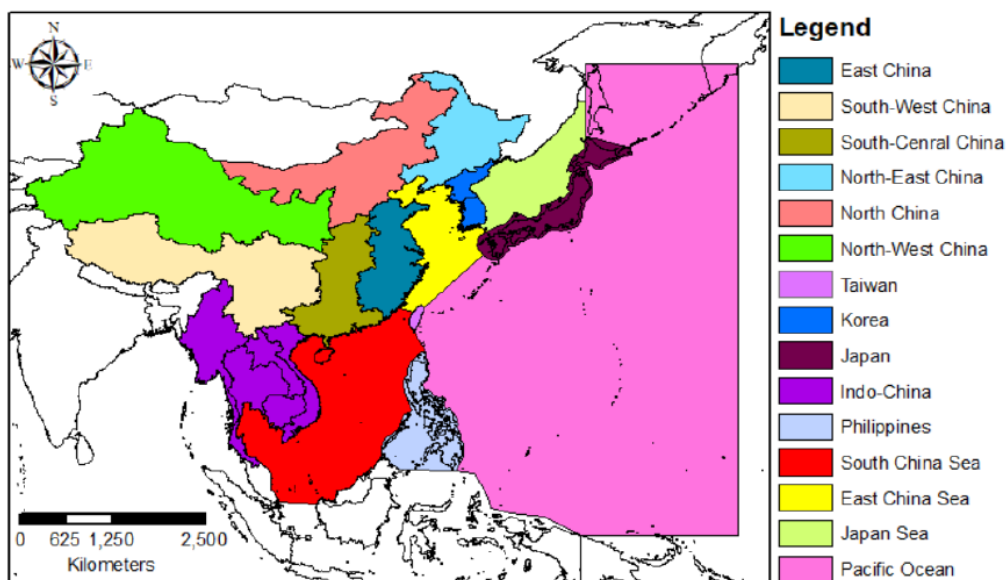


Figure 5.1: Regions for which the contribution to the footprint simulated by the NAME model is quantified.

In order to quantify the contribution of various geographical regions to each footprint, the domain was divided into 15 regions using shapefiles produced by ArcGIS, a geographic information system (GIS) (Figure 5.1). The 15 regions were determined by country boundaries and China was split into regions using province boundaries. The output underpinning the NAME footprints, a mass density residence time ( $\text{g m}^{-3} \text{ s}$ ) in each model grid cell, is summed across all grid cells within each of these 15 regions. These regional quantities are used to assess the possible relationships between emissions from specific regions and the mixing ratios of CFC-11 observed in Taiwan.

Additionally, the NAME footprints were combined with emission inventories of carbon monoxide (CO) taken from the Representative Concentration Pathway 8.5 (RCP 8.5) (Riahi et al., 2011) for the year 2010 to generate modelled CO mixing ratios at Taiwan resulting only from emissions occurring within the 12-day timescale of the NAME trajectories (Oram et al., 2017; Mohd Hanif, 2019). The RCP uses decade long averages and 2010 is used as it is the closest to the years of the campaigns in Taiwan. CO is a tracer of anthropogenic emissions and in this study the modelled CO is divided into various anthropogenic emission sectors e.g. ‘industry (combustion and processing)’ and ‘residential and commercial’. The correlations between the CFC-11 mixing ratios in Taiwan and the modelled CO from the emission sectors in East Asia were then calculated to investigate the spatial distribution of CFC-11 emissions.

### 5.2.3 Correlations of CFC-11 with other trace gases

The relationship between mixing ratios of CFC-11 and other halocarbons were investigated using the Spearman's rank correlation coefficient (R). Spearman's was selected as these data are not normally distributed with a few samples having particularly high halocarbon mixing ratios, including those of CFC-11. Spearman's

method gave slightly lower correlation coefficients for these data than the Pearson's method. The significance of the correlations were tested using a two-tailed Student's t-distribution. The background mixing ratios for the months of the campaign were subtracted from each year to account for any long-term trends. For CFC-11, CFC-12 and CCl<sub>4</sub> the NOAA Northern Hemisphere background was used (<https://www.esrl.noaa.gov/gmd/dv/ftpdata.html>). For CH<sub>2</sub>Cl<sub>2</sub> and CHCl<sub>3</sub> NOAA does not provide background values so the 10th percentile of our measurements for each year were used. To calculate the interspecies ratios the enhancements of CFC-11 above its background were plotted against the enhancements of each compound above their respective backgrounds. The slopes were calculated by total least squares regression using the Williamson-York method to account for uncertainties in mixing ratios of both species (Cantrell, 2008). These slopes were then used to estimate CFC-11 emissions (Fang et al., 2012; Wang et al., 2014).

#### 5.2.4 Estimation of CFC-11 emissions from China

Similar to the approach used in some previous studies of halocarbon emissions from China (Fang et al., 2012; Wang et al., 2014), we estimated emissions of CFC-11 using the slope of CFC-11 mixing ratio enhancements against those of other compounds which had a good correlation with CFC-11 and had published emissions. The compounds chosen were CCl<sub>4</sub>, CHCl<sub>3</sub>, CH<sub>2</sub>Cl<sub>2</sub> and HCFC-22. Equations (5.1) and (5.2) were used to calculate emissions of CFC-11 and their uncertainties.

$$E_{CFC-11} = S E_x \frac{M_{CFC-11}}{M_x} \quad (5.1)$$

$$\sigma_{E_{CFC-11}} = E_{CFC-11} \sqrt{\frac{\sigma_S^2}{S} + \frac{\sigma_{E_x}^2}{E_x}} \quad (5.2)$$

$E_{CFC-11}$  and  $E_x$  represent emissions of CFC-11 and halocarbon  $x$  respectively;  $M_{CFC-11}$  and  $M_x$  represent the molecular weights of CFC-11 and halocarbon  $x$  respectively; and  $S$  represents the slope of the correlation.  $\sigma_{E_{CFC-11}}$  is the uncertainty in the CFC-11 emissions;  $\sigma_S$  is the uncertainty in the slope of the correlation; and  $\sigma_{E_x}$  is the uncertainty in the emissions of halocarbon  $x$ .

The CCl<sub>4</sub> emissions used in this study were calculated by Lunt et al. (2018) for eastern China in 2009-2016 using a top-down approach with atmospheric measurements from Gosan, South Korea, and two atmospheric inversion models, NAME: 17 (11-24) Gg yr<sup>-1</sup> and FLEXPART: 13 (7-19) Gg yr<sup>-1</sup>. The CHCl<sub>3</sub> emissions used in this study were calculated by Fang et al. (2019) for eastern China in 2015 using measurements from Gosan and from Hateruma, Japan and the same two atmospheric inversion models, NAME: 82 (70-101) Gg yr<sup>-1</sup>, FLEXPART: 88 (80-95) Gg yr<sup>-1</sup>. The HCFC-22 emissions used were taken from Li et al. (2016), who calculated 134 (100-167) Gg yr<sup>-1</sup> for China in 2016 using an emission-factor based (bottom-up) method. Two reported emission

estimates for CH<sub>2</sub>Cl<sub>2</sub> were used: bottom-up emissions in China of 318 (254-384) Gg yr<sup>-1</sup> for 2016 were calculated by Feng et al. (2018) based on a survey of known consumption and emission factors in industrial sub-sectors; and 455 (410-501) Gg yr<sup>-1</sup> (2016) were calculated by Oram et al. (2017), based on chlorocarbon production and sales information for 2015. The main difference between these two estimates is the amount of CH<sub>2</sub>Cl<sub>2</sub> produced. Oram et al. (2017) estimated Chinese CH<sub>2</sub>Cl<sub>2</sub> production in 2015 to be 715 Gg using the reported production of HCFC-22, whilst Feng et al. (2018) estimated 600 Gg of CH<sub>2</sub>Cl<sub>2</sub> production in 2016, based on surveys in the Chinese chloro-alkali industry.

### **5.2.5 Estimation of changes in CFC-11 emissions from China**

One key question is whether CFC-11 emissions from China have increased in recent times and, if so, by how much. The Taiwan measurements only cover the period 2014-2018 and so to look at CFC-11 emissions in China over a longer period of time, back to 2008, we compared the emissions derived here with previous studies (Wan et al., 2009; Kim et al., 2010; An et al., 2012; Fang et al., 2012; Wang et al., 2014; Fang et al., 2018; Rigby et al., 2019). There are some differences in the methods used in these studies to calculate the emissions. All emission estimates from these studies are top-down except those from Wan et al. (2009) and Fang et al. (2018) which are bottom-up estimates. Wan et al. (2009), Fang et al. (2012), Wang et al. (2014) and Fang et al. (2018) are emission estimates for the whole of China. Those from Kim et al. (2010), An et al. (2012) and Rigby et al. (2019) are for eastern China. We have included all these estimates accepting that we are not always comparing like with like as there was no clear difference between CFC-11 emission estimates for the whole of China and eastern China (Figure 5.10). Also, we decided to include as many studies as possible to increase the confidence in our estimate and in-order to show the possible uncertainty. For further information see Table A1.

## **5.3 Results and discussion**

### **5.3.1 CFC-11 mixing ratios in Taiwan**

Across all five years the CFC-11 mixing ratios in Taiwan range from 226 ppt to 272 ppt (Figure 5.2, Table 5.1). They are on average 3 % higher than the northern hemispheric background mixing ratios as represented by Mauna Loa, Hawaii. Some of the measurements are consistent with the background, while many, especially those in years 2016-2018, contain higher mixing ratios than those observed at Mauna Loa implying that CFC-11 is enhanced on a regional scale (Figure 5.2). Samples with particularly high CFC-11 mixing ratios provide observational evidence of CFC-11 emissions from relatively nearby sources.

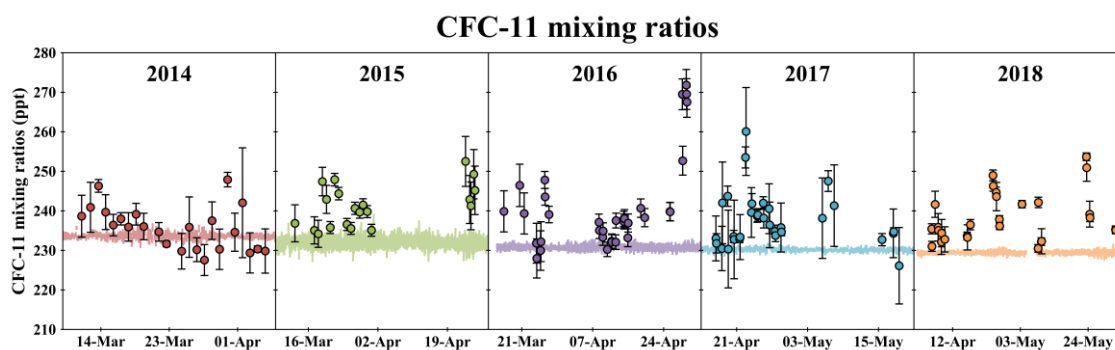


Figure 5.2: CFC-11 mixing ratios in Taiwan 2014-2018. The measurement campaigns lasted for 1-3 months each year. Uncertainties represented by the error bars are described in the text. Hourly in situ measurements of CFC-11 mixing ratios at Mauna Loa, Hawaii from the NOAA/ESRL Global Monitoring Division are included for comparison (<ftp://ftp.cmdl.noaa.gov/hats/cfcs/cfc11/insituGCs/CATS/hourly/>). The standard deviation error bars of the Mauna Loa measurements are plotted in the same colour as the data.

Table 5.1: The sampling sites in Taiwan, the dates of the campaign period, the number of samples collected, the average and range of CFC-11 mixing ratios and the NOAA mixing ratios for each year of the campaign.

Site	Year	Campaign period		No. of samples	Mean (ppt)	Median (ppt)	Range (ppt)	Manua Loa range (ppt)
		start	end					
Cape Fuguei	2014	11-Mar-14	04-Apr-14	23	236	236	228-248	232-236
Hengchun	2015	12-Mar-15	25-Apr-15	20	241	241	234-253	228-238
Cape Fuguei	2016	16-Mar-16	29-Apr-16	33	241	238	228-272	229-232
Cape Fuguei	2017	17-Apr-17	18-May-17	31	238	236	226-260	229-231
Cape Fuguei	2018	05-Apr-18	01-Jun-18	28	238	236	230-254	228-231

### 5.3.2 CFC-11 source regions

For all years combined, the strongest positive correlation is between CFC-11 mixing ratios and contributions to the NAME footprints from the East China region, with a Spearman's correlation coefficient of  $R = 0.495$ ,  $p < 0.01$  (Figure 5.3). All other regions have a correlation with CFC-11 mixing ratios of  $R < 0.3$ . East China includes major industrialized areas such as the Yangtze River Delta that have previously been identified as the source region of other chloromethanes: methyl chloride (Li et al., 2017) and carbon tetrachloride (Lunt et al., 2018). Rigby et al. (2019) also focused on eastern mainland China but they identified the Shandong and Hebei provinces as the main source of CFC-11 emissions. Shandong is part of our East China region, but Hebei is slightly further north than our East China region.

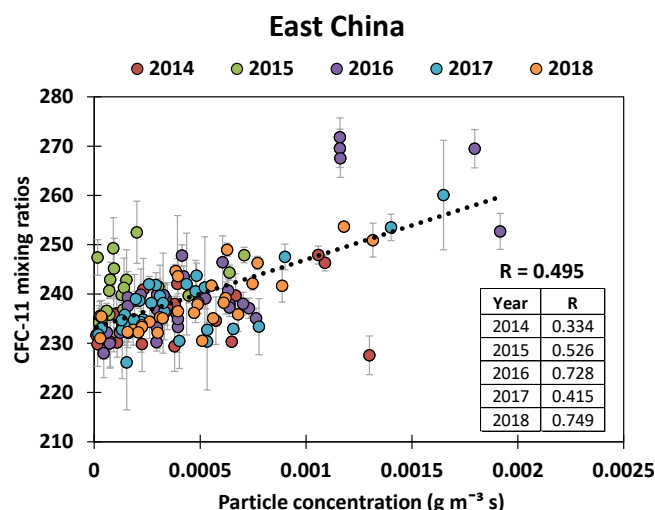


Figure 5.3: CFC-11 mixing ratios (ppt) against particle concentration from the East China source region arriving at Taiwan at the time the analysed samples were collected as simulated by the NAME particle dispersion model. The dashed line is the trend line calculated using ordinary least squares regression.

While our analysis highlights East China as a potentially important source region for CFC-11 in East Asia, it is possible that other important emission regions exist but have less influence on the observations in Taiwan. Monthly average NAME footprints were used to investigate typical air transport during the sampling period. In the spring air generally travels eastwards across the northern half of China and then curves southwards towards Taiwan (Figure 5.4; Mohd Hanif, 2019). Taiwan is an island and the measurement sites are on the coast, so based on the mass density residence times ( $\text{g m}^{-3} \text{ s}$ ) of the 12-day NAME footprints, most of the influence on air samples (on average about two-thirds) is from ocean regions: i.e. East China Sea, Pacific Ocean and the South China Sea. When comparing only the land-based source regions, East China and North China typically contributed the most to air sampled in Taiwan. Other potential source regions had much less of an influence on the samples collected in Taiwan, each contributing to about 1-4 % of the air in Taiwan based on the mass density residence times. Therefore, CFC-11 emissions from other source regions will have had a small impact on the air samples collected in Taiwan during the times of year of the present study.

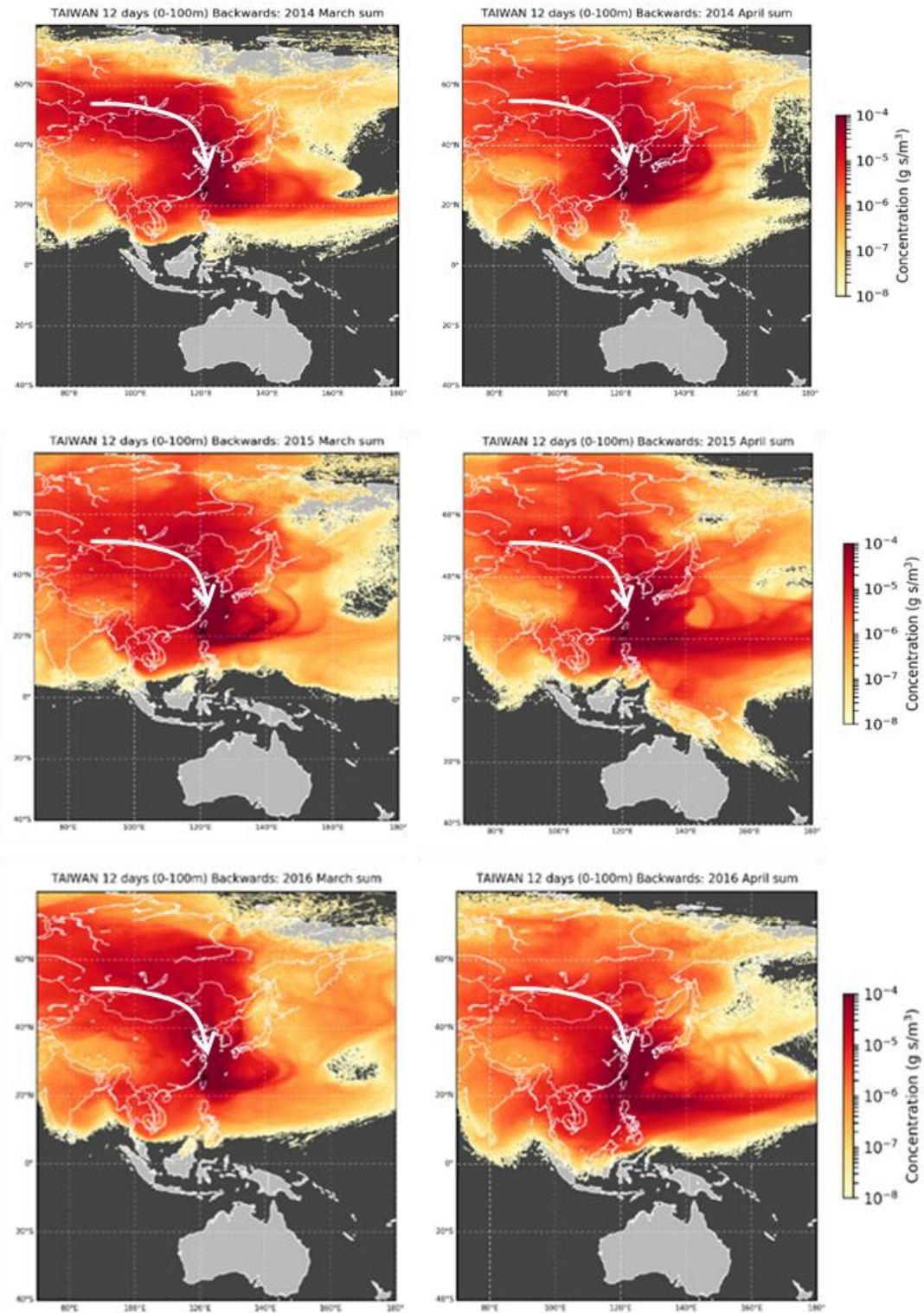


Figure 5.4: Monthly averages of the individual NAME footprints for Taiwan for March and April in 2014, 2015 and 2016. They are a combination of the daily NAME footprints for each month. The twelve-day air mass history footprints were calculated for three hourly periods and these have been integrated into monthly footprints. The sampling site is denoted by a black cross. The white arrows indicate the general direction of air transport during the spring.

For all years combined the correlations (Spearman's  $p < 0.01$ ) between CFC-11 mixing ratios in Taiwan and modelled CO mixing ratios from a range of sources were found to be very similar: agricultural waste burning on fields ( $R = 0.545$ ); residential and commercial sector ( $R = 0.491$ ); solvent sector ( $R = 0.483$ ); and industry (combustion and processing) ( $R = 0.469$ ) (Figure 5.5). The correlation between CFC-11 and power plants, energy conversion and extraction was somewhat lower ( $R = 0.384$ ,  $p < 0.01$ ). CO tracers that we do not find to significantly correlate ( $R < 0.25$ ) with CFC-11 are waste (landfills, waste water, incineration), forest burning, grassland burning, international shipping, surface transportation, agriculture (animals, rice and soil) and aviation.

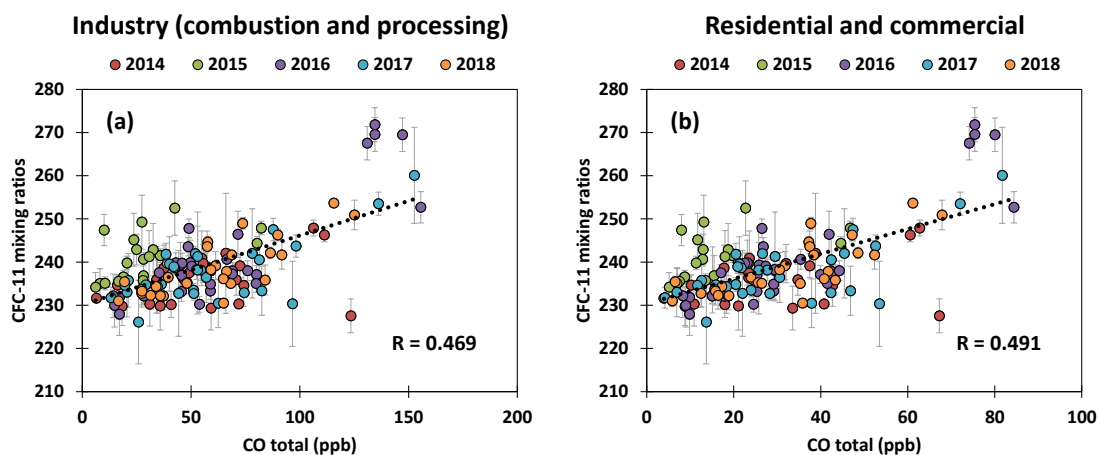


Figure 5.5: CFC-11 mixing ratios against simulated CO total from (a) Industry and (b) Residential and commercial. The dashed line is the trend line calculated using ordinary least squares regression. The trend line is calculated after subtracting the CFC-11 background mixing ratios from each year to remove the influence of long-term trends.

Some of the CO emission sectors most likely have very similar correlations because they are generally co-located with each other, so it is not possible to discriminate between the different sources (Figure 5.6). These sources are predominantly in eastern China, between Shanghai and Beijing, similar to the area identified by Rigby et al. (2019) as a major source of CFC-11 emissions. This gives additional indirect evidence of CFC-11 emissions from eastern China.

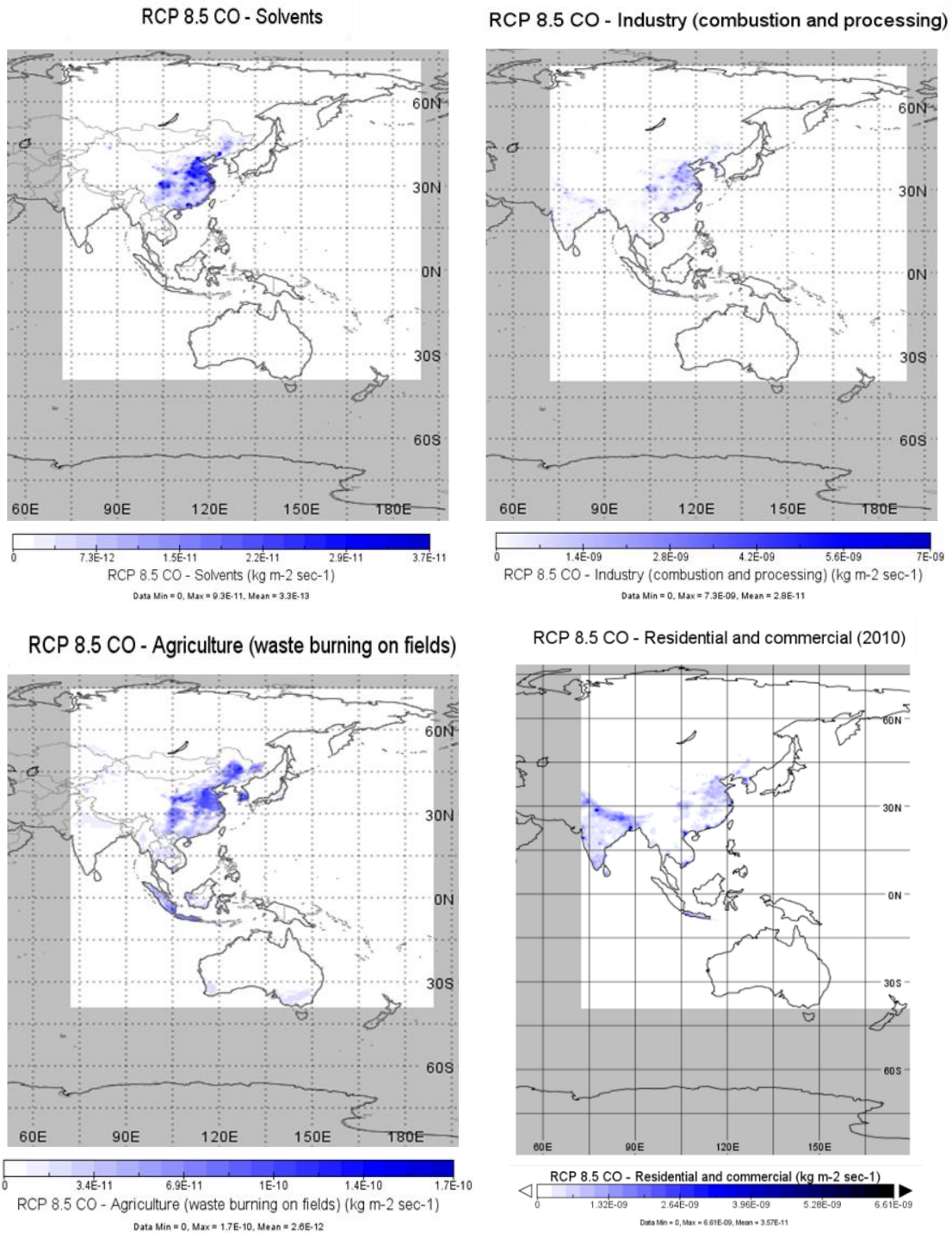


Figure 5.6: The distribution of carbon monoxide (CO) emissions ( $\text{kgm}^{-2}\text{s}^{-1}$ ) taken from the Representative Concentration Pathway 8.5 (2010) inventories of CO for four emission sectors: industry, residential and commercial, solvents and agriculture waste burning.

### 5.3.3 Correlations of CFC-11 with other trace gases

The strongest positive correlations (Spearman's  $p < 0.01$ ) between CFC-11 and other halocarbons when measurements from all years are combined are:  $\text{CHCl}_3$  ( $R = 0.720$ ),  $\text{CCl}_4$  ( $R = 0.713$ ), HCFC-141b ( $\text{C}_2\text{H}_3\text{Cl}_2\text{F}$ ) ( $R = 0.671$ ), HCFC-142b ( $\text{CH}_3\text{CClF}_2$ ) ( $R = 0.667$ ),  $\text{CH}_2\text{Cl}_2$  ( $R = 0.622$ ) and HCFC-22 ( $\text{CHClF}_2$ ) ( $R = 0.593$ ) (Figure 5.7). These correlations concur with a previous study that also found correlations of HCFC-22 and  $\text{CH}_2\text{Cl}_2$  with CFC-11 in measurements from Hawaii when air masses originated from East Asia (Montzka et al., 2018).

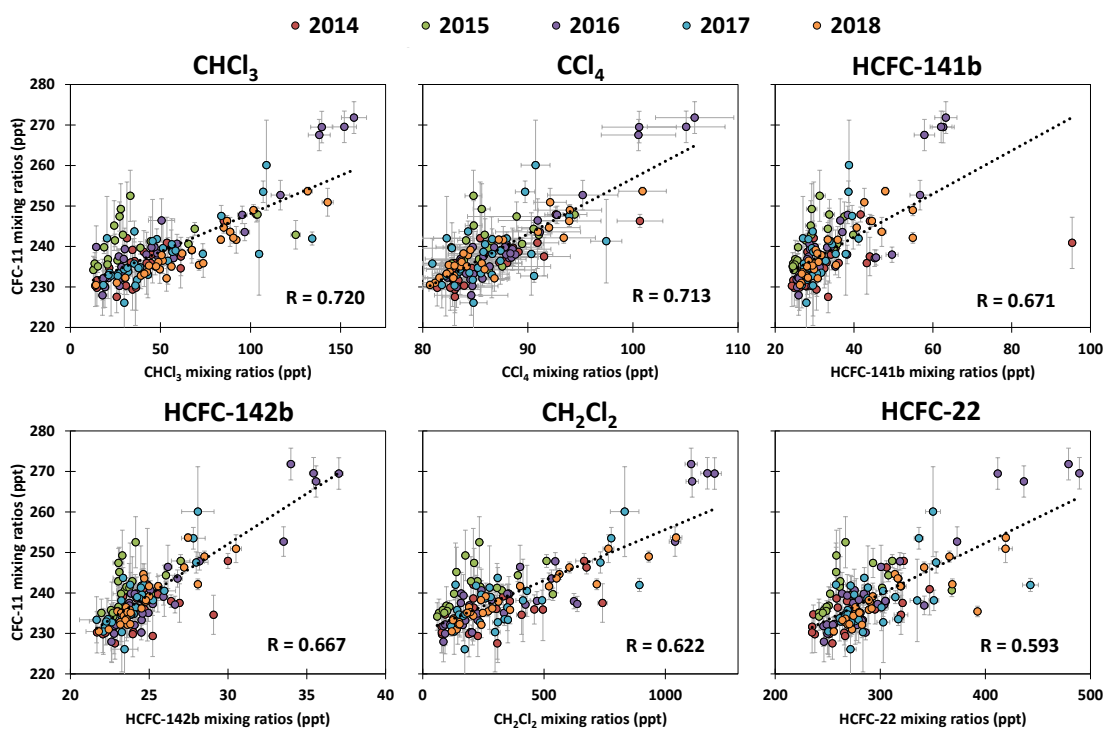


Figure 5.7: Interspecies correlations of CFC-11 mixing ratios with those of other halogenated trace gases. The dashed line is the trend line calculated by total least squares regression using the Williamson-York method.

Compounds generally have correlated mixing ratios in the atmosphere when their emissions are released from a similar location or when atmospheric mixing ratio gradients are present (vertically or horizontally) that are sampled by different wind patterns. CFC-11 emissions are probably found in many locations. The emissions of CFC-11 and other compounds from a production facility are likely to be low as it is not economically viable for a production facility to release their products into the atmosphere (UNEP 2018b; UNEP 2019b). If CFC-11 is used as a foam blowing agent then about 4 % (e.g. appliance foams) to 25 % (e.g. spray foams) of the CFC-11 emissions would be released from the foam blowing stage when the foam is made (UNEP 2018a; UNEP 2019b). The rest of the CFC-11 emissions would be gradually released from foam degradation or when the foam is broken up e.g. during demolition of buildings (UNEP 2018a; Harris et al., 2019).

CFC-11 has historically been widely used in polyurethane foam applications (UNEP 2018a). As CFC-11 was phased out HCFC-141b became commonly used as a replacement (UNEP 2018a; UNEP 2019b). HCFC-142b and HCFC-22 are also used in the foam blowing industry in extruded polystyrene production (UNEP 2018a). The correlations between these compounds may be related to them all being used as foam blowing agents in building insulation and co-location of built environments and foam-blowing facilities.

The other compounds that CFC-11 has a good correlation with,  $\text{CHCl}_3$ ,  $\text{CH}_2\text{Cl}_2$ ,  $\text{CCl}_4$  and HCFC-22, are all involved in the same production chain.  $\text{CHCl}_3$  and  $\text{CH}_2\text{Cl}_2$  are co-produced through chlorination of methyl chloride ( $\text{CH}_3\text{Cl}$ ) with a small amount of  $\text{CCl}_4$  produced as a by-product (Oram et al., 2017). Almost all the chloroform ( $\text{CHCl}_3$ ) produced is then used as a feedstock in HCFC-22 production (Oram et al., 2017; UNEP 2019b). China has a large chloromethanes industry and recent studies have found emissions of  $\text{CCl}_4$  (Lunt et al., 2018),  $\text{CHCl}_3$  (Fang et al., 2019) and  $\text{CH}_2\text{Cl}_2$  (Oram et al., 2017) from eastern China. Most of the emissions of  $\text{CCl}_4$  are thought to be due to its production as a by-product. Most of the emissions of CFC-11,  $\text{CHCl}_3$ ,  $\text{CH}_2\text{Cl}_2$  and HCFC-22 will likely come from their applications rather than from production facilities; therefore, these correlations indicate co-location of the uses of CFC-11 and chloromethanes, possibly in urban areas.

CFC-11 has historically been produced via fluorination of  $\text{CCl}_4$  to produce a mixture of CFC-11 ( $\text{CCl}_3\text{F}$ ) and CFC-12 ( $\text{CCl}_2\text{F}_2$ ) (UNEP 2019b). The production ratio has typically been between 30:70 and 70:30 (UNEP 2019b). Therefore, if enhanced mixing ratios of CFC-12 were observed coincident with enhanced mixing ratios of CFC-11, this might suggest the cause of the increased CFC-11 emissions to be new production. However, we found no correlation between mixing ratios of CFC-11 and CFC-12 ( $R = 0.285$ ) in the Taiwan measurements even after removing the decreasing background trend in CFC-12 to focus on enhancements in mixing ratios above the background. CFC-12 mixing ratios in the Taiwan air samples do not show any major enhancements and are similar to the levels at Mauna Loa, Hawaii (Figure 5.8). This agrees with findings in previous studies that also found no evidence for an increase in CFC-12 emissions (Rigby et al., 2019; Montzka et al., 2018) and adds to the evidence that emissions of CFC-11 from eastern China are not directly associated with emissions of CFC-12.

Operating conditions could be controlling the relative proportions of CFC-12 and CFC-11; close to 100 % CFC-11 production is difficult to achieve but not impossible (UNEP 2019b). Alternatively CFC-12 may still be being co-produced but is destroyed or used as a refrigerant, which is considered to be a non-emissive source as release of the CFC-12 will take place over a long period of time (UNEP 2019b; Harris et al., 2019).

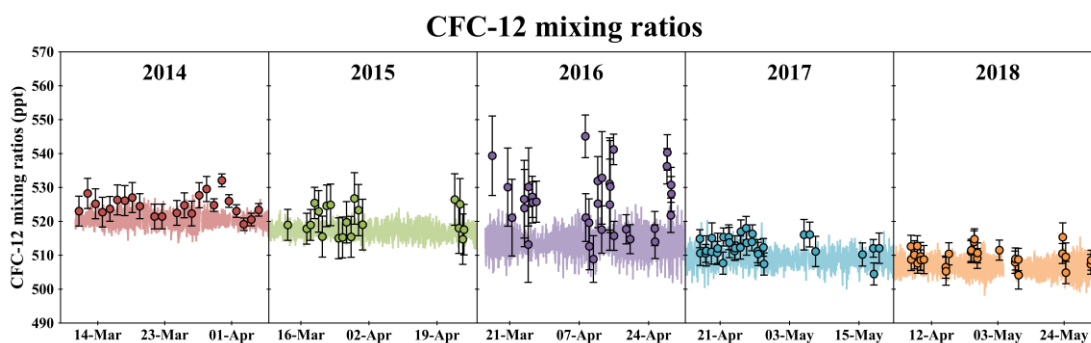


Figure 5.8: CFC-12 mixing ratios in Taiwan 2014-2018. The measurement campaigns lasted for 1-3 months each year. Uncertainties represented by the error bars are described in the text. In 2016 CFC-12 eluted close to the end of the retention window and so peak heights were used instead of peak areas to calculate CFC-12 mixing ratios. This led to larger uncertainties in 2016 in comparison to the other years. Hourly in situ measurements of CFC-12 mixing ratios at Mauna Loa, Hawaii from the NOAA/ESRL Global Monitoring Division are included for comparison (<ftp://ftp.cmdl.noaa.gov/hats/cfcs/cfc12/insituGCs/CATS/hourly/>). The standard deviation error bars of the Mauna Loa measurements are plotted in the same colour as the data.

### 5.3.4 CFC-11 emissions from China

The CFC-11 emission estimates in this study are based on emission estimates for the whole of China and eastern China and therefore, when the CFC-11 emission estimates are combined together they are referred to as CFC-11 emissions from '(eastern) China'. CFC-11 emissions from (eastern) China for the period 2014-2018 are estimated based on interspecies ratios of CFC-11 with other halocarbons for which we found good correlations. There is a large range in the estimates of CFC-11 emissions from (eastern) China derived during this study (Figure 5.9). Most of the uncertainty in the CFC-11 emission estimates is due to the uncertainty in the emissions estimates of the other compounds rather than the uncertainty in the slope of the interspecies ratios. The lowest estimate is 12 (9-14) Gg yr<sup>-1</sup> using the Feng et al. (2018) estimate of CH<sub>2</sub>Cl<sub>2</sub> emissions. The largest CFC-11 emission estimate is 27 (20-33) Gg yr<sup>-1</sup>, based on HCFC-22 emissions from Li et al. (2016). The two compounds with the strongest correlations with CFC-11 are CHCl<sub>3</sub> and CCl<sub>4</sub> (Table 5.2) and the estimates derived from these are in the middle of the range (17-22 Gg yr<sup>-1</sup>) (Figure 5.9). It is important to note that the HCFC-22 and CH<sub>2</sub>Cl<sub>2</sub> based emissions estimates are for the whole of China, whilst the CHCl<sub>3</sub> and CCl<sub>4</sub> based emissions are for eastern China only. There is no consistent pattern of higher emissions for the whole of China and lower emissions for eastern China (Figure 5.9). The mean of all the individual estimates is 19 (14-23) Gg yr<sup>-1</sup>. The uncertainties were calculated as the standard deviation of the mean of the individual estimates.

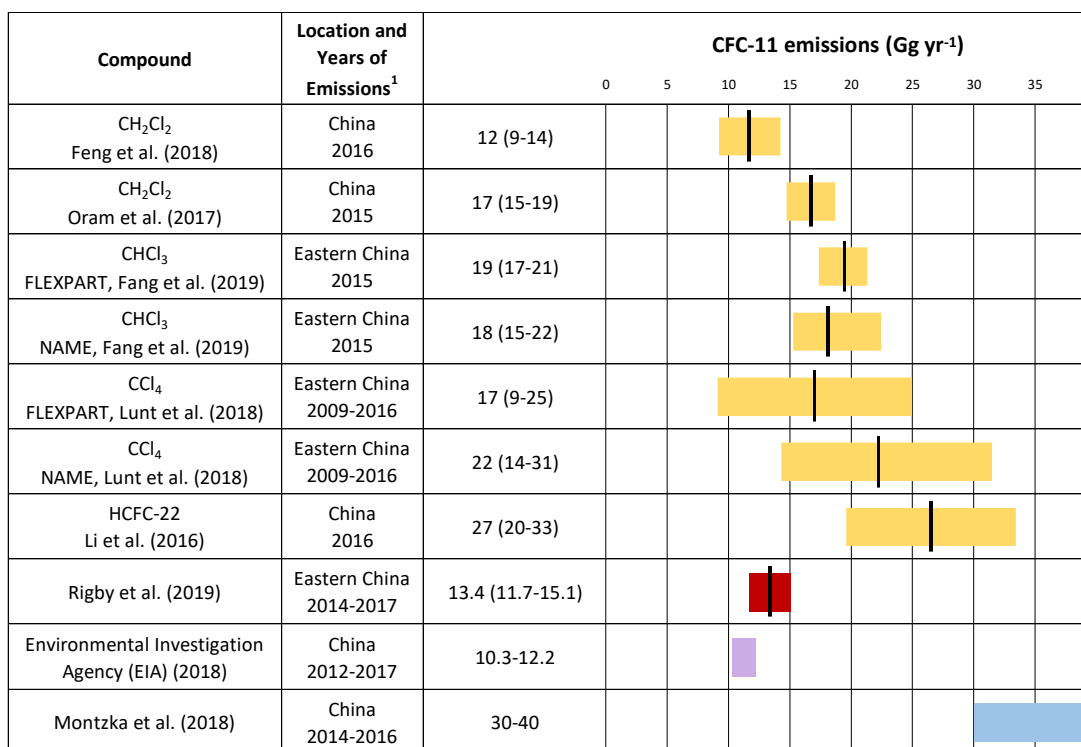


Figure 5.9: CFC-11 emission estimates and the upper and lower limits based on the interspecies ratios with CHCl<sub>3</sub>, CH<sub>2</sub>Cl<sub>2</sub>, CCl<sub>4</sub> and HCFC-22 in our Taiwan measurements from 2014-2018 and published halocarbon emission estimates. The vertical lines indicate the best estimate. Recently published CFC-11 emission estimates for eastern mainland China and China are also shown (Montzka et al., 2018; EIA, 2018; Rigby et al., 2019). The emission estimates from this study are coloured yellow and the emission estimates from other studies are different colours. <sup>1</sup> For the estimates from the current study based on interspecies correlations the location and years of emissions are based on the region for the emission estimate of compound x.

Table 5.2: Emission estimates based on the correlation slopes with CHCl<sub>3</sub>, CH<sub>2</sub>Cl<sub>2</sub>, CCl<sub>4</sub> and HCFC-22. The molecular weight used for CFC-11 was 137.36 g mol<sup>-1</sup>.

Compound	CH <sub>2</sub> Cl <sub>2</sub>	CH <sub>2</sub> Cl <sub>2</sub>	CHCl <sub>3</sub>	CHCl <sub>3</sub>	CCl <sub>4</sub>	CCl <sub>4</sub>	HCFC-22
<b>Molecular Weight</b>	84.93	84.93	119.37	119.37	153.82	153.82	86.47
<b>Spearman's R</b>	0.622	0.622	0.720	0.720	0.713	0.713	0.593
<b>Trendline (total linear least squares regression)</b>	y = 0.023x + 2.436	y = 0.023x + 2.436	y = 0.192x + 1.635	y = 0.192x + 1.635	y = 1.466x + 0.573	y = 1.466x + 0.573	y = 0.125x + 2.718
<b>Emissions (Gg yr<sup>-1</sup>)</b>	318 (254-384)	455 (410-501)	88 (80-95)	82 (70-101)	13 (7-19)	17 (11-24)	134 (100-167)
<b>Location of Emissions</b>	China	China	East China	East China	East China	East China	China
<b>Years of Emissions</b>	2016	2015	2015	2015	2009-2016	2009-2016	2016
<b>Reference</b>	Feng et al., 2018	Oram et al., 2017	Fang et al., 2019 (FLEXPART)	Fang et al., 2019 (NAME)	Lunt et al., 2018 (FLEXPART)	Lunt et al., 2018 (NAME)	Li et al., 2016
<b>CFC-11 emissions (Gg yr<sup>-1</sup>)</b>	11.7 (9.2-14.2)	16.7 (14.7-18.7)	19.4 (17.4-21.3)	18.1 (15.3-22.4)	17.0 (9.1-24.9)	22.2 (14.3-31.5)	26.5 (19.6-33.4)

The CFC-11 emission estimates in this study are generally comparable with the other estimates in the literature, although there are some important differences. The Environmental Investigation Agency (EIA), in a non-peer reviewed report, estimated CFC-11 emissions from China's rigid polyurethane foam blowing industry to be 10.3-12.2 Gg yr<sup>-1</sup> for 2012-2017. This estimate is based on surveys with industry experts, reported production data and a number of assumptions on emission rates and the extent of CFC-11 use (EIA, 2018). This estimate is at the lower end of our range and as the EIA estimate is covering only one source it neither rules in nor rules out the possibility of other emission sources.

A recent study estimated CFC-11 emissions of 30-40 Gg yr<sup>-1</sup> from China, over the period 2014-2016, based on correlations of CFC-11 with HCFC-22 mixing ratios in Hawaii (Montzka et al., 2018 Extended Data Figure 5). This is a rough estimate of relative emission magnitudes as it is based on measurements far from source regions. It is somewhat higher than our estimates, but agrees, within the uncertainties, with our estimate based on HCFC-22, 27 (20-33) Gg yr<sup>-1</sup> (Figure 5.9).

Another recent study used CFC-11 measurements at Gosan, Jeju Island, Korea and Hateruma, Japan and two atmospheric inversion models to calculate CFC-11 emissions from eastern mainland China to be 13.4 ± 1.7 Gg yr<sup>-1</sup> in 2014-2017 (Rigby et al., 2019). These estimates are at the lower end of the range that we calculate here based on the Taiwan samples. The reason for this might be that the Rigby et al. (2019) estimates are

confined to provinces to which the measurements were most sensitive. Rigby et al. (2019) mentioned that including the provinces adjacent to their ‘eastern mainland China’ region increased their emissions by 15 %. The  $\text{CHCl}_3$  emissions that we use in our calculations (Fang et al., 2019) are based on observations from the same measurement sites as Rigby et al. (2019). The  $\text{CCl}_4$  emissions that we use in our calculations are based on observations in Gosan, Korea (Lunt et al., 2018). These studies (Lunt et al., 2018; Fang et al., 2019) derived emissions for ‘eastern China’, but a slightly larger area to that used by Rigby et al. (2019).

The regions of our CFC-11 emission estimates are the same as the regions used to calculate the emissions of the other compounds. It is assumed that the interspecies ratio will be the same in one region as it is in the other. So whilst our estimates based on  $\text{CHCl}_3$  and  $\text{CCl}_4$  emissions are largely restricted to eastern China, those using HCFC-22 and  $\text{CH}_2\text{Cl}_2$  emission estimates are for the whole of China (Li et al., 2016; Feng et al., 2018; Oram et al., 2017). Our overall emission estimate (19 (14-23)  $\text{Gg yr}^{-1}$ ) based on the Taiwan measurements is a combination of estimates for eastern China and the whole of China.

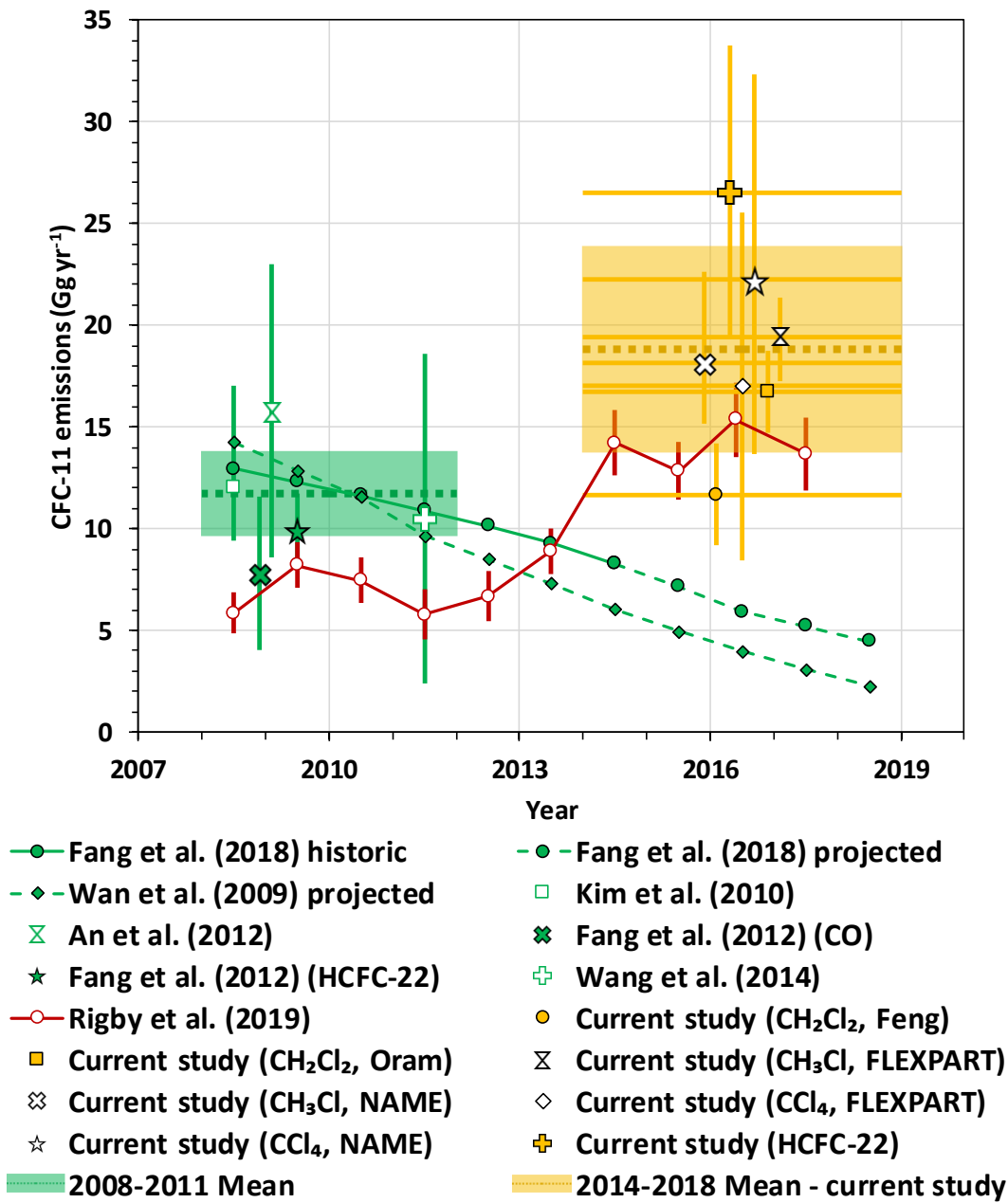


Figure 5.10: CFC-11 emissions in China and eastern China (Wan et al., 2009; Kim et al., 2010; An et al., 2012; Fang et al., 2012; Wang et al., 2014; Fang et al., 2018; Montzka et al., 2018; Rigby et al., 2019). Data that cover means of several years have horizontal error bars to indicate the periods that they relate to. Vertical error bars show the uncertainties in the emission estimates. Data from the same years are offset slightly so that the error bars are visible. The data points joined by dashed lines are projections. The 2008-2011 mean is the mean of the estimates in Wan et al. (2009), Kim et al. (2010), An et al. (2012), Fang et al. (2012), Wang et al. (2014) and Fang et al. (2018). The 2014-2018 mean is the mean of the seven interspecies correlation estimates in this study. Emissions for the whole of China have filled data points and emissions for eastern China have clear data points.

### 5.3.5 Changes in CFC-11 emissions from China

There is variation in the CFC-11 emission estimates between different studies, but the combined evidence suggests an increase in CFC-11 emissions in (eastern) China from 2008-2011 to 2014-2018. Rigby et al. (2019) emission estimates for 2008-11 are lower than the other estimates for this period. Possibly because Rigby et al. (2019) estimates are limited to 'eastern mainland China' whereas some of the other estimates cover larger areas (see above). Averaging published emission estimates for 2008-2011, and excluding Rigby et al. (2019) gives CFC-11 emissions of 12 (10-14) Gg yr<sup>-1</sup> (green bar, Figure 5.10)(Wan et al., 2009; Kim et al., 2010; An et al., 2012; Fang et al., 2012; Wang et al., 2014; Fang et al., 2018). The uncertainties were calculated using the standard deviation of the individual estimates.

CFC-11 emissions from (eastern) China for the period 2014-2018 are estimated in this study to be 19 (14-23) Gg yr<sup>-1</sup> (golden bar, Figure 5.10) by combining the seven interspecies correlation emission estimates (Figure 5.9). This gives an increase of 7 (2-12) Gg yr<sup>-1</sup> since 2008-2011. The uncertainties are the square root of the sum of the uncertainties for each time period squared.

This increase in emissions between 2008-2011 and 2014-2018 that we estimate is similar to the increase estimated by Rigby et al. (2019) of  $7.0 \pm 3.0$  Gg yr<sup>-1</sup> between 2008-2012 and 2014-2017. If we include the Rigby et al. (2019) emissions in our analysis, this gives us slightly lower CFC-11 emissions for both the earlier and later time periods, as the Rigby et al. (2019) estimates are generally lower than the other estimates we use in our study (Table A1). Including the Rigby et al. (2019) estimates in our averages still gives an absolute increase of  $\sim 7$  Gg yr<sup>-1</sup> in CFC-11 emissions (Table A1). The consistency between our results and those of Rigby et al. (2019), obtained by different, independent methods, provides some confidence in this estimated size of the CFC-11 emissions in eastern China, although it is recognized that both estimates have uncertainty in them.

In our study, the emission estimates are based on measurements of samples collected during springtime each year when Taiwan is consistently impacted by air masses transported from mainland China. This minimises dilution so the observed interspecies concentration ratios will better reflect their emission ratios. Seasonal variations in emission ratios in this region are not well constrained. Kim et al. (2010) in their estimates of halocarbons emissions from China, assumed emissions were constant throughout the year. However, their observed ratio between CFC-12 and HCFC-22 enhancements suggest higher values in the summer. Seasonally varying ratios of halocarbon enhancements were also observed in the US in the 1990s (Barnes, 2003). Limited seasonal sampling will therefore introduce some error into our analysis but by using interspecies ratios of CFC-11 with four different halocarbons, we aim to reduce this error. Interspecies emission ratios may also vary with location and this approach assumes sources to be perfectly co-located, which is unlikely. This is partly accounted for in the uncertainty of the observed interspecies ratios. Additionally, we are

combining emission estimates from multiple studies that used different methods and are for different time periods and regions. Furthermore, it is possible that climate change may be leading to changes in boundary layer height which could influence the observed CFC-11 mixing ratios (Aulagnier et al., 2010). Therefore, our CFC-11 emission estimates will have some unaccounted for uncertainties.

CFC-11 emissions were expected to have decreased since 2012, due to the diminishing size of the banks, assuming compliance with the Montreal Protocol. This means the difference between projected bottom-up emissions and actual emissions may be larger than the increase in CFC-11 emissions from 2008-2011 to 2014-2018 (Rigby et al., 2019; Montzka et al., 2018; Engel and Rigby et al., 2018). Previous studies projected future CFC-11 Chinese emissions using bottom-up estimates of reported production, estimates of the size of the CFC-11 bank and assumed emission rates (Wan et al., 2009; Fang et al., 2018). These bottom-up estimates agree with the top-down estimates in 2008-2011 but decrease such that they disagree in 2014-2018 with the top-down estimates (Figure 5.10). Averaging the estimates for the individual years between 2014 and 2018 from Wan et al. (2009) and Fang et al. (2018) gives 5 (3-7) Gg yr<sup>-1</sup>. The uncertainties are the standard deviation of the estimates for the individual years. If we subtract 5 (3-7) Gg yr<sup>-1</sup> from our estimate of 19 (14-23) Gg yr<sup>-1</sup> this leads to 14 (9-19) Gg yr<sup>-1</sup> more emissions of CFC-11 in China than projected.

### 5.3.6 Comparison to global CFC-11 emissions

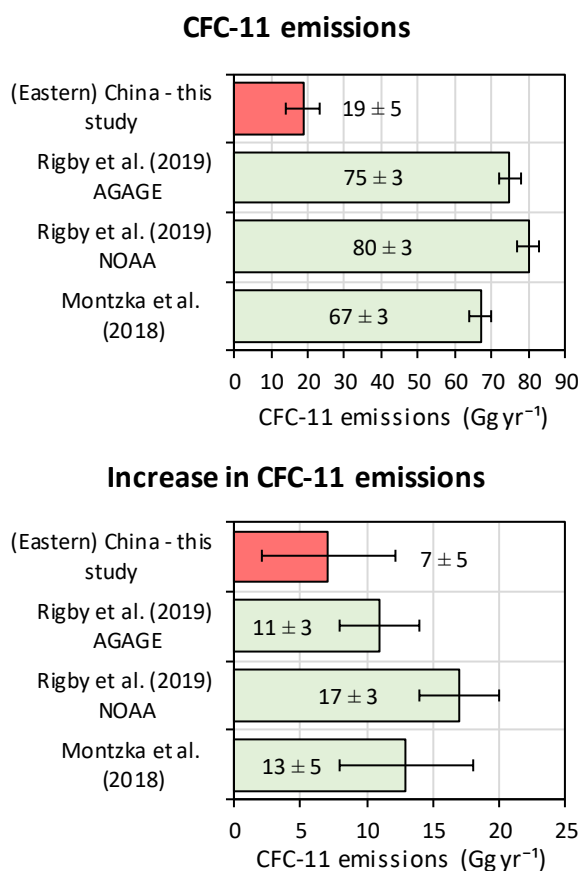


Figure 5.11: Top: Global CFC-11 emissions (green bars) compared to the (eastern) China emissions in this study (red bar). Bottom: Increase in global CFC-11 emissions (green bars) compared to the increase in (eastern) China emissions (red bar). These estimates are for slightly different time periods. The estimates from Montzka et al. (2018) are for 2014–2016 compared to the 2002–2012. The Rigby et al. (2019) estimates are for 2014–2017 compared to 2008–2012. This study’s emission estimates are for 2014–2018 compared to 2008–2011.

Montzka et al. (2018) used NOAA observations to calculate global CFC-11 emissions of  $67 \pm 3$  Gg yr<sup>-1</sup> in 2014–2016 which was an increase of  $13 \pm 5$  Gg yr<sup>-1</sup> above the 2002–2012 mean. Rigby et al. (2019) calculated global CFC-11 emissions in 2014–2017 to be  $80 \pm 3$  Gg yr<sup>-1</sup> based on NOAA observations and  $75 \pm 3$  Gg yr<sup>-1</sup> based on AGAGE observations. These are increases since 2008–2012 of  $17 \pm 3$  Gg yr<sup>-1</sup> (NOAA) and  $11 \pm 3$  Gg yr<sup>-1</sup> (AGAGE). The NOAA-derived CFC-11 emissions in Rigby et al. (2019) differ from the NOAA-derived Montzka et al. (2018) CFC-11 emissions because Rigby et al. (2019) includes an additional year (2017) and uses a shorter atmospheric lifetime for CFC-11. The atmospheric lifetime contributes to the differences in emission estimates given in the different studies but has very little effect on the change in emissions over the short time period.

In the section above, (eastern) China emissions were estimated to be 19 (14–23) Gg yr<sup>-1</sup> in 2014–2018 and the increase estimated to be 7 (2–12) Gg yr<sup>-1</sup> compared to 2008–2011.

These regional emissions of 19 (14-23) Gg yr<sup>-1</sup> are 25% (19%-32%) of the total global emissions (Figure 5.11). This is the proportion of our (eastern) China emissions compared to the average of the three global estimates. The uncertainties are based on the square root of the sum of squares of the uncertainty in our (eastern) China estimate and the standard deviation of the three global estimates. The increase in (eastern) China CFC-11 emissions are a large proportion of the increase in global CFC-11 emissions but are also highly uncertain (Figure 5.11). They are 52% (13%-91%) of the increase in global emissions (Figure 5.11). Where the remaining CFC-11 emissions are coming from is not well known as there are many parts of the world that are not well covered by the global networks, including South America, Africa and the rest of Asia (Harris et al., 2019). Note these CFC-11 emission estimates do not consider possible changes in atmospheric dynamics which could slow-down the rate of decline in global CFC-11 mixing ratios and lead to an over estimation of global CFC-11 emissions (Montzka et al., 2018).

## **5.4 Conclusions**

Overall, the current study finds independent evidence of continuing and significant CFC-11 emissions from China, in particular from eastern China, using different observations and methods to previous studies. Comparing with past studies implies a recent increase in (eastern) China CFC-11 emissions, which will have contributed to a substantial proportion of the increase in global CFC-11 emissions. However, the extent of this contribution still has considerable uncertainty and further investigation is needed to better understand the recent changes in CFC-11 emissions.

## **Acknowledgements**

This work was supported by the NERC IOF awards NE/J016047/1 and NE/J016012/1. This work was also supported by Sources and Impacts of Short-Lived Anthropogenic Chlorine (SISLAC) NE/R001782/1. Karina Adcock was funded by the UK Natural Environment Research Council through the EnvEast Doctoral Training Partnership (grant number NE/L002582/1). Norfazrin Mohd Hanif was funded through a PhD studentship by the Ministry of Education Malaysia (MOE) and Universiti Kebangsaan Malaysia (UKM). Johannes C. Laube received funding from the UK Natural Environment Research Council (Research Fellowship NE/I021918/1) and the ERC project EXC<sup>3</sup>ITE (EXC3ITE-678904-ERC-2015-STG). Lauren J. Gooch received funding from UK Natural Environment Research Council (studentship NE/1210143). Charles C.-K. Chou received funding from the Academia Sinica through grant AS-KPQ-106-DDPP and the Ministry of Science and Technology of Taiwan through grant 105-2111-M-001-005-MY3 to support the sampling activities at Cape Fuguei Research Station. We are grateful for the work of the NOAA-ESRL Global Monitoring Division who provided the Manua Loa data. We acknowledge use of the NAME atmospheric dispersion model and associated NWP meteorological datasets made available to us by the UK Met Office. We also acknowledge the significant storage resources and analysis

facilities made available to us on JASMIN by STFC CEDA along with the corresponding support teams.

## References

- Adcock, K. E., Reeves, C. E., Gooch, L. J., Leedham Elvidge, E., Ashfold, M. J., Brenninkmeijer, C. A. M., Chou, C., Fraser, P. J., Langenfelds, R. L., Mohd Hanif, N., O'Doherty, S., Oram, D. E., Ou-Yang, C.-F., Moi Phang, S., Abu Samah, A., Röckmann, T., Sturges, W. T. and Laube, J. C.: Continued increase of CFC-113a ( $\text{CCl}_3\text{CF}_3$ ) mixing ratios in the global atmosphere: emissions, occurrence and potential sources, *Atmos. Chem. Phys.*, 18(7), 1–15, doi:10.5194/acp-18-4737-2018, 2018.
- An, X., Henne, S., Yao, B., Vollmer, M. K., Zhou, L. and Li, Y.: Estimating emissions of HCFC-22 and CFC-11 in China by atmospheric observations and inverse modeling, *Sci. China Chem.*, 55(10), 2233–2241, doi:10.1007/s11426-012-4624-8, 2012.
- Aulagnier, C., Rayner, P., Ciais, P., Vautard, R., Rivier, L. and Ramonet, M.: Is the recent build-up of atmospheric  $\text{CO}_2$  over Europe reproduced by models. Part 2: An overview with the atmospheric mesoscale transport model CHIMERE, *Tellus, Ser. B Chem. Phys. Meteorol.*, 62(1), 14–25, doi:10.1111/j.1600-0889.2009.00443.x, 2010.
- Barnes, D. H., Wofsy, S. C., Fehla, B. P., Gottlieb, E. W., Elkins, J. W., Dutton, G. S. and Montzka, S. A.: Urban/industrial pollution for the New York City–Washington, D.C., corridor, 1996–1998: 2. A study of the efficacy of the Montreal Protocol and other regulatory measures, *J. Geophys. Res. D Atmos.*, 108(D6), doi:10.1029/2001jd001117, 2003.
- Cantrell, C. A.: Technical Note: Review of methods for linear least-squares fitting of data and application to atmospheric chemistry problems, *Atmos. Chem. Phys.*, 8(17), 5477–5487, doi:10.5194/acp-8-5477-2008, 2008.
- Carpenter, L. J., Daniel, J. S., (Lead Authors), Fleming, E. L., Hanaoka, T., Hu, J., Ravishankara, A. R., Ross, M. N., Tilmes, S., Wallington, T. J. and Wuebbles, D. J.: Chapter 6 Scenarios and Information for Policymakers, in *Scientific Assessment of Ozone Depletion: 2018*, Global Ozone Research and Monitoring Project–Report No. 58, World Meteorological Organization, Geneva, Switzerland., 2018.
- Dameris, M., Jöckel, P. and Nützel, M.: Possible implications of enhanced chlorofluorocarbon-11 concentrations on ozone, *Atmos. Chem. Phys.*, 19(22), 13759–13771, doi:10.5194/acp-19-13759-2019, 2019.
- Dhomse, S. S., Feng, W., Montzka, S. A., Hossaini, R., Keeble, J., Pyle, J. A., Daniel, J. S. and Chipperfield, M. P.: Delay in recovery of the Antarctic ozone hole from unexpected CFC-11 emissions, *Nat. Commun.*, 10(1), 1–12, doi:10.1038/s41467-019-13717-x, 2019.
- Engel, A., Rigby, M., (Lead Authors), Burkholder, J. B., Fernandez, R. P., Froidevaux, L., Hall, B. D., Hossaini, R., Saito, T., Vollmer, M. K., and Yao, B.: Chapter 1 Update

on Ozone-Depleting Substances (ODSs) and Other Gases of Interest to the Montreal Protocol, in: Scientific Assessment of Ozone Depletion: 2018, Global Ozone Research and Monitoring Project–Report No. 58, World Meteorological Organization, Geneva, Switzerland, 2018.

Environmental Investigation Agency (EIA): BLOWING IT: Illegal Production and Use of Banned CFC-11 in China's Foam Blowing Industry, 8<sup>th</sup> July 2018. [online] Available from: [https://content.eia-global.org/posts/documents/000/000/761/original/Blowing-It\\_CFC11\\_Report\\_EIA.pdf?1531089183](https://content.eia-global.org/posts/documents/000/000/761/original/Blowing-It_CFC11_Report_EIA.pdf?1531089183) (Accessed 30 March 2020), 2018.

Fang, X., Wu, J., Su, S., Han, J., Wu, Y., Shi, Y., Wan, D., Sun, X., Zhang, J. and Hu, J.: Estimates of major anthropogenic halocarbon emissions from China based on interspecies correlations, *Atmos. Environ.*, 62, 26–33, doi:10.1016/j.atmosenv.2012.08.010, 2012.

Fang, X., Ravishankara, A. R., Velders, G. J. M., Molina, M. J., Su, S., Zhang, J., Hu, J. and Prinn, R. G.: Changes in Emissions of Ozone-Depleting Substances from China Due to Implementation of the Montreal Protocol, *Environ. Sci. Technol.*, 52(19), 11359–11366, doi:10.1021/acs.est.8b01280, 2018.

Fang, X., Park, S., Saito, T., Tunnicliffe, R., Ganesan, A. L., Rigby, M., Li, S., Yokouchi, Y., Fraser, P. J., Harth, C. M., Krummel, P. B., Mühle, J., O'Doherty, S., Salameh, P. K., Simmonds, P. G., Weiss, R. F., Young, D., Lunt, M. F., Manning, A. J., Gressent, A. and Prinn, R. G.: Rapid increase in ozone-depleting chloroform emissions from China, *Nat. Geosci.*, 12(2), 89–93, doi:10.1038/s41561-018-0278-2, 2019.

Feng, Y., Bie, P., Wang, Z., Wang, L. and Zhang, J.: Bottom-up anthropogenic dichloromethane emission estimates from China for the period 2005–2016 and predictions of future emissions, *Atmos. Environ.*, 186(May), 241–247, doi:10.1016/j.atmosenv.2018.05.039, 2018.

Fraser, P., Dunse, B., Krummel, P., Steele, P. and Derek, N.: Australian & Global Emissions of Ozone Depleting Substances. Report prepared for Department of the Environment, CSIRO Oceans and Atmosphere Flagship, Collaboration for Australian Weather and Climate Research, Aspendale, Australia, iii, 29 pp. [online] Available from: <https://www.environment.gov.au/system/files/resources/1b3c0ae6-e2ec-440a-b147-4d868f0da01f/files/australian-global-emissions-ods-2015.pdf> (Assessed 16 April 2020), 2015.

Harris, N. R. P., Montzka, S. A., and Newman, P. A.: SPARC Stratosphere-Troposphere Processes And their Role in Climate, Newsletter no. 53, July 2019, Report on the International Symposium on the Unexpected Increase in Emissions of Ozone-Depleting CFC-11, Vienna, Austria ISSN 1245-4680, [online] Available from: <https://www.sparc-climate.org/publications/newsletter/sparc-newsletter-no-53/> (Assessed 16 April 2020), 2019.

Hu, L., Montzka, S. A., Lehman, S. J., Godwin, D. S., Miller, B. R., Andrews, A. E., Thoning, K., Miller, J. B., Sweeney, C., Siso, C., Elkins, J. W., Hall, B. D., Mondeel, D. J., Nance, D., Nehrkorn, T., Mountain, M., Fischer, M. L., Biraud, S. C., Chen, H. and Tans, P. P.: Considerable contribution of the Montreal Protocol to declining greenhouse gas emissions from the United States, *Geophys. Res. Lett.*, 44(15), 8075–8083, doi:10.1002/2017GL074388, 2017.

Jones, A., Thomson, D., Hort, M. and Devenish, B.: The U.K. Met Office's Next-Generation Atmospheric Dispersion Model, NAME III, in *Air Pollution Modeling and Its Application XVII*, edited by C. Borrego and A.-L. Norman, pp. 580–589, Boston, MA, Springer US., 2007.

Keeble, J., Abraham, N. L., Archibald, A. T., Chipperfield, M. P., Dhomse, S., Griffiths, P. T. and Pyle, J. A.: Modelling the potential impacts of the recent, unexpected increase in CFC-11 emissions on total column ozone recovery, *Atmos. Chem. Phys.*, 20(12), 7153–7166, doi:10.5194/acp-20-7153-2020, 2020.

Keller, C. A., Hill, M., Vollmer, M. K., Henne, S., Brunner, D., Reimann, S., O'Doherty, S., Arduini, J., Maione, M., Ferenczi, Z., Haszpra, L., Manning, A. J. and Peter, T.: European Emissions of Halogenated Greenhouse Gases Inferred from Atmospheric Measurements, *Environ. Sci. Technol.*, 46(1), 217–225, doi:10.1021/es202453j, 2012.

Kim, J., Li, S., Kim, K. R., Stohl, A., Mühle, J., Kim, S. K., Park, M. K., Kang, D. J., Lee, G., Harth, C. M., Salameh, P. K. and Weiss, R. F.: Regional atmospheric emissions determined from measurements at Jeju Island, Korea: Halogenated compounds from China, *Geophys. Res. Lett.*, 37(12), 2007–2011, doi:10.1029/2010GL043263, 2010.

Laube, J. C., Keil, A., Bönisch, H., Engel, A., Röckmann, T., Volk, C. M. and Sturges, W. T.: Observation-based assessment of stratospheric fractional release, lifetimes, and ozone depletion potentials of ten important source gases, *Atmos. Chem. Phys.*, 13(5), 2779–2791, doi:10.5194/acp-13-2779-2013, 2013.

Leedham Elvidge, E. C., Oram, D. E., Laube, J. C., Baker, A. K., Montzka, S. A., Humphrey, S., O'Sullivan, D. A. and Brenninkmeijer, C. A. M.: Increasing concentrations of dichloromethane, CH<sub>2</sub>Cl<sub>2</sub>, inferred from CARIBIC air samples collected 1998-2012, *Atmos. Chem. Phys.*, 15(4), 1939–1958, doi:10.5194/acp-15-1939-2015, 2015.

Li, S., Park, M.-K., Jo, C. O. and Park, S.: Emission estimates of methyl chloride from industrial sources in China based on high frequency atmospheric observations, *J. Atmos. Chem.*, 74(2), 227–243, doi:10.1007/s10874-016-9354-4, 2017.

Li, Z., Bie, P., Wang, Z., Zhang, Z., Jiang, H., Xu, W., Zhang, J. and Hu, J.: Estimated HCFC-22 emissions for 1990–2050 in China and the increasing contribution to global emissions, *Atmos. Environ.*, 132, 77–84, doi:10.1016/j.atmosenv.2016.02.038, 2016.

Lunt, M. F., Park, S., Li, S., Henne, S., Manning, A. J., Ganesan, A. L., Simpson, I. J., Blake, D. R., Liang, Q., O'Doherty, S., Harth, C. M., Mühle, J., Salameh, P. K., Weiss, R. F., Krummel, P. B., Fraser, P. J., Prinn, R. G., Reimann, S. and Rigby, M.: Continued Emissions of the Ozone-Depleting Substance Carbon Tetrachloride From Eastern Asia, *Geophys. Res. Lett.*, 45(20), 11,423-11,430, doi:10.1029/2018GL079500, 2018.

Manning, A. J., Ryall, D. B., Derwent, R. G., Simmonds, P. G. and O'Doherty, S.: Estimating European emissions of ozone-depleting and greenhouse gases using observations and a modeling back-attribution technique, *J. Geophys. Res.*, 108(D14), 4405, doi:10.1029/2002JD002312, 2003.

Mohd Hanif, N.: The tropospheric abundances, emissions, and transport of halogenated substances on regional and global scales, PhD, School of Environmental Sciences, University of East Anglia. Available from: <https://ueaeprints.uea.ac.uk/72024/>, 2019.

Montzka, S. A., Dutton, G. S., Yu, P., Ray, E., Portmann, R. W., Daniel, J. S., Kuijpers, L., Hall, B. D., Mondeel, D., Siso, C., Nance, J. D., Rigby, M., Manning, A. J., Hu, L., Moore, F., Miller, B. R. and Elkins, J. W.: An unexpected and persistent increase in global emissions of ozone-depleting CFC-11, *Nature*, 557, 413–417, doi:10.1038/s41586-018-0106-2, 2018.

National Oceanic and Atmospheric Administration (NOAA): Combined Chlorofluorocarbon-11 data from the NOAA/ESRL Global Monitoring Division. Available from: <ftp://ftp.cmdl.noaa.gov/hats/cfcs/cfc11/combined/>, (Accessed 27 July 2019), 2019.

Oram, D. E., Ashfold, M. J., Laube, J. C., Gooch, L. J., Humphrey, S., Sturges, W. T., Leedham-Elvidge, E., Forster, G. L., Harris, N. R. P., Mead, M. I., Samah, A. A., Phang, S. M., Ou-Yang, C.-F., Lin, N.-H., Wang, J.-L., Baker, A. K., Brenninkmeijer, C. A. M. and Sherry, D.: A growing threat to the ozone layer from short-lived anthropogenic chlorocarbons, *Atmos. Chem. Phys.*, 17(19), 11929–11941, doi:10.5194/acp-17-11929-2017, 2017.

Riahi, K., Rao, S., Krey, V., Cho, C., Chirkov, V., Fischer, G., Kindermann, G., Nakicenovic, N., and Rafaj, P.: RCP 8.5-A scenario of comparatively high greenhouse gas emissions, *Climatic Change*, 109, 33-57, doi:10.1007/s10584-011-0149-y, 2011.

Rigby, M., Park, S., Saito, T., Western, L. M., Redington, A. L., Fang, X., Henne, S., Manning, A. J., Prinn, R. G., Dutton, G. S., Fraser, P. J., Ganesan, A. L., Hall, B. D., Harth, C. M., Kim, J., Kim, K.-R., Krummel, P. B., Lee, T., Li, S., Liang, Q., Lunt, M. F., Montzka, S. A., Mühle, J., O'Doherty, S., Park, M.-K., Reimann, S., Salameh, P. K., Simmonds, P., Tunnicliffe, R. L., Weiss, R. F., Yokouchi, Y. and Young, D.: Increase in CFC-11 emissions from eastern China based on atmospheric observations, *Nature*, 569(7757), 546–550, doi:10.1038/s41586-019-1193-4, 2019.

Say, D., Ganesan, A. L., Lunt, M. F., Rigby, M., O'Doherty, S., Harth, C., Manning, A. J., Krummel, P. B. and Bauguitte, S.: Emissions of halocarbons from India inferred

through atmospheric measurements, *Atmos. Chem. Phys.*, 19(15), 9865–9885, doi:10.5194/acp-19-9865-2019, 2019.

United Nations Environment Programme (UNEP): Rigid and Flexible Foams Technical Options Committee (FTOC) 2018 Assessment Report, ISBN: 978-9966-076-57-1. [online] Available from: <https://ozone.unep.org/sites/default/files/2019-04/FTOC-assessment-report-2018.pdf> (Accessed 14 April 2020), 2018a.

United Nations Environment Programme (UNEP): Medical and Chemicals Technical Options Committee (MCTOC) Assessment Report 2018, ISBN: 978-9966-076-51-9. [online] Available from: <https://ozone.unep.org/sites/default/files/2019-04/MCTOC-Assessment-Report-2018.pdf> (Accessed 14 April 2020), 2018b.

United Nations Environmental Programme (UNEP): Handbook for the Montreal Protocol on Substances that Deplete the Ozone Layer Thirteenth edition (2019), ISBN: 978-9966-076-59-5. [online] Available from: [https://ozone.unep.org/sites/default/files/Handbooks/MP\\_Handbook\\_2019.pdf](https://ozone.unep.org/sites/default/files/Handbooks/MP_Handbook_2019.pdf) (Accessed 14 April 2020), 2019a.

United Nations Environment Programme, (UNEP): Technology and Economic Assessment Panel (TEAP) Report, Volume 3 Decision XXX/3 TEAP Task Force Report on Unexpected Emissions of CFC-11, ISBN: 978-9966-076-65-6. [online] Available from: [http://conf.montreal-protocol.org/meeting/oewg/oewg-41/presession/Background-Documents/TEAP\\_Task\\_Force\\_Dec\\_XXX-3\\_on\\_Unexpected\\_CFC-11\\_Emissions\\_May\\_2019.pdf](http://conf.montreal-protocol.org/meeting/oewg/oewg-41/presession/Background-Documents/TEAP_Task_Force_Dec_XXX-3_on_Unexpected_CFC-11_Emissions_May_2019.pdf) (Accessed 14 April 2020), 2019b.

United Nations Environment Programme (UNEP): Report of the Thirty-First Meeting of the Parties to the Montreal Protocol on Substances that Deplete the Ozone Layer, Rome, 4–8 November 2019, UNEP/OzL.Pro.31/9, Annex II Summaries of presentations by members of the assessment panels and technical options committees, A. Interim report of the Scientific Assessment Panel on increased emissions of CFC-11. [online] Available from: <http://conf.montreal-protocol.org/meeting/mop/mop-31/report/SitePages/Home.aspx> (Accessed 30 March 2020), 2019c.

United Nations Environment Programme (UNEP): Report of China on progress made in the monitoring and management of ozone-depleting substances. Thirty-First Meeting of the Parties to the Montreal Protocol on Substances that Deplete the Ozone Layer, Rome, 4–8 November 2019, UNEP/OzL.Pro.31/INF/9. [online] Available from: <https://undocs.org/en/UNEP/OZL.PRO.31/INF/9> (Accessed 30 March 2020), 2019d.

Wan, D., Xu, J., Zhang, J., Tong, X. and Hu, J.: Historical and projected emissions of major halocarbons in China, *Atmos. Environ.*, 43(36), 5822–5829, doi:10.1016/j.atmosenv.2009.07.052, 2009.

Wang, C., Shao, M., Huang, D., Lu, S., Zeng, L., Hu, M. and Zhang, Q.: Estimating halocarbon emissions using measured ratio relative to tracers in China, *Atmos. Environ.*, 89, 816–826, doi:10.1016/j.atmosenv.2014.03.025, 2014.

Wu, J., Fang, X., Martin, J. W., Zhai, Z., Su, S., Hu, X., Han, J., Lu, S., Wang, C., Zhang, J. and Hu, J.: Estimated emissions of chlorofluorocarbons, hydrochlorofluorocarbons, and hydrofluorocarbons based on an interspecies correlation method in the Pearl River Delta region, China, *Sci. Total Environ.*, 470–471, 829–834, doi:10.1016/j.scitotenv.2013.09.071, 2014.

## Chapter 6: Summary, conclusions and future work

---

The ozone layer is a part of the atmosphere that blocks harmful ultraviolet radiation from reaching the Earth's surface and so protects human health and the environment. Industrially produced halogenated trace gases that contain chlorine and bromine enhance natural ozone destruction in the stratosphere and their increasing mixing ratios lead to the formation of 'the ozone hole' over Antarctica. Due to this an international agreement called the Montreal Protocol on Substances that Deplete the Ozone Layer was introduced in 1989. Parties of the Montreal Protocol agreed to phase out and eventually stop almost all production and consumption of many ozone-depleting substances. This agreement was largely successful and mixing ratios of ozone-depleting substances, such as the major CFCs, Halons,  $\text{CCl}_4$  and  $\text{CCl}_3\text{CH}_3$ , are now decreasing in the atmosphere and the ozone layer is starting to show signs of recovery (Engel and Rigby et al., 2018).

However, continued monitoring of ozone-depleting substances in the atmosphere is necessary to verify ongoing compliance with the Montreal Protocol and identify new threats that could undermine previous progress and delay the expected long-term recovery of the ozone layer. In this study, air samples collected from a variety of ground-based measurement sites and aircraft campaigns were measured for 30-50 ozone-depleting substances and other trace gases using a high sensitivity Gas Chromatograph - Mass Spectrometer (GC-MS) instrument.

This study investigates changes in mixing ratios of ozone-depleting substances in the atmosphere with a special focus on ozone-depleting substances in East Asia. East Asia is a region of particular importance for ozone-depleting substances as it is a region with potentially fast transport of air from the surface into the lower stratosphere. Additionally, it has rapidly developed in recent years with a large part of its industry producing and using many halocarbons.

The main conclusions of this thesis are that mixing ratios of CFC-113a ( $\text{CCl}_3\text{CF}_3$ ) are still increasing in the atmosphere (Chapter 4) and emissions of CFC-11 ( $\text{CCl}_3\text{F}$ ) have increased in eastern China (Chapter 5), despite a global ban on almost all production of CFCs since 2010. Also, there are enhanced mixing ratios of chlorine-containing very short-lived ozone-depleting substances in the lower stratosphere above the Asian summer monsoon (Chapter 3).

## 6.1 Outline of major research findings

### 6.1.1 Transport of chlorine-containing very short-lived ozone-depleting substances by the Asian summer monsoon

Chapter 3 discusses aircraft-based observations of ozone-depleting substances (ODSs) in the upper troposphere and lower stratosphere in and above the Asian summer monsoon. In this study mixing ratios of 27 ozone-depleting substances were measured, in 118 air samples collected on board the Geophysica high-altitude research aircraft. Two aircraft campaigns took place, over the Mediterranean in 2016 (AMO-16 campaign) and over Nepal and northern India in 2017 (AMA-17 campaign). These measurements were used to investigate the importance of transport of very short-lived substances (VSLs) by the Asian summer monsoon into the lower stratosphere.

Very short-lived ozone-depleting substances are not included in the Montreal Protocol. It was, until relatively recently, thought that VSLs are largely removed in the troposphere before they reach the stratosphere and therefore contribute relatively little to ozone depletion. However, in air samples collected during the AMA-17 campaign the mixing ratios of the chlorine-containing very short-lived ozone-depleting substances,  $\text{CH}_2\text{Cl}_2$ ,  $\text{CHCl}_3$  and  $\text{CH}_2\text{ClCH}_2\text{Cl}$  were enhanced above expected levels. This indicates that the Asian summer monsoon anticyclone is rapidly transporting very short-lived substances into the lower stratosphere where they will contribute to ozone depletion.

The CLaMS model (a global stratospheric model focused on transport and chemistry) was used to run 15-day backward trajectories for samples collected during the AMA-17 campaign. The trajectories were used to constrain the last location where the air was in the model boundary layer, i.e. 2-3 km above the surface, and the time taken by the trajectory to reach the model boundary layer. The source locations for most of the air samples were located mostly around southern China with less frequent sources in the rest of South-East Asia. Transport times were generally fast, with 32 samples having trajectories reaching the model boundary layer within 15 days. This agrees with previous research that air is mostly confined within the Asian summer monsoon anticyclone and subsequently rapidly transported from the anticyclone to the lower stratosphere. There was not a significant correlation between shorter transport times and higher  $\text{CH}_2\text{Cl}_2$  mixing ratios, but this may be due to the impact of other factors.

The Equivalent Chlorine (ECI) and Equivalent Effective Stratospheric Chlorine (EESC) were derived to investigate the importance of VSLs in comparison to total chlorine and bromine loading under these conditions.

Equivalent Chlorine (ECI) is the sum of the mixing ratios of bromine atoms (multiplied by 60) and chlorine atoms from all halogen source gases. A regional ECI was calculated for the tropopause region using measurements from the AMA-17 campaign. For comparison a global estimate of ECI was calculated using tropospheric mixing ratios for long-lived compounds and estimated mixing ratios at the Level of Zero Radiative

Heating (LZRH) from the WMO 2018 report for very short-lived compounds (Engel and Rigby et al., 2018). The total equivalent chlorine of the AMA-17 campaign is the highest estimate but the ranges of the two estimates overlap (4186-4499 ppt vs 4331-5057 ppt). This is due to the AMA-17 ECl estimate having some samples with higher long-lived chlorine, higher long-lived bromine, similar very short-lived bromine, and higher very short-lived chlorine than the global estimate (89-132 ppt vs 169-393 ppt). Very short-lived chlorine is a relatively small fraction of the total equivalent chlorine in the tropopause region but has a larger percentage contribution to the ECl in the AMA-17 estimate (4-8 %) than in the global estimate (2-3 %).

The Equivalent Effective Stratospheric Chlorine (EESC) is similar to ECl but takes into account the effects of stratospheric transport (mean age-of-air) and chemistry (Fractional Release Factors, FRFs). Fractional Release Factors and mean age-of-air were derived using tropospheric trends from the same data sets as the ECl and mixing ratios from the aircraft samples. Our FRFs agree within the uncertainties for most compounds when compared to previous studies that used the same method to calculate FRFs.

The EESC calculated for the AMA-17 campaign was found to be more than 100 ppt higher than the EESC calculated for the AMO-16 campaign at a mean age-of-air of 2.4 years (e.g. relevant age: 1483-1495 ppt vs 1630-1650 ppt). This is likely because the AMO-16 campaign sampled air masses of Northern Hemispheric extra-tropical air and outflow from the Asian monsoon, which would be more well-mixed air not recently polluted with ODSs, and so in general has lower ODS mixing ratios.

The regional EESCs in this study were generally higher than other estimates in the literature. For example, the AMO-16 relevant age-based EESC is 1861-1872 ppt for age-of-air of 3 years, in comparison to the WMO 2018 reported relevant age-based EESC of 1649 ppt (Engel and Rigby et al., 2018). This is most likely because the Asian monsoon region has large continental emissions and more input into the stratosphere compared to globally averaged estimates which also include areas with less input.

The contribution of VSLs to the EESC was also estimated and their contribution increased the long-lived EESC by about 8-26 %. This suggests VSLs have an important effect on the amount of EESC and therefore the amount of ozone destruction, especially in the northern hemispheric extra-tropical lower stratosphere.

The contribution of Cl-VSLs to the ECl and EESC are substantial in comparison to the size of the decreasing trend in ODS mixing ratios in the atmosphere. For example, Cl-VSLs contribute about 75-123 ppt to the EESC at a mean age-of-air of 3 years based on the AMO-16 campaign, whereas, EESC at mid-latitudes has been decreasing by about 14-16 ppt per year (Engel and Rigby et al., 2018). This shows that the contribution from VSLs is large compared to the size of the decreasing trend.

Although this is only one part of the atmosphere the additional input of chlorine into the stratosphere, if it continues, could delay the recovery of the ozone layer.

### **6.1.2 CFC-113a mixing ratios and emissions in the atmosphere**

Chapter 4 investigates the ozone-depleting substance CFC-113a ( $\text{CCl}_3\text{CF}_3$ ). A recent study found increasing mixing ratios and emissions of CFC-113a in the atmosphere (Laube et al., 2014). This trend is investigated further using measurements of air samples collected at multiple sites all over the world.

The long-term time series of CFC-113a mixing ratios at Cape Grim was updated with an additional four years. The CFC-113a mixing ratios were found to have continued increasing from 0.5 ppt in December 2012 to 0.7 ppt in February 2017. These mixing ratios remain small in comparison to other CFCs, but continue to rapidly increase, and the causes of this increase are uncertain.

A previous study used the CFC-113a measurements at Cape Grim with a 2D atmospheric chemistry-transport model to estimate, top-down, global annual emissions of CFC-113a (Laube et al., 2014). In this thesis, the emission estimates were updated, and it was found that CFC-113a emissions began in the 1960s and gradually increased until 2010. Then there was a sharp increase in CFC-113a emissions from  $0.9 \text{ Gg yr}^{-1}$  ( $0.6\text{-}1.2 \text{ Gg yr}^{-1}$ ) in 2010 to  $1.9 \text{ Gg yr}^{-1}$  ( $1.5\text{-}2.4 \text{ Gg yr}^{-1}$ ) in 2012. After the increase in 2010-2012, emissions were on average  $1.7 \text{ Gg yr}^{-1}$  ( $1.3\text{-}2.4 \text{ Gg yr}^{-1}$ ) between 2012 and 2016.

Measurements of CFC-113a mixing ratios were also made on air samples collected at the Tacolneston tall tower in the UK and as part of the CARIBIC campaign onboard commercial aircraft flights between Germany and South Africa. These CFC-113a mixing ratios indicate a persistent interhemispheric difference with larger CFC-113a emissions in the Northern Hemisphere.

Air samples were also collected at ground-based measurement sites in Taiwan between 2013 and 2016, in the spring of each year, and were measured for multiple halogenated trace gases including CFC-113a. Some of the samples collected in Taiwan had enhanced mixing ratios of CFC-113a up to 3 ppt indicating relatively nearby emissions of CFC-113a.

The NAME particle dispersion model was used to produce footprints of where the air sampled during the Taiwan campaigns had previously been close to the Earth's surface. When air samples were collected with enhanced CFC-113a mixing ratios the NAME footprints in general showed a larger influence from eastern China or the Korean Peninsula. This indicates emissions of CFC-113a may be coming from these areas.

In the Taiwan samples CFC-113a mixing ratios had a good correlation with CFC-113 and HCFC-133a mixing ratios. This indicates that sources of these compounds may be co-located or that these substances are being co-produced. CFC-113 emissions have

dramatically decreased since 1989 but have not declined to zero. Therefore, CFC-113 and CFC-113a could be co-produced, along with HCFC-133a, possibly as fugitive emissions during the large-scale production of CFC-alternatives such as HFC-134a and HFC-125 production. Other possible sources of CFC-113a emissions are from its use as an agrochemical intermediate or as an impurity in CFC-113 banks. Emissions of CFC-113a are small enough that they could be completely due to these sources which are permitted under the Montreal Protocol. Therefore, the main conclusion of this study is that while CFC-113a mixing ratios continue to increase in the atmosphere there is no evidence of illegal production of this compound under the current terms of the Montreal Protocol.

### **6.1.3 CFC-11 mixing ratios and emissions in East Asia**

Chapter 5 investigates CFC-11 ( $\text{CCl}_3\text{F}$ ) using atmospheric observations in Taiwan. Global CFC-11 mixing ratios were recently found to be declining at a slower rate than expected due to an increase in global CFC-11 emissions (Montzka et al., 2018). A study in East Asia concluded that emissions of CFC-11 were coming from eastern mainland China using inversion modelling and measurements in Japan and Korea (Rigby et al., 2019). It has been suggested that this increase is very likely from illegal production of CFC-11 for its use as a foam blowing agent in building insulation.

In this thesis, 135 air samples were collected at ground-based measurement sites in Taiwan between 2014 and 2018 in spring each year. The samples were measured for multiple halogenated trace gases including CFC-11. CFC-11 mixing ratios in Taiwan were often consistent with ‘background’ mixing ratios in Hawaii,  $\sim 231$  ppt, but were sometimes enhanced up to 272 ppt.

The NAME particle dispersion model was again used to investigate the history of air arriving at the sampling sites in Taiwan. The NAME footprints mass density residence times from the region of East China had the strongest correlation with CFC-11 mixing ratios in the air samples. This, therefore, suggests that East China is the region most likely to be the source of CFC-11 emissions.

Measured CFC-11 mixing ratios were also compared to modelled CO mixing ratios from 12 emission sectors in the Representative Concentration Pathway 8.5 (Riahi et al., 2011; Mohd Hanif, 2019). The emissions sectors with the strongest correlations with CFC-11 mixing ratios were agricultural waste burning on fields, the residential and commercial sector, the solvent sector, and industry (combustion and processing). As these emission sectors were predominantly co-located in eastern China, it was not possible to clearly identify an emissions sector as the source of CFC-11. Although, it does provide further indirect evidence of CFC-11 emissions in eastern China.

CFC-11 mixing ratios were found to have good interspecies correlations with  $\text{CHCl}_3$ ,  $\text{CCl}_4$ , HCFC-141b, HCFC-142b,  $\text{CH}_2\text{Cl}_2$ , and HCFC-22 in the Taiwan samples. This is most likely due to co-location of emissions as eastern China is a very industrialized

densely populated area with a large chloromethane industry. The traditional method of CFC-11 production also produces large quantities of CFC-12. However, it was found that CFC-12 mixing ratios do not have a good correlation with those of CFC-11 so the possible production method of CFC-11 in recent years is still uncertain.

Interspecies ratios of CFC-11 with compounds that it has a good correlation with, and which have published emission estimates, were used to estimate CFC-11 emissions. Multiple studies were used with emission estimates for the whole of China and eastern China. When the CFC-11 emission estimates from the whole of China and eastern China were combined they were termed CFC-11 emissions from “(eastern) China” and were estimated to be 19 (14–23) Gg yr<sup>-1</sup> in 2014–2018.

When CFC-11 emission estimates from earlier studies for eastern China and the whole of China were combined CFC-11 emissions in (eastern) China in 2008–2011 were estimated to be 12 (10–14) Gg yr<sup>-1</sup>. This indicates an increase in CFC-11 emissions in (eastern) China of 7 (2–12) Gg yr<sup>-1</sup>. This is similar to the increase of  $7 \pm 3$  Gg yr<sup>-1</sup> in eastern mainland China estimated by Rigby et al. (2019). The consistency between these estimates, based on independent methods, increases the confidence in these conclusions. An increase in CFC-11 emissions in (eastern) China is very much counter to the intentions of the Montreal Protocol.

To investigate the importance of (eastern) China CFC-11 emissions these emission estimates were compared to three global CFC-11 emission estimates. (Eastern) China CFC-11 emissions were about one-quarter of global emissions. Also, the contribution of (eastern) China emissions to the global increase in CFC-11 emissions is highly uncertain, about  $50 \pm 40$  % of the increase in emissions that occurred around 2013.

## **6.2 Suggestions for future work and policy implications**

### **6.2.1 Transport of chlorine-containing very short-lived ozone-depleting substances by the Asian summer monsoon**

There are a number of ways this work could be extended. In Chapter 3 the conclusions are based on VLS measurements made during one Asian summer monsoon season and so they are spatially and temporally limited. Therefore, measurements during other Asian summer monsoons would be advantageous to determine the impact of interannual monsoon variability on VLSs mixing ratios. Although due to the high cost of research aircraft campaigns this is likely to be prohibitively expensive.

In addition, it is uncertain how mixing ratios of chlorine-containing VLSs will change in the future. For example, if CH<sub>2</sub>Cl<sub>2</sub> mixing ratios continue to increase at the same rate as between 2004 and 2014 (2.85 ppt yr<sup>-1</sup>) it could delay the return of total lower stratospheric chlorine to pre-1980 levels by 15–17 years, (Hossaini et al., 2017). However, this growth rate may not be consistent with expected future demand

(McCulloch, 2017). Therefore, continued surface measurements would be most beneficial to track future trends.

Something to potentially consider is adding VSLs, such as  $\text{CH}_2\text{Cl}_2$ , to the list of controlled substances in the Montreal Protocol.  $\text{CH}_2\text{Cl}_2$  has an atmospheric lifetime of about 6 months, 180 (95–1070) days, is predominantly anthropogenic in origin, and its average global tropospheric mixing ratios were 32–39 ppt in 2016 (WMO, 2018).  $\text{CH}_2\text{Cl}_2$  currently contributes very little ( $\sim 1\text{--}3\%$ ) to stratospheric chlorine input but it will likely become relatively more important in the future as emissions from long-lived compounds decrease. The WMO, 2018 report suggests that the elimination of both  $\text{CH}_2\text{Cl}_2$  emissions and the unexpected increase in CFC-11 emissions would have larger positive impacts on future ozone than any of the other mitigation options considered (Carpenter and Daniel et al., 2018, Figure 6-1). In addition, as  $\text{CH}_2\text{Cl}_2$  is short-lived the impacts of any mitigation efforts would be seen in the atmosphere relatively quickly.

### **6.2.2 CFC-113a mixing ratios and emissions in the atmosphere**

In Chapter 4 it was shown that emissions of CFC-113a have varied in recent years. After a sudden increase in emissions in 2010-2012, CFC-113a emissions remained stable at about  $1.7\text{ Gg yr}^{-1}$  in 2012-2016. The UEA will continue collecting about 4 subsamples each year from the Cape Grim Air Archive. This record can carry on being used to monitor the long-term trends of global background CFC-113a mixing ratios and discover if CFC-113a emissions remain stable in the future.

If CFC-113a emissions are coming from HFC-134a and HFC-125 production, the phase out of these compounds under the Montreal Protocol may affect future CFC-113a emissions. Although, CFC-113a emissions may also be from agrochemical production or impurities in CFC-113 banks. In addition, there have been some patent applications for the use of CFC-113a in the production of HFOs (Baldychev et al., 2019; Peng et al., 2019), the replacement compounds for HCFCs and HFCs. Therefore, fugitive emissions of CFC-113a might continue in the future from these sources.

In addition, air samples will keep being collected in Taiwan in the spring of each year. These samples can be used to investigate if there continues to be enhanced mixing ratios of CFC-113a in Taiwan. Also, to further investigate the correlations of CFC-113a mixing ratios with other compounds, discussed in Chapter 4, such as CFC-113, HCFC-133a, HCFC-123, HCFC-124 and CFC-114a. These compounds are also involved in the production of HFC-134a, HFC-125 and agrochemicals, and they had inconsistent correlations with CFC-113a, in the Taiwan air samples, in Chapter 4. More measurements could make the correlations clearer and provide more evidence to better determine the sources of CFC-113a emissions. In addition, the measurements could be compared to NAME footprints of the sampled air to further narrow the source regions of CFC-113a emissions.

In Chapter 4 it was reported that the isomers CFC-113a and CFC-113 have different long-term atmospheric trends. This is in addition to another study that found different trends in the isomer's CFC-114a and CFC-114 (Laube et al., 2016). If a complete understanding of the impacts of individual isomers was desired, then it could be required that isomers be reported separately to the UNEP. Also, the increasing emissions of CFC-113a indicate that the uses of ozone-depleting substances (ODSs) as chemical feed-stock or intermediates is becoming more important. Therefore, these uses of ODSs might need to be regulated if we want to accelerate the rate of decrease of ODSs and/or aim to eventually have zero emissions of ODSs. Although, compared to other CFCs, the current background mixing ratios of CFC-113a are very low (0.7 ppt vs CFC-12: ~510 ppt, CFC-11: ~230 ppt, CFC-113: ~70 ppt in 2016). Therefore, CFC-113a emissions are still small enough that they are not a major threat to the ozone layer and there are more important compounds to focus on, such as CFC-11 and VLSs.

### **6.2.3 CFC-11 mixing ratios and emissions in East Asia**

In Chapter 5 emissions of CFC-11 in (eastern) China were estimated to be about one-quarter of global CFC-11 emissions. However, there are still many parts of the world without current regional CFC-11 emission estimates including South America, Africa, and parts of Asia including the rest of China (Harris et al., 2019). Other regional studies would help to better constrain the sources of the increase in global CFC-11 emissions. In addition, a better understanding is needed of the influence of changes in atmospheric dynamics on global top-down emission estimates.

Investigations into the foam blowing industry in China could determine to what extent this is the cause of the recent increase in CFC-11 emissions. In the non-peer-reviewed literature, the Environmental Investigation Agency (EIA), based in the UK and the US, interviewed representatives from 21 foam production companies and 18 of them admitted to using CFC-11 (EIA, 2018a). Many also said that the use of CFC-11 was wide-spread in the industry. A New York Times investigation also found evidence of CFC-11 production in the foam blowing industry in China (Buckley and Fountain, 2018). Additionally, the EIA tested three samples of foam and found all of them contained CFC-11 (EIA, 2018b). In response to the reports about CFC-11, China launched a nationwide investigation and have undertaken several enforcement actions (EIA, 2018b). It was reported in November 2019 that they had fined six enterprises for using CFC-11 illegally and closed down three CFC-11 production facilities (UNEP, 2019a). There is preliminary evidence that these enforcement efforts have been successful and that both global and East Asian emissions of CFC-11 declined in 2018 and 2019 (UNEP, 2019b). Enforcement efforts will need to continue in the future to get the CFC-11 issue under control.

The recent changes in CFC-11 trends shows the necessity of constant monitoring to make sure existing legislation is being followed and shows that despite the success of the Montreal Protocol we must not become complacent.

#### 6.2.4 Further research directions

One of the limitations of the studies in Chapters 4 and 5 was that samples in Taiwan were collected during only springtime each year. The conclusions assume that mixing ratios and emissions are similar during other times of the year. This assumption is especially important for the CFC-11 emission estimates in Chapter 5. It would be interesting to know what the results would be if air samples were collected during other times of the year. A larger number of samples than usual were collected in Taiwan in 2019, 52 samples between March and May. Another way to extend this study would be to incorporate the measurements from these air samples and the future campaigns planned for later years.

In addition, the air samples collected in Cape Grim and Taiwan were measured for 30-50 halogenated trace gases, not all of which have been fully investigated. Possible studies in the future could investigate other compounds in these samples. Furthermore, continuing to make intercomparison measurements between the different standards used at the UEA (Section 2.8) is needed for quality assurance purposes, especially for the compounds that were found to be unstable, in order to enable comparisons between different datasets and laboratories, such as NOAA-GMD, to carry on in the future.

This thesis focused on three areas of concern in regards to ozone-depleting substances: VSLs, CFC-113a & CFC-11. Future studies could focus on some of the other areas of concern that were mentioned in the introduction but have not been investigated here such as: changes in mixing ratios and emissions of other ozone-depleting substances such as CCl<sub>4</sub>, CFC-13, CFC-114, CFC-114a & CFC-115 or the impacts of greenhouse gases and climate change on ozone recovery.

Investigation of ozone-depleting substances in general is needed in the future. Excellent progress has been made in reducing levels of ozone-depleting substances. The ozone layer is projected to return to 1980s levels in the middle of this century but there are many factors that could influence this including changes in the mixing ratios of ozone-depleting substances. The 21<sup>st</sup> century will be a time of change in this area as countries transition away from using HCFCs and HFCs because of the requirements of the Montreal Protocol. It will be important to continue making measurements of halogenated trace gases to understand their atmospheric abundance, trends, geographical distribution, and global and regional emissions so that the progress of the Montreal Protocol can be monitored effectively and to identify new threats to the ozone layer.

## References

Baldychev, I. S., Brandstadter, S. M., Cheung, P. and Nappa, M. J.: United States Patent Application, Integrated process for the production of Z-1,1,1,4,4,4-Hexafluoro-2-butene, The Chemours Company FC, LLC, Appl. No.: 16/262,834, Pub. No.: US 2019/0248719 A1, Pub. Date: 15<sup>th</sup> August 2019. [online] Available from: <http://www.freepatentsonline.com/y2019/0248719.html>, (Accessed 30 March 2020), 2019.

Buckley, C. and Fountain, H.: In a High-Stakes Environmental Whodunit, Many Clues Point to China, New York Times, 24th June [online] Available from: <https://www.nytimes.com/2018/06/24/world/asia/china-ozone-cfc.html>, (Accessed 30 March 2020), 2018.

Carpenter, L. J., Daniel, J. S., (Lead Authors), Fleming, E. L., Hanaoka, T., Hu, J., Ravishankara, A. R., Ross, M. N., Tilmes, S., Wallington, T. J. and Wuebbles, D. J.: Chapter 6 Scenarios and Information for Policymakers, in Scientific Assessment of Ozone Depletion: 2018, Global Ozone Research and Monitoring Project–Report No. 58, World Meteorological Organization, Geneva, Switzerland., 2018.

Engel, A., Rigby, M., (Lead Authors), Burkholder, J. B., Fernandez, R. P., Froidevaux, L., Hall, B. D., Hossaini, R., Saito, T., Vollmer, M. K. and Yao, B.: Chapter 1 Update on Ozone-Depleting Substances (ODSs) and Other Gases of Interest to the Montreal Protocol, in Scientific Assessment of Ozone Depletion: 2018, Global Ozone Research and Monitoring Project–Report No. 58, World Meteorological Organization, Geneva, Switzerland., 2018.

Environmental Investigation Agency (EIA): BLOWING IT: Illegal Production and Use of Banned CFC-11 in China’s Foam Blowing Industry, 8<sup>th</sup> July 2018. [online] Available from: [https://content.eia-global.org/posts/documents/000/000/761/original/Blowing-It\\_CFC11\\_Report\\_EIA.pdf?1531089183](https://content.eia-global.org/posts/documents/000/000/761/original/Blowing-It_CFC11_Report_EIA.pdf?1531089183) (Accessed 30 March 2020), 2018a.

Environmental Investigation Agency (EIA): Tip of the Iceberg: Implications of Illegal CFC Production and Use. EIA Briefing to the 30th Meeting of the Parties to the Montreal Protocol, 4<sup>th</sup> November 2018. [online] Available from: <https://eia-international.org/report/tip-iceberg-implications-illegal-cfc-production-use/> (Accessed 30 March 2020), 2018b.

Harris, N. R. P., Montzka, S. A. and Newman, P. A.: SPARC Stratosphere-Troposphere Processes And their Role in Climate, Newsletter no. 53, July 2019, Report on the International Symposium on the Unexpected Increase in Emissions of Ozone-Depleting CFC-11; ISSN 1245-4680; Vienna, Austria, 2019 [online] Available from: <https://www.sparc-climate.org/publications/newsletter/sparc-newsletter-no-53/> (Accessed 30 March 2020), 2019.

Hossaini, R., Chipperfield, M. P., Montzka, S. A., Leeson, A. A., Dhomse, S. S. and Pyle, J. A.: The increasing threat to stratospheric ozone from dichloromethane, *Nat. Commun.*, 8, 15962, doi:10.1038/ncomms15962, 2017.

Laube, J. C., Newland, M. J., Hogan, C., Brenninkmeijer, C. A. M., Fraser, P. J., Martinerie, P., Oram, D. E., Reeves, C. E., Röckmann, T., Schwander, J., Witrant, E. and Sturges, W. T.: Newly detected ozone-depleting substances in the atmosphere, *Nat. Geosci.*, 7(March), 10–13, doi:10.1038/NGEO2109, 2014.

Laube, J. C., Mohd Hanif, N., Martinerie, P., Gallacher, E., Fraser, P. J., Langenfelds, R., Brenninkmeijer, C. A. M., Schwander, J., Witrant, E., Wang, J.-L., Ou-Yang, C.-F., Gooch, L. J., Reeves, C. E., Sturges, W. T. and Oram, D. E.: Tropospheric observations of CFC-114 and CFC-114a with a focus on long-term trends and emissions, *Atmos. Chem. Phys.*, 16(23), 15347–15358, doi:10.5194/acp-16-15347-2016, 2016.

McCulloch, A.: Dichloromethane in the environment, A note prepared for the European Chlorinated Solvents Association (ECSA) and the Halogenated Solvents Industry Alliance (HSIA), 9th November 2017. [online] Available from: [http://www.chlorinated-solvents.eu/images/Documents/Newsroom/Dichloromethane paper.pdf](http://www.chlorinated-solvents.eu/images/Documents/Newsroom/Dichloromethane%20paper.pdf) (Accessed 19 February 2018), 2017.

Mohd Hanif, N.: The tropospheric abundances, emissions, and transport of halogenated substances on regional and global scales, PhD, School of Environmental Sciences, University of East Anglia. Available from: <https://ueaeprints.uea.ac.uk/72024/>, 2019.

Montzka, S. A., Dutton, G. S., Yu, P., Ray, E., Portmann, R. W., Daniel, J. S., Kuijpers, L., Hall, B. D., Mondeel, D., Siso, C., Nance, J. D., Rigby, M., Manning, A. J., Hu, L., Moore, F., Miller, B. R. and Elkins, J. W.: An unexpected and persistent increase in global emissions of ozone-depleting CFC-11, *Nature*, 557, 413–417, doi:10.1038/s41586-018-0106-2, 2018.

Peng, S., Nappa, M. J., Jackson, A. and Lousenberg, R. D.: United States Patent Application Process for Producing Halogenated Olefins. The Chemours Company FC, LLC, Appl. No.: 16/320,320, Pub. No.: US 2019/0233353 A1, Pub. Date: 1<sup>st</sup> August 2019 [online] Available from: <http://www.freepatentsonline.com/y2019/0233353.html> (Accessed 30 March 2020), 2019.

Riahi, K., Rao, S., Krey, V., Cho, C., Chirkov, V., Fischer, G., Kindermann, G., Nakicenovic, N., and Rafaj, P.: RCP 8.5-A scenario of comparatively high greenhouse gas emissions, *Climatic Change*, 109, 33-57, doi:10.1007/s10584-011-0149-y, 2011.

Rigby, M., Park, S., Saito, T., Western, L. M., Redington, A. L., Fang, X., Henne, S., Manning, A. J., Prinn, R. G., Dutton, G. S., Fraser, P. J., Ganesan, A. L., Hall, B. D., Harth, C. M., Kim, J., Kim, K.-R., Krummel, P. B., Lee, T., Li, S., Liang, Q., Lunt, M. F., Montzka, S. A., Mühle, J., O'Doherty, S., Park, M.-K., Reimann, S., Salameh, P. K., Simmonds, P., Tunnicliffe, R. L., Weiss, R. F., Yokouchi, Y. and Young, D.: Increase

in CFC-11 emissions from eastern China based on atmospheric observations, *Nature*, 569(7757), 546–550, doi:10.1038/s41586-019-1193-4, 2019.

United Nations Environment Programme (UNEP): Report of China on progress made in the monitoring and management of ozone-depleting substances. Thirty-First Meeting of the Parties to the Montreal Protocol on Substances that Deplete the Ozone Layer, Rome, 4–8 November 2019, UNEP/OzL.Pro.31/INF/9. [online] Available from: <https://undocs.org/en/UNEP/OZL.PRO.31/INF/9> (Accessed 30 March 2020), 2019a.

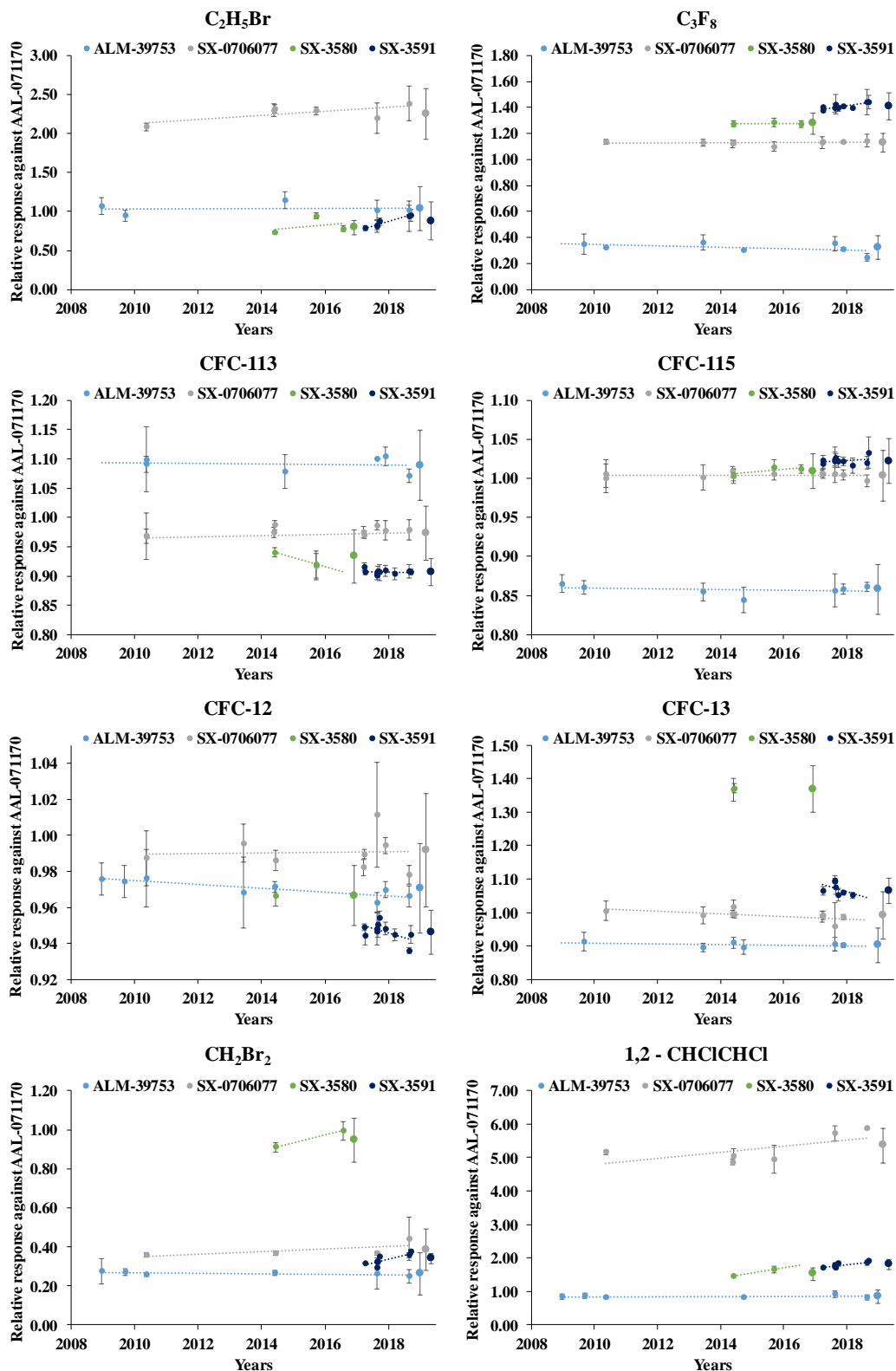
United Nations Environment Programme (UNEP): Report of the Thirty-First Meeting of the Parties to the Montreal Protocol on Substances that Deplete the Ozone Layer, Rome, 4–8 November 2019, UNEP/OzL.Pro.31/9, Annex II Summaries of presentations by members of the assessment panels and technical options committees, A. Interim report of the Scientific Assessment Panel on increased emissions of CFC-11. [online] Available from: <http://conf.montreal-protocol.org/meeting/mop/mop-31/report/SitePages/Home.aspx> (Accessed 30 March 2020), 2019b.

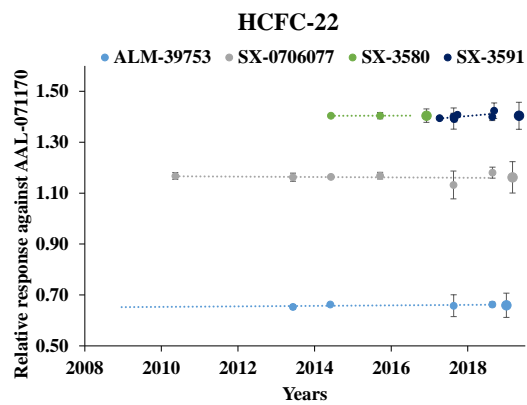
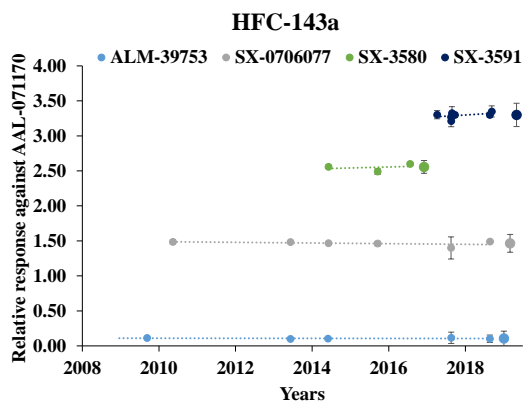
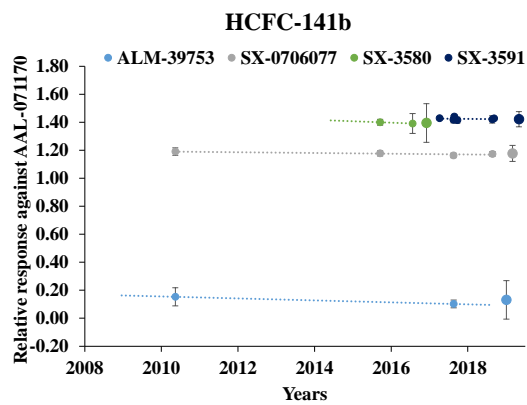
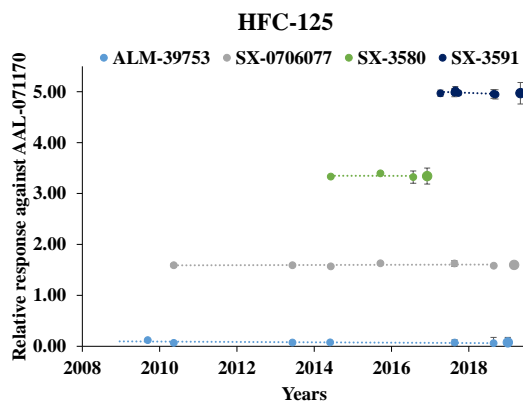
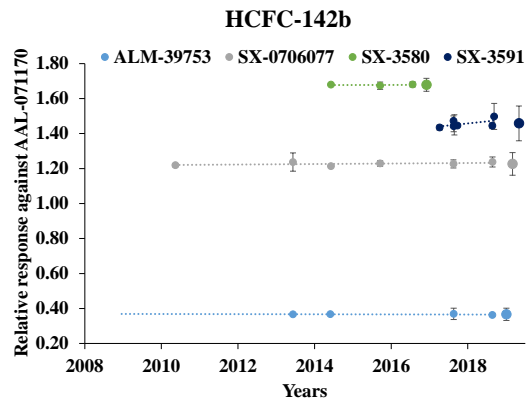
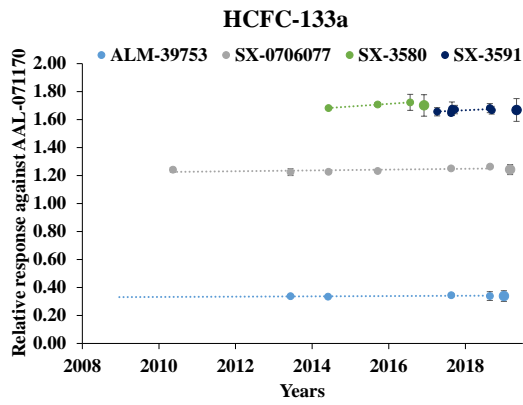
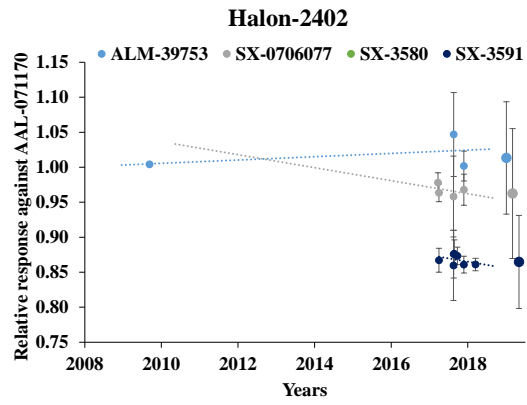
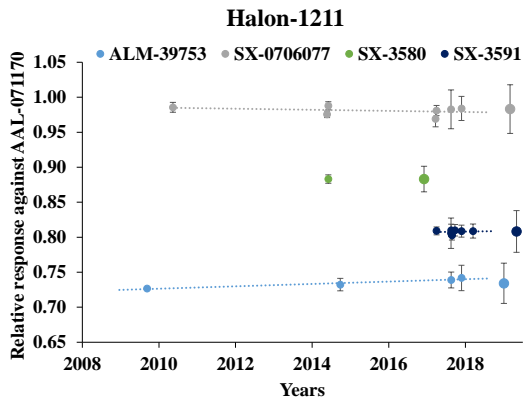
WMO (World Meteorological Organization): Scientific Assessment of Ozone Depletion: 2018 World Meteorological Organization Global Ozone Research and Monitoring Project—Report No. 58., ISBN: 978-1-7329317-1-8, 2018.

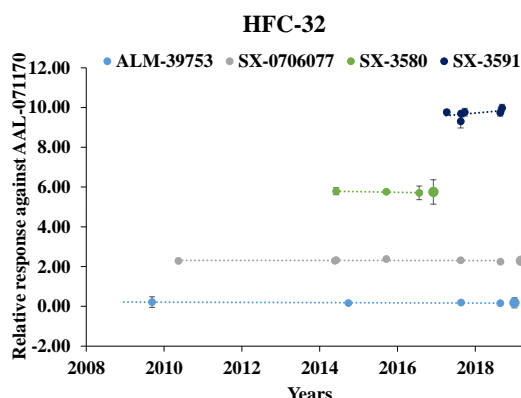
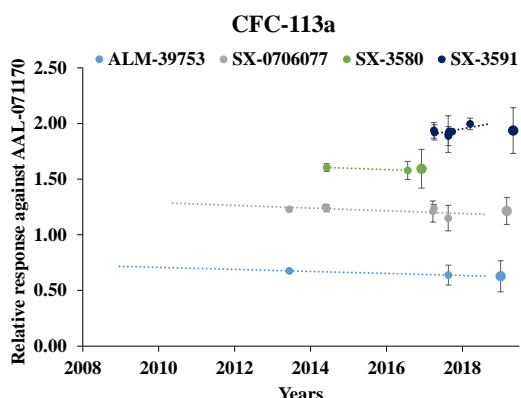
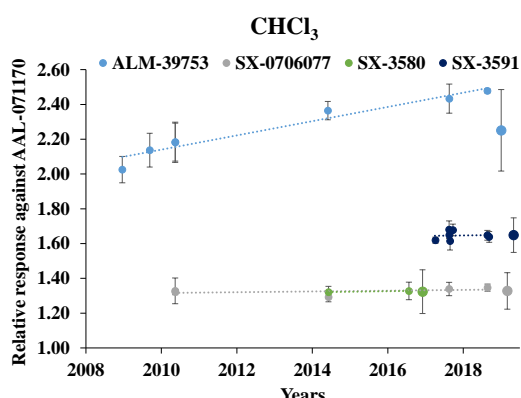
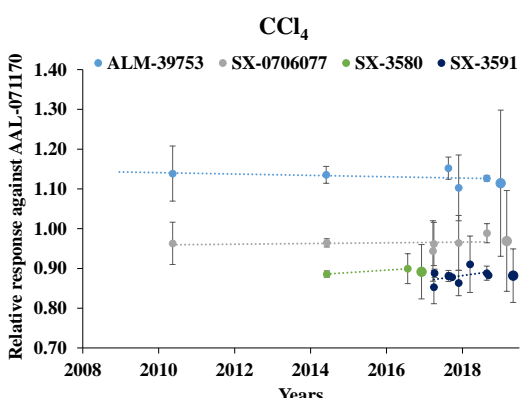
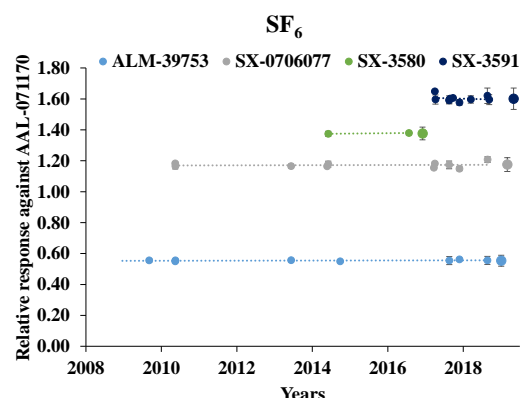
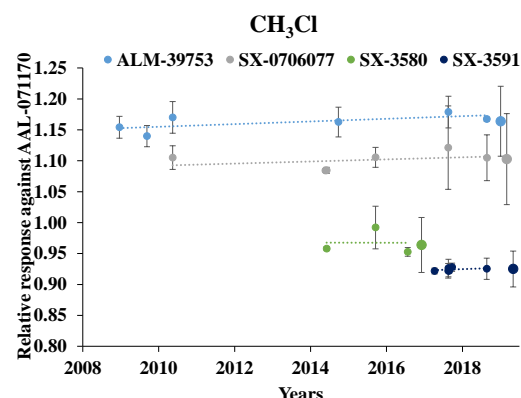
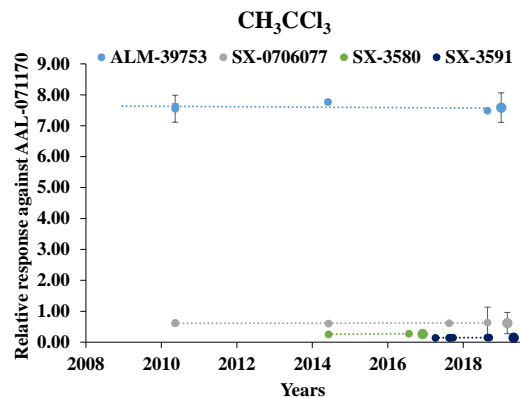
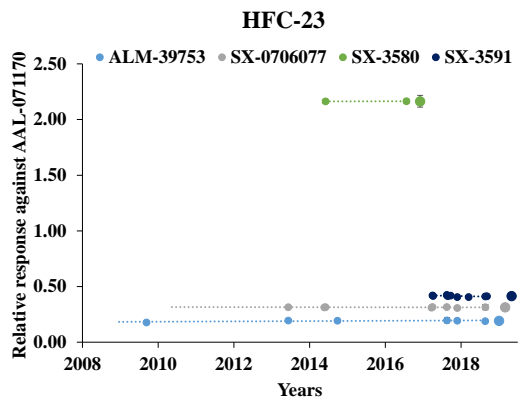
# Appendix

## A1. Intercomparison results

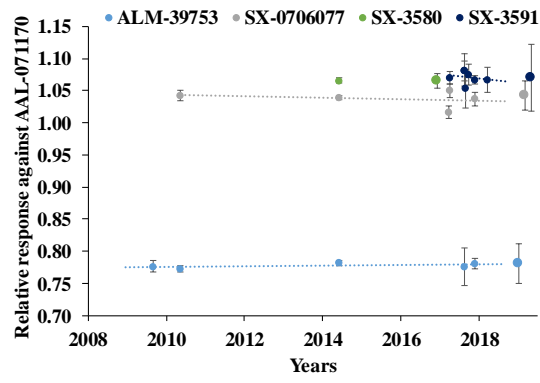
Relative responses of the standards against AAL-071170 between 2008-2018 from Section 2.8.





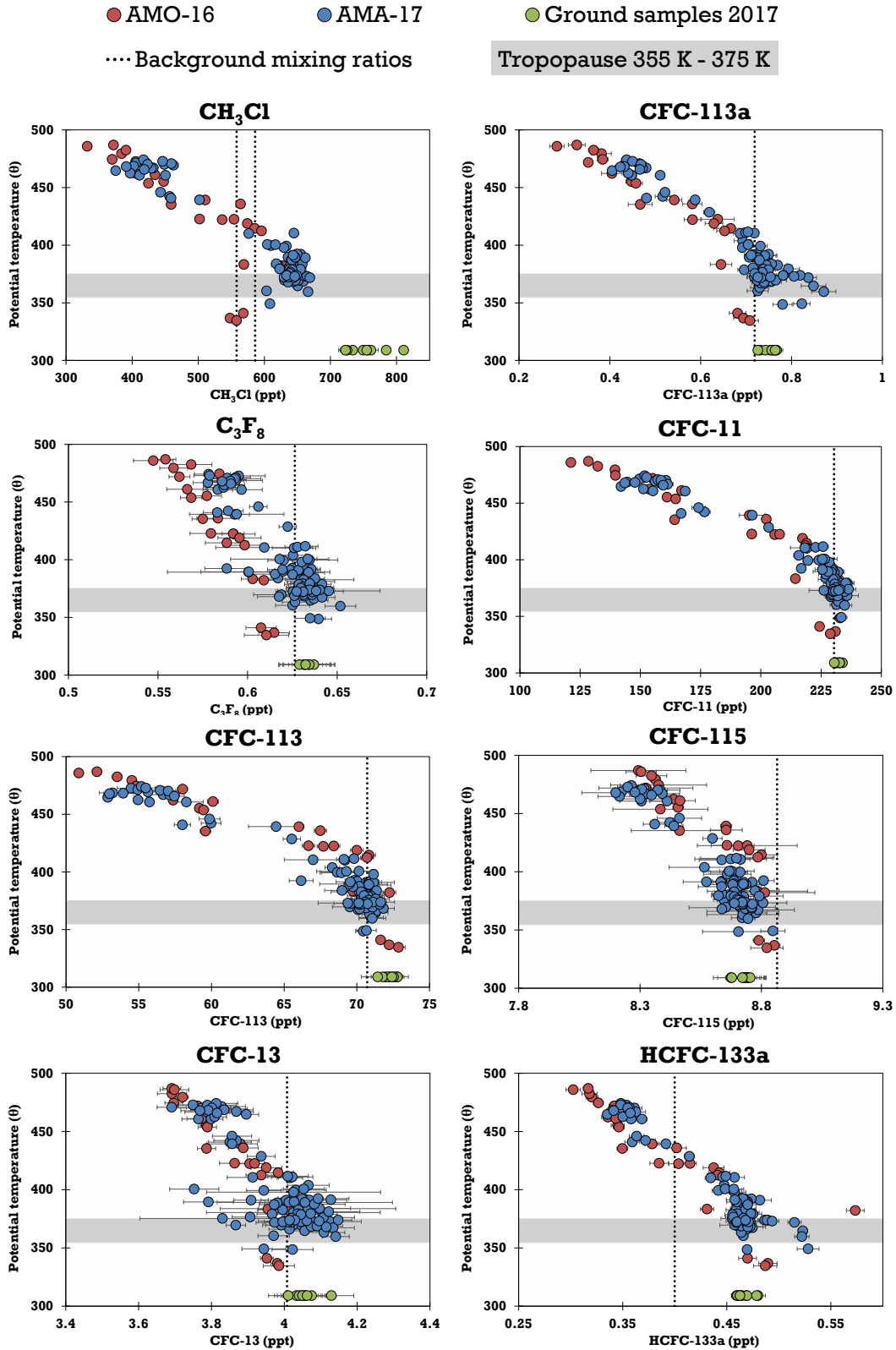


### Halon-1301



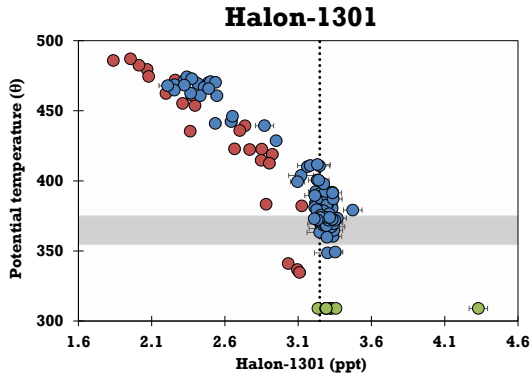
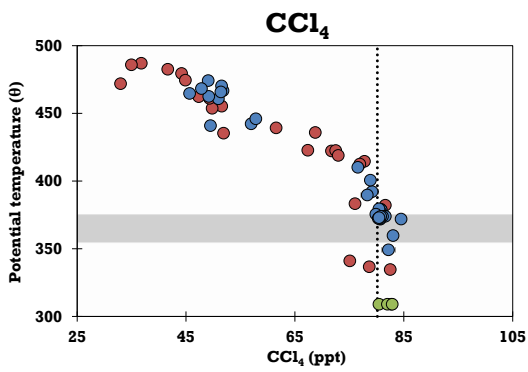
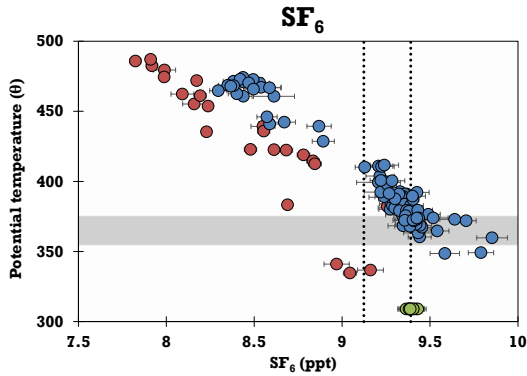
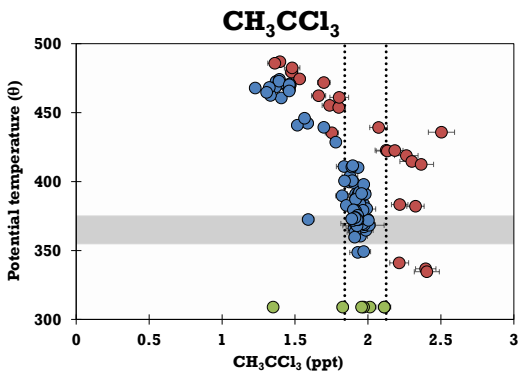
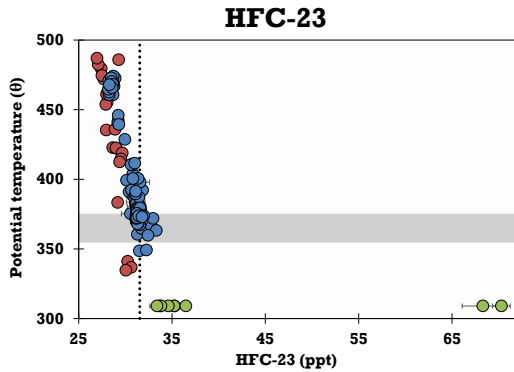
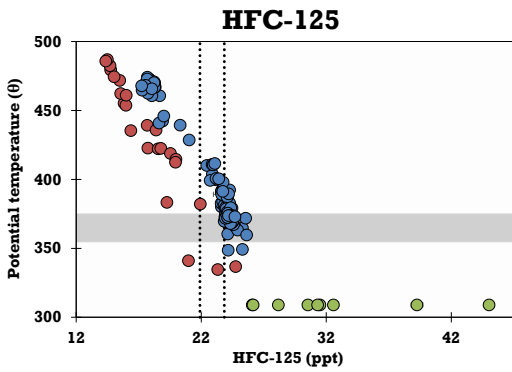
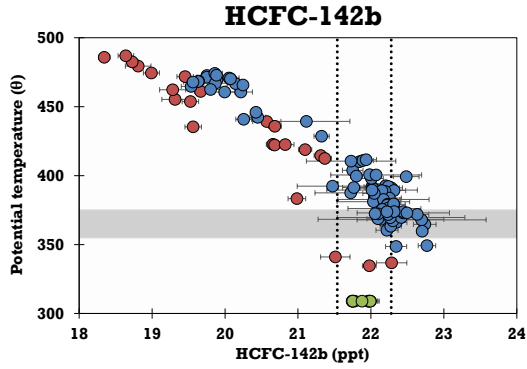
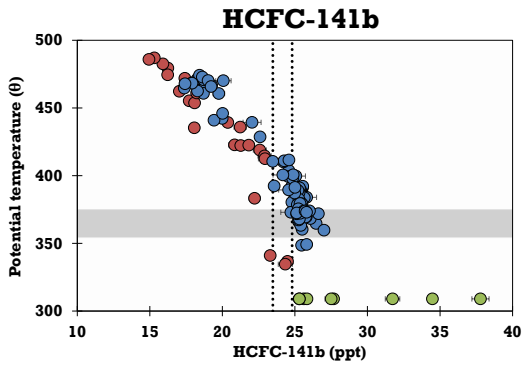
## A2. AMO-16 and AMA-17 mixing ratios

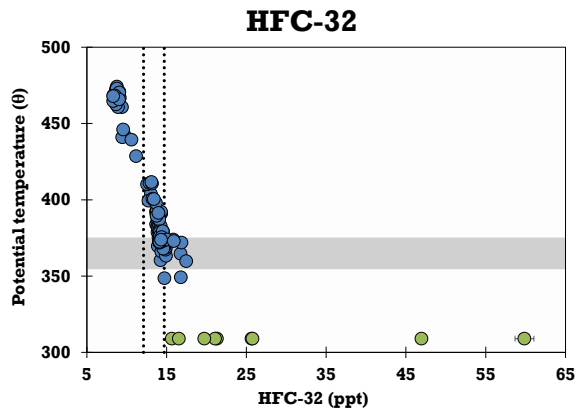
Mixing ratios as a function of potential temperature (a pseudo-vertical coordinate) for AMO-16, AMA-17 and the ground samples collected during AMA-17. The dotted vertical lines indicate the background mixing ratios. The horizontal grey bar represents the location of the chemical tropopause at 355 K – 375 K.



● AMO-16      ● AMA-17  
 ⋯ Background mixing ratios

● Ground samples 2017  
 Tropopause 355 K - 375 K

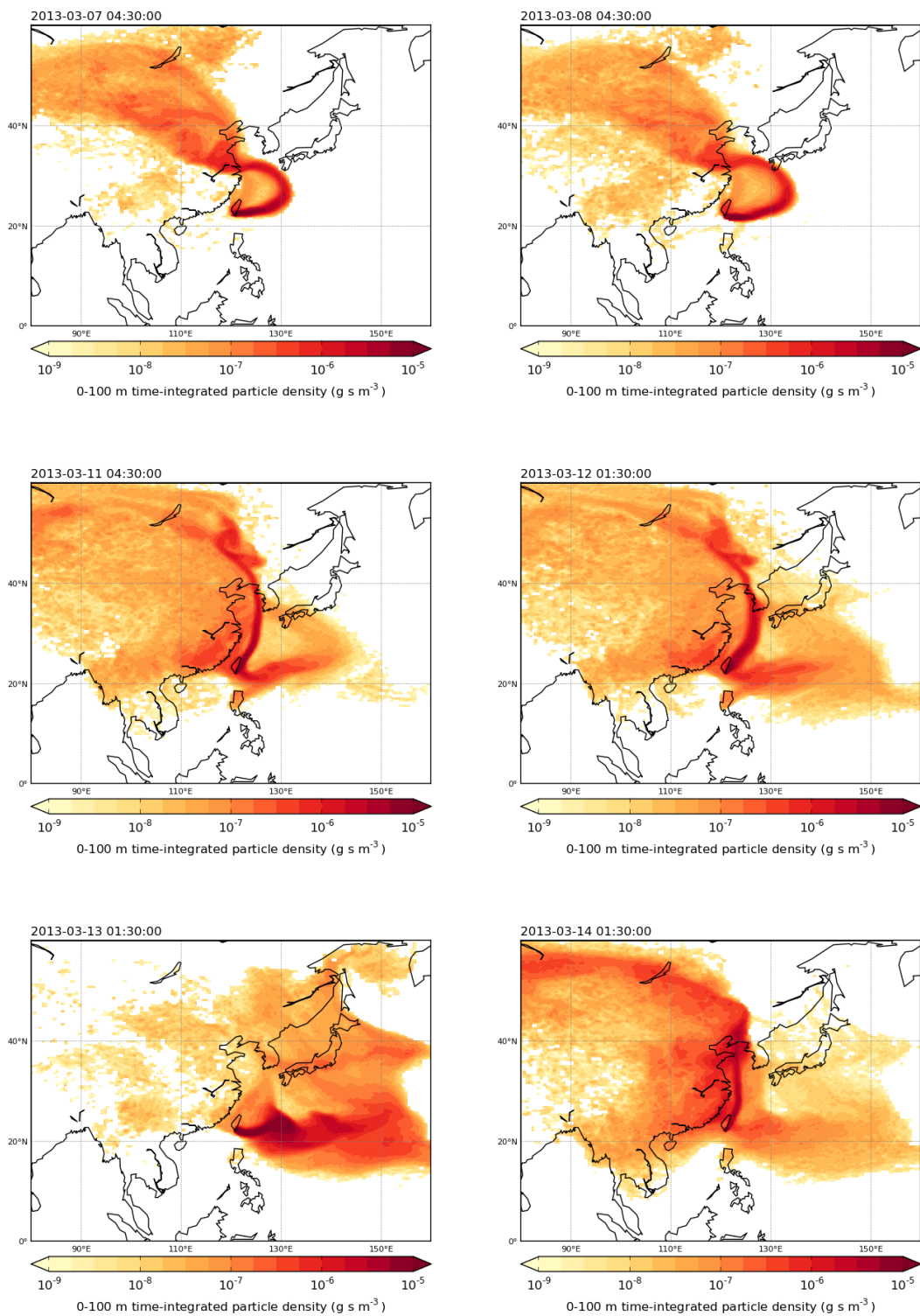


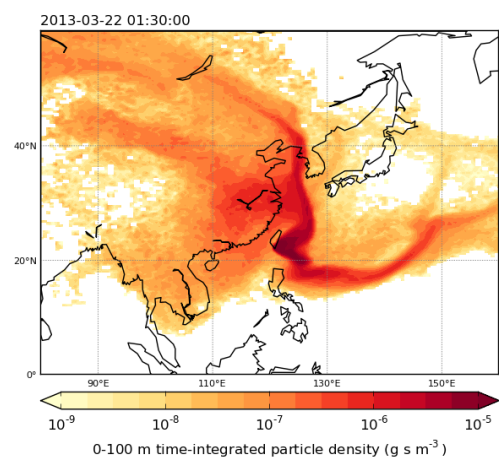
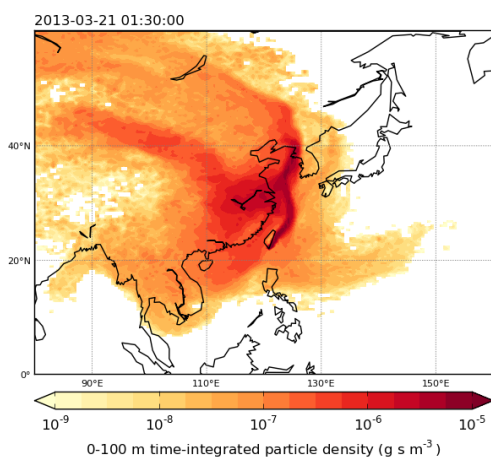
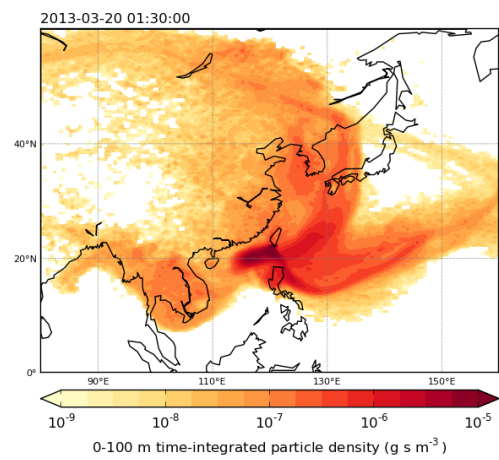
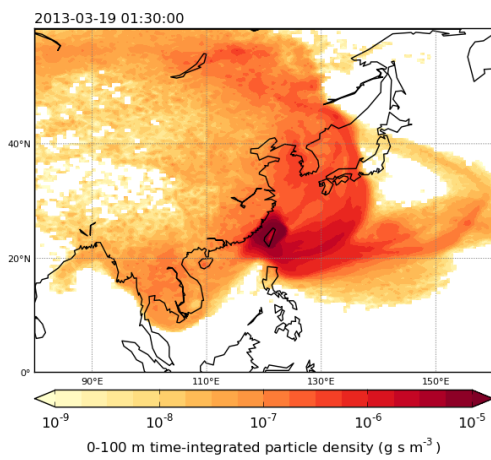
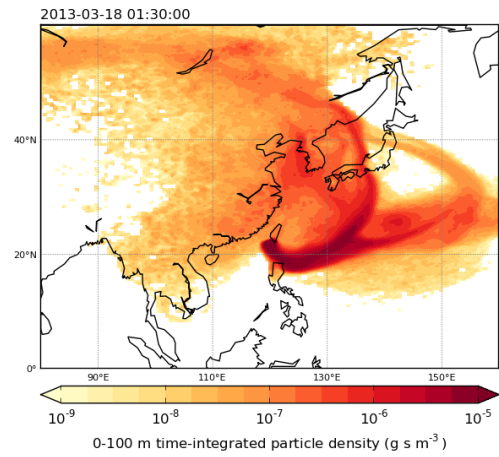
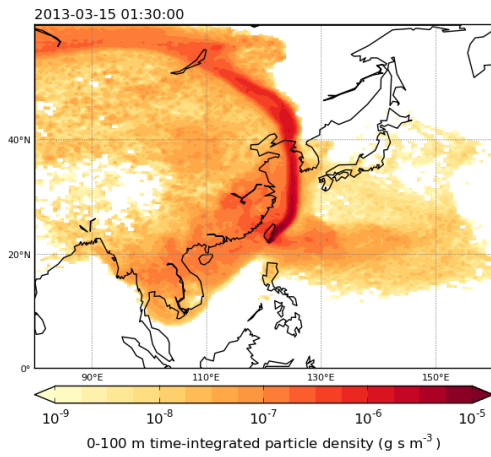


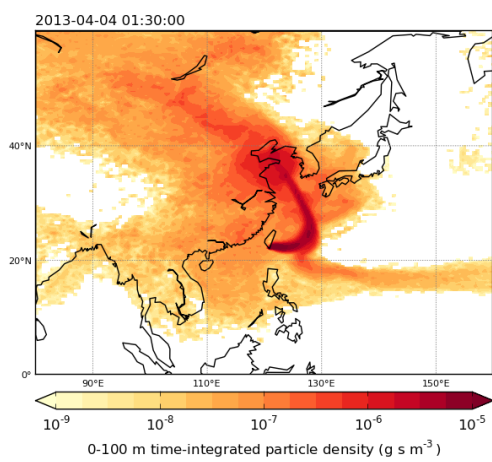
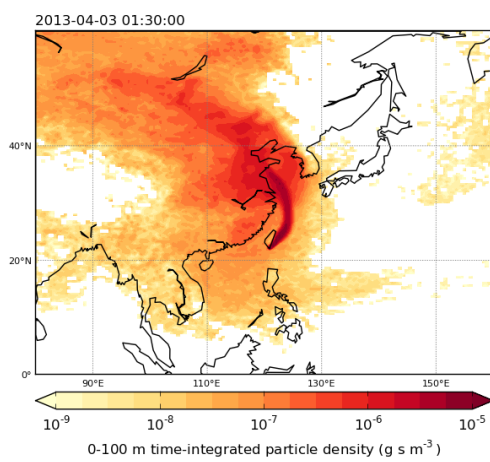
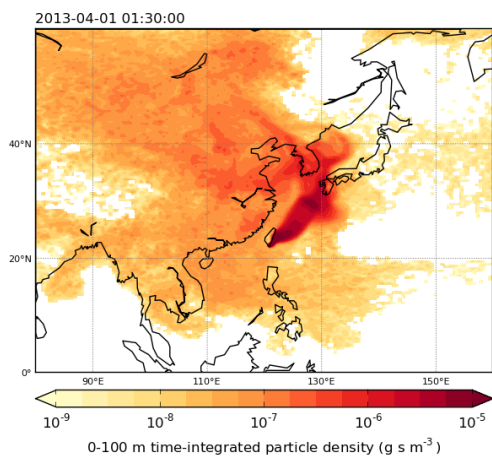
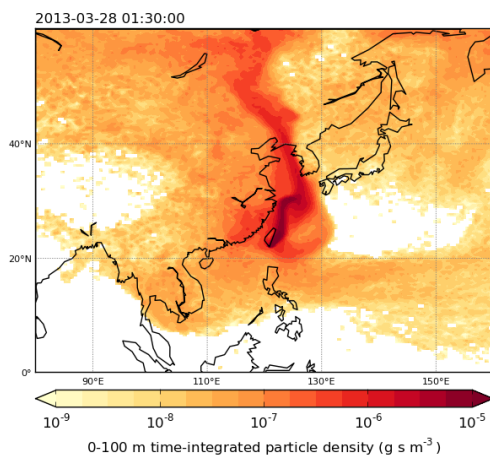
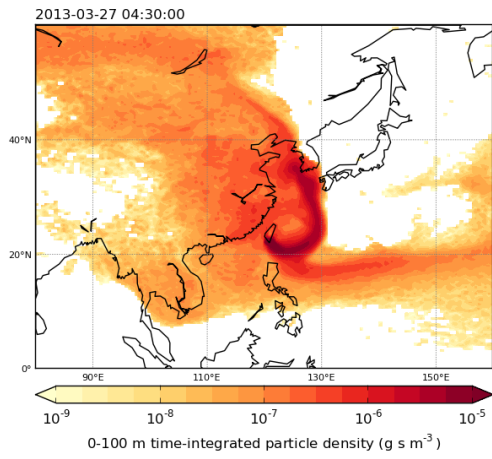
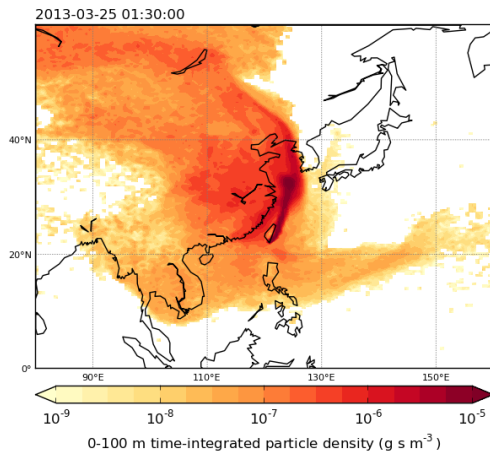
### A3. NAME footprints

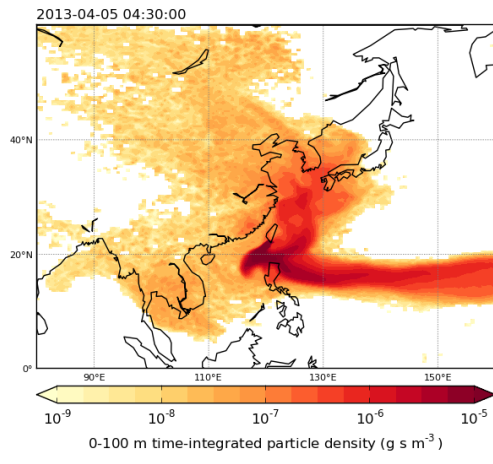
The NAME footprints derived from 12-day backward simulations and showing the time integrated density of particles below 100 m altitude for the approximate times when samples were collected during the Taiwan campaigns at Hengchun in 2013 and 2015 and Cape Fuguei in 2014 and 2016.

#### 3.1 NAME footprints for the Hengchun, Taiwan 2013 campaign

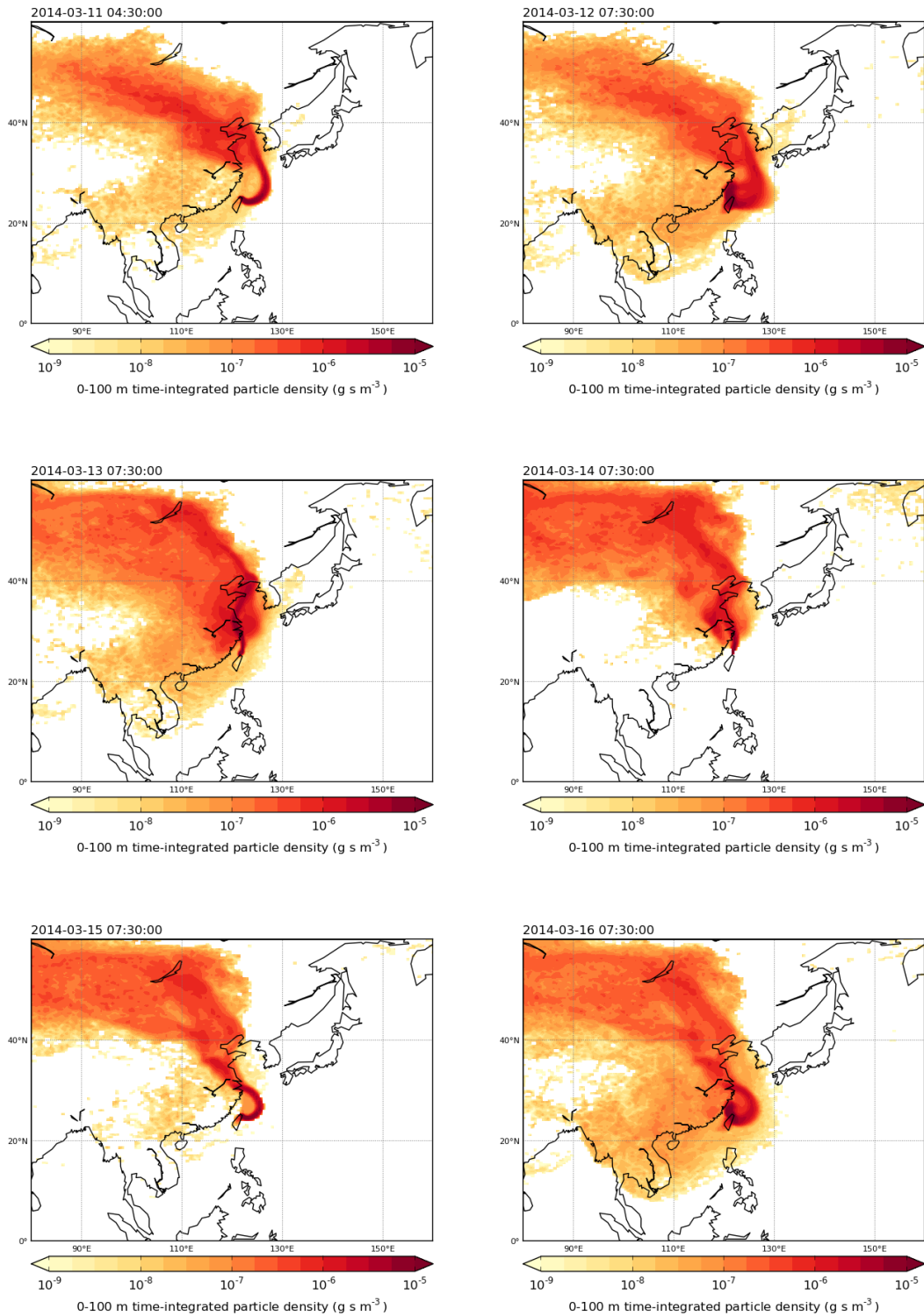


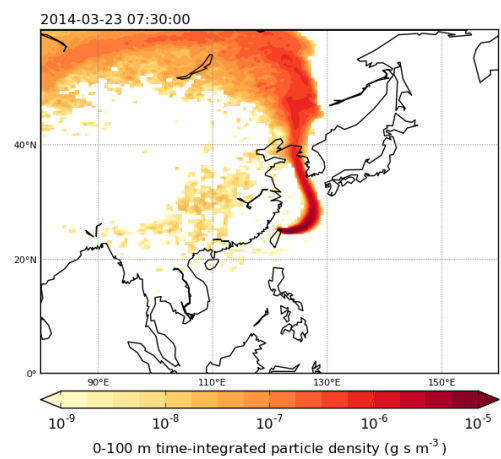
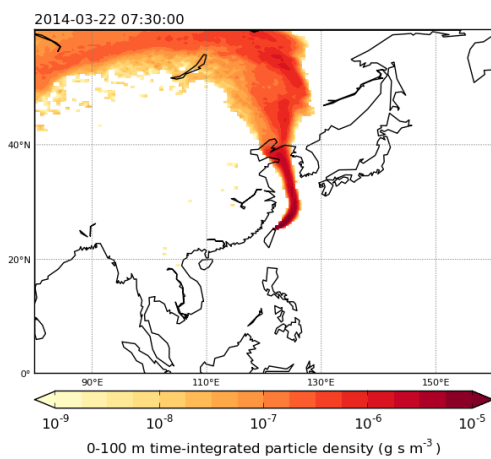
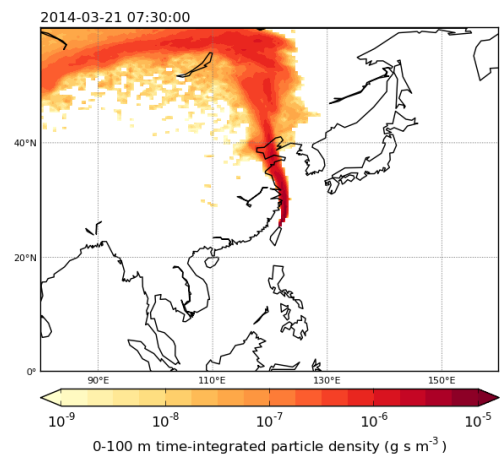
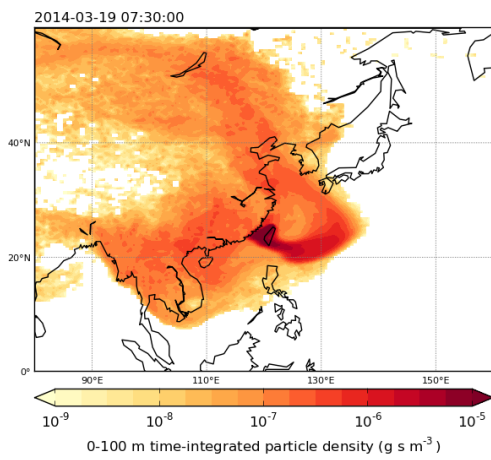
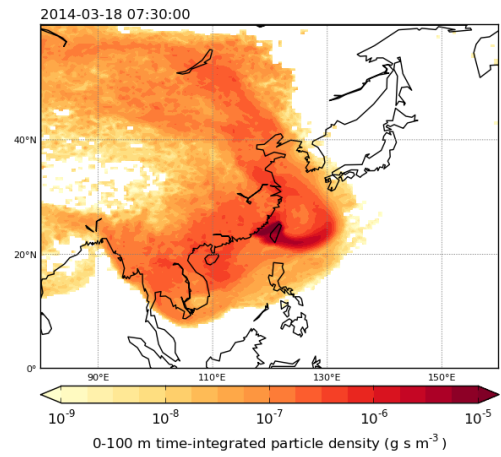
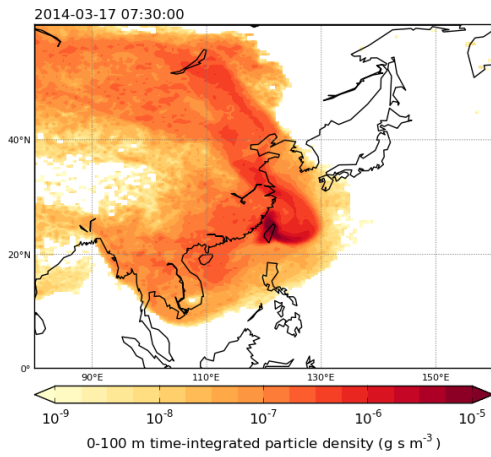


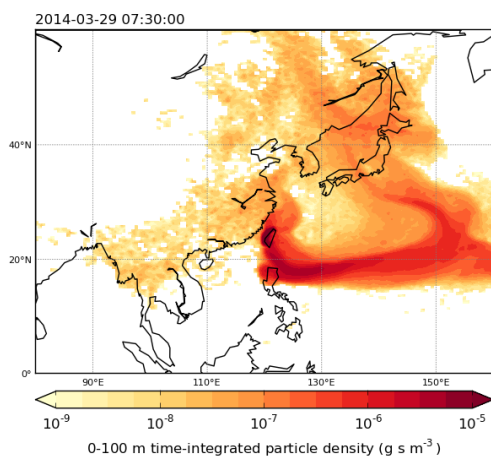
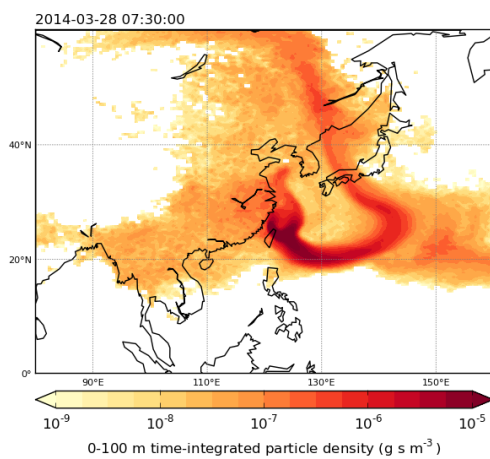
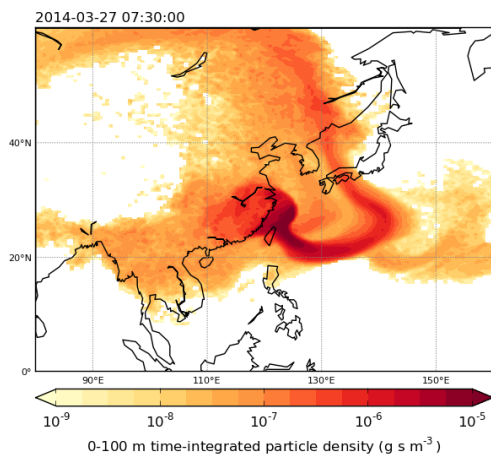
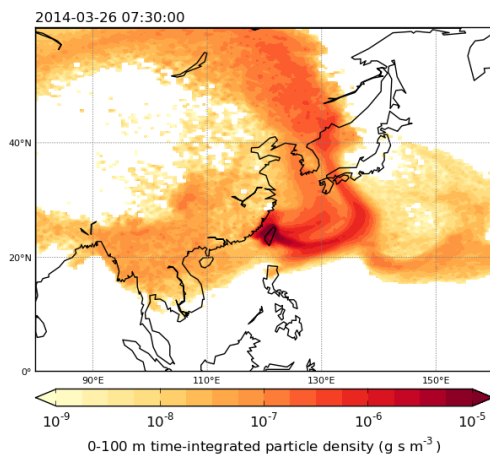
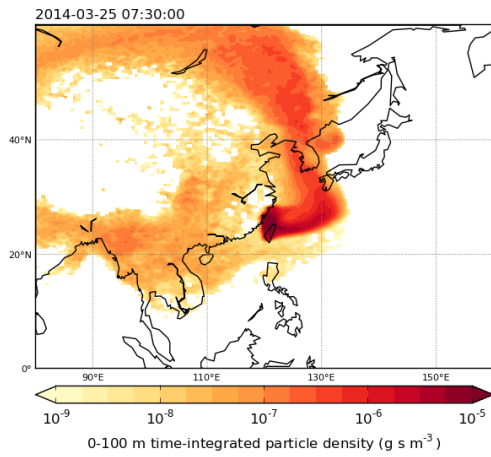
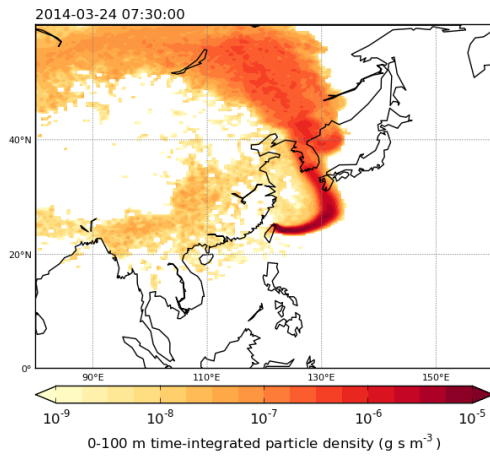


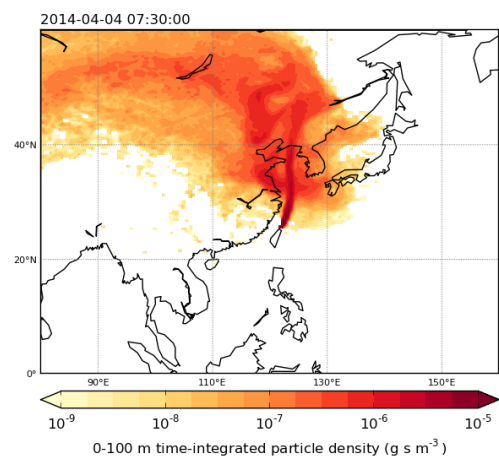
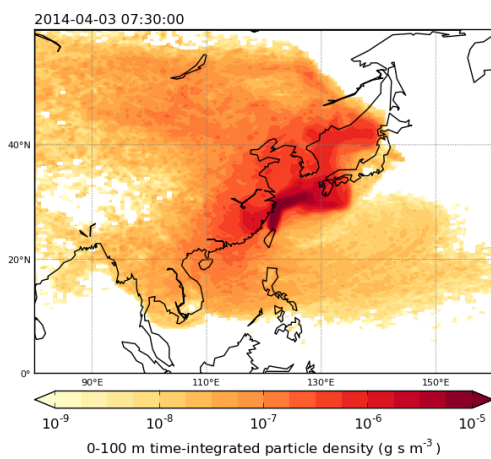
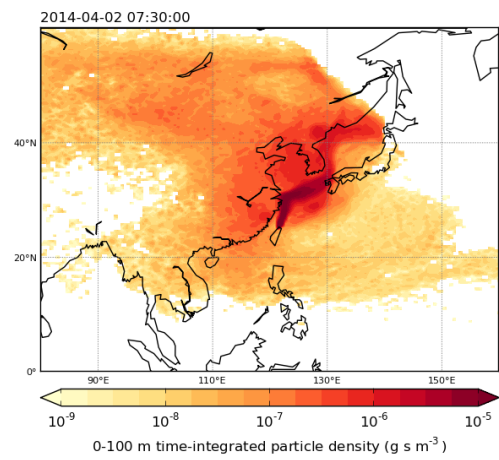
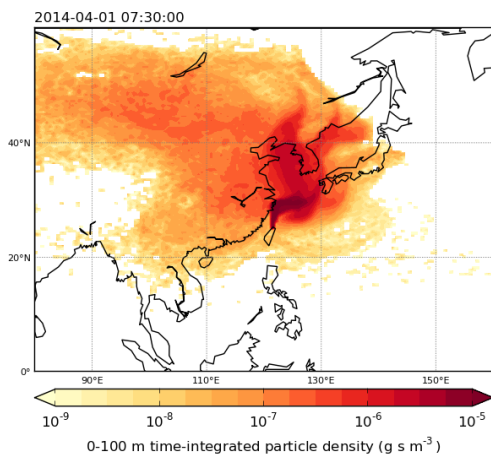
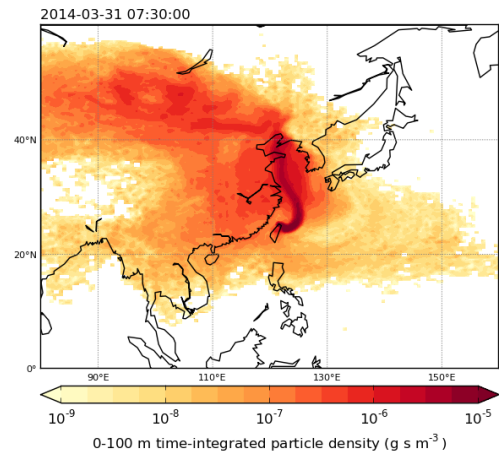
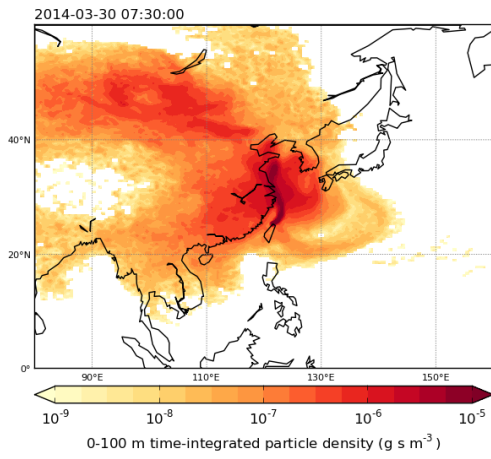


### 3.2 NAME footprints for the Cape Fuguei, Taiwan 2014 campaign

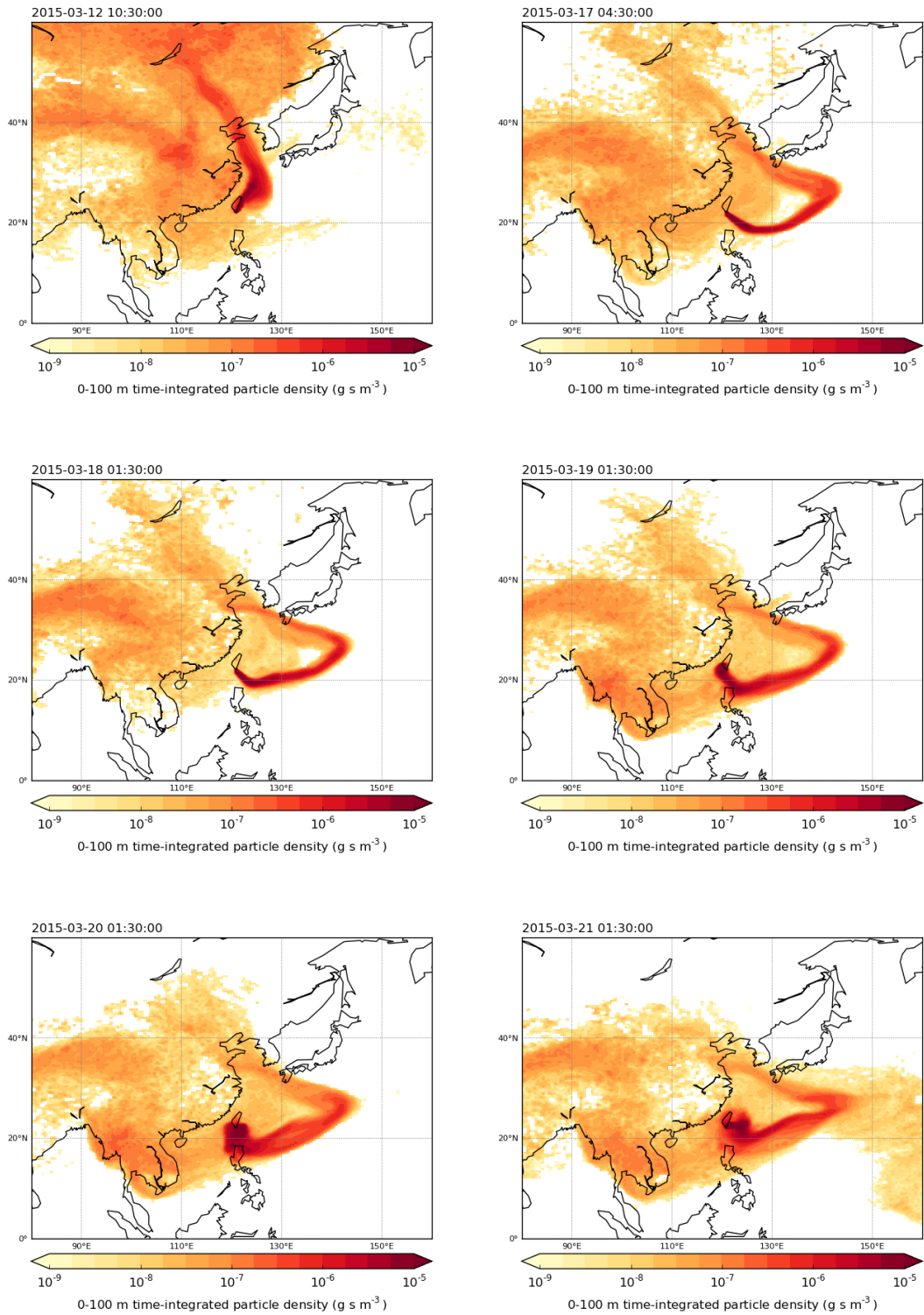


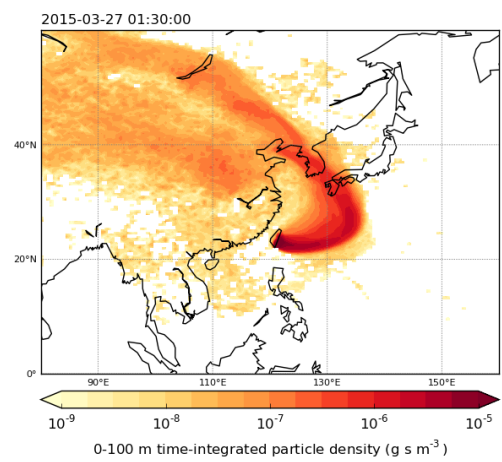
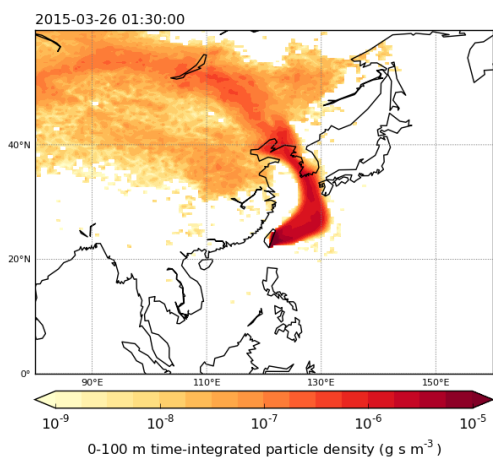
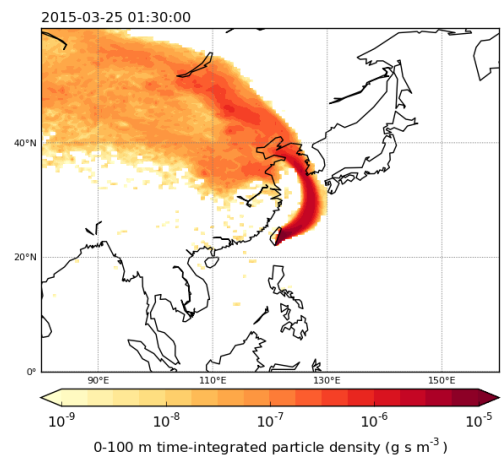
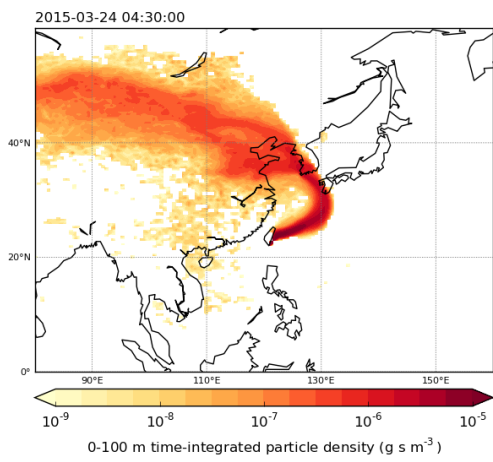
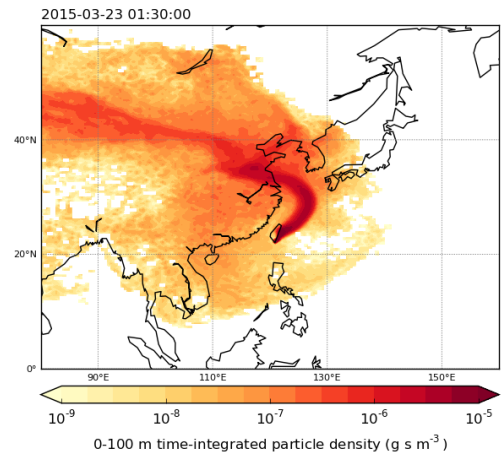
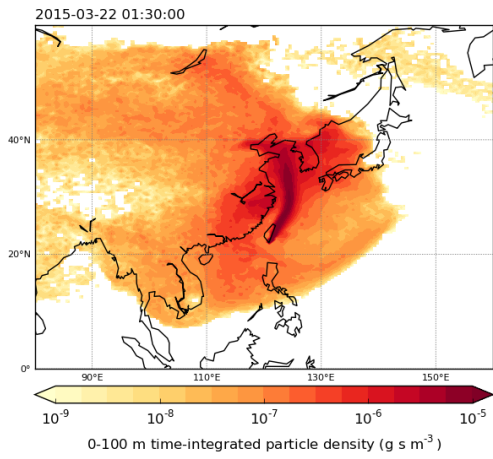


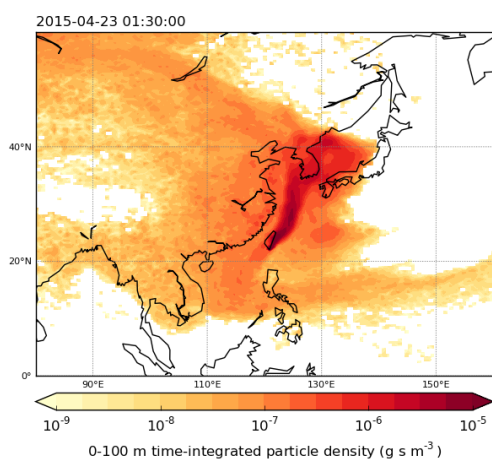
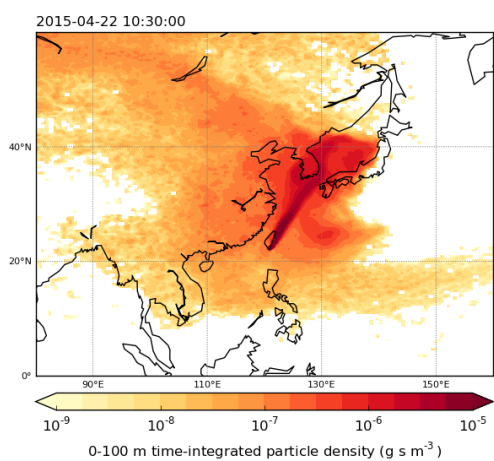
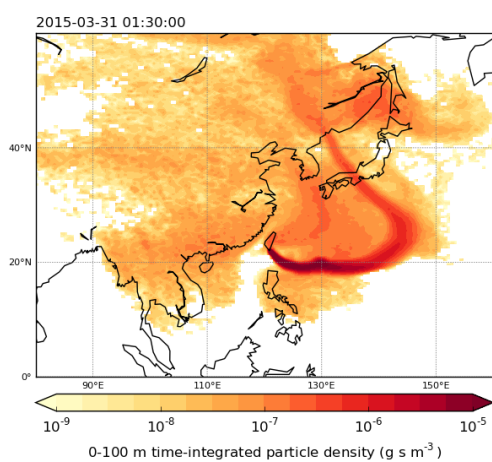
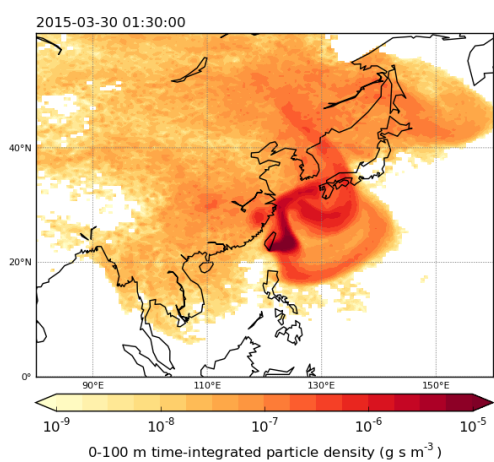
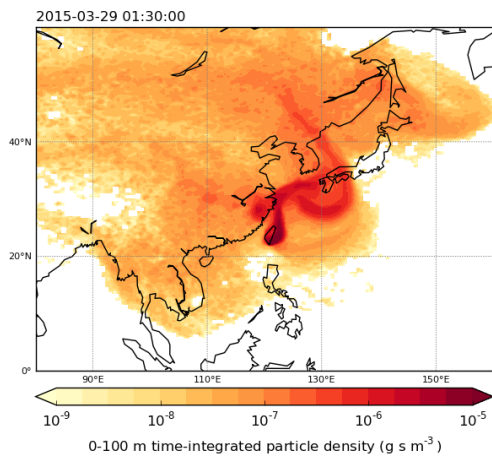
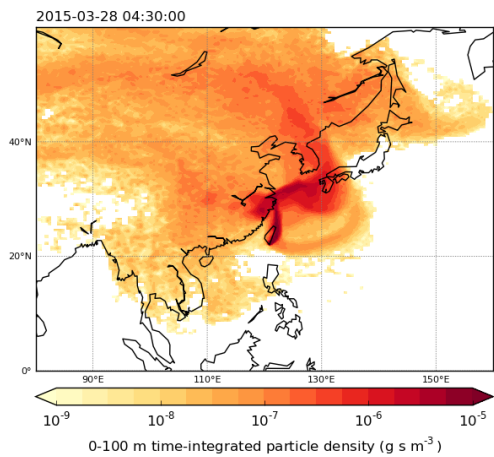


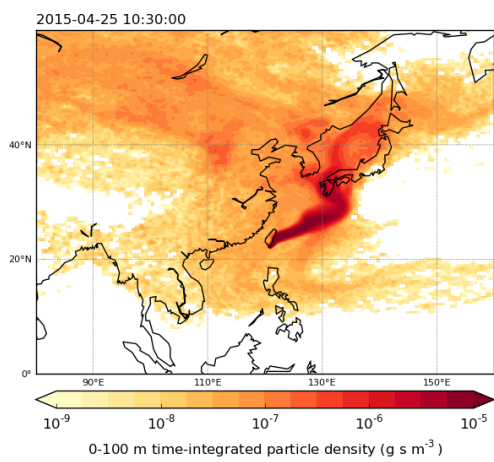
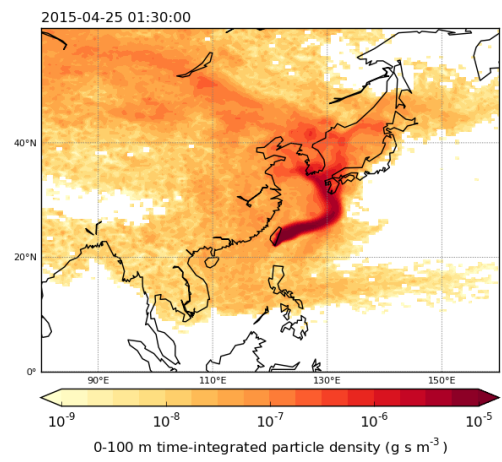
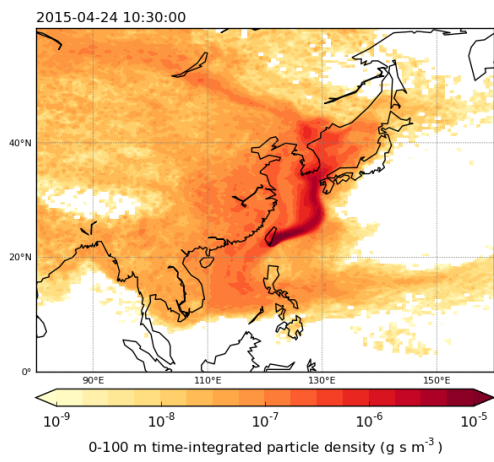
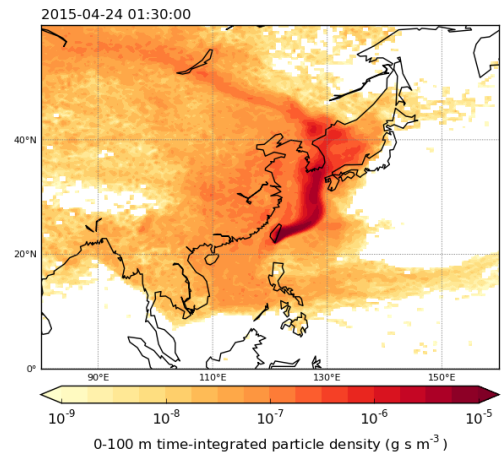
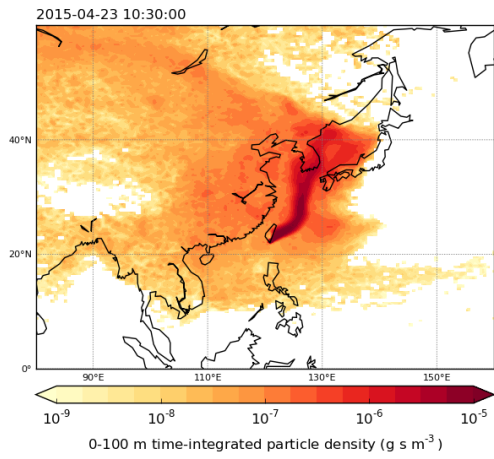


### 3.3 NAME footprints for the Hengchun, Taiwan 2015 campaign

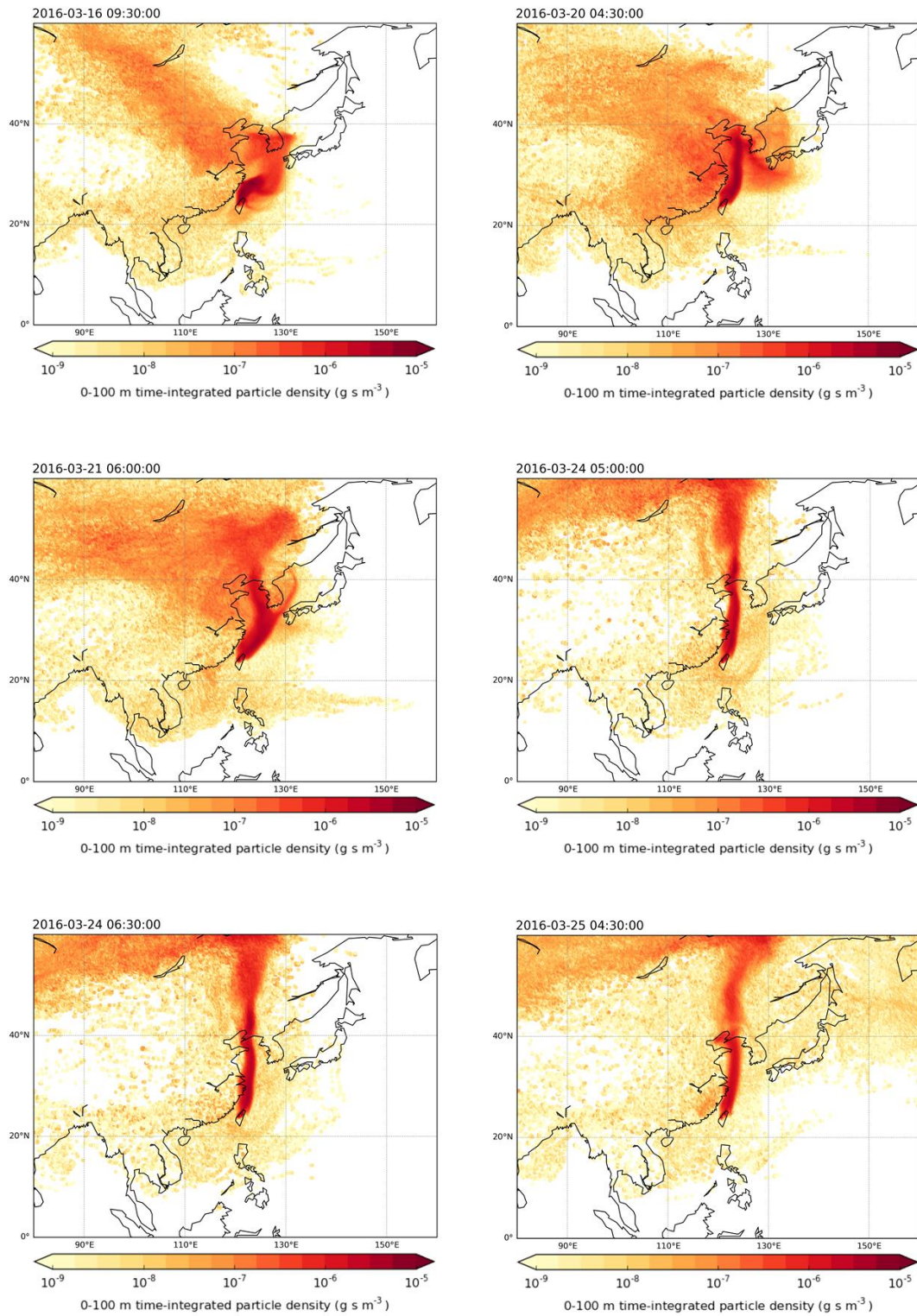


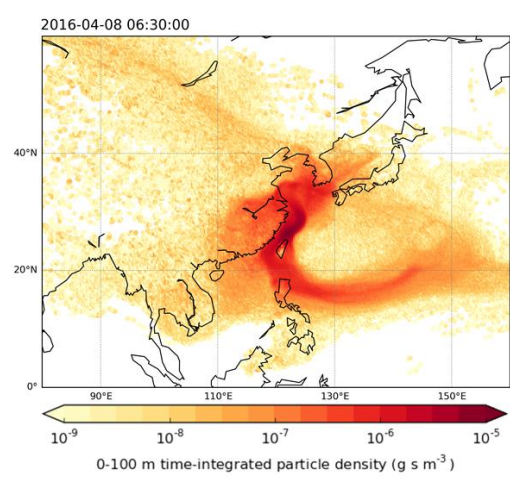
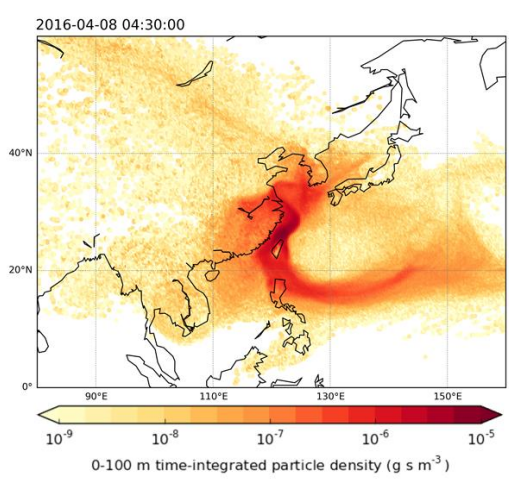
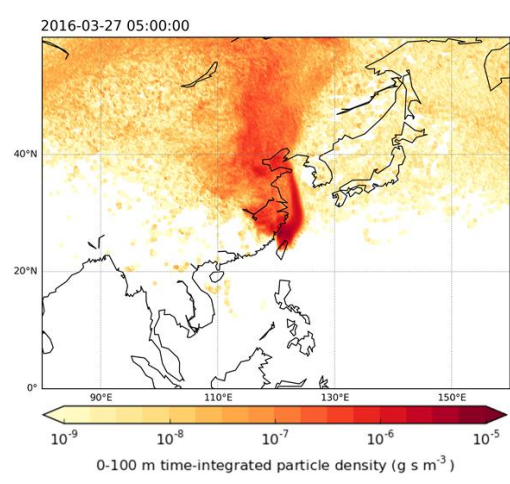
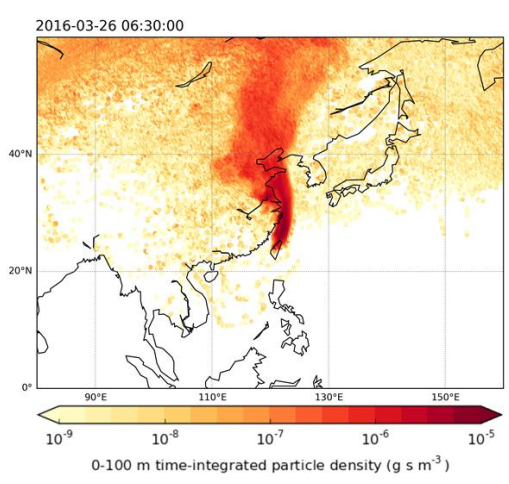
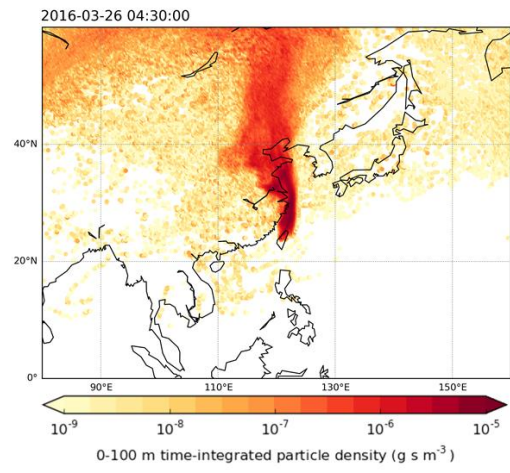
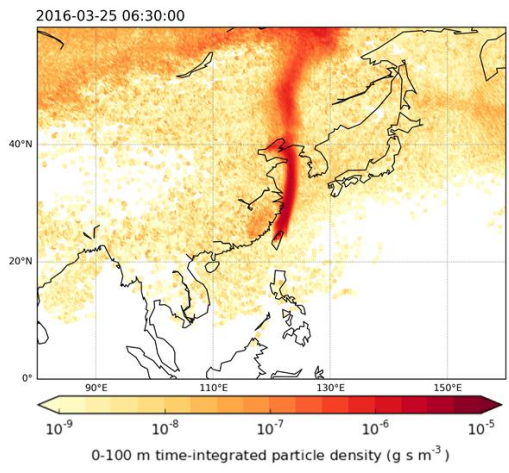


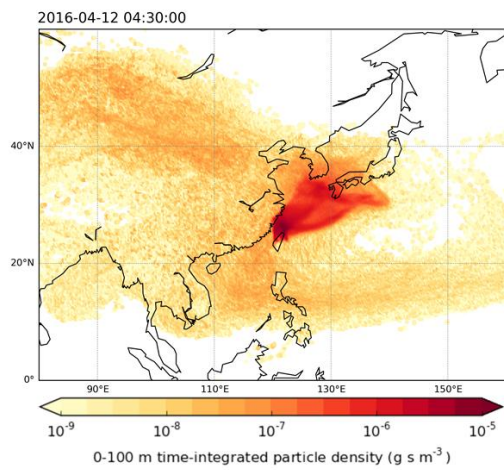
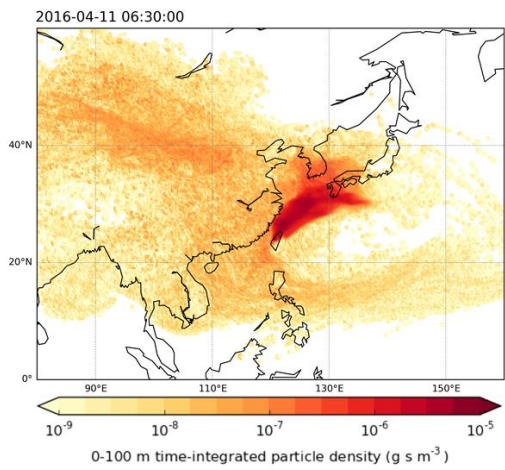
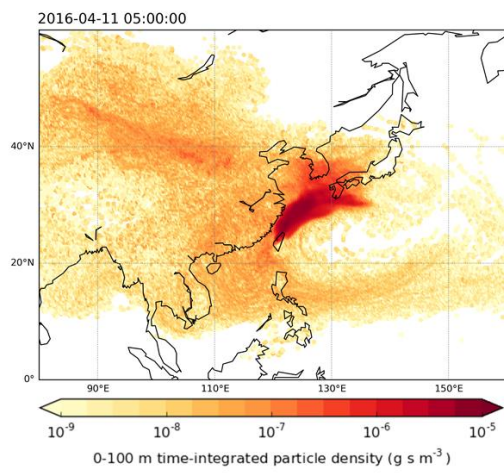
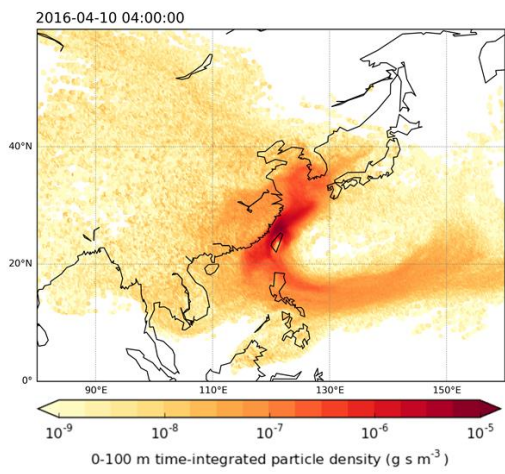
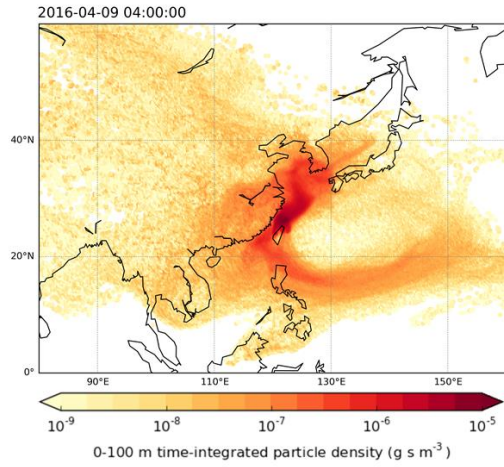
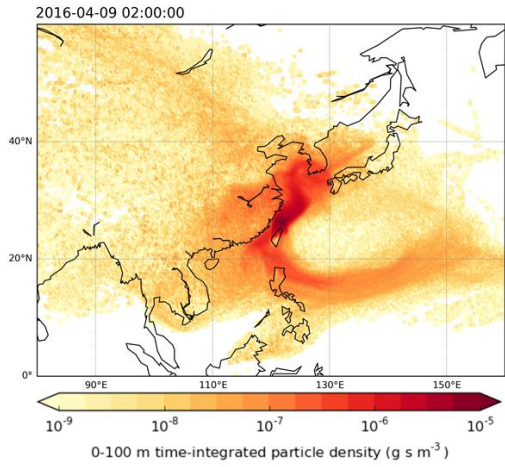


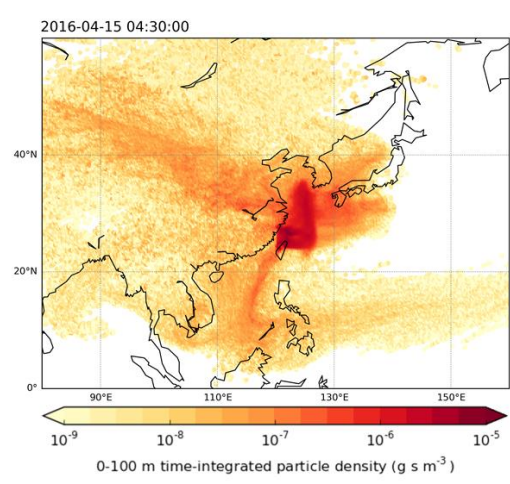
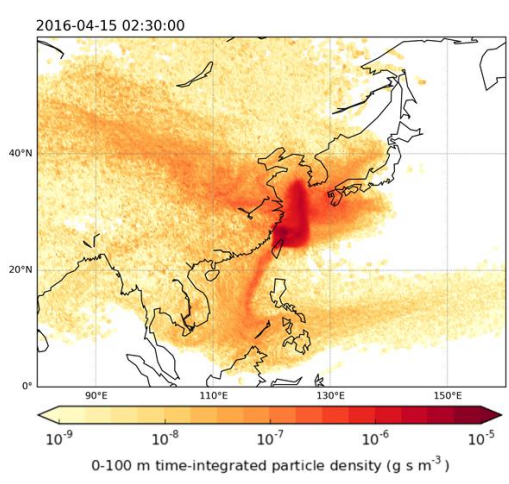
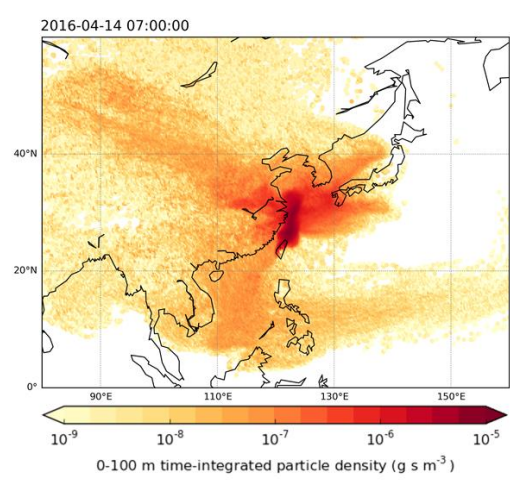
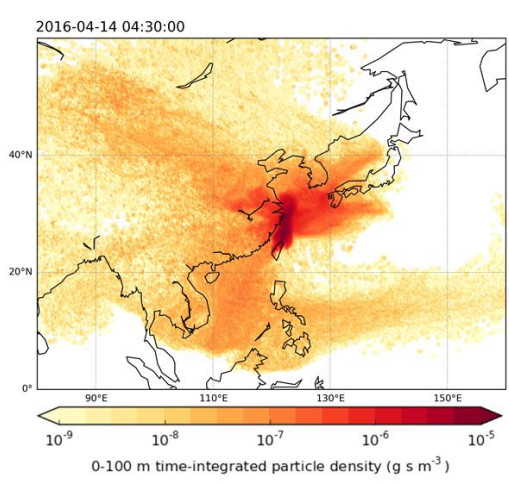
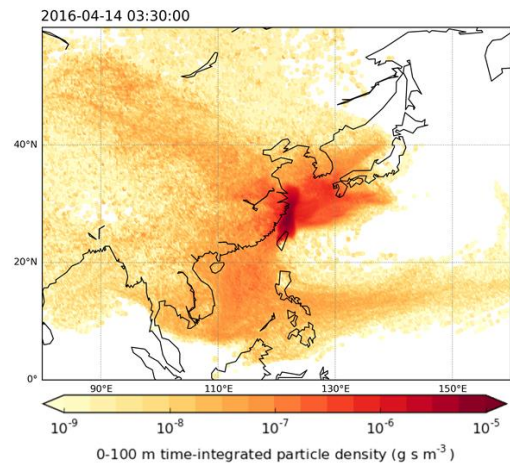
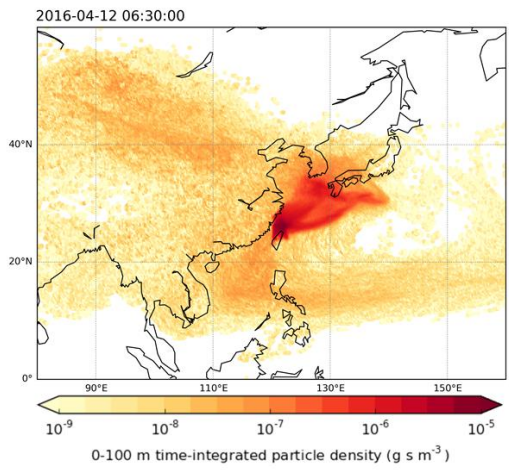


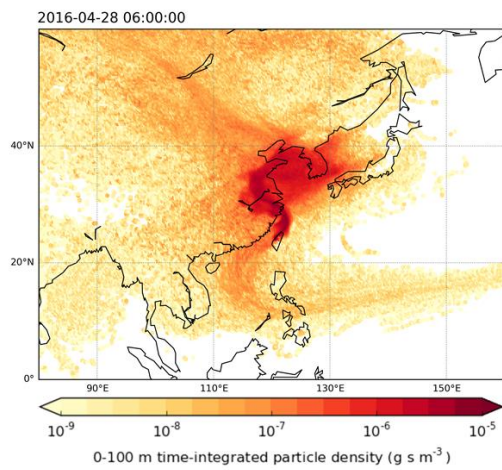
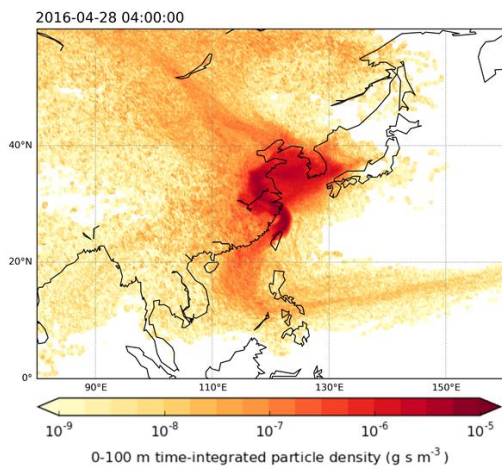
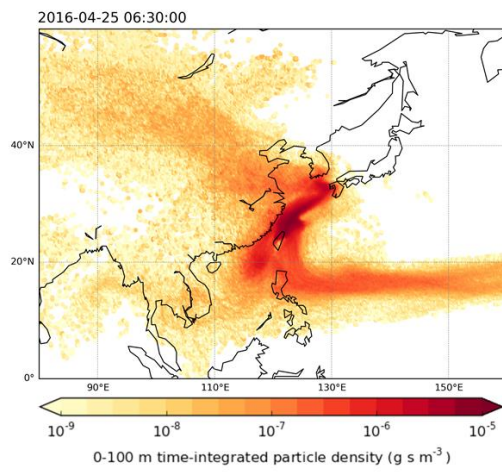
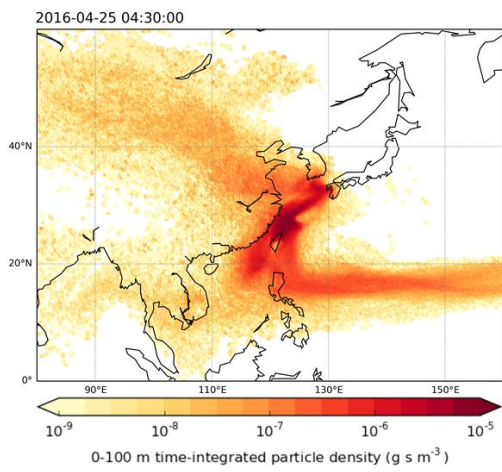
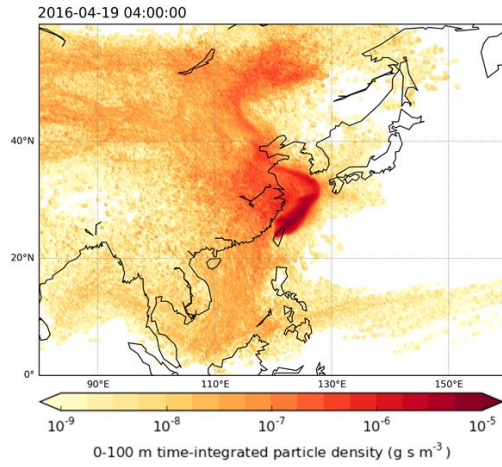
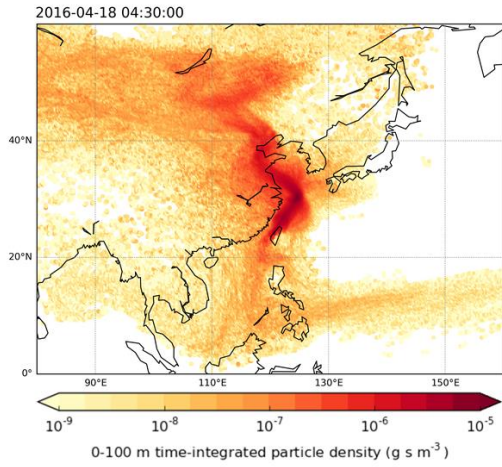
### 3.4 NAME footprints for the Cape Fuguei, Taiwan 2016 campaign

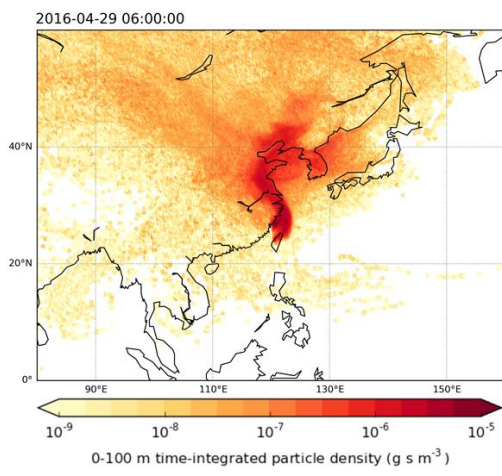
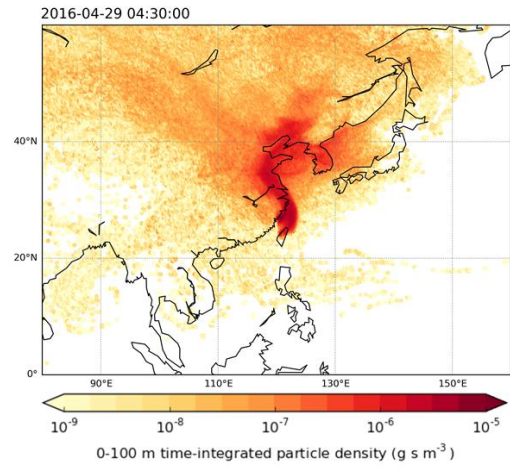
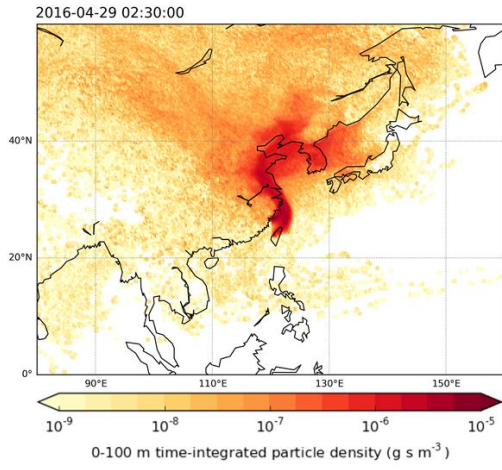












#### A4. CFC-11 emission estimates

Table A1: CFC-11 emission estimates from previous studies for China or eastern China; the years the estimates are for; the uncertainties in the estimates; and comments on the methods used.

Reference	Year	Best estimate (Gg yr <sup>-1</sup> )	Lower uncertainty (Gg yr <sup>-1</sup> )	Upper uncertainty (Gg yr <sup>-1</sup> )	Method
<b>Earlier period</b>					
Wan et al. (2009)	2008	14.259			Bottom-up method based on reported production and estimated emission rates
Wan et al. (2009)	2009	12.858			
Wan et al. (2009)	2010	11.541			
Wan et al. (2009)	2011	9.638			
Fang et al. (2018)	2008	13.0			Bottom-up method based on reported production and estimated emission rates
Fang et al. (2018)	2009	12.3			
Fang et al. (2018)	2010	11.6			
Fang et al. (2018)	2011	10.9			
Kim et al. (2010)	2008	12	9.4	17	Measurements at Gosan, Jeju Island, Korea and atmospheric inversion modeling using FLEXPART
An et al. (2012)	2009	15.8	8.6	23	Measurements at Shangdianzi Global Atmosphere Watch (GAW) Regional Station (SDZ) which is 120 km North East of Beijing and atmospheric inversion modeling using FLEXPART. Limited coverage in South and Central China
Fang et al. (2012)	2009	7.8	4	11.6	Measurements in 2009/10 at Peking University Station (PKU) in Beijing using correlations with CO mixing ratios and CO emission estimates
Fang et al. (2012)	2009	10	8.4	11.7	Measurements in 2009/10 at PKU in Beijing using correlations with HCFC-22 mixing ratios and HCFC-22 emission estimates
Wang et al. (2014)	2011	10.5	2.4	18.6	CO correlations based on measurements in Shangdong Peninsula, 2010-2011. Uncertainty +/-8.1 kt/y
Rigby et al. (2019)	2008-2012	6.4	5.2	7.6	Measurements at Gosan, Jeju Island, Korea and Hateruma, Japan and NAME and FLEXPART atmospheric inversions
<b>Combined estimates of earlier period</b>					

Mean of earlier estimates (excluding Rigby et al., 2019)	2008-2011	11.7	9.6	13.8	Uncertainties are standard deviation of the estimates
Mean of earlier estimates (including Rigby et al., 2019)	2008-2012	10.3	7.4	13.2	Uncertainties are standard deviation of the estimates
<b>Later period</b>					
Current study (CH <sub>2</sub> Cl <sub>2</sub> , Feng)	2014-2018	11.7	9.2	14.2	Taiwan interspecies correlation with CH <sub>2</sub> Cl <sub>2</sub> emission estimate from Feng et al., (2018)
Current study (CH <sub>2</sub> Cl <sub>2</sub> , Oram)	2014-2018	16.7	14.7	18.7	Taiwan interspecies correlation with CH <sub>2</sub> Cl <sub>2</sub> emission estimate from Oram et al., (2017)
Current study (CH <sub>3</sub> Cl, FLEXPART)	2014-2018	19.4	17.4	21.3	Taiwan interspecies correlation with CH <sub>3</sub> Cl emission estimate from Fang et al., (2019) using FLEXPART inversion model
Current study (CH <sub>3</sub> Cl, NAME)	2014-2018	18.1	15.3	22.4	Taiwan interspecies correlation with CH <sub>3</sub> Cl emission estimate from Fang et al., (2019) using NAME inversion model
Current study (CCl <sub>4</sub> , FLEXPART)	2014-2018	17.0	9.1	24.9	Taiwan interspecies correlation with CCl <sub>4</sub> emission estimate from Lunt et al., (2018) using FLEXPART inversion model
Current study (CCl <sub>4</sub> , NAME)	2014-2018	22.2	14.3	31.5	Taiwan interspecies correlation with CCl <sub>4</sub> emission estimate from Lunt et al., (2018) using NAME inversion model
Current study (HCFC-22)	2014-2018	26.5	19.6	33.4	Taiwan interspecies correlation with HCFC-22 emission estimate from Li et al., (2016)
Rigby et al. (2019)	2014-2017	13.4	11.7	15.1	Measurements at Gosan, Jeju Island, Korea and Hateruma, Japan and NAME and FLEXPART atmospheric inversions
<b>Combined estimates of later period</b>					
Mean of current study	2014-2018	18.8	14.2	23.5	Uncertainties are standard deviation of the estimates
Mean of current study and Rigby et al. (2019)	2014-2018	17.1	12.7	21.5	Uncertainties are standard deviation of the estimates
<b>Increase</b>					
Average increase from 2008-2011 to 2014-2018 (excluding Rigby et al., 2019)	2014-2018	7.1	2.0	12.2	The uncertainties are the square root of the sum of the uncertainties for each time period squared
Average increase from 2008-2011 to 2014-2018 (including Rigby et al., 2019)	2014-2018	6.7	1.5	12.0	The uncertainties are the square root of the sum of the uncertainties for each time period squared
<b>Other estimates</b>					

EIA (2018)	2012-2017		10.3	12.2	Bottom-up method based on surveys with industry experts, reported production data and assumptions on emission rates and the extent of CFC-11 use
Wan et al. (2009)	2014	6.038			Bottom-up method based on reported production and estimates of emission rates
Wan et al. (2009)	2015	4.941			
Wan et al. (2009)	2016	3.982			
Wan et al. (2009)	2017	3.088			
Wan et al. (2009)	2018	2.256			
Fang et al. (2018)	2014	8.3			Bottom-up method based on reported production and estimates of emission rates
Fang et al. (2018)	2015	7.2			
Fang et al. (2018)	2016	5.9			
Fang et al. (2018)	2017	5.2			
Fang et al. (2018)	2018	4.5			
Average of Wan et al. (2009) and Fang et al. (2018)	2014-2018	5.1	3.3	6.9	Uncertainties are standard deviation of the estimates
Mean of current study minus average of Wan et al. (2009) and Fang et al. (2018)	2014-2018	13.7	8.7	18.7	The uncertainties are the square root of the sum of the uncertainties for the estimates